



**THE DEVELOPMENT OF NEW ARTIFICIAL INTELLIGENCE
BASED HYBRID TECHNIQUES COMBINING BEES ALGORITHM,
DATA MINING AND GENETIC ALGORITHM FOR DETECTION,
CLASSIFICATION AND PREDICTION OF FAULTS IN INDUCTION
MOTORS**

Ammar Khaleel Ibrahim Al-Musawi

**School of Engineering
Cardiff University
Wales, United Kingdom**

**A thesis submitted to the Cardiff University in Candidature for the
degree of Doctor of Philosophy**

2019

DECLARATION

This work has not been submitted in substance for any other degree or award at this or any other university or place of learning, nor is being submitted concurrently in candidature for any degree or other award.

Ammar Al-Musawi (PhD Candidate)

Date:

STATEMENT 1

This thesis is being submitted in partial fulfilment of the requirements for the degree of PhD.

Ammar Al-Musawi (PhD Candidate)

Date:

STATEMENT 2

This thesis is the result of my own independent work/investigation, except where otherwise stated, and the thesis has not been edited by a third party beyond what is permitted by Cardiff University's Policy on the Use of Third Party Editors by Research Degree Students. Other sources are acknowledged by explicit references. The views expressed are my own.

Ammar Al-Musawi (PhD Candidate)

Date:

STATEMENT 3

I hereby give consent for my thesis, if accepted, to be available online in the University's Open Access repository and for inter-library loan, and for the title and summary to be made available to outside organisations.

Ammar Al-Musawi (PhD Candidate)

Date:

ACKNOWLEDGMENT

This work was carried out at the School of Engineering, Cardiff University, United Kingdom.

*First and foremost, I thank **ALLAH** for helping me to complete this thesis.*

I am grateful to Cardiff University for providing the opportunity and resources required for my study to complete this project. Special thanks for Cardiff University staff especially research office, teaching office, finance office, IT support team, electrical and mechanical workshops.

*I would like to express my deepest gratitude to my academic supervisors, **Dr. Fatih Anayi** and **Dr. Michael Packianather** for their excellent guidance during this research. I am deeply grateful for my external examiner **Professor Duc Truong Pham** and internal examiner **Dr. Turgut Meydan** for their insightful comments and suggestions for this research.*

*Of equal importance is my thanks to my small lovely family, my love **Rusul El-Dujeili** and gorgeous daughter **Fatimah** and my little son **Ibrahim**, I am really grateful for their supporting and motivating me during my study. My greatest thanks are reserved to my parents, brothers and my grandparents, for their unconditional love, support and encouragement in whole of my life.*

Last but not least, I deeply thank the Ministry of Higher Education and Scientific Research / Iraq (University of Wasit) via its representative, the Iraqi Cultural Attaché in London for their financial support of this research.

Ammar Al-Musawi

ABSTRACT

This thesis focuses on applying Artificial Intelligence (AI) methods for detecting, classifying and predicting the faults in induction motors in order to prevent any failures happening during their operation due to loading conditions. It is very important to monitor and detect any faults in the motor during its operation in order to alert the operators so that potential problems could be avoided. In this study, a new AI algorithm has been developed and applied to detect, classify and predict the induction motor faults at an early stage. This is based on a hybrid approach using the Bees Algorithm (BA) and Data Mining called Bee for Mining (B4M), which overcomes the drawbacks of current AI methods in achieving higher classification accuracy with reduced rule set generated from the training data. The proposed B4M algorithm has been implemented, tested and validated using the University of California at Irvine (UCI) dataset, and was compared with other well-known classifiers.

Later, the proposed B4M algorithm was applied in dealing with two most common faults, firstly, that of rotor (one rotor bar, four rotor bars and eight rotor bars), and secondly, bearing defects (inner race, outer race and ball bearing defects). In this research, three condition monitoring techniques involving thermal imaging, current and vibration signal processing have been used to monitor these faults. Further, features such as image metrics and Discrete Wavelet Transform (DWT) coefficients were extracted from the thermal images, and DWT coefficients from the current and vibration signals. Later, five-feature selection methods were applied in order to select the best features for defect classification. Finally, an improvement to the proposed B4M was made by producing a new hybrid classification algorithm by combining

The Development of New Artificial Intelligence based Hybrid Techniques Combining Bees Algorithm, Data Mining and Genetic Algorithm for Detection, Classification and Prediction of Faults in Induction Motors

Genetic Algorithm (GA) with B4M referred to as GA-B4M where the GA was used for feature selection. The new algorithms were successfully implemented on MATLAB and its performance was tested on real data and compared with other algorithms using the WEKA software.

The results obtained for the thermal image monitoring data showed 98.97% classification accuracy with a reduced rule set containing 10 rules for B4M while a 100% accuracy with a larger rule set of 63 and 72 rules were achieved by Decision Table and OneR classifiers respectively. For the current monitoring data, the classification accuracy fell to 79.62% with only 8 rules for B4M, while 79.20% with 837 rules was achieved by Random Tree. Similarly, for the vibration monitoring data the B4M achieved 80.05% with 7 rules in comparison with Naïve Bayes tree at 79.25% with 31 rules. Furthermore, the results achieved by the proposed hybrid approach GA-B4M on thermal imaging dataset also showed an overall improvement on the classification accuracy reaching 99.85% with 7 rules. Similarly, on the current and vibration dataset the GA-B4M obtained 79.98% with 16 rules and 98.74% with 7 rules respectively. This study has shown that the new proposed classification algorithms B4M and GA-B4M are able to detect, classify and predict the induction motor faults more reliably.

LIST OF ABBREVIATIONS AND NOMENCLATURES

LIST OF ABBREVIATION

μAnt-Miner	Classification algorithm
2D	Two Dimensions
A	Approximations coefficients
ABC	Artificial Bees Colony
AC	Alternative Current
ACO	Ant Colony Optimization
AI	Artificial Intelligence
ANF	Adaptive Neuro-Fuzzy
ANN	Artificial Neural Network
AntMiner_{mbc}	AntMiner multiple-based classifiers
ART-NN	Adaptive Resonance Theory Neural Network
ATM	Automated Teller Machine
B4M	Bee for Mining
BA	Bees Algorithm
BEE-Miner	Classification algorithm
BEMD	Bi-Dimensional Empirical Mode Decomposition
BPNN	Back Propagation Neural Network
C_Healthy	Healthy current dataset
C4.5	Classification algorithm
C5.0	Classification algorithm
CA	Classification Accuracy
cAnt-Miner	Classification algorithm
CART	Classification And Regression Tree
CFS	Correlation based Feature Selection
CN2	Classification algorithm
CT	Current Transformer
CWT	Continuous Wavelet Transform
D	Details coefficients

The Development of New Artificial Intelligence based Hybrid Techniques Combining Bees Algorithm, Data Mining and Genetic Algorithm for Detection, Classification and Prediction of Faults in Induction Motors

DAG-SVM	Directed Analytic Graph Support Vector Machine
DAQ	Data Acquisition
db	Daubechies (wavelet name)
DBN	Deep Belief Network
DC	Direct Current
DM	Data Mining
DT	Decision Tree
DWT	Discrete Wavelet Transform
FCFS	Fast Correlation-based Feature Selection
FCM	Fuzzy C-Mean clustering
FEM	Finite Element Model
FFT	Fast Fourier Transform
FK-NN	Fuzzy K-Nearest Neighbour
FL	Fuzzy Logic
FLIR	Forward Looking Infrared Radiometer (thermal cameras)
FN	False Negative
FP	False Positive
FPA	Focal Plane Array
Fuzzy-BP	Fuzzy Back Propagation
G₀	Low pass filter
GA	Genetic Algorithm
GDA	Generalized Discriminant Analysis
H₀	High pass filter
HH	High-High
HL	High-Low
HP	Horse Power
HSB	Hue-Saturation-Brightness
HSI	Hue-Saturation-Intensity
HSL	Hue-Saturation-Lightness/luminance
HSV	Hue-Saturation-Value
HT	Hilbert Transform
ICA	Independent Component Analysis

The Development of New Artificial Intelligence based Hybrid Techniques Combining Bees Algorithm, Data Mining and Genetic Algorithm for Detection, Classification and Prediction of Faults in Induction Motors

idwt	Inverse Discrete wavelet transform
IEEE	The Institute of Electrical and Electronics Engineers
IFO	Indirect Field Oriented
IM	Induction Motors
IR	Infrared
IRT	Inferred Thermograph
JPEG, MPEGZ, PNG	Image file extension
Jrip	Implantation of “Repeated Incremental Pruning to Produce Error Reduction (RIPPER)
KNN	K-Nearest Neighbours algorithm
LH	Low-High
LL	Low-Low
LP	Logic Programing
LV	Laser Vibrometer
MATLAB	Matrix Laboratory Software
MBF	Markov Blanket Filter
MCSA	Motor Current Signature Analysis
MLPNN	Multi-Layer Perceptron Neural Network
MMF	Magnetic Motive Field
MoASoID	Method of Areas Selection of Image Differences
MRA	Multiresolution analysis
MRAS	Model Reference Adaptive System
MSAF-RATIO15	Method of Selection of Amplitudes of Frequencies-Ratio 15%
NETA	InterNational Electrical Testing Association
NI LabVIEW	National instruments Laboratory Virtual Instrument Engineering Workbench software
PART	Classification algorithm
PCA	Principal Component Analysis
PDT	Power Decomposition Technique
PH	Phase

The Development of New Artificial Intelligence based Hybrid Techniques Combining Bees Algorithm, Data Mining and Genetic Algorithm for Detection, Classification and Prediction of Faults in Induction Motors

PPNN	Parzen Probabilistic Neural Network
PSD	Power Spectral Density
PSNR	Peak Signal to Noise Ratio
PSO	Particle Swarm Optimization
PSO/ACO	A hybrid Particle Swarm Optimisation/Ant Colony Optimisation algorithm for classification
PSP	Problem Solving and Planning
PSVM	Proximal Support Vector Machine
PV	Prediction Value
PWM	Pulse Width Modulation
RBF	Radial-Basis Function
REGAL	Classification algorithm
RGB	Red, Green and Blue
RMS	Root Mean Square
ROI	Regime of Interest
RPM	Rotation Per Minutes
RTD	Resistance Temperature Detectors
RVM	Relevant vector machine
SBS	Sequential Backward Selection
SFBS	Sequential Floating Backward Selection
SFFS	Sequential Floating Forward Selection
SFS	Sequential Forward Selection
SOM	Self-Organizing Map
STD	Standard Deviation
STFT	Short Time Fast Fourier Transform
SURF	Speeded-Up Robust Features selection method
SVM	Support Vector Machine
SWPT	Stationary Wavelet Packet Transform
THI_Healthy	Healthy thermal dataset
UCI	University of California at Irvine Machine Learning Repository
UMP	Unbalanced magnetic pull

The Development of New Artificial Intelligence based Hybrid Techniques Combining Bees Algorithm, Data Mining and Genetic Algorithm for Detection, Classification and Prediction of Faults in Induction Motors

V_Healthy	Healthy vibration dataset
VI_s	Virtual Instrumentation
WEKA	Waikato Environment for Knowledge Analysis machine learning software
WPT	Wavelet Pocket Transform
WSN	Wireless Sensor Network
WT	Wavelet Transform

LIST OF NOMENCLATURES

$\psi(t)$	Analysing wavelet
θ	Angle
C	Celsius
cm	Centimetre
ψ^*	Complex conjugate of ψ
G	Edge gradient
E	Efficiency
EMF	Electromotive Force
f_s	Fundamental frequency
Hz	Hertz
kW	Kilowatt
α	KNN-based classification error
K	Kurtosis
ω_e	Line frequency
I_m	Magnetizing current
S_x and S_y	Mask direction in image segmentation operators
μ	Mean
MSE	Mean Square Error
MW	Megawatt
$\mu\text{m/V}$	Micrometre/voltage
mm	Millimetre

The Development of New Artificial Intelligence based Hybrid Techniques Combining Bees Algorithm, Data Mining and Genetic Algorithm for Detection, Classification and Prediction of Faults in Induction Motors

mm/s/V	Millimetre/second/voltage
f_{min} and f_{max}	Minimum and maximum values of the attribute, which represent the range of the feature
NB	Naïve Bayes classifier
NN	Nearest Neighbour
ngh	Neighbourhood size for each selected patch (local search)
e	Number of elite bees
nep	Number of recruited bees for elite (e) sites
nsp	Number of recruited bees for other best (m-e) sites
n	Number of scout bees
m	Number of selected bees
N_f	Number of selected features
N	Number of turns in each phase winding
Ω	Ohm
f	Original feature values
P	Poles number
N_r	Rotor speed
rcp	Rule coverage percentage
rfv	Rule fitness value
a	Scale parameter
S	Skewness
S	Slip speed
f_e	Stator frequency
N_s	Synchronous speed
β	The coverage-weight
G_y and G_x	The derivatives of X and Y points
∇f	The gradient
N and M	The height and width of reference image respectively
W	The image
LB and UB	The Lower and Upper Bound
g	The noisy image

The Development of New Artificial Intelligence based Hybrid Techniques Combining Bees Algorithm, Data Mining and Genetic Algorithm for Detection, Classification and Prediction of Faults in Induction Motors

α	The quality-weight
$x(i,j)$	The reference image
r and c	The row and column coordinates
$y(i,j)$	The threshold image
b	Time parameter
N	Total value of the predicted class by the rules
TN	True Negative
TP	True Positive
k_1, k_2	Two different random numbers between 0 and 1
VA	Validation Accuracy
V	Voltage
rfv	Rule fitness value
rcp	Rule coverage percentage

TABLE OF CONTENT

DECLARATION	II
ACKNOWLEDGMENT.....	III
ABSTRACT	IV
LIST OF ABBREVIATIONS AND NOMENCLATURES	VI
TABLE OF CONTENT	XIII
LIST OF TABLES	XVIII
LIST OF FIGURES	XXI
LIST OF PUBLICATIONS	XXVII
CHAPTER 1: INTRODUCTION AND THESIS OBJECTIVES	1
1.1 Introduction.....	2
1.2 Research Aim and Objectives.....	4
1.2.1 Research Objectives	4
1.3 Thesis Outline	7
CHAPTER 2: INDUCTION MOTORS AND RELATED FAULTS	10
2.1 Induction Motor Structure.....	11
2.2 Induction Motor Principle.....	16
2.3 Faults of Induction Motors.....	18
2.3.1 Electrical Faults.....	19
2.3.2 Mechanical Faults	24
CHAPTER 3: LITRETURE REVIEW	29
3.1 Introduction.....	30
3.2 Thermal Monitoring.....	30

The Development of New Artificial Intelligence based Hybrid Techniques Combining Bees Algorithm, Data Mining and Genetic Algorithm for Detection, Classification and Prediction of Faults in Induction Motors

3.2.1 Thermal Protection based on Traditional Methods	32
3.3 Current Monitoring	35
3.3.1 Current Protection based on Traditional Methods	36
3.4 Vibration Monitoring	43
3.4.1 Vibration Protection based on Traditional Methods	43
3.5 Artificial Intelligence Techniques for Motor Faults Diagnosis	46
3.5.1 Thermal Monitoring based on AI.....	47
3.5.2 Current Monitoring based on AI	54
3.5.3 Vibration Monitoring based on AI	57
3.6 Common Softwares for IM Fault Detection	60
3.7 Data Mining based on Optimization Algorithm for Classification Task.....	61
3.7.1 Optimization Algorithms based on Data Mining for Classification Tasks	62
3.8 Previous Work Observations	65
CHAPTER 4: PROPOSED BEE FOR MINING (B4M)	69
4.1 The Bees Algorithm (BA).....	70
4.2 Proposed Bee for Mining (B4M)	71
4.2.1 Data Pre-Processing	73
4.2.2 Evaluation Function (fitness function).....	74
4.2.3 Rule Format.....	75
4.2.4 Rule Discovery and Extraction	75
4.2.5 Rule Pruning.....	77
4.2.6 Prediction Strategy	77
4.3 Testing of B4M Performance on selected UCI Datasets	80
4.3.1 Description of Datasets	80
4.3.2 The B4M Parameters.....	81
4.3.3 The B4M Test Results.....	82
4.4 Comparison of B4M with Other Algorithms	85

**The Development of New Artificial Intelligence based Hybrid Techniques
Combining Bees Algorithm, Data Mining and Genetic Algorithm for Detection,
Classification and Prediction of Faults in Induction Motors**

CHAPTER 5: PROPOSED METHODS FOR DATA PRE-PROCESSING AND FEATURE SELECTION	89
5.1 HSV Colour Model	90
5.2 Image Segmentation.....	92
5.2.1 Image Segmentation based on Edge Detection.....	93
5.3 Image Metrics	99
5.4 Wavelet Transform for Thermal Image, Current and Vibration Signals ...	104
5.4.1 Continuous Wavelet Transform (CWT).....	107
5.4.2 Discrete Wavelet Transform (DWT)	108
5.5 Feature Selection Methods.....	115
5.5.1 Sequential Forward Selection (SFS).....	117
5.5.2 Sequential Backward Selection (SBS).....	118
5.5.3 Sequential Floating Selection.....	119
CHAPTER 6: GENETIC ALGORITHM BASED FEATURE SELECTION FOR B4M (GA- B4M)	121
6.1 Introduction.....	122
6.2 Genetic Algorithm.....	123
6.3 GA Theoretical Background	126
6.4 GA based Feature Selection	128
CHAPTER 7: EXPERIMENTAL SETUP AND MEASUREMENTS.....	137
7.1 Introduction.....	138
7.2 Condition Monitoring Scheme.....	138
7.3 Test Rig Equipment's and Data Collection.....	141
7.4 Rig Setup.....	147
7.5 Fault Generation.....	147
7.6 Healthy Motor	149

The Development of New Artificial Intelligence based Hybrid Techniques Combining Bees Algorithm, Data Mining and Genetic Algorithm for Detection, Classification and Prediction of Faults in Induction Motors

7.7	Faulty Rotor	150
7.7.1	One Bar Rotor Fault	151
7.7.2	Four Bars Rotor Fault.....	153
7.7.3	Eight Bars Rotor faults.....	155
7.8	Faulty Bearings	158
7.8.1	Outer Race Bearing Fault.....	159
7.8.2	Ball Bearing Fault	160
7.8.3	Inner Race Bearing Fault	162
CHAPTER 8: DATA AND SIGNAL ANALYSIS.....		165
8.1	Thermal Image Analysis	166
8.2	Thermal Image Analysis for Rotor Faults.....	166
8.2.1	Thermal Image Analysis for Four Bars Rotor Fault	167
8.2.2	Thermal Image Wavelet Analysis for Rotor Bars Fault.....	176
8.3	Current and Vibration Signals Analysis based on DWT	183
8.3.1	Current Signal Analysis	186
8.3.2	Vibration Signal Analysis	192
CHAPTER 9: RESULTS AND DISCUSSION		197
9.1	B4M Classification based on Thermal Image for Fault Detection	198
9.1.1	Feature Extraction	198
9.1.2	Feature Selection.....	201
9.1.3	Classification Results	202
9.1.4	Comparison of B4M Performance with other Classification Algorithms	206
9.2	B4M Classification based on Current Signal for Fault Detection	210
9.2.1	Feature Extraction	210
9.2.2	Feature Selection.....	214
9.2.3	Classification Results	215
9.2.4	Comparison of B4M Performance with other Classification Algorithms.....	220

The Development of New Artificial Intelligence based Hybrid Techniques Combining Bees Algorithm, Data Mining and Genetic Algorithm for Detection, Classification and Prediction of Faults in Induction Motors

9.3	B4M Classification based on Vibration Signal for Fault Detection	223
9.3.1	Feature Extraction	223
9.3.2	Feature Selection	226
9.3.3	Classification Results	227
9.3.4	Comparison of B4M Performance with other Classification Algorithms	231
9.4	GA-B4M	233
9.4.1	Classification Results	234
9.5	Classification Results for Testing Dataset based on B4M	237
9.6	Classification Results for Testing Dataset based on GA-B4M	239
CHAPTER 10: CONCLUSIONS AND FUTURE WORK		242
10.1	Overview	243
10.2	Conclusions	244
10.3	Future Work	249
REFERENCES		251
APPENDIX A - THERMAL IMAGE ANALYSIS		271
APPENDIX B - CURRENT AND VIBRATION SIGNALS ANALYSIS		280
APPENDIX C – MATLAB CODE		286

LIST OF TABLES

CHAPTER 2

Table 2-1: Common faults in induction motors.28

CHAPTER 3

Table 3-1: Sources of abnormal temperature and causes.....30

Table 3-2: Some previous research experimental setup for induction motor faults
detection based on thermography.....51

Table 3-3: Common differences between the vibration and current signals.....67

CHAPTER 4

Table 4-1: BA parameters.70

Table 4-2: classification rule format.75

Table 4-3: Five selected UCI dataset characteristics.81

Table 4-4: B4M parameters.81

Table 4-5: P-value for B4M parameters based on T-test.82

Table 4-6: Classification and Validation Accuracy with 10-fold cross-validation using
B4M.....84

Table 4-7: Comparison the results of B4M with other classification algorithms.86

CHAPTER 5

Table 5-1: HSV colour space distribution.....90

Table 5-2: Image neighborhood (center pixel).....93

Table 5-3: Masks for S_x direction.....94

Table 5-4: Masks for S_y direction.....94

Table 5-5: Masks for S_x direction.....94

Table 5-6: Masks for S_y direction.....94

Table 5-7: Masks for S_x direction in Robert's operators.....95

Table 5-8: Masks for S_y direction in Robert's operators.....95

Table 5-9: Masks for G_x direction in LoG.....98

The Development of New Artificial Intelligence based Hybrid Techniques Combining Bees Algorithm, Data Mining and Genetic Algorithm for Detection, Classification and Prediction of Faults in Induction Motors

Table 5-10: Masks for G_y direction in LoG.....	98
Table 5-11: Comparison of the performance of CWT and DWT.....	111
Table 5-12: Taxonomy of feature selection algorithms.....	116

CHAPTER 6

Table 6-1: Comparative terminology to human genetics.....	129
Table 6-2: GA parameters values.....	131

CHAPTER 7

Table 7-1: Current transformer specification.....	143
Table 7-2: Bearing specifications.....	158

CHAPTER 8

Table 8-1: Frequency levels of wavelet coefficients.....	186
---	-----

CHAPTER 9

Table 9-1: Sample of thermal image dataset features.....	199
Table 9-2: The selected features for the thermal image dataset.....	202
Table 9-3: Thermal image dataset description.....	203
Table 9-4: The proposed B4M classification results.....	204
Table 9-5: Confusion matrix of the proposed B4M for the thermal image dataset.....	205
Table 9-6: Sample of current signal dataset features.....	212
Table 9-7: The selected features for the current signal dataset.....	214
Table 9-8: Current signal dataset description.....	215
Table 9-9: The proposed B4M classification results.....	216
Table 9-10: Confusion matrix of the proposed B4M for the current signal dataset.....	218
Table 9-11: Sample of vibration signal dataset features.....	224
Table 9-12: The selected features for the vibration signal dataset.....	226
Table 9-13: Vibration signal dataset description.....	227
Table 9-14: The proposed B4M classification results.....	228

**The Development of New Artificial Intelligence based Hybrid Techniques
Combining Bees Algorithm, Data Mining and Genetic Algorithm for Detection,
Classification and Prediction of Faults in Induction Motors**

Table 9-15: Confusion matrix of the proposed B4M for the vibration signal dataset.
.....229

Table 9-16: The selected features for all the condition monitoring dataset based on
GA.....234

LIST OF FIGURES

CHAPTER 2

Figure 2-1: Parts of induction motor [13].	11
Figure 2-2: Induction motor wound rotor [14].	12
Figure 2-3: Induction motor squirrel cage rotor [19].	13
Figure 2-4: Induction motor rotor and stator magnetic circuit [18].	14
Figure 2-5: Block diagram of IM faults [21].	18
Figure 2-6: Probability of fault-occurrence in induction motors [21].	18
Figure 2-7: Squirrel cage of IM broken rotor bar [23].	19
Figure 2-8: Different stator windings faults caused by insulation damage [30].	23
Figure 2-9: Bearing faults [33].	25
Figure 2-10: Different types of IM eccentricity faults [37].	26
Figure 2-11: Misalignment types [38].	26

CHAPTER 3

Figure 3-1: Sample of thermal signature for induction motor (during and after starting)[45].	31
Figure 3-2: Flow chart for motor current measurement [37].	36
Figure 3-3: Basic MCSA equipment system [58].	36
Figure 3-4: AI flow chart for IM fault diagnosis [86].	47

CHAPTER 4

Figure 4-1: Basic BA flowchart.	71
Figure 4-2: Proposed B4M flowchart.	73
Figure 4-3: B4M rule discovery flowchart.	76
Figure 4-4: Classification procedure of proposed B4M.	79
Figure 4-5: Comparison of classification accuracy (X - different methods; Y - % classification accuracy) achieved by B4M with other methods for five UCI datasets.	85
Figure 4-6: Comparison of classification accuracy (%) for five UCI datasets.	88

Figure 4-7: Compression of average rules number for five UCI datasets.88

CHAPTER 5

Figure 5-1: How to detect the edge by non-maximum suppression.97

Figure 5-2: Thermal image processing diagram. 103

Figure 5-3: Wavelet families (a) Harr, (b) Daubechies, (c) Coiflet, (d) Symlet, 105

Figure 5-4: DWT decomposition signal to approximation and detail using filters
[181]. 109

Figure 5-5: DWT two channel filters [185]. 109

Figure 5-6: Filter bank structure of the DWT analysis [185]. 110

Figure 5-7: Filter bank structure of the reverse DWT synthesis [185]. 110

Figure 5-8: Daubechies wavelet families [189]. 112

Figure 5-9: Procedure for thermal image analysis in MATLAB using wavelet toolbox.
..... 113

Figure 5-10: Current and vibration signals processing procedure. 114

CHAPTER 6

Figure 6-1: Population in GA 124

Figure 6-2: Crossover structure..... 125

Figure 6-3: Mutation changing. 125

Figure 6-4: GA flow chart..... 126

Figure 6-5: GA based feature selection. 130

Figure 6-6: Pseudo code for creation the initial population..... 131

Figure 6-7: GA fitness function based on the KNN..... 133

CHAPTER 7

Figure 7-1: Condition monitoring scheme. 139

Figure 7-2: Research framework for motor fault classification..... 140

Figure 7-3: Induction motor specification. 141

Figure 7-4: Dynamometer parts: a- Electric motor dynamometer, b- Dynamometer
sensor (R.P.M., torque, power, and torque rise), c- Dynamometer barker
control. 142

The Development of New Artificial Intelligence based Hybrid Techniques Combining Bees Algorithm, Data Mining and Genetic Algorithm for Detection, Classification and Prediction of Faults in Induction Motors

Figure 7-5: Current transformer setup for collecting the stator current.....	143
Figure 7-6: National Instrument Data Acquisition card (NI DAQ USB-6211 16 AI multifunction I/O).....	144
Figure 7-7: LabView circuit for collecting the stator current data.	144
Figure 7-8: Thermal image specifications.	145
Figure 7-9: Laser vibrometer: a: Front panel, b: Optical head and c: Oscilloscope.	146
Figure 7-10: The experimental test rig.....	147
Figure 7-11: IM faults scheme.....	148
Figure 7-12: Healthy conditions.	149
Figure 7-13: Thermal image for healthy motor, a: No load, b: 50% load c: 100% load.	149
Figure 7-14: The current and vibration signals of healthy IM, a, b, and c represent the current signals at (a) no load, (b) 50% load and (c) 100% load respectively, while d, e and f represent the vibration signal at different load conditions.....	150
Figure 7-15: IM circuit diagram.....	151
Figure 7-16: One bar fault has been created artificially in the experiment (left figure) and description of the rotor cage-related faults in circuit diagram (right figure).....	152
Figure 7-17: Thermal images of one bar rotor fault: a: No load, b: 50% load and c: 100% load.....	152
Figure 7-18: The current and vibration signals for one bar fault, a, b, and c represent the three-phase current signal at (a) no load, (b) 50% load and (c) 100% load respectively, while d, e and f represent the vibration signal at different load conditions.	153
Figure 7-19: Artificially four bars fault have created in the experiment(left figure) and description of the rotor cage-related faults in circuit diagram (right figure).....	154
Figure 7-20: Thermal images of four rotor bars fault: a: No load, b: 50% load and c: 100% load.	154

Figure 7-21: The current and vibration signals for four bars rotor faults, a, b, and c represent the three phase current signal at (a) no load, (b) 50% load and (c) 100% load respectively, while d, e and f represent the vibration signal at different load conditions. 155

Figure 7-22: IM rotor circuit diagram with eight bars rotor fault and eight rotor bar faults has been created artificially in the experiment. 156

Figure 7-23: Thermal images of eight rotor bars fault: a: No load, b: 50% load and c: 100% load. 157

Figure 7-24: The current and vibration signals for eight rotor bars fault, a, b, and c represent the three-phase current signal at (a) no load, (b) 50% load and (c) 100% load respectively, while d, e and f represent the vibration signal at different load conditions. 157

Figure 7-25: Bearing with outer race defect. 159

Figure 7-26: Thermal images of outer race bearing defect: a: No load, b: 50% load, and c: 100% load..... 159

Figure 7-27: The current and vibration signals for outer race bearing defect, a, b, and c represent the three phase current signal at (a) no load, (b) 50% load and (c) 100% load respectively, while d, e and f represent the vibration signal at different load conditions. 160

Figure 7-28: Bearing with ball defect. 161

Figure 7-29: Thermal images of ball bearing defect: a: No load, b: 50% load and c: 100% load. 161

Figure 7-30: The current and vibration signals for ball bearing defect, a, b, and c represent the three-phase current signal at (a) no load, (b) 50% load and (c) 100% load respectively, while d, e and f represent the vibration signal at different load conditions. 162

Figure 7-31: Bearing with inner race defect. 162

Figure 7-32: Thermal images of inner race defect: a: No load, b: 50% load and c: 100% load. 163

Figure 7-33: The current and vibration signals for inner race defect, a, b, and c represent the three-phase current signal at (a) no load, (b) 50% load and

(c) 100% load respectively, while d, e and f represent the vibration signal at different load conditions. 163

CHAPTER 8

Figure 8-1: Thermal image analysis for four bars rotor fault with no load condition a) original image, b) HSV image, c) Hue image, d) Saturation image, e) Value image, f) Sobel image for Hue, g) Prewitt image for Hue, h) Roberts image for Hue, i) Canny image for Hue, j) LoG image for Hue, k) Otsu image for Hue. 169

Figure 8-2: Thermal image analysis for four bars rotor fault with 50% load condition a) Original image, b) HSV image, c) Hue image, d) Saturation image, e) Value image, f) Sobel image for Hue, g) Prewitt image for Hue, h) Roberts image for Hue, i) canny image for Hue, j) LoG image for Hue, k) Otsu image for Hue. 171

Figure 8-3: Thermal image analysis for four bars fault with 100% load condition a) Original image, b) HSV image, c) Hue image, d) Saturation image, e) Value image, f) Sobel image for Hue, g) Prewitt image for Hue, h) Roberts image for Hue, i) Canny image for Hue, j) LoG image for Hue, k) Otsu image for Hue. 173

Figure 8-4: a) The MSE values, and b) The PSNR values for three different load conditions..... 174

Figure 8-5: a) The variance value, and b) The mean values for different load conditions..... 174

Figure 8-6: a) The thermal image Skew values and b) Thermal image Kurtosis values for different load conditions. 175

Figure 8-7: Thermal image wavelet analysis for four bars rotor fault with no load condition. 177

Figure 8-8: Thermal image wavelet analysis for four bars rotor faults with 50% load condition. 178

Figure 8-9: Thermal image wavelet analysis for four bars rotor faults with 100% load condition. 179

Figure 8-10: Approximation coefficients level (a1) for four bars rotor fault at different load conditions. 180

Figure 8-11: Approximation coefficients level (a2) for four bars rotor fault at different load conditions. 181

Figure 8-12: Approximation coefficients level a3 for four bars rotor fault at different load conditions. 182

Figure 8-13: Wavelet analysis for healthy current signal with three different load conditions a) No-load, b) 50 % load, c) 100% load..... 187

Figure 8-14: Wavelet analysis for four bars faulty rotor based on current signal for with three different load conditions a) No-load, b) 50 % load, c) 100% load..... 189

Figure 8-15: The d5 and d3 wavelet analysis coefficients for healthy and faulty rotor based on the current signal with no load condition. 190

Figure 8-16: The d5 and d2 wavelet coefficients for healthy and faulty (four bars) rotor current signal with 50% load condition. 191

Figure 8-17: The d5 and d3 wavelet coefficients for healthy and faulty rotor (four bars) current signal with 100% load condition. 191

Figure 8-18: Wavelet analysis for healthy vibration signal of induction motor with three different load conditions a) No-load, b) 50% load and c) 100% load. 193

Figure 8-19: Wavelet analysis for faulty rotor (four bars) vibration signal of with three different load conditions a) No-load, b) 50% load and c) 100% load.194

Figure 8-20: The d5 and d3 wavelet coefficients for healthy and faulty rotor (four bars) based on the vibration signal with no-load condition. 195

Figure 8-21: The d5 and d2 wavelet coefficients for healthy and faulty rotor (four bars) based on the vibration signal with 50% load condition. 195

Figure 8-22: The d5 and d3 wavelet coefficients for healthy and faulty rotor (four bars) based on the vibration signal with 100% load condition. 196

CHAPTER 9

Figure 9-1: The proposed B4M classification accuracy and number of rules based on thermal image dataset.....205

Figure 9-2: Comparison of the classification accuracy for different feature selection and classification algorithms based on the thermal image dataset.....208

Figure 9-3: Comparison of the number of rules for different feature selection and classification algorithms based on the thermal image dataset.....209

Figure 9-4: Comparison of the classification accuracy for different feature selection and classification algorithms based on current signal dataset.....221

Figure 9-5: Comparison of the number of rules for different feature selection and classification algorithms based on current signal dataset.....222

Figure 9-6: Comparison of the classification accuracy for different feature selection and classification algorithms based on the vibration signal dataset.....232

Figure 9-7: Comparison of the number of rules for different feature selection and classification methods based on the vibration signal dataset.....233

Figure 9-8: The comparison of classification and number of rules for different classification methods based on the thermal image dataset.....235

Figure 9-9: The comparison of classification accuracy and number of rules for different classification methods based on the current signal dataset. ...236

Figure 9-10: The comparison of classification accuracy and number of rules for different classification algorithms based on the vibration signal dataset.236

Figure 9-11: Classification accuracy for test dataset of thermal image.....238

Figure 9-12: Classification accuracy for test dataset of current signal.....238

Figure 9-13: Classification accuracy for test dataset of vibration signal.....239

Figure 9-14: Classification accuracy of thermal image test dataset based on GA-B4M.240

Figure 9-15: Classification accuracy of current test dataset based on GA-B4M....241

Figure 9-16: Classification accuracy of vibration test dataset based on GA-B4M.241

LIST OF PUBLICATIONS

- [1] M. S. Packianather, A. K. Al-Musawi, and F. Anayi, "Bee for mining (B4M) – A novel rule discovery method using the Bees algorithm with quality-weight and coverage-weight," Proc. Inst. Mech. Eng., 2019.
- [2] A. K. Al-Musawi, F. Anayi, and M. S. Packianather, "Three-Phase Induction Motor Faults Detection based on Thermal Image Segmentation" has been submitted to the Infrared Physics and Technology.

CHAPTER 1

INTRODUCTION AND THESIS OBJECTIVES

“This chapter describes the main purposes of maintenance strategies. It also introduces condition monitoring and describes the different types of condition monitoring systems and techniques. Finally, the research aim, objectives and the thesis structure have been presented”.

1.1 Introduction

The induction machine condition monitoring plays a vital role in the industrial facilities as it guarantees both the reliability and low cost operation [1]. Condition monitoring gives an opportunity to maintain the machine at early stage or before any possible disastrous accident or any dangerous damage. Furthermore, it allows having a schedule or planned service for the technician, which will decrease the possibility of production losses. Induction motors (IM) have been widely used in most of industrial applications due to their robustness, low cost and operation (operate with an easily available power supply). However, IM may fail far sooner than its designed lifetime because of the installation issues, duties, and operational environments. Recently, the approach of “run-to-fail” has been rejected for most manufacturing process and operations. For that reason, the condition monitoring has been required as an alternative system to protect the motor based on the motor data collection and analysis during its operation, which makes it acceptable and more desirable due to its capability of detecting the motor faults in early stage [2]. Moreover, most of the companies and industries are searching/looking for the best condition monitoring methods in order to reduce the damage to the environments or the maintenance cost, which may mitigate any possible injuries to the operators or technicians. There are three essential maintenance strategies as follows [3], [4]:

- a) **Preventive maintenance (time-based-maintenance):** the machine are thoroughly inspected and tested at a set of intervals, and any necessary maintenance has to be carried out to remedy faults present within the system.

- b) **Breakdown maintenance:** the machines are run until they completely fail, this kind of maintenance is considered as a very expensive in terms of machine damage and lost output, or it may also lead to dangerous occurrences.
- c) **Predictive maintenance:** this strategy requires a continuous monitoring in order to detect and diagnose any defects happened to the machine. If the defects have been detected, the maintenance must be planned and executed as soon as possible.

The main objectives of these maintenance are assisting the machine for productivity improvements, extend the machine life, minimise the number of maintenance and replacements routine and producing a high quality products [1], [5]. In the induction motors, faults could be occur in the rotor, bearing, stator or any other peripheral devices that are connected to the induction motor. These faults have been broadly classified into broken rotor bars, bearing faults, eccentricity, gearbox failure and many others. In other word, the mentioned faults may produce one or more symptoms such as unbalanced line current and voltages, excessive heating, torque pulsations, vibration and noise and other symptoms.

The recent development in the computer software and electrical equipment based on the Artificial Intelligence (AI) systems (machine learning) attract the attention of the electrical engineers to launch an extensive researches to apply the AI techniques for motor fault detection and diagnosis [6]. The AI techniques such as Artificial Neural Network (ANN), Fuzzy Logic (FL), Genetic Algorithm (GA) and many others have been applied to induction motor faults detection and diagnosis. These techniques have used association, reasoning and decision-making process as would the human brain in solving diagnosis problems [7].

1.2 Research Aim and Objectives

The aim of this research is to investigate and recommend a new condition monitoring technique based on three common approaches, which are thermal image, motor current signal analysis and vibration signal analysis. The thermal image has been captured using FILR thermal camera, the motor current signals have been collected using current transformers and the vibration signals have been collected using laser vibrometer.

Specifically, the aim of this research is:

- To develop and improve a new artificial intelligence technique based on Bees Algorithm (optimization algorithm), data mining and Genetic Algorithm to be used for detecting, classifying and predicting the motor faults at an early stage.

1.2.1 Research Objectives

In the last decades, there has been a huge amount of research into creating a new condition monitoring technique for electrical machines based on AI [8]–[10]. The research and development of designing a newer and alternative diagnostic system is continuous. However, since condition monitoring and fault diagnosis system should always suite new, the condition monitoring based on the AI has been developed rapidly to cover all the induction motor situations under any circumstances. This continuous development and research have argued by the fact that there is no specific system/technique could be considered generally or the best for all existing applications, since an operator must treat each motor drive as a unique entity. In this respect, the fundamental causes, mechanical load characteristics, potential failure

modes and operational conditions have to be carefully taken into consideration when designing a monitoring system for specific applications [11].

Additionally, all previous studies that are carried out in the field of condition monitoring show that there have been many challenges and opportunities for engineers and researchers to focus on. Several solutions and recommendations concerning the condition monitoring methods have been given in this area, generally depending on the machine type, operating conditions (loading), size, cost constraints, available instruments etc. Besides, several fields of technology and science such as thermal, electrical, mechanical and sometime chemical engineering should be considered and combined whenever possible, in order to allow analysts to correlate different aspects of each technology to troubleshoot symptoms and determine a course of action to avert failures. This is also a stringent requirement when aiming to build or design a competitive condition monitoring system.

In this research, three computational tools would be extensively used. These are NI LabVIEW, MATLAB and WEKA software's. NI LabVIEW is systems engineering software for applications that require test, measurements and control with rapid access to hardware and data insight. MATLAB is a very ubiquitous scientific and technical computing tool that has found wide applicability. WEKA is a machine learning environment created by University of Waikato. This research was oriented to achieve the following objectives:

In terms of machine learning

- 1- To develop a new innovative, non-intrusive, accurate, reliable and simple artificial intelligence technique based on Bees Algorithm (optimization

algorithm) and data mining approach, called Bee for Mining (B4M) that is able to detect and diagnose the motor faults in an early stage.

- 2- To validate the new proposed classification algorithm based on the University of California at Irvine Machine Learning Repository (UCI machine learning datasets).
- 3- To compare the capability of the new algorithm with other well-known classification algorithms based on the UCI machine-learning datasets.

In terms of condition monitoring

- 1- To explore induction motor failures modes and understand condition-monitoring techniques.
- 2- To design and construct a test rig with the associated instrumentation for induction motor faults to collect the real data from the induction motor with seven faulty cases and three different condition monitoring technique, thermal image, motor current signature analysis and vibration signal.
- 3- Apply different feature extraction and feature selection methods with purpose of extracting and selecting the best fault information from the raw images and signals for all three condition-monitoring techniques.
- 4- To apply the new proposed classification algorithm that are relying on the Bees Algorithm and Data Mining approaches (B4M) in the suggested condition monitoring techniques.

- 5- To compare the capability of the new algorithm with other well-known classification algorithms based on the thermal image, current and vibration signals.

In terms of the machine learning hybrid system

- 1- To build a new hybrid classification system based on the Genetic Algorithm and the proposed classification algorithm (B4M), which is called (GA-B4M), in order to make the classification system more robust and accurate for classifying the motor faults correctly.
- 2- To apply the new hybrid system to the seven faulty cases and three suggested condition-monitoring techniques.

1.3 Thesis Outline

- **Chapter 1: Introduction and Thesis Objectives.** It presents the research objectives and the thesis outline.
- **Chapter 2: Induction Motors and Related Faults.** Since the induction motor is aimed to study in this research, this chapter introduces background information about the induction motor such as induction motor structure and principle. It also introduces the most common types of electrical and mechanical faults, because they are the problems that are aimed to be solved.
- **Chapter 3: Literature Review.** The previous related work on condition monitoring is presented in this chapter.

- **Chapter 4: Proposed Bee for Mining (B4M).** In this chapter, the combination of the Bees Algorithm and Data Mining have been described in detail in order to produce the proposed Bee for Mining (B4M).
- **Chapter 5: Proposed Methods for Data Pre-Processing and Feature Selection.** In this chapter, the proposed methods for pre-processing the induction motor dataset have been explained for all condition monitoring approach, thermal image, current and vibration signals.
- **Chapter 6: Genetic Algorithm based Feature Selection for B4M (GA-B4M).** This chapter explains how the Genetic Algorithm has been used as feature selection method and how it works theoretically.
- **Chapter 7: Experimental Setup and Measurements.** The practical work of this research starts in this chapter. It shows what equipment was used in experiments, how the induction motor test rig was built, and the procedure of the experiments, how the required measurements were taken and how the acquired data were stored in order to be proceeded in the next chapter. It also shows the induction motor healthy and the faulty signals and how the faults have been generated.
- **Chapter 8: Data and Signal Analysis.** It explains how to analyse the motor data and signals based on the proposed methods that are explained in previous chapters. It also shows the signal analysis for all three condition monitoring approaches (thermal image, current and vibration condition monitoring).
- **Chapter 9: Results and Discussion.** The results that were obtained from the induction motor conditions (healthy and faulty) are discussed using MATLAB

and WEKA software's. Then, the results of the other classification algorithms have been discussed and compared with the proposed technique.

- **Chapter 10: Conclusions and Future Work.** All the discussions about the results of testing the proposed techniques in both simulation and practical work are concluded in this chapter. It also introduces some recommendations for future work.

CHAPTER 2

INDUCTION MOTORS AND RELATED FAULTS

“In this chapter, the concept of induction motor and a brief review of what are the main types of induction machine faults are presented. In order to cover the understanding of the induction motors, the induction motor structure and its fundamental are introduced first. Then brief review of induction motors symptoms and mechanisms of the electrical and mechanical faults are presented”.

2.1 Induction Motor Structure

Induction Motors are also known as asynchronous motors and are typically Alternative Current (AC) electric motors. In induction motors, electric current is required to generate the torque to drive the motor [12]. It has been considered as asynchronous machine since they operate at speed lower than the synchronous speed. Worth noting, asynchronous speed is the speed of rotating magnetic field, which depends upon the machine pole numbers and the supplied frequency. The driving torque is achieved by electromagnetic induction that is obtained from the electromagnetic field of the stator coils. IM contains magnetic circuits, which are connected to two electric circuit, these circuits are:

- a) Magnetic circuit, which is responsible for carrying the magnetic flux that is made of laminated magnetic material generally steel.
- b) Electrical circuit, which is normally made of insulated aluminium or copper to carry the current.

These two circuits are very important for rotating the main part of the induction motor, which is rotating part (rotor) as illustrated in figure 2-1.

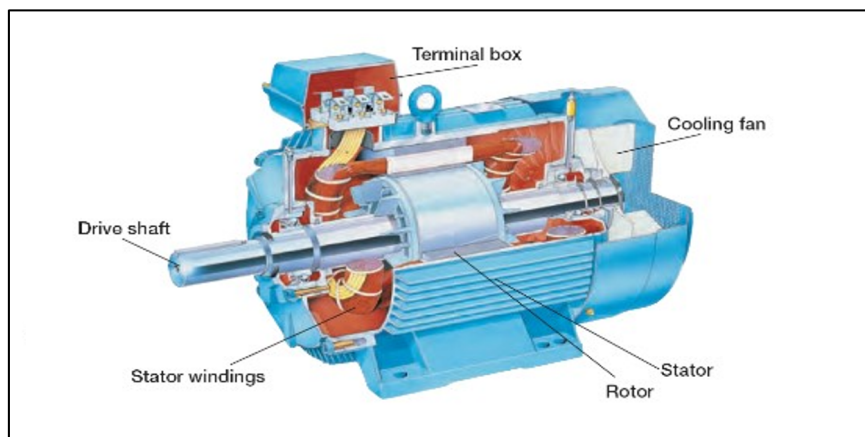


Figure 2-1: Parts of induction motor [13].

Chapter 2: Induction Motor and Related Faults

A series of thin aluminium pieces permanently attached to a laminated cylinder make up the rotor structure. The rotor pieces are attached in a horizontal fashion and parallel to the rotor shaft. Towards the edge of the rotor, aluminium plates are intertwined with a shorting ring. There are two types of rotor: wound and squirrel cage rotors. The wound rotor of an induction motor is similar to a three-phase stator winding because it carries a poly-phase winding. In addition, three isolated slip rings are connected to a rotor winding which are mounted on rotor shaft. In this type of rotor (wound rotor) as shown in figure 2-2, an external changeable resistance is connected to the slip rings in order to limit the rotor heating and starting current.

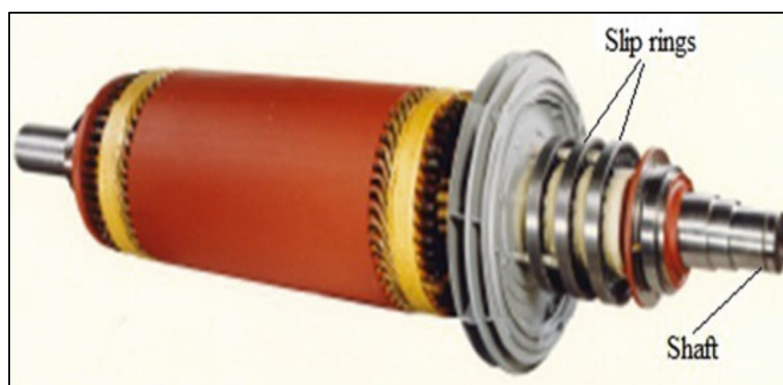


Figure 2-2: Induction motor wound rotor [14].

During starting up, the inserted resistance to the wound rotor produces less starting current with high starting torque than the squirrel cage rotor [13]. So far, wound rotor has been concerned; the structure and functions of squirrel cage rotor will be explained. It consists of parallel slots with a laminated cylinder core in order to carry rotor conductor, no wires are connected but it has a thick bars of aluminium or copper. Furthermore, it has two end rings that are braced or welded, and these ends are short circuit. For that reason, it is impossible to connect or add any external variable resistance. The shaft is usually not parallel to the rotor bars, it is a little bit skewed, as shown in figure 2-3.

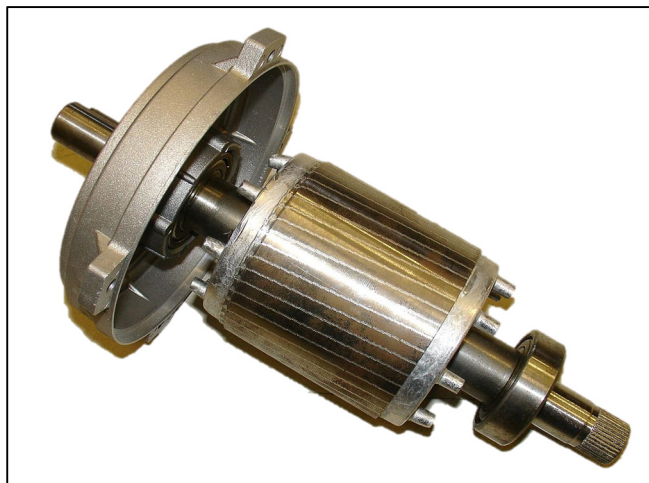


Figure 2-3: Induction motor squirrel cage rotor [19].

The squirrel cage rotor is different from the wound rotor in a number of aspects. The main difference is that the squirrel cage rotor is economical, simpler and more rugged than the wound rotor. Additionally, if a constant frequency and constant voltage connected to the squirrel cage rotor, it produces a constant speed. Thus, it is compatible with stationary speed drive system [13][14]. Otherwise, many industries required adjustable speed or various speed for products applications. In addition, it is important to ask why squirrel cage induction motors are preferred in most industries than DC motors.

In terms of Direct Current (DC) motor has been used in order to obtain adjustable range of speeds. Nevertheless, because of the DC motors are very expensive and the brushes and commutators need to be serviced frequently, the squirrel cage induction motors are preferred in most industries because as mentioned above, rugged, cheap and no need for commutators. Recently, the squirrel cage motors are used in high and low-performance applications owing to its versatility.

Moving on now to consider the stator, it is fabricated in such a way that windings of low resistance (copper) wire coils are permanently attached to the motor body/frame.

Chapter 2: Induction Motor and Related Faults

Whenever a current and high potential is applied to the stationary runs/coils, a strong magnetic field is induced in the stator coils [15]. The stator windings are arranged in a pattern that the magnetic field appears to synchronously rotate around the motor housing [16]. Through the electromagnetic induction, the power will transfer from one part to other. When stator windings are powered from a three-phase AC source, a rotating magnetic field is induced, then it converts electrical energy into mechanical energy [17].

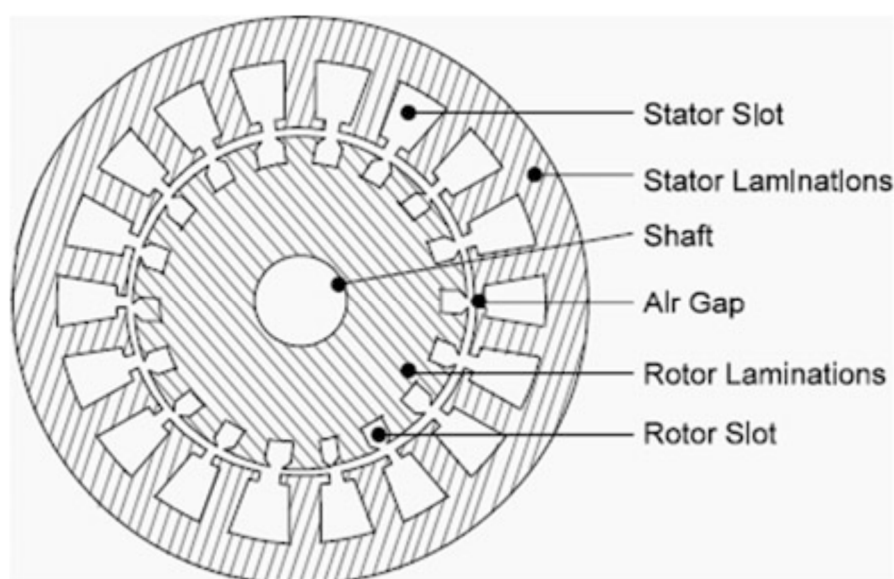


Figure 2-4: Induction motor rotor and stator magnetic circuit [18].

Induction motors operate under a complex system of current, voltage and magnetic field in a synchronized manner to induce the rotary effect. For the case of three-phase AC induction motors, however, no excitation is required for it to start. Instead, the motor is a self-starting device [15]. In between the rotor and stator, an air gap/space allows free movement for the rotor during its operation [18] as illustrated in figure 2-4 above. In effect, a synchronous speed is established in the stator. An electromotive force (EMF) is induced in the rotor bars by the magnetic field produced in the stator windings. Afterwards, a current is generated in the rotor and a separate magnetic field is generated within the rotor windings, whose polarity is opposite to that of the stator

windings. This current is created due to the relative speed between rotor conductor and the rotating flux. Consequently, a magnetic flux generate a force that pulls the field in the rotor, thereby inducing a turning effect on the rotor. As described in Lenz's Law, the rotor spins in a similar direction in order to reduce the causing effect that is the relative speed. The resultant rotation is in accordance with Faraday's law of electromagnetic induction "EMF is induced in a circuit due to changing magnetic flux linkage experienced within the circuitry."

In addition to the above two main parts of induction motor, there are other parts which are:

- a) **Bearings:** two bearings have been used for supporting the rotor at each end in order to rotate the shaft.
- b) **End flanges:** two flanges are placed in both ends of induction motor for supporting the bearings, and
- c) **Shaft:** is used for transmitting the generated torque to load.

Another significant aspect on induction motors is that these motors are generally suitable for continuous speed operations. Furthermore, compared to other alternatives, induction motors are cheaper to acquire and maintain. While designing induction motor, operational features can be examined using several calculations described in the subsequent subsections. By applying these calculations, an electrical engineer will be in a position to select a motor that best suits a particular job. The section below describes briefly the IM principles.

2.2 Induction Motor Principle

The magnetic field distribution between the air gap and the rotation is one of the most fundamental concept. Because of non-ideal winding distribution, the effect of the space harmonic and slots have been neglected. The sinusoidal current in the three-phase induction machine is impressed on the stator winding, as it is given below [19]:

$$\begin{aligned}i_a &= I_m \cos \omega_e t \\i_b &= I_m \cos(\omega_e t - 120^\circ) \\i_c &= I_m \cos(\omega_e t + 120^\circ)\end{aligned}\tag{2-1}$$

Where: I_m : maximum current, ω_e : line frequency.

In order to produce Magnetic Motive Field (MMF) wave and distribute it sinusoidally, each phase will work individually to produce the MMF, which pulses about the X-axis and Y-axis. The expressions of instantaneous MMF at spatial angle (θ) are given below [19]:

$$\begin{aligned}F_a(\theta) &= Ni_a \cos \theta \\F_b(\theta) &= Ni_b \cos\left(\theta - \frac{2\pi}{3}\right) \\F_c(\theta) &= Ni_c \cos\left(\theta + \frac{2\pi}{3}\right)\end{aligned}\tag{2-2}$$

Where: N : number of turns in each phase winding, θ : spatial angle.

The MMF are:

$$\begin{aligned}F(\theta) &= F_a(\theta) + F_b(\theta) + F_c(\theta) \\F(\theta) &= Ni_a \cos \theta + Ni_b \cos\left(\theta - \frac{2\pi}{3}\right) + Ni_c \cos\left(\theta + \frac{2\pi}{3}\right)\end{aligned}\tag{2-3}$$

The MMF has been distributed sinusoidally, which rotates the air gap at frequency (ω_e). Furthermore, for two poles induction motors the current variation has one

revolution per cycle, which is created by $F(\theta, t)$. Thus, the rotational speed for P-pole motor can be as given below:

$$f_e = \frac{\omega_e}{2\pi} \quad , \quad N_s = \frac{120f_e}{P} \quad (2-4)$$

Where: N_s : synchronous speed (RPM), f_e : stator frequency (Hz), P : number of pole pairs.

The motor synchronous speed indicates the speed of rotation for stator magnetic field. N_s is a function of pole number and the frequency of the power source in the motor as explained above in the equation (2-4). The rotor conductors are subjected to rotating magnetic field when the induction motor rotor is stationary and inducing the short circuit rotor current to rotate at the same rotor frequency. Hence, the interactions between the rotor MMF and the air gap flux will produce the torque. The difference between the rotor speed and synchronous (stator) field speed gives the slip speed. The slip speed of an induction motor is calculated and expressed as a fraction of the synchronous speed. Slip speed is an important parameter in the motor because without slip, the induction motor will produce a torque equivalent to zero. The motor slip equation is expressed as follows:

$$S = \frac{N_s - N_r}{N_s} \quad (2-5)$$

Where: S : slip, N_r : rotor speed (RPM).

Furthermore, the motor efficiency should also be considered. This is determined by comparing the input and output power. Higher efficiency is desired in induction motors since they are used for energy conversion. Low values of efficiency implies that the motor is less productive and it should be substituted.

$$E = \frac{\text{output power}}{\text{input power}} \times 100\% \quad (2-6)$$

2.3 Faults of Induction Motors

Induction motors are reliable electric machines [9]. However, they are susceptible to several electrical and mechanical faults as shown in figure 2-5. Flaws in induction motor often lead to unbalanced stator current and voltages [20], reduction in efficiencies, torque oscillations, excessive vibrations, overheating and torque reduction.

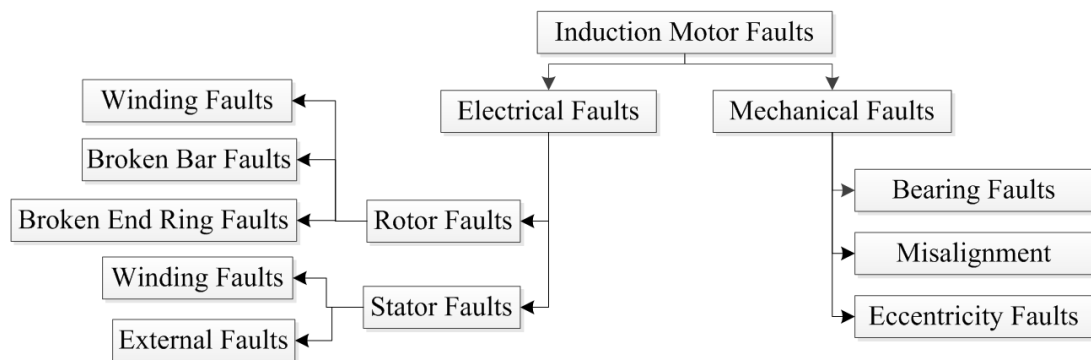


Figure 2-5: Block diagram of IM faults [21].

As illustrated in figure 2-6 [21], faults in induction motor occur in varied magnitudes with bearing faults assuming higher probabilities of occurrence followed by stator faults, but rotor faults assume the least probability of occurrence but it still need to monitored due to the environment change.

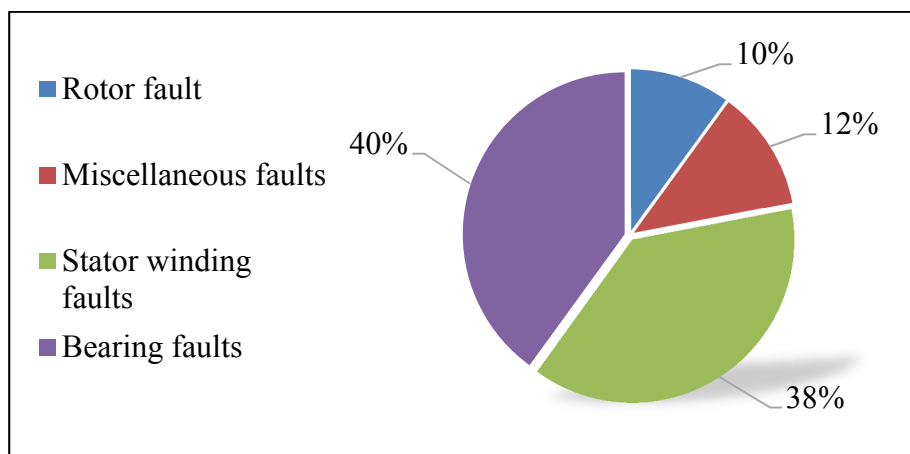


Figure 2-6: Probability of fault-occurrence in induction motors [21].

The most common electrical and mechanical faults of the induction motors will be explained below.

2.3.1 Electrical Faults

Electrical faults in an IM can stem from rotor bars and stator faults, which are briefly explained below.

2.3.1.1 Rotor Faults

Figure 2-7 shows a squirrel cage for an AC induction motor that comprises of end rings and rotor bars. A broken bar can be completely or partially cracked. Such bars are susceptible to breaking due to constant starts at rated voltages, manufacturing defects, mechanical stresses or thermal stresses caused by metal fatigue [22].

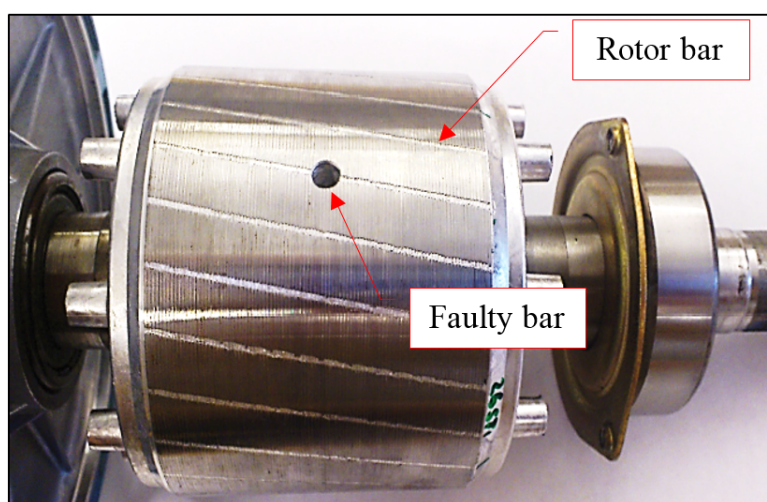


Figure 2-7: Squirrel cage of IM broken rotor bar [23].

Many reasons of causing broken rotor bar, due to manufacturing fault, such as irregular metallurgical stress might happen during brazing processes, which sometimes lead to rotor rotation failure, and an extra stress on the rotor bars due to large centrifugal force, which caused by heavy end ring. These faults have also effect on the rotor currents asymmetrical distribution [24]. In addition, some faults have been occurred in

different locations of the rotor such as at the joint between end ring and bars. **A. Bonnet and G. Soukup** [25] stated that the most rotor faults are happened at the joint between the end ring and bars due to manufacturing fault or any other possibilities, for instance if the motor is subject to stop and start frequently or long time to start up. Recently, broken rotor bars are common faults in induction motors. Furthermore, the main reasons that causes the faults in induction motors rotors are described below [26]:

- a) Manufacturing defects as mentioned earlier in the last section.
- b) Thermal stress, which is caused by the hot spot, sparking, excessive losses or thermal overload.
- c) Mechanical stress due to bearing failure, fatigued parts and lose lamination.
- d) Magnetic stress due to unbalance magnetic pull, vibration, electromagnetic force and electromagnetic noise.
- e) Dynamic stress due to cyclic stress, shaft torques and centrifugal forces.
- f) Environmental stress due to moisture and chemical into the rotor material.

A broken bar in an induction motor induces a series of side effects. One of the commonly known effect is the appearance of sideband components. The so-called sidebands are observed in the power continuum of the stator current towards the right edges and left sides of the fundamental frequency. The lower side band element is triggered by magnetic and electrical asymmetries of the rotor cage within AC asynchronous motors. Consequently, constant speed ripples produced by the resulting force pulsations instigate the right side band element. These side band frequencies are

determined by classical twice slip frequency sidebands, therefore occur at $\pm 2s f_s$ around the supply frequency as follows [27]:

$$f_b = f_s \left(\frac{k}{p} (1 - s) \pm s \right) \quad (2-7)$$

Where f_s : fundamental frequency, $\frac{k}{p} = 1, 5, 7, 11, 13 \dots$ due to normal configuration of winding, s : slip per unit.

Sideband elements, as explained earlier, are widely used for reorganization/correction of induction motor faults. Other electric properties created by the broken bars including stator current envelopes, oscillations speed, instantaneous power oscillations and torque ripples have been used for motor fault detection [28].

The previous section has explained the squirrel cage rotor faults in induction motors. Turning now to wound rotor faults, rotor windings of wound rotor are linked to external resistance via slip rings. By adjusting the resistance, it is possible to control the torque/speed properties of the induction motor. Further, it is possible to start the motor with low in-rush current through insertion of high- resistance windings in the rotor circuit. However, as the motor accelerates towards higher speed, the resistance of winding decreases, which is leading to faults. In addition, slip rings that are used in wound rotor motors are susceptible to damage. Subsequently, current in the rotor windings drops below the expected values [29]. Just like stator windings, rotor windings are also susceptible to failure due to a number of catastrophe issues such as:

- a) Insulation faults due to motor breakdown.
- b) Overheating which is caused by an electrical overload, leading to power-surge within the rotor coils or unbalanced motor supply voltage, and open-rotor bars could lead to winding overheating.

- c) Rotor locks emanating from mechanical faults can generate current that exceeds the starting current. However, rotor overheating may increase rotor losses. At a heightened levels, the motor temperatures may increase up to 350 °C.

2.3.1.2 Stator Faults

Stator faults are caused by one of the following factors, which create short-circuiting and effects on the stator coils:

- a) Mechanical forces and stresses.
- b) Thermal stresses and normal ageing process.
- c) Environmental pollution.
- d) Switching transient and electrical overloads.

Short-circuiting in stator windings is common feature in induction motors. It occurs between turns of two phases, or between turns of a single phase, or between turns of all phases. In addition, short-circuiting is observed between the stator core and windings of the conductor. The following section summarizes the faults in stator windings:

Short circuiting effects between turns of a similar phase as illustrated in figure 2-8a below. Winding short circuits are illustrated in figure 2-8b. Figure 2-8c and figure 2-8d illustrate short-circuiting between stator core and windings respectively. Similarly, figure 2-8e captures short-circuiting throughout the connections, while figure 2-8f illustrates short-circuiting between two phases due to abrasion and stator voltage

transients [30]. Over-rated and sub-rated voltage supplies could also create these faults [31].

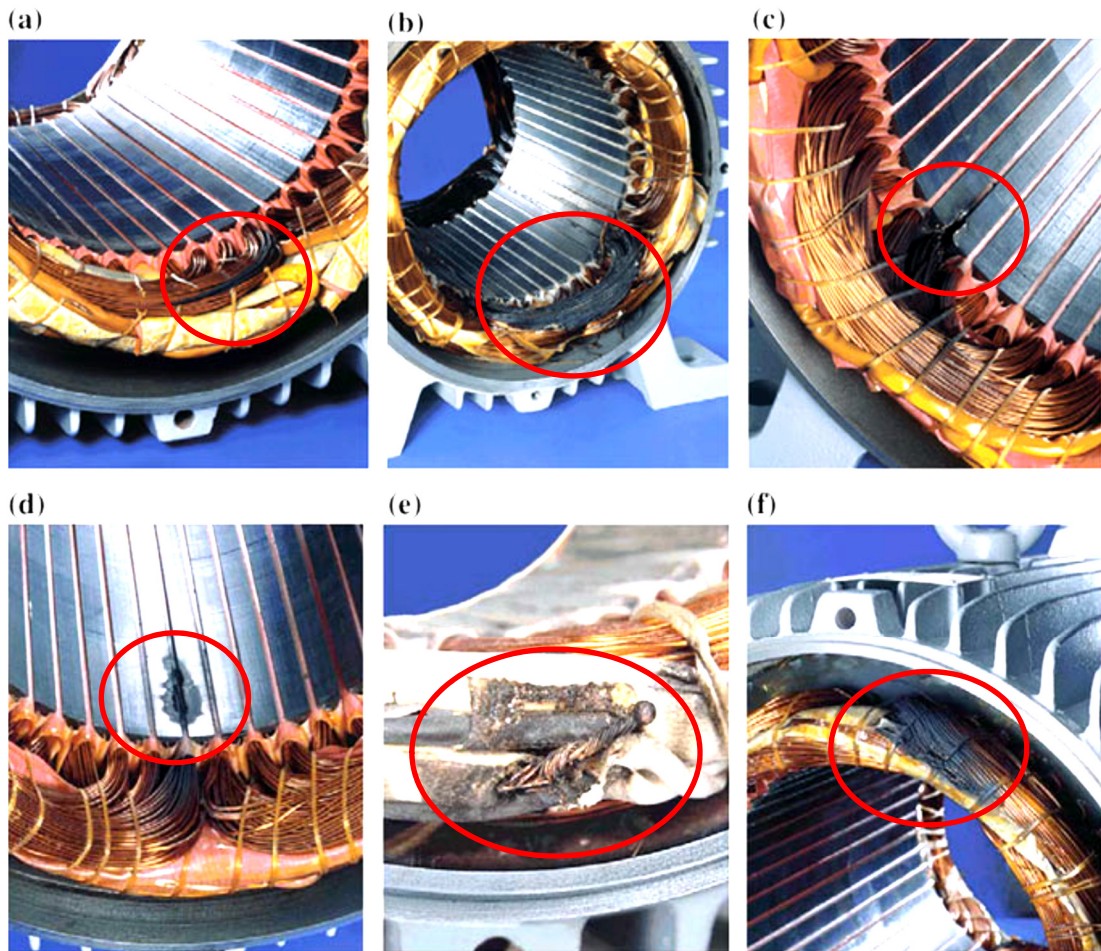


Figure 2-8: Different stator windings faults caused by insulation damage [30].

The stator faults could also be effected by an external faults as described briefly below:

a) Single-Phase Faults

The induction motors are subjected to loss one of their phases and this issue will have an effect on the power system distribution. This kind of fault causes a serious problem, because it prevents the motor to operate in actual horsepower. Furthermore, to detect the single-phase fault, for some cases the negative phase current has been used during the motor operation. Thus, the motor voltage and

current measurement was used for detecting the phase fault before loading the motor.

b) Phase Unbalance Faults

The probability of the unbalance faults is less than full phase faults, but if it happened, it may have similar consequences. Recently, more attention has been paid for the new induction motor installation in order to distribute the balance equally.

Having discussed the electrical faults and their causes, the final section of this chapter addresses the most common mechanical faults in induction motors.

2.3.2 Mechanical Faults

Mechanical faults can be caused by either of the following faults: bearing faults, eccentricity and misalignment. These faults account for 40% to 50% of the total faults observed in the motor [32].

2.3.2.1 Bearing Faults

Bearing faults are complications encountered in either the rolling element or the ball bearings that touch the inner and outer rings [9]. Ball bearings or the rolling elements continuously rotate in tracks inside the bearing ring. Bearing fault defects on outer ring, ball or inner ring. These faults could occur by internal stresses, vibrations, currents and inherent eccentricity that influence the formation of mechanical faults. A clear analysis of motor history helps to arrive at a conclusive statement that motors were previously driven by variable frequency drives lead to exhibited several premature failures. Misalignment faults and bearing faults within the load drive system

may generate periodic variations to motor. Figure 2-9 illustrates four types of rolling bearing misalignments [33].

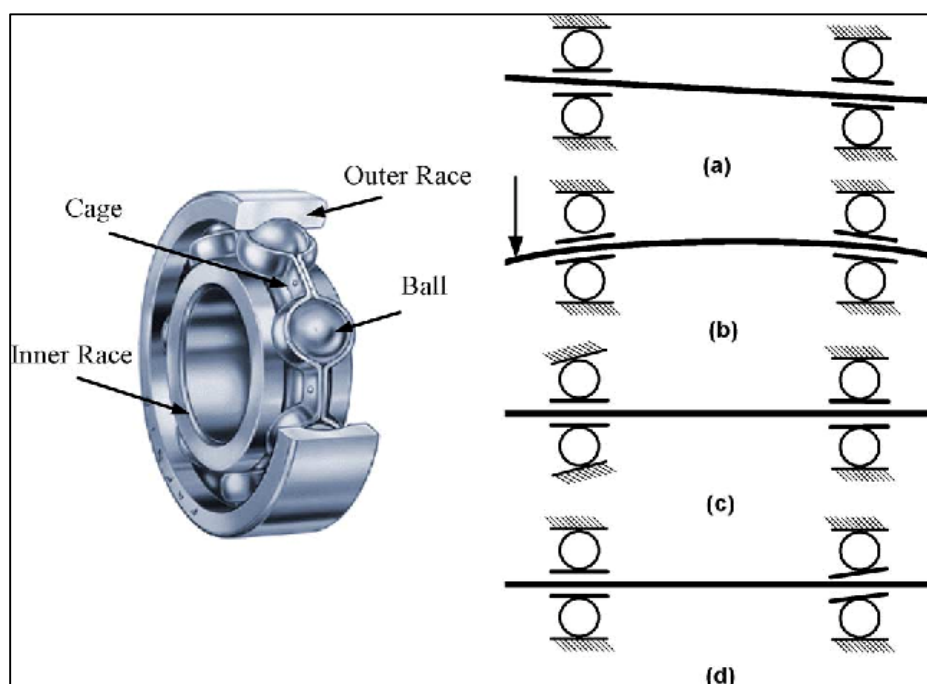


Figure 2-9: Bearing faults [33].

2.3.2.2 Eccentricity Faults

Eccentricity fault is also known as air gap eccentricity, which occurs in two primary forms namely, dynamic and static forms [34]. In static eccentricity fault, rotation of the axis is displaced from the centre with the position of the least air gap length being fixed in space. The fault occurs due to inaccurate positioning of the stator or/and rotor during the construction phase [35]. The displacement of the rotor from the central axis within the stator bar makes the distribution field in the air gap to be asymmetrical. As a result, a non-uniform air gap is created, thus generating a radial force of the electromagnetic origin. The effect is commonly termed as “Unbalanced Magnetic Pull” (UMP) which works towards the minimum air gap.

Furthermore, static eccentricity stimulates dynamic eccentricity as well. In dynamic eccentricity, the rotor does not spin within its own axis, but the least air gap spins with the rotor. Dynamic eccentricity may lead to several problems: For example; it might cause bending to the shaft, may lead to mechanical resonance, misalignment, bearing wear or may cause the static eccentricity [36]. Figure 2-10 illustrates several eccentricity faults in an induction motor where: a) without eccentricity, b) static eccentricity, c) dynamic eccentricity, d) mixed eccentricity respectively.

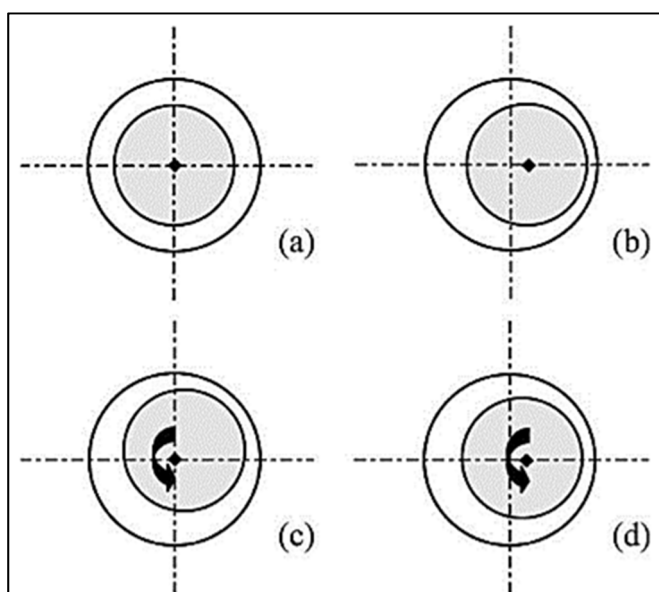


Figure 2-10: Different types of IM eccentricity faults [37].

2.3.2.3 Misalignment Faults

There are three common types of misalignment faults, which are parallel, angular and combination as shown in figure 2-11.

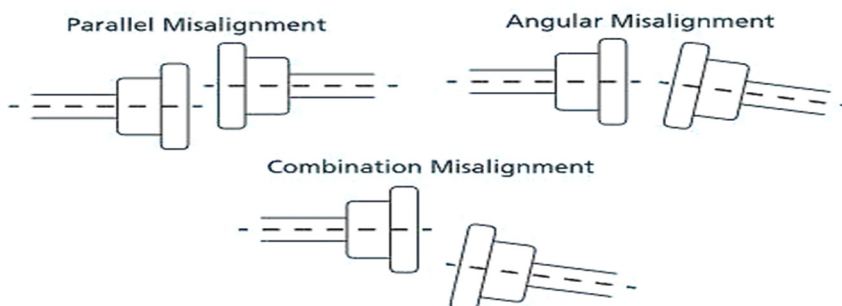


Figure 2-11: Misalignment types [38].

- a) **Parallel misalignment:** this fault occurs when the centre line of both shafts are parallel. These shafts could be displaced right/left, offset vertically/horizontally.
- b) **Angular misalignment:** this fault occurs when the driven equipment are set to angle with the motor. The mismatch angle could be to below/above, or to right/left. The centre line of the driven equipment and the motor can be cross each other if they are extended rather than in parallel. By the time this fault can damage both the drive equipment and the motor.
- c) **Combination misalignment:** this fault occurs when both shafts are suffering from parallel misalignment besides the angular misalignment.

Currently, AC induction motors have been widely used in the industries. In fact, over 85% of induction motors are in consumer and industrial markets. They are grouped as polyphase, or single phase. Induction motors are distinct from DC motors since they are consistently manoeuvre higher workloads that exceed a horsepower i.e. (746 Watts). Notably, 3-phase induction motors are required for intensive, power-driven applications [39], [40].

What follows next is an account of faults that occur in all kind of the induction motors. Electrical machines are considerably insecure because of detrimental operating environments or exposed unexpected fault which depend on the special circumstances such as start/stops, overload, unstable cooling, insufficient lubrication, etc. Thus, all these conditions are predicted to put all motors beneath risks of failures [41]. According to the IEEE standard 493-1997, table 2-1 [42] stated the most common faults in induction motors and statistical appearances recorded, based on different faults in industry.

Chapter 2: Induction Motor and Related Faults

Table 2-1: Common faults in induction motors [42].

Type of faults	Number of faults/failures				
	Induction motors	Synchronous motors	Wound rotor motors	DC motors	All motors
Bearing	152	2	10	2	166
Winding	75	16	6	--	97
Rotor	8	1	4	--	13
Shaft	19	--	--	--	19
Brushes or slip rings	--	6	8	2	16
External device	10	7	1	--	18
Others	40	9	--	2	51

The next chapter explains the way of protecting the induction motors by using the traditional and artificial intelligence methods for three common condition monitoring techniques thermal image processing, current and vibration signals processing.

CHAPTER 3

LITERATURE REVIEW

“In this chapter, condition monitoring methods on induction motor faults detection have been presented. For example, traditional methods (motor current signature analysis MCSA, signal processing techniques) and artificial intelligence techniques. Additionally, this review will also cover the development of the condition monitoring from earlier studies to most recent”.

3.1 Introduction

Condition monitoring and fault diagnosis of induction motors are quite challenging for electrical engineers. There are several methods of condition monitoring, which are thermal, current, vibration monitoring, etc. However, thermal and vibration monitoring require very sensitive sensors and highly specialized equipment. In both cases of motor faults electrical and mechanical, an effective condition monitoring technique should be able to provide adequate warning about the machine fault before failing in its critical component. This process will prevent any maintenance schedule or any other cost that causes by the fault. The technology provides highly selective, sensitive and cost effective techniques for online/offline diagnosing and monitoring of industrial machinery.

3.2 Thermal Monitoring

Last decades there have been a numerous approaches to monitor the operation of induction motors by thermal protection technique by using for example relays, thermocouples, thermography (thermal cameras) and others, which are suitable for low cost applications. Providing thermal protection for induction machines, different types of relays have been already developed for overload and thermal monitoring [43].

Table 3-1 illustrates the sources of abnormal heating and their possible causes.

Table 3-1: Sources of abnormal temperature and causes [43].

Origen	Faults
Thermal	Finishing problem, lubricant refrigeration and deficient cooling.
Environmental	Lubricate contamination, dust and dirtiness.
Mechanical	Overload, bearing, transmission problem and misalignment.
Electrical	Supply voltage, connection defects, broken rotor bars, voltage unbalance and harmonic distortion.

Chapter 3: Literature Review

In order to avoid the thermal overload, thermal sensors have been widely used for stator winding monitoring. However, these sensors are highly undesirable for some applications.

Moving on now to consider some reasons of having both electrical stress and high thermal faults on the rotor cage and stator winding. The most common reasons are the high current and long starting time, which have an effects on the rotor cage or stator winding, which make it unable to be cooled. As results of these stresses, the small induction motors take long starting time than the large motors [44].

Most of induction motors start with high torque and high starting current with low voltage. Throughout the motor starting time, the current of the rotor and the stator are much higher than rated current, which cause very high thermal stress for rotor and stator. Thus, the temperature peak of induction motor is naturally appears during the motor starting instead of loading condition. Figure 3-1 illustrates the temperature of the rotor cage and stator winding during and after starting [45]. Furthermore, the rotor cage temperature could be rise to 600°C in some induction motors [46].

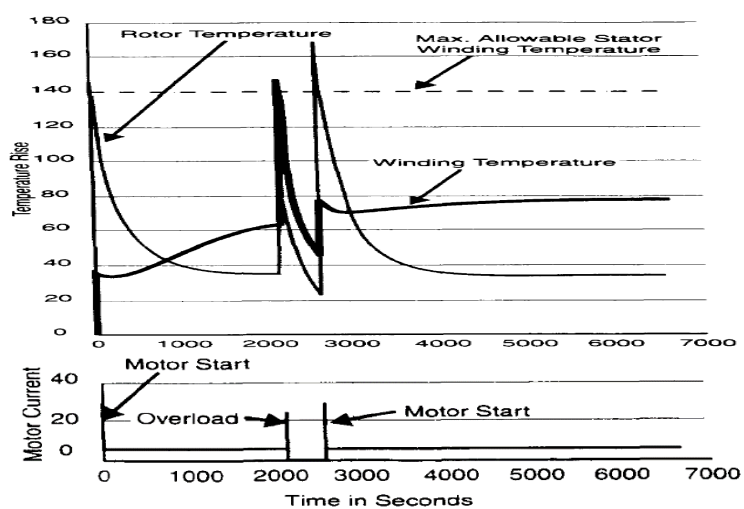


Figure 3-1: Sample of thermal signature for induction motor (during and after starting) [45].

As previously stated, the rotor will be affected by the high temperature, which reduces not only the mechanical performance, but also it could lead to dilate the rotor, all these are lead to rotor cage failure. Consequently, the thermal protection for the rotor and the stator of the induction motor is essential during both cases of steady and transient state in order to prevent the catastrophic failure in the motors.

3.2.1 Thermal Protection based on Traditional Methods

Rotor temperature contains many information about the motor status, thus it is very important that researchers take the rotor temperature into account for detecting and diagnosing the induction machine faults. There are two important rotor-monitoring temperature approaches, the first approach is relying on the rotor resistance [47]–[49]. The second approach is direct measurement of the rotor temperature by different thermal sensors such as infrared cameras, thermocouples, etc. The first approach has been proposed in order to overcome the disadvantages of the direct measurements, but this technique requires advance knowledge of rotor speed and parameters.

Many researches have proposed parameter-based approaches in order to estimate the rotor temperature from rotor resistance variations. **Beguenane et al** [47] published a paper in which they described the Model Reference Adaptive System (MRAS) and apply it for rotor flux observer based on the inverse time constant and rotor speed. The results indicate that the proposed method has ability to be applied to an Indirect Field Oriented (IFO) control of induction motor without speed sensors but it requires high performance of torque control in order to be suitable to apply for induction motor vector control.

Habetler et al [48] have proposed a new method for estimating the rotor and stator resistance based on Model Reference Adaptive System (MRAS) for the purpose of

monitoring the rotor conductor and stator winding temperature. Their results show that the MRAS provides an accurate estimation in case of the motor is heavily loaded and it has the ability to track R_s (stator resistance) and R_r (rotor resistance). While, a sensorless rotor temperature estimator based on the harmonic spectral estimation of the current has been proposed. Experimental results have been proven that the proposed system was suitable for rotor thermal protection because it was very reliable and accurate [49].

Gao et al [50] pointed out an investigation in the estimated rotor temperature error with the unbalance supply and the impaired cooling by applying the Goertzel algorithm to the voltage space vector and complex current. Goertzel algorithm has been widely used in touch-tone telephone services in order to detect the signals with multi-frequencies, which is employed to a complex space vector for extracting the efficient and fast component of positive sequence of fundamental frequency.

Gao et. al. [51], which are related to the latter articles, proposed a pipelined architecture for estimating rotor temperature (squirrel cage induction motors) in both steady state and dynamic operations. This was based on the current and voltage measurements without including any (temperature or speed) sensors. Two super-heterodyne receivers have been also applied on a complex current vector, which are operated in parallel with pipelined architecture. The first super-heterodyne receiver has been used for detecting the motor speed based on the instantaneous rotor slot harmonic frequency, which is extracted from the complex current vector, and the latter one has been used for the same complex current vector in order to extract a new complex fundamental current vector. The results indicate that the proposed system allows the modern microprocessors to handle all the data in parallel, as a result in the

superior performance during rotor temperature estimation in the absence of speed and temperature sensors.

Reigosa et al [52] have suggested a new approach for estimating the rotor temperature based on a high-frequency signal injection, the results show that the worst case has been happened in the thermal transients. The estimated temperature error in the transients state was $< 5^{\circ}\text{C}$, while in the steady state reduces to $< 2^{\circ}\text{C}$. Furthermore, **Huang and Gühmann** [53] proposed an implementation for fourth order Kalman filter algorithm in Wireless Sensor Network (WSN) for the purpose of rotor temperature estimation. Six sensors have been used for acquiring current and voltage data from the stator, which means that the temperature could be estimated correctly without recording the mechanical load and rotor speed as long as the current goes through the stator windings. The experimental results have been proved that the Kalman filter implementation is suitable for real time rotor temperature estimation. Consequently, the approach of rotor resistance estimation has shown its robustness for rotor fault detection in many applications but it still needs further testing, since some parameters or values of the typical per-unit of induction motors are different from each other. In addition to this, the accuracy of these approaches are limited in case of fast transient state such as starting, because they have been designed for slow transient or steady state.

International Electrical Testing Association (NETA) proposed a standard to rotating machinery and electrical systems for thermal inspection [54], these guidelines have helped for estimating and detecting faults severity. **Singh and Naikan** [55] have tested the thermal image monitoring (FLIR E60 camera) based on the two hot spot profiles of stator temperature for induction motor faults (cooling system failure and inter-turn),

which has been used in compliance with International Electrical Testing Association (NETA). The results show that the proposed profiles have efficiently diagnosed the motor faults.

Lim [56] has demonstrated omnidirectional thermal imaging system for condition monitoring by designing a custom and specific Infrared (IR) reflected hyperbolic mirror set. In this study, log-polar mapping technique has been applied to have a panoramic form by unwarping the captured thermal image. The results show that the proposed system obtain high accuracy for detecting the machine faults.

Turning on to the experimental evidence on the traditional current monitoring technique and discuss the most helpful method for motor fault detection based on the current signal.

3.3 Current Monitoring

High performance electrical drives currently employ sophisticated control techniques. In fact, the demand for such drives are currently on the rise. This demand has been necessitated by cost, size and efficiency of induction motors. Currently, research is being undertaken to examine load oscillation, unsymmetrical supply voltage and motor monitoring techniques to enhance the safety and serviceability. The Motor Current Signature Analysis (MCSA) has been employed for decades as a tool for diagnosing the motor faults. In spite of these efforts, induction motors are still faced myriad of uncontrolled challenges that reduce their lifespan [57]. Squirrel cage motors are preferred than other types of induction motors since they are robust and work under fault conditions longer for a reasonable period before they fail.

3.3.1 Current Protection based on Traditional Methods

MCSA has been applied to identify most of motor faults for example, broken rotor bars, short-circuited turns and eccentricity. Furthermore, MCSA technique can also be applied to determine mechanical faults such as load oscillations, bearing and gearbox. By using the current harmonics, it is possible to detect the type of fault within components of the rotating flux. Fault monitoring and diagnosis based on MCSA proceeds as shown in figure 3-2.

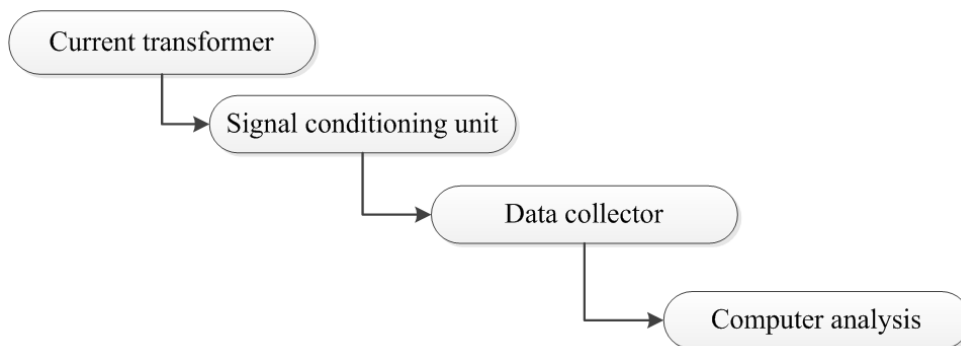


Figure 3-2: Flow chart for motor current measurement [37].

To diagnose faults in a motor, figure 3-3 illustrates the basic MCSA equipment system, MCSA uses current spectra, which has potential information of motor faults.

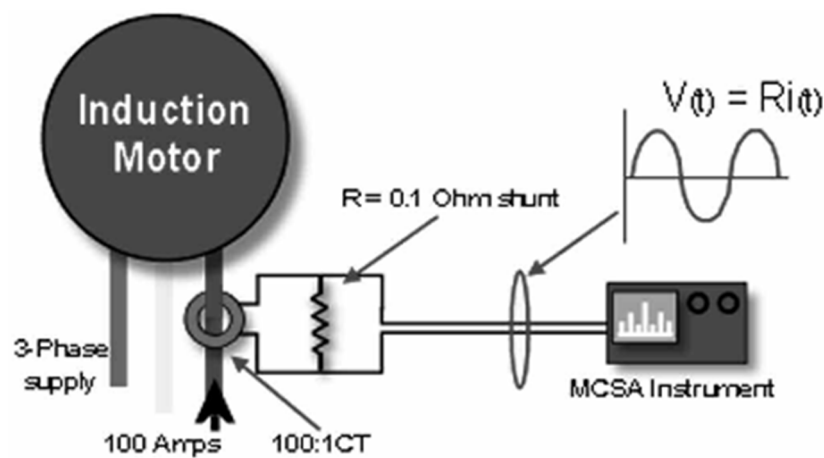


Figure 3-3: Basic MCSA equipment system [58].

Past decades have seen the rapid development of condition monitoring and series of reviews have been made by many researchers. They offer a good overview on how current monitoring progress has been made. MCSA is the state-of-the-art techniques [59]. This technique has many advantages. It is non-invasive, where stator current is measured and monitored and no other special equipment is needed. Numerous faults can be diagnosed using MCSA: damaged rotor bar, such as, broken rotor bars, eccentricities; for example, due to unbalanced rotor; bearing defects; stator winding short circuit [24][60].

A notable change is in the progress from the use of traditional Fourier transform e.g. Fast Fourier Transform (FFT) to the use of Wavelet Transform (WT) e.g., Discrete Wavelet Transform (DWT), to identify fault based on current spectrum and extract a unique features for fault diagnosis. In addition, FFT is a traditional tool for MCSA analysis, it has been able to locate individual fault based on current spectrum. This approach has been successfully used for broken rotor bars and eccentricities faults detection [15].

Schoen et. al. [61] have addressed the application of MCSA to detect the rolling-element bearing damage in induction machines. This study investigates the efficacy of current monitoring for bearing fault detection by correlating the relationship between vibration and current frequencies caused by incipient bearing failures. Experimental results, clearly illustrate that the stator current signature can be used to identify the presence of bearing fault.

Benbouzid et al [60] have stated that the preventive maintenance of electric drive systems with induction motors by monitoring their operation for detecting the abnormal electrical and mechanical conditions, because this may lead to a system

failure. Intensive research efforts have been done on the motor current signature analysis. This technique utilizes the results of spectral analysis of the stator current. Their investigations show that the frequency signature of some asymmetrical motor faults can be well identified using the Fast Fourier Transform (FFT), which is leading to a better interpretation for the motor current spectra. Furthermore, the laboratory experiments indicate that the FFT based motor current signature analysis is a reliable tool for asymmetrical faults detection.

Thomson et. al. [62] have presented an appraisal of on-line current monitoring techniques to detect airgap eccentricity in three-phase induction motors. On-line current monitoring is proposed as the most applicable method in the industrial environment. The results verify that the interpretation of the current spectrum proposed in this study was successful in diagnosing airgap eccentricity problems.

Benbouzid et. al. [16] have investigated in the efficacy of current spectral analysis on induction motor fault detection. The frequency signatures of some asymmetrical motor faults, including air gap eccentricity, broken bars, shaft speed oscillation, rotor asymmetry and bearing failure were identified. This work verified the feasibility of current spectral analysis. Current spectral analysis was applied to other types of electrical machines too. For example, [59], [62] verified that the use of the current spectrum was successful in diagnosing air gap eccentricity problems in large, high-voltage, three-phase induction motors but not with low voltage motors.

Benbouzid [9] made a review of MCSA as a medium tool for fault detection. This study introduces in a concise manner the motor signature analysis for motor faults detection and localization that indicate or may lead to a failure of induction motors. It is based on the behaviour of the current at the side band associated with the fault. It

has been explained that when the load torque varies with rotor position, the current will contain spectral components, which coincide with those caused by the fault condition. Researchers have concluded that Fourier analysis is very useful for many applications where the signals are stationary. However, it is not appropriate for analysing a signal that has a transitory characteristic such as drifts, abrupt changes and frequency trends. To overcome this problem, Fourier analysis has been adapted to analyse small sections of the signal in time; this technique is known as the Short Time Fast Fourier Transform (STFT). STFT represents a sort of compromise between time and frequency-based views of a signal and provides information about both.

Arkan et al. [63] have presented a non-invasive online method for stator winding faults detection in three-phase induction motors from the observation of negative sequence supply current. A Power Decomposition Technique (PDT) was used to derive positive and negative sequence components of measured voltages and currents. The results show that the negative sequence impedance could vary between 10% and 50% during an inter-turn short circuit.

Miletic and Cettolo [64] have acknowledged that Motor Current Signature Analysis (MCSA) is one of the widely used as diagnostic method. This method is based on measurement of sidebands in the stator current spectrum. These sidebands are usually located close to the main supply frequency. Frequency converter causes changing in the supply frequency slightly in time as a result of some additional harmonics in the current spectrum. These harmonics could be easily misinterpreted as sidebands, which are caused by the rotor faults. In this study, the experimental results of fault diagnosis carried out using standard supply and using frequency converter were presented and compared.

In current spectral analysis, the actual harmonics measured from a running machine are always compared with known values (thresholds) obtained from a healthy motor. In practical applications, the thresholds change with motor operating conditions. Therefore, **Obaid and Habetler** [65] have proposed tracking method for the normal values of a healthy motor at different load conditions. For each load condition, a corresponding threshold was determined and compared with the on-line measurement to determine the motor condition. Besides, the FFT technique used in spectral analysis, other techniques in advanced digital signal processing and pattern recognition have been applied to motor current signal as well. Five different motor conditions were studied (the healthy machine and having up to four broken rotor bars), each at nine different loads. The results of this study show that if there is any broken rotor bar will directly affect the induced voltages in the stator windings and the waveform of the stator currents. Therefore, the spectrum analysis of the line current (motor current signature analysis) is one of the best non-intrusive method. While [66] utilized the result of spectral analysis of stator current to diagnose rotor faults. The diagnosis procedure was performed by using virtual instrumentation (VI). Several virtual instruments (VIs) were built up in LabVIEW. These VIs were used for both controlling and data processing. The measured current signals were processed using the Fast Fourier Transformation (FFT). The power spectral density of the measured phase current was plotted. The results obtained from the healthy motor and those having rotor faults were compared, especially looking for the sidebands components those are appeared in the special frequencies. The significance presence of some well-defined sidebands frequencies are clearly indicate the motor rotor faults.

Stack et. al. [67] have proposed a method for detecting bearing faults via stator current. Current-based condition monitoring offers significant economic savings and

implementation advantages over vibration-based techniques. This method filter the stator current and remove the frequency content that is unrelated to bearing faults. As bearing health degrades, the modelled spectrum deviates from its baseline value; the mean spectral deviation is then used as the fault index. This fault index is able to track changes in machine vibration due to developing bearing faults. Due to the initial filtering process, this method is robust to many influences including variations in supply voltage, cyclical load torque variations, and other (non-bearing) fault sources. Experimental results from 10 different faulty bearings are used to verify the proficiency of this method.

An experiment to diagnose the induction motor broken rotor bar fault conducted in [68]. The Motor Current Signature Analysis (MCSA) has been used to diagnose the rotor fault. The rotor bar was damaged by drilling into the rotor. The spectra of healthy and faulty motors were compared. Stator current spectrum of faulty motor shows the side bands at particular frequencies due to presence of broken rotor bars with great reliability. Finally, researchers concluded that the MCSA is a reliable technique for diagnosing the broken rotor bar faults.

Jung et. al. [69] have proposed an online induction motor diagnosing system using MCSA with advanced signal and data processing algorithms. The advanced algorithms were made-up of the optimal slip-estimation algorithm. The optimal slip-estimation algorithm suggested the optimal slip-estimator based on the Bayesian method of estimation. To verify the generality of the suggested algorithm, laboratory experiments were performed with 3.7 kW and 30 kW squirrel-cage induction motors. The proposed system was able to discover four kinds of motor faults and diagnose

them. Experimental results have successfully verified the operations of the proposed diagnosis system and algorithms.

Frosini et. al. [70] have proposed a new approach of using the induction motor stator current and its efficiency as indicators of rolling-bearing faults. This study illustrates the experimental results on four different types of bearing defects: crack in the outer race, hole in the outer race, deformation of the seal and corrosion. Another novelty introduced by this study is to analyse the decrease in the efficiency of the motor with a double purpose: as alarm of incipient faults and as evaluation of the energy waste resulting from the fault condition before the machine breakdown.

Different fault diagnosis methods by means of data processing in LabVIEW were compared in [71]. The results obtained by experiments verified that the three-phase current vector, the instantaneous torque and the outer magnetic field could be used for diagnosing the rotor faults. At last, authors stated that due to its simplicity, the MCSA is the mostly used in industrial applications.

This section has described the traditional methods of induction motor fault diagnosis based on the current spectral, and has argued that the MCSA is the best-known fault diagnosis techniques used today. In fact, MCSA requires simplified sensor calibrations and installations. However, the main drawback to MCSA is that the stator current data must be sampled whenever the motor attains steady-state speeds.

The next section of this chapter will describe another condition monitoring technique (vibration), and how it diagnoses the machine faults.

3.4 Vibration Monitoring

Vibration analysis is one of the most important condition monitoring and fault diagnosis tool for all rotating machinery because the majority of the rotating machine problems are caused by bearing defects which in turn effects the shaft [72]. Rotating machinery generate a vibration signal during their operation, this signal has many information about the machine. It generates three types of vibration signals, which are stationary, noise and random vibrations. These signals are used for detecting the motor faults based on digital signal processing [73]. In the electrical machines, the vibration and noise could be caused by many forces such as mechanical, magnetic and aerodynamic [74]. Consequently, various types of asymmetries and faults in the electric machine could be detected by analysing the vibration signals [75]. Bearing faults, unbalanced rotor, rotor eccentricity and gear faults have been detected by the vibration signals.

3.4.1 Vibration Protection based on Traditional Methods

Dorrell and Smith [76] have suggested an analytical model for static eccentricity fault in induction motor. In this approach, the air gap between the stator magneto-motive forces and rotor has been used for producing unbalanced magnetic pull. In addition to this, an experiment has been done in order to confirm the model results and they have found that both the measured and predicted results are good for two cases at low slip in the rotor cage, when using blank rotor. They have concluded that the winding harmonics order and the skew of the rotor have a big impact on the unbalanced magnetic pull.

Finley et. al. [77] have analysed the electromagnetic force of stator and rotor based on the vibration patterns. These two forces are subjected to reach their peaks when the

stator magnetizing current flow has reached its maximum value. However, these signals are very sensitive to some problems especially for motor base stiffness and frame and eccentricity.

Trutt [78] has studied the relationships between two induction motor components, which are electrical winding damage and vibration faults. The results show that these two faults has good quantifiable correlation, which was probably used as a basis in condition monitoring for induction motors.

Müller and Landy [79] have investigated in the factors that effects on the axial force based on broken rotor bar which have been done theoretically and experimentally. A mathematical model has been developed in this study in order to find the interaction of the stator flux and the inter-bar current with axial direction force. The results have been experimentally confirmed, but the main disadvantage of this study is that it could only be applied for the devices that have inter-bar current.

The Pulse Width Modulation (PWM) inverter has been used as feeder for induction motors, which has been studied and investigated in [80] by comparing the healthy and faulty signals based on current and vibration monitoring. The vibration signal has been collected at different frequencies, which can be used for detecting the stator winding faults at an early stage. In order to have a full view, the results should be updated for any changes in the motor status in predictive program. The results indicate that establishing condition monitoring for induction motor from one data set was probably unachievable and undesirable.

Vandeveldel and Melkebeek [81] have designed a Finite Element Method (FEM) model for analysing and predicting the induction motor faults numerically based on noise and vibration signals, which are resulted from magnetic equivalent circuit of

electromechanical analysis. It has been claimed by the researchers that their results overcome the weaknesses inherited in the model analysis but all the analyses were not made of lower order forces.

Zhang et. al. [82] have demonstrated the Wavelet Pocket Transform (WPT) and Power Spectral Density (PSD) for monitoring the turbo generator based on the vibration monitoring. The results show that the WPT overcome the drawbacks of constant time-frequency resolution in feature extraction, and it was promising compared to Fourier-based approach.

Stack et. al.[83] have developed a fault signature model and detection scheme for detecting the inner race defect of induction motor bearing faults using vibration signal. It examines the spectrum of vibration signal for peaks with the phase-coupled sidebands that occurring at predicted spacing by the model. The results show that the inner race faults could be easily detected, and it can possibly handle the cage or rolling element defects.

Rahman and Uddin [84] have used the vibration and current signals of unbalanced rotor and analysed them by several techniques: Fast Fourier Transform (FFT), Hilbert Transform (HT), and Discrete Wavelet Transform (DWT) in order to detect the fault severity and its location at different conditions. The Daubechies wavelet has been selected for analysing the healthy and faulty signals. The results show that the DWT is best for identifying the fault locations. However, wavelet analysis may not be accurate in analysing some of the harmonics presence.

Artigao et. al. [5] have used the vibration signal for detecting the wind turbine bearing fault mainly based on the frequency domain of vibration signal that has been analysed by FFT. In this research 1.5 MW wind turbine has been used with doubly-fed induction

generator. The results conducted that the FFT was helpful for detecting the bearing faults in the wind turbine.

Previous sections have demonstrated traditional methods for induction motor fault detection based on different condition monitoring techniques. It is now necessary to explain the course of artificial intelligence (AI) techniques and their applications for saving the rotating machinery and avoid catastrophic consequence.

3.5 Artificial Intelligence Techniques for Motor Faults Diagnosis

Recently, artificial intelligence has grown significantly in popularity because of its powerful capabilities. It has been widely used for improving the effectiveness and efficiency of fault detection and prediction in the electrical machine especially in rotating machinery. Artificial intelligence technique for motor fault diagnosis was achieved through the notion of human intelligence in machine operations to mimic the human features and thinking process [85]. AI comprises a series of branches including Artificial Neural Network (ANN), Genetic algorithms (GA), Problem Solving and Planning (PSP), Fuzzy Logic (FL), Logic Programming (LP) and so forth. These techniques deal in vast quantities of data and handle non-linear problems. Upon training, they can produce a model for predicting the class for new incoming data [18]. Figure 3-4 illustrates the steps of AI in induction motors faults diagnosis [86].

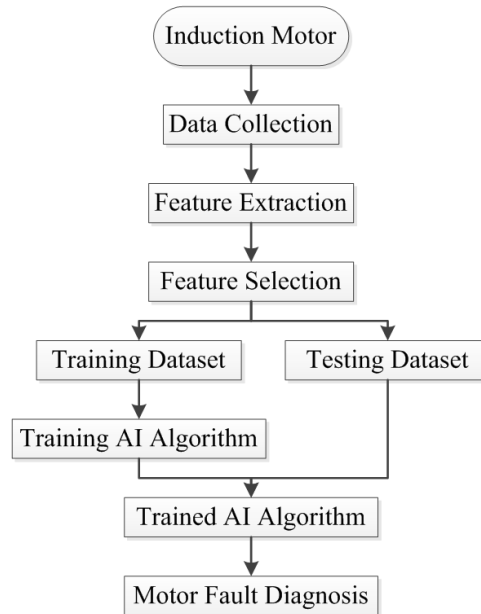


Figure 3-4: AI flow chart for IM fault diagnosis [86].

3.5.1 Thermal Monitoring based on AI

Thermal imaging has been widely used and successfully applied in many fields as a fault diagnosis method such as medical, mechanical system, energy and electronics and electrical systems. It becomes an important technology for protecting and monitor the behaviour of the most rotating machinery in industries, which may have effects on product quality, productivity, time efficiency and maintenance cost [87]. Furthermore, the electrical device preservation has been increasing (induction motors, transformers and generator) so as for improving the power supply, enhancing the reliability of operation, reducing the operating cost and superior service to customer [88].

Infrared Thermograph (IRT) is a non-intrusive and non-contact measuring technique. It has advantage of capability to display the temperature distribution in real time and any changes in the object temperature. Lately, the most common method for condition monitoring and fault diagnosis for electrical equipments is Infrared Thermography (IRT) or thermal monitoring [89]. This could be done by comparing a hot spot of

healthy thermal image (reference) and a hot spot of the faulty image. The reliability of the input power for the electrical equipment must be checked frequently in order to be sure that all equipment working normally. However, if the temperature of any machine has exceeded the limit, it will lead to a fail of the certain machine. Meanwhile, to diagnose and detect the faults for the electrical equipments by IRT, some of image processing methods have been applied for extracting the best features from the healthy and faulty images. Thermal images have a vital information on radiation of machine temperatures. This information could be extracted by using different image processing techniques and classified by using different classification algorithms.

In the classification field, **Nunez et. al.** [90] have proposed a low cost thermographic analysis for detecting the induction motor bearing faults by applying the thermal differential technique in order to make the faults detectable even if there is any changing in the surrounding environment. The result prove that the low cost thermal camera has been able to detect the bearing faults and it has been also found that the absolute thermogram was not enough for the determining the bearing defects unless by considering the ambient temperature.

A. Glowacz and Z. Glowacz [91] have produced a new method for extracting the features from the thermal image of three-phase induction motors called “Method of Areas Selection of Image Differences”, (MoASoID). Three types of induction motor faults have been considered in this study, which are healthy, squirrel cage ring fault and two broken rotor bars. Then, three classification methods have been applied for detecting the faults severity (Nearest Neighbour NN, Back Propagation Neural Network BPNN and k-means clustering) by using the best-extracted features from the thermal images based on MoASoID. The proposed technique was very useful for

detecting the induction motor faults and it could be used for other rotating machinery (generators, DC motors, and synchronous machines) for fault detection.

Khamisan et. al. [92], 300 thermal images have been captured for detecting the normal and abnormal of induction motor bearing faults. The SURF (Speeded-Up Robust Features) feature based selection method, active contour segmentation and RGB (Red, Green and Blue) colour space statistical algorithms have been applied for feature selection in order to differentiate between the normal and abnormal images. The results show that the proposed technique has been able to distinguish between the normal and abnormal of motor state and it could be implemented and used for improving the classification accuracy.

Huo et. al. [93] have proposed a new self-adaptive method using infrared thermography for induction motor bearing fault detection. Six bearing faults with different conditions have been experimentally tested, which are healthy, inner race, multi-fault, outer race, worn damage and roller element damages. In addition, wavelet approximation coefficient and decomposition level of “dmey” have been used for feature extraction from the image based on histogram of approximation coefficients. Furthermore, Genetic Algorithm (GA) has been used for feature selection and Nearest Neighbour (NN) for classification. The experimental results indicate that the proposed method was able to achieve above 95% of classification accuracy for detecting the motor faults.

Younus et. al. [94] have applied different classification algorithms such as Support Vector Machine (SVM), Parzen Probabilistic Neural Network (PPNN), Adaptive Resonance Theory Neural Network (ART-NN) and Fuzzy K-Nearest Neighbour (FK-NN) for induction motor faults detection based on thermal imaging. In addition,


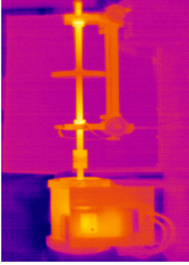
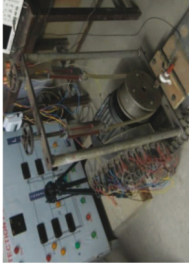
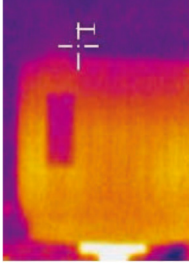
Principal Component Analysis (PCA) and Independent Component Analysis (ICA) have been applied for reducing the data dimensionality. The results show that the ICA provide better clustering performance than the PCA and the SVM has achieved better classification accuracy (98.33%) than other classification algorithms.

Lim et. al. [95] have suggested and developed an intelligence feature-based fault diagnosis based on the thermal images (FILIR, SC 5000) of motor faults detection (normal, bearing fault and misalignment) and then compare the results with the vibration signal. In this paper, Support Vector Machine (SVM) has been used for classifying the machine faults. The results indicate that the proposed method obtained 95% classification accuracy using thermal image based on three features only, while the classification accuracy was 96.25% using vibration signal based on over four features.

Table 3-2 shows some previous research experimental setup for induction motor faults detection based on thermography [93 – 98].

Chapter 3: Literature Review

Table 3-2: Some previous research experimental setup for induction motor faults detection based on thermography [93 – 98].

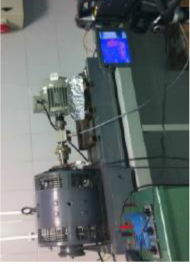
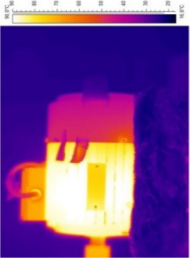
Authors	Camera type	Fault type	Experimental setup	Thermal image	Methods	Results
Tran et. al [96].	FLIR-A40.	<ul style="list-style-type: none"> ➤ Healthy. ➤ Misalignment. ➤ Bearing. ➤ Mass-unbalance. 			<ul style="list-style-type: none"> ➤ Propose bi-dimensional empirical mode decomposition (BEMD) for enhancing the image. ➤ Generalized discriminant analysis (GDA) for feature reduction. ➤ Relevant vector machine (RVM) for fault classification. 	<ul style="list-style-type: none"> ➤ The proposed system has been experimentally tested and compared with other classifiers (SVM and Adaptive Neuro-Fuzzy (ANF)), which indicate that the system was able to improve the classification accuracy and detect the rotating machinery faults.
Chaturvedi et. al [97].	Uncooled FPA microbolometer.	<ul style="list-style-type: none"> ➤ Healthy. ➤ Cooling system failure. 			<ul style="list-style-type: none"> ➤ Colour based segmentation technique for identifying the hot regions. ➤ Implementation of changing in the red colour intensity algorithm for recognizing the hot spot. 	<ul style="list-style-type: none"> ➤ The analysis results showed that the proposed method able to monitor the health condition of IM.

Chapter 3: Literature Review

Picazo-Rodenas et. al. [98]

- Healthy.
- Bearing damage.
- Ventilation damage.

FLIR-S65 series.


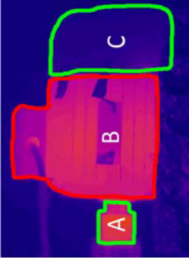



- Build a new model based on the thermodynamics first law and induction motor thermal images.
- The model could be successfully applied for induction motor fault detection by obtaining eventual alarms if the motor working in abnormal conditions.

Karvelis et. al. [99].

- Healthy.
- Rotor bar.
- Stator unbalance.
- Bearing failure.
- Fan failure.

FLIR-S65 series.

- Proposed object matching method for IM faults detection based on the image segmentation.
- C4.5 tree and Naïve Bayes (NB) have been used for fault classification (Weka software).
- The results have achieved good accuracy with the C4.5 classifier rather than other classifiers, and the proposed method needs more implementation in order to increase the classification accuracy.

Chapter 3: Literature Review

- Healthy.
- Unbalance.
- Looseness.
- Misalignment.
- Bearing (inner race, outer race, cage and ball defect).

Widodo et. al. [100].
FLIR-SC5000.

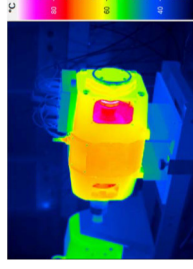


- Develop the Self-Organizing Map (SOM) for motor fault detection based on the thermal image.
- Thermal image data and vibration signal.
- Regions of Interest (ROI), Otsu and k-Mean clustering for feature extraction.
- Thermal features: area, central moments and perimeter.
- Vibration features: mean, RMS, kurtosis and skewness.

- The results show that good accuracy have been obtained by using both features, thermal and vibration.
- It also shows that the thermography could be used as alternative way for condition monitoring.

- Healthy.
- Humidity influence.
- Atmospheric temperature influence.

Fantidis et. al. [101].
Jenoptik camera VarioCAM 7800.



- Induction motor temperature measurements.
- Describing the humidity and the environment influences on the motor.

- The results show that the IM temperature measurements could be applied for fault detection.

3.5.2 Current Monitoring based on AI

Electrical monitoring such as current signature, negative-sequences and zero-sequences current monitoring, Park's vector and other more have been used for monitoring the motor status and analysing the stator current signal for diagnosing the faults severity. Consequently, the current monitoring has been used as sensorless method for fault detection, could be implemented and applied without any extra hardware.

Considerable amount of literatures have been published on the current monitoring technique as briefly discussed in the following, **Haji, and Toliyat** [102] have developed a pattern recognition technique based on Bāyes minimum error classifier to detect broken rotor bar faults in induction motors at steady state. The proposed algorithm uses only stator current as input without the need for any other variables. First, the rotor speed is estimated from the stator current, and then appropriate features are extracted. Once normalized mean and variance plus mean and covariance of each class, the technique can be used in online condition monitoring. The theoretical approach and experimental results show that the strength of the proposed method without loss of generality, the algorithm could be revised to include other faults such as eccentricity and phase unbalance.

Nejjari and Benbouzid [103] have applied the artificial neural network (ANN) for induction motor fault detection by examining the shapes and the patterns of the Park's vector of supplied faults based on the backpropagation algorithm. The method has been experimentally tested and the results show that the accuracy level was satisfactory.

Bouzid et. al. [104] have used a feed forward Multi-Layer Perceptron Neural Network (MLPNN) for detecting and locating the stator inter-turn short circuit automatically based on the backpropagation technique. The input for the NN is the phase differences between the line current and the phase voltage of IM and the output is set to either (0 or 1). Thus, if there is a short circuit fault in the stator the NN will give 1, otherwise it gives 0.

Sonje et. al. [105] have proposed a machine learning classifier for multi class to diagnose the faults. The classification system based on random forest classifier for individual and mix faults. After acquiring the stator current data with different load conditions, fourteen statistical parameters (minimum, maximum, mean, median, standard deviation, variance, sum, skewness, kurtosis, energy, R.M.S value, absolute value of sum, shape factor and peak factor) have been extracted from the signal to be used as input for the classifier. Thus, the result shows that the proposed system was more accurate and obtained better performance comparing to the Multi-Layer Perceptron Neural Network (MLPNN).

Martins et. al. [106] have studied the unsupervised NN for online fault detection based on stator current data. This method has been used alfa-beta stator currents as input variables. This system has applied with help of the Hebbian-based unsupervised NN, which was used to extract principle component from the stator current dataset. The result was satisfactory for detecting and verifying the faults severity.

Abid et. al. [107] have presented a support vector machine (SVM) classifier for detecting bearing faults by motor current signature analysis. The authors proposed a novel strategy for detecting the rotating machinery faults using Directed Analytic Graph Support Vector Machine (DAG-SVM) and Stationary Wavelet Packet

Transform (SWPT). Four bearing fault conditions (Normal, Inner, Outer and Cage defects) have been tested. The experimental results show that the proposed method is considerably reduces the number of descriptors from 4 to 2 under 5 different load conditions, as a result the classification accuracy was above 95%.

The wavelet NN and fuzzy logic systems have been proposed by **Abiyev and Kaynak** [108] for controlling and identifying the fault of uncertain system. In this work, the gradient decent algorithm has been used for updating the wavelet parameters. The test results show that the proposed system has more adaptive and fast for classifying new data.

A novel hybrid techniques of MCSA and fuzzy logic has been presented by **Soomro et. al.** [109] for induction motor mechanical faults (eccentricity and bearing) detection. The MCSA was used for locating the fault by using particular harmonics of line current spectral analysis, while the Fuzzy logic was used for assessing the motor operating condition and detect the faults severity. The test results show that the proposed technique has been able to detect and locate the faults successfully, thus it could be used to analyse all major motor faults.

Glowacz et. al. [110] have presented three different types of classifiers (Nearest Neighbour, Linear Discriminant Analysis and Bayes) for detecting four types of faults. These faults are healthy, one rotor bar, two rotor bars and ring of squirrel cage. The best features have been selected by using Method of Selection of Amplitudes of Frequencies-Ratio 15% (MSAF-RATIO15). The results obtained from three classifiers were good in classification accuracy (above 90%), which indicate that they have been able to protect other electrical rotating machinery.

3.5.3 Vibration Monitoring based on AI

The time-frequency domain analysis and neural network has been implemented and used in [111] for detecting rolling bearing faults based on vibration signal. In [112] the Short Time Fourier Transform (STFT) has been adopted for processing and analysing the vibration signal and use it as input for NN, then use analytical redundancy to train the model for motor fault detection. This system has used the spreading of vibration signal and its random nature for detecting the fault.

Chow et. al. [8] have used the NN approach for detecting the rolling bearing faults based on the vibration signal. The method has been simulated and experimentally tested. The results indicate that this system able to detect a range of motor faults based on the vibration signal. Furthermore, they have used the FFT in order to obtain the vibration spectrum, which has specific frequencies based on the defect. The maximum amplitude, mean and kurtosis parameters have been also considered in NN training model.

Jack and Nandi [113] have combined two AI techniques, which are genetic algorithm and ANN, in order to select the most important features for detecting the IM faults based on the estimation of vibration signal. A large set of vibration data has been collected and only six important features have been selected by genetic algorithm for fault identification. The result of classification accuracy was at 99.8%, which is good for detecting the fault correctly.

Wu and Chow [114] have developed the radial-basis function (RBF) of ANN for motor faults detection. Four features have been extracted from the power spectrum of the vibration signal and they used them as input for the developed system. These features are skewness, total average frequency and normalized of vibration signal. The

proposed system was used for electrical and mechanical faults at different speeds. For electrical fault, the inter-turn short circuit fault for the stator was injected by connecting an additional resistor across the phase to change the stator electromagnetic force. For mechanical fault, they have removed one of the screws that have been used for holding the motor. Consequently, the results indicate that the system is not only be able to detect the faults but also able to estimate the fault extension.

The Deep Learning approach has been developed for the purpose of learning the best features from the distributed frequency in the vibration signal relying on the Deep Belief Network (DBN) [115]. It has been built by using restricted Boltzmann machine and train it layer-by-layer (pre-training algorithm), which combine the extracted features with a well-known classification algorithm in order to detect the induction motor faults. The test results point out that this system able to model large dimensional data and learn the best representation of multiple layers. Accordingly, the classification accuracy has been improved and less training error has been obtained.

Patel and Giri [116] have used random forest classifier for induction motor bearing faults detection based on the vibration signal, which was collected by accelerometer sensor. The random forest classifier used the extracted features from the vibration signal. Four types of faults (normal, outer race, ball fault and inner raceway) have been generated and the results have been compared with neural network. The results indicate that the proposed classifier false prediction was only two out of 1600 dataset, while the neural network false prediction was 14 out of 1600 dataset.

Samanta [117] has studied the comparison of support vector machine and artificial neural network for detecting gear faults. In this study, two cases have been applied for the feature extraction: one was using GA for selecting the input features and the other

without GA. The obtained results with the use of GA-based selection have produced equal classification accuracy by using both SVM and ANN, but SVM produces higher classification accuracy than ANN without using GA-based selection.

Similarly in [118] GA-based selection has been applied for selecting the best input features and use them as input for different ANN classifier in order to detect the bearing faults using vibration signal. The outcomes show that the GA-based selection was very effective for increasing the ANN classification accuracy.

Satish and Sarma [119] have demonstrated the combination of two artificial intelligence techniques to create a cost effective and approach hybrid system of ANN and Fuzzy back propagation (Fuzzy-BP) for detecting and predict the medium and small bearing faults. This system has been built to overcome the individual disadvantages of each system. The results confirm that the proposed system was well suitable for bearing fault detection based on vibration signal.

Saimurugan et. al. [120] have considered two faults of rotating machinery, which are bearing and shaft based on the vibration signal. In this study, two types of SVM classification (cSVC and nuSVC) have been used for detecting both faults. In the same time the Decision Tree (DT) classifier has been used for selecting the best features to be used as input for four different kernel function types of SVM (linear, three degree polynomial, radial basis function (RBF) and Sigmund). The results indicate that the four different speeds of RBF in cSVC model produce better classification accuracy than nuSVC model.

Saravanan et. al. [121] have used a piezoelectric transducer for collecting the vibration data from the rotating machinery. In this study, Continuous Wavelet Transform (CWT) (multilevel 1 D wavelet decomposition) with Morlet wavelets have

been applied for extracting the important features from the vibration data, then decision tree J48 has been used for identifying and selecting the best features by using MATLAB software. The selected features were used as input to two different classification algorithms (Proximal Support Vector Machine (PSVM) and Artificial Neural Network (ANN)) by using “Weka” software. The results show that the Morlet wavelet and the decision tree J48 for extracting and selecting the features respectively, have the ability to increase the classification accuracy of PSVM and ANN algorithms, which was above 90%.

3.6 Common Softwares for IM Fault Detection

Many different softwares have been used for induction motor fault diagnosis, these softwares were able to be used in both traditional and artificial intelligence techniques. These softwares include: MATLAB software, LabVIEW software, ABAQUS software, COMSOL Multiphysics software, Ansys software, JMAG software, Solidwork software, Motor Monitor software, PAM software, COSMOS work software, Fault tolerance software, STRANDS7 software, Neural net. Software, Free Master software, Sim 20 software, Maxwell PC software, SAMCEF software and many others.

Having discussed how to construct an AI system for detecting and predicting the faults in induction motor, the final section of this chapter addresses ways of how data mining approach has been combined with the most well-known optimization algorithms in order to build a strong system for early fault detection.

3.7 Data Mining for Classification Task

The recent growth in IT infrastructure and data storage have made large volumes of data to become more readily available and affordable. However, raw data in itself has no value unless knowledge is extracted from it. One of the methods used for manipulating and customizing raw data is Data Mining (DM). DM is the most common method used for the classification, regression and clustering of large data. Three important categories in the data mining should be considered:

- a) Discovery: a process of searching in the entire database in order to find the hidden patterns without default preset.
- b) Predictive modelling: a process to discover patterns in the databases and employ them to predict the future.
- c) Forensic analysis: a process to apply the extracted patterns to find out unusual elements.

In data mining all statistical features such as standard deviation, variance, mean, etc. could be used to illustrate all related properties with a signal. Motor faults can be classified effectively by using these features. Obtaining information from the motor signal by using a suitable signal processing technique followed by a good technique of data mining, which plays a vital role in order to monitor the behaviour of induction motors. In addition to this, DM technique is able to improve the fault classification accuracy even in poor condition [122].

The modern techniques of fault classifications were used to avoid the limitations of the traditional methods because it does not need any previous knowledge about the induction motor parameters and it is capable to encompass a numerous range of motor

behaviour operations. These technologies motivate the researcher to improve an efficient memory based data driven approach for fault discrimination. Thus, by discovering a useful knowledge from thermal image, motor current or vibration signals in a different form is very important step to develop many algorithms.

Furthermore, rule discovery is one of the DM processes, which is commonly used by interdisciplinary fields, such as artificial intelligence, statistics, knowledge engineering and other domains [123]. The aim of classification rule discovery is to assign the given data to the most suitable class in the dataset. There are many factors that make classification rule discovery a challenging task. Firstly, the bigger the dataset the more complex the task of rule discovery and rule identification. Secondly, the noise in the data may lead to insufficient and irrelevant rule generation. Thirdly, in addition to others, the overfitting problem is difficult to overcome because it affects data classification [124]. Hence, an algorithmic approach is necessary to overcome these issues. As such, the evolutionary algorithm was very popular because of its use in DM [125], which includes many biologically-inspired algorithms used in DM, such as Genetic Algorithm (GA) [126], Particle Swarm Optimization (PSO) [127] and Ant Colony Optimization (ACO) [128].

3.7.1 Optimization Algorithms based on Data Mining for Classification Tasks

In the recent literature, many optimization approaches and algorithms have been developed and proposed in DM in order to solve several problems in the field of classification.

Traditional methods use different strategies for handling datasets, such as conquer and separate. Some algorithms have their own measurements for calculating the performance of the extracted rules upon the dataset. Nevertheless, most of those

algorithms produce a very long list of complex rules, and might have an overfitting issue depending on the dataset [129]. For instance, a GA has been applied in DM in order to carry out both tasks: feature selection and mining the data simultaneously by improving the chromosome structure [130]. A Support Vector Machine (SVM) has been used with fuzzy rules in order to extract fuzzy “IF-THEN” rules from the training dataset as the SVM provides the extraction mechanism for fuzzy rules [131]. In addition, A PSO algorithm has been used in DM, which is based on coordinated movement in bird flocks [127]. The use of PSO in DM was proposed by **Silva et al.** [132]. **Sarath and Ravi** [133] have developed a binary particle swarm optimization based on association rule miner and it has been applied for real bank dataset which produced good results compared to a Priori Algorithm (PA). Furthermore, ACO has been successfully applied for data classification for generating multiple rule sets, which is called AntMiner_{mbc} (AntMiner multiple-based classifiers) [134]. Correspondingly in [135] ACO has been developed for rule extraction and applied for acoustic emission for classification tasks. Another optimization algorithm which is Artificial Bees Colony (ABC) has been used in DM for classification tasks, which are based on the search dimension of the bees and best food source [136].

Most of the optimization algorithms were converted for the use of data classification through data mining rule discovery as mentioned above, but these algorithms still have problems with classification accuracy, validation accuracy and number of rules, which all play a vital role in data classification. Lately, researchers have considered combining two or three algorithms together in order to overcome the disadvantages of each algorithm and gain accurate rules for big data classification.

Up to now, the researchers have tended to focus on the Bees Algorithm (BA) (optimization algorithm) rather than other well known optimization algorithm, this is because it is different from other swarm intelligence methods since it merges neighbourhood search and random search together based on the natural bee swarms for finding the best food sources [137]. The BA has been effectively applied to a number of optimization problems and multi-objective optimization problems. Several studies have indicated that the BA has been used for many applications. For example, it has been successfully applied for feature selection with Multi-Layer Perceptron (MLP) whereby the combination features with the lowest classification error are selected. Moreover, many engineering problems have been solved by using the BA, such as machine shop scheduling [138], dynamic control problems [137], non-linear model identification [139], pattern classifier training [140] and robotic swarm coordination [141]. It has also been used successfully with slope angle and hill climbing algorithms with the aim of improving the performance of the BA for solving single machine scheduling [142].

Equally important, the BA has been applied for the identification of defects in wood veneer sheets [143]. In [144], a new version of BA was introduced by using pheromone as a new technique to recruit the bees in order to conduct the local and global random searches. It has been successfully applied for optimizing Fuzzy C-Mean (FCM) clustering [145]. Simultaneously, **Tapkan et al.** [146] have proposed a combination of BA with a cost-sensitive classification algorithm, known as BEE-Miner, for classification tasks. It achieved good results, relying on the misclassification cost and classification accuracy. However, the problem of the accuracy and the number of rules still exist when compared to other classification algorithms.

3.8 Previous Work Observations

As was pointed out in the literature review, the history of condition monitoring and fault diagnosis is as old as the induction motor itself. The induction motors have been initially relied on simple protection such as over-current and over-voltage to ensure safe operation. In spite of these tools, many companies are still faced unexpected system failures and reduced motor lifetime. Redundancy and conservative design techniques have been adopted for improving the reliability of induction motor drive systems against a variety of faults that could occur. However, these techniques are expensive to realize.

Condition monitoring is leading to incipient fault detection and prediction of induction motors, which has attracted many researchers in the past few years owing to its considerable influence on the safe operation of many industrial processes. Early detection, prediction and correct diagnosis of incipient faults could allow preventive maintenance to be performed and provide sufficient time for controlling the shutdown of product line. It could reduce the financial losses and avoid catastrophic consequences. As discussed above this topic could be treated under three headings: thermal, current and vibration monitoring. These methods have its own advantages and disadvantages, this is the reason of why that the thermal monitoring and vibration monitoring have been paid less attention than current monitoring. Previous studies of condition monitoring have not dealt with thermal monitoring and have paid less attention because of the thermal sensors, which are needed to access the motor performance such as thermocouples, resistance temperature detectors (RTD), winding thermostat and thermistor. It has been reported that the thermal monitoring was important because any overheating to the stator winding will decrease the motor coil

insulation life, which have effects on the motor resistance to either environmental or mechanical effects [147], [148].

Such approaches, however, have failed to address the induction motor faults without thermal monitoring technique. In one hand, recently, the researchers have used thermal cameras to monitor the rotating machinery and read the device temperature in healthy and faulty conditions without any access to the motor (contactless) based on the image processing technique to detect the motor faults. On the other hand, up to now, the research has tended to focus on the current monitoring (electrical monitoring) because it does not need to any additional sensors, as the current and voltage transformers are connected to the protection system at all times. Thus, the MCSA was very popular for monitoring the induction motor since it is non-intrusive detection (does not disconnect the electrical circuit), safe to operate (no contact between the motor and the current transformer) and remote sensing (current transformer could be place anywhere for monitoring) [9], [69], [149]–[152].

All the studies reviewed so far, however, suffer from the fact that MCSA is not appropriate for analysing the non-stationary signals. Another problem with this approach is that it fails to take the low signal to noise ratio into account, which makes the MCSA non-sensitive under certain conditions such as in inverter-fed motor as stated in [4], [147], [153], [154]. There would be therefore a definite need for vibration monitoring for mechanical faults detection because it allows different locations for sensors to be mounted on the motor, while MCSA relying on the radial rotor movement. Consequently, in case of bearing fault, the MCSA has difficulty in distinguishing non-drive-end or drive-end if two bearings have similar physical

Chapter 3: Literature Review

characteristics. Furthermore, the vibration signal has higher signal to noise ratio than the MCSA as shown in table 3-3 [155].

Table 3-3: Common differences between the vibration and current signals [152].

Fault type	VIB	MCSA
Electrical faults detection	×	√
Radial rotor movement analysis	×	√
Cheap installation	×	√
Able to apply in rough environment	×	√
Mechanical faults detection at early stage	√	×
Easy to distinguish between different bearings	√	×
Mean Time To Failure (MTTF)	√	×
Higher signal to noise ratio	√	×

Moving on to consider the AI techniques for induction motor faults detection based on data mining. As indicated previously, most of AI techniques such as (ANN, GA, NN and SVM) have been applied and validated successfully for diagnosing the motor faults with different classification accuracy. Although extensive research has been carried out on the use of AI for induction motor fault detection and prediction, no single study exist shows that there is one best technique for all kind of motors to diagnose the faults. This is because, the bigger the dataset the more complex task for classification, the noise in the data may lead to insufficient and irrelevant to original class, and the overfitting problem is difficult to overcome because it affects the classification system. Therefore, several studies have revealed that the development of induction motor fault detection based on AI techniques is still in its early stages. Consequently, despite that the considerable work have been done in this field, much more work are required to bring such techniques into the mainstream of induction motor fault diagnosis. Due to the limitations and strengths of these techniques, the findings from these studies suggest that the combinations of intelligence techniques

could have an effect on the developing on the rotating machinery condition monitoring for fault diagnosis scheme.

The previous sections have shown that many researches have been performed for IM fault detection by relying on the traditional methods and some AI techniques. Furthermore, the problem of IM fault still exists in many manufacturing applications. For that reason, the need for data mining algorithms are very important to detect and predict the fault before it happens based on the motor previous behaviour (data) in order to reduce the breakdowns of the electric machines.

Considering the aforementioned shortcomings of the methods that were used in motor condition monitoring, this research is aimed to address these disadvantages by presenting new classification technique. This technique is based on data mining rule discovery that are simple in algorithm design, and easy to apply for three kinds of condition monitoring technique, which are thermal, current and vibration monitoring, based on simple digital image and signal processing.

The next chapter describes the proposed hybrid approach by combing the Bees Algorithm and Data Mining methods that are used for condition monitoring in order to detect, classify and diagnose the induction motor faults at an early stage.

CHAPTER 4

PROPOSED BEE FOR MINING (B4M)

“In this chapter, the combination of the proposed methods Bees Algorithm and Data Mining for induction motor faults detection have been described and explained in details, so called Bee for Mining (B4M). The proposed method (B4M) has been tested and validated based on the UCI dataset and its performance has been compared with other well-known classifiers. The proposed method has been translated as a software code or toolbox package using MATLAB software version “R2015a””.

4.1 The Bees Algorithm (BA)

The Bees Algorithm is one of the most important types of swarm intelligence algorithm used to find the optimal solution inspired by honeybees' natural foraging behaviour. The BA will require from the user to set values for the parameters as described in table 4-1 before it can start to optimize the given problem.

Table 4-1: BA parameters.

Description	Symbol
Number of scout bees	n
Number of selected bees	m
Number of elite bees	e
Number of recruited bees for elite (e) sites	nep
Number of recruited bees for other best (m-e) sites	nsp
Neighbourhood size for each selected patch (local search)	ngh

First, in the search space, the basic BA begins with a number of scout bees arriving at random positions for global search or exploration. These bees will evaluate their positions and maximize the solutions to the problem by ranking them from the highest to the lowest according to their fitness value. The second stage is to select (m) best sites for local search or exploitation and abandon the remaining sites. Then the best of the best sites, which is called the elite sites (e), are chosen for intense exploitation. Further, the size of the neighbourhood search space is chosen for recruitment the bees, where fewer bees will be assigned for the non-elite sites (m-e), while more bees for the elite sites (e) in order to conduct the local search. Simultaneously, while the recruited bees are busy exploiting around the neighbourhood of the best solutions found so far, the global search will be carried out on the remaining sites where the

scout bees will be sent randomly [142]. This procedure will be repeated iteratively as shown in figure 4-1 until one of the following stopping criteria given below is met:

- a) A solution has been found, which is equal to real optimum value.
- b) The iteration number has reached the preset value.
- c) If there is no improvement over a preset number of iterations.

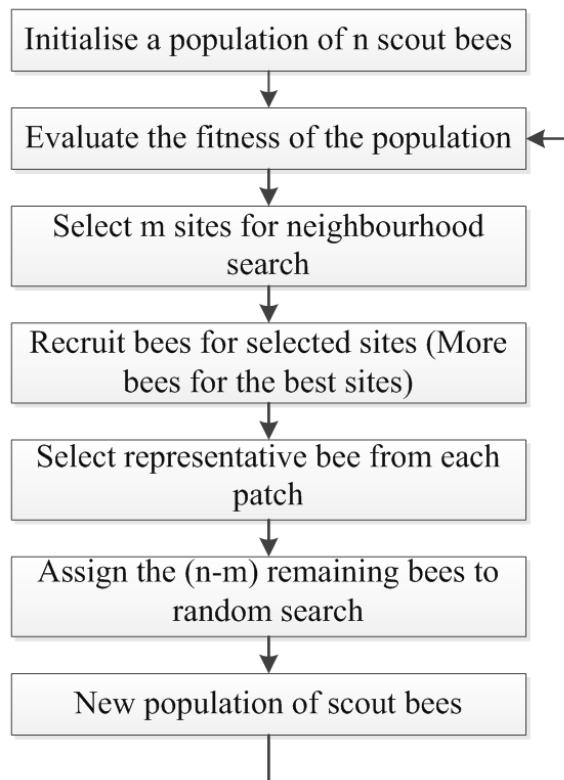


Figure 4-1: Basic BA flowchart.

Procedure and concept for the proposed Bee for Mining (B4M) will be introduced in the following sections.

4.2 Proposed Bee for Mining (B4M)

The Bees Algorithm which has been reconfigured in a novel way to enable it to act as a Data Mining (DM) tool and it is referred to as Bee for Mining (B4M) in this research.

The main thrust of B4M is its ability for rule discovery and rule pruning. The proposed B4M utilizes the basic Bees Algorithm within its process. Among other steps, the steps followed by the proposed B4M are as follows. When the rule discovery process is faced with an ambiguous situation, it will rely on the newly introduced parameters namely quality and coverage weight in the proposed B4M to overcome this issue, the details are graphically shown in figure 4-2. This has been done through a process of Meta-Pruning i.e., examining the discovered rules by referring to itself and measuring their contribution to the class assignment in terms of their quality and coverage before pruning. The main steps followed by the proposed B4M are summarised and described here below:

- 1) Data Pre-Processing.
- 2) Evaluation Function (fitness function).
- 3) Rule Format.
- 4) Rule Discovery and Extraction.
- 5) Rule Pruning.
- 6) Prediction Strategy.

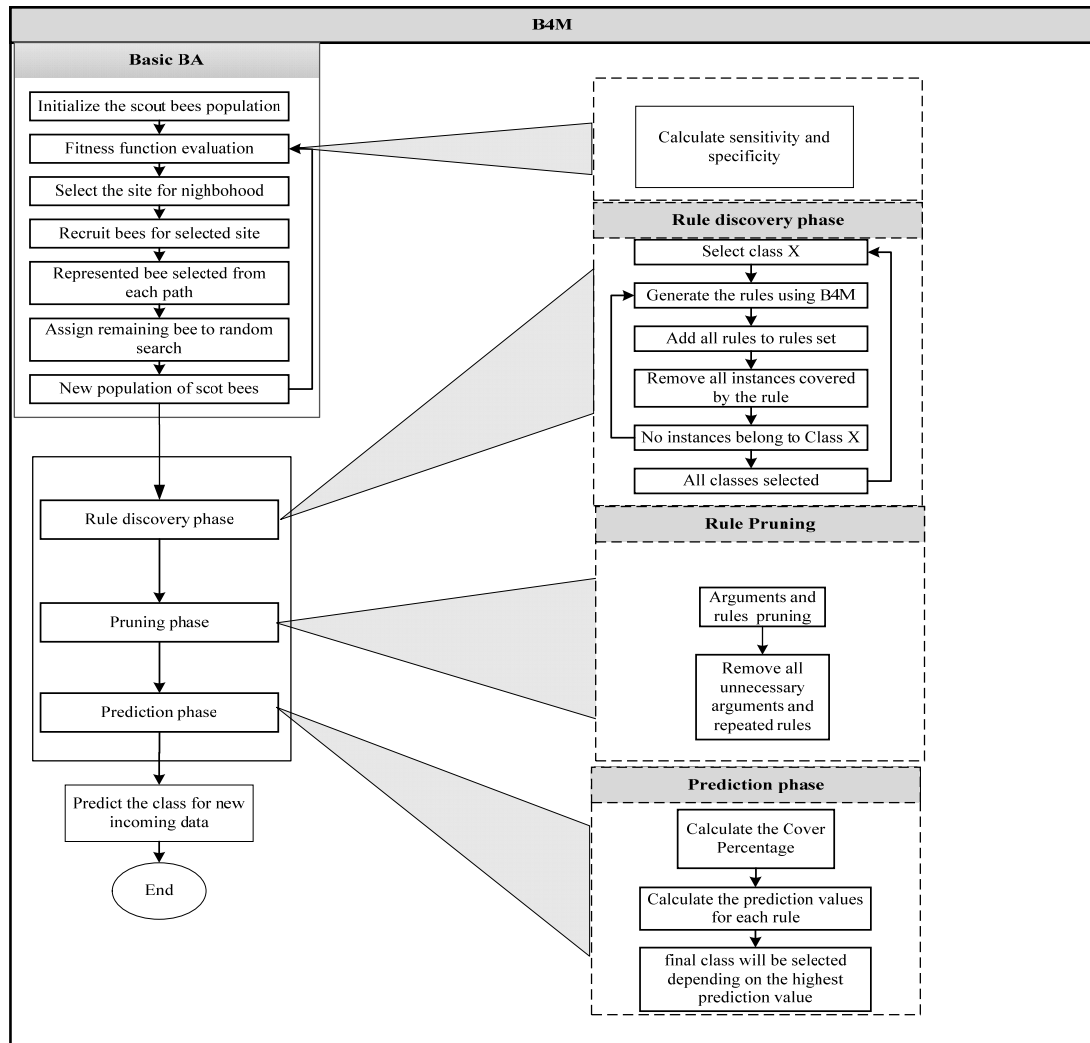


Figure 4-2: Proposed B4M flowchart.

4.2.1 Data Pre-Processing

In data pre-processing stage, there is a need to delete all non-coherent and incomplete data, since some data can confuse the algorithm when detecting the class based on the features provided. Otherwise, this can lead to having inaccurate classification rules (overlapping problem) for the new and unseen data presented for prediction and generalisation.

4.2.2 Evaluation Function (fitness function)

BA has been used to minimize the fitness function as the best and nearest food source, but in the classification task the fitness function will be used to evaluate the fitness value of the rules, as defined in the equation below [146]:

$$\text{Fitness function} = \text{Sensitivity} \times \text{Specificity} = \frac{TP}{(TP + FN)} \times \frac{TN}{(TN + FP)} \quad (4-1)$$

Where TP (True Positive): the records or datasets that have been covered by the rules and these rules have predicted their class correctly. FN (False Negative): the records that have not been covered by the rules, but the rules have predicted their class correctly. FP (False Positive): the records that have been covered by the rules and the rules have not predicted their class correctly and TN (True Negative): the records that have not been covered by the rules and the rules have not predicted their class correctly.

In addition, there are two important concepts that need to be considered in the rule discovery, as described below:

- a) The algorithm will measure and examine all data features. If the value of the feature is between the lower and the upper bounds then this feature is covered by the rule.
- b) If the class predicted by the rule is the same as the evaluated class then this indicates that this class has been predicted by the rule correctly.

4.2.3 Rule Format

The format of the classification rule has two parts namely antecedent and consequent as shown in table 4-2. The antecedent part deals with the condition and the consequent part deals with the outcome.

All datasets have their own features starting with feature 1 to feature N. Each feature or attribute has its own values, which are divided into two categories, the lowest value (Lower Bound) and the highest value (Upper Bound) for the rule. Furthermore, three important values related to the classification rule discovery namely fitness value, class prediction and cover percentage, which are described in the following section, should be taken into account.

Table 4-2: classification rule format.

Antecedent	Consequent
If $(X_j \leq U_{i-j})$ and $(X_j \geq L_{i-j})$	then class 'X'

4.2.4 Rule Discovery and Extraction

The most important part in the classification method is the rule set phase because it identifies the group of data into a specific class. Therefore, figure 4-3 shows the flowchart of B4M rule discovery procedure.

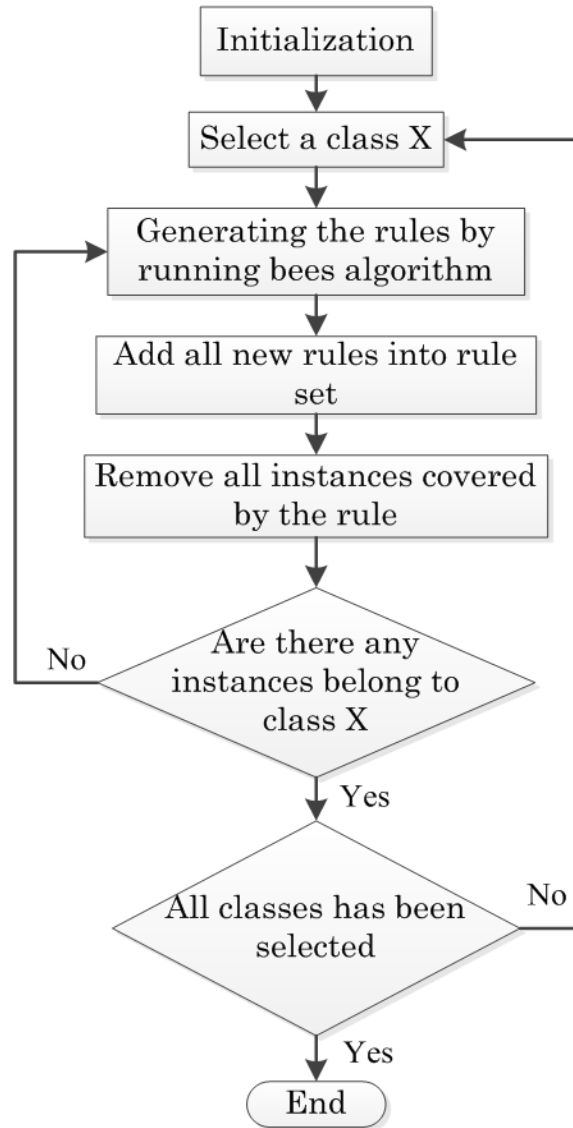


Figure 4-3: B4M rule discovery flowchart.

The values for all the attributes will be calculated and set in the dataset by using two equations as given below [156]:

$$\text{Lower Bound (LB)} = f - k_1 \times (f_{max} - f_{min}) \quad (4-2)$$

$$\text{Upper Bound (UB)} = f + k_2 \times (f_{max} - f_{min}) \quad (4-3)$$

Where k_1, k_2 are two different random numbers between 0 and 1 and f represents the original feature values. The f_{min} and f_{max} are the minimum and the maximum values of the attribute, which represent the range of the feature. k_1 , and k_2 have been created in order to discover the rules. LB and UB represent the lower and upper bound

respectively. The rules will be generated automatically for each class by using the classification rule-mining algorithm. This process will be repeated for each class until all instances that belong to that class are covered. Moreover, at the end of rule discovery process the rule set will have many rules, and each rule will abide by the rule structure.

4.2.5 Rule Pruning

This is where the redundant rules are removed. Once all the rule sets have been generated for each class, each rule will be subject to rule pruning. The main purpose of pruning rules is to remove all unwanted rules, which may affect the classification accuracy. Rule pruning helps the algorithm to increase the classification accuracy due to the removal of some dispensable attributes or rules which negatively affects the classification results. This process will keep running until the performance of the reduced rules set cannot be improved further. In this work, a “Meta-Pruning” process is followed where the discovered rules themselves are made subject to the rule pruning mechanism.

4.2.6 Prediction Strategy

After the pruning process, the obtained rules set can be used for predicting the class of new incoming data. If more than one rule lead to the same class then some strategies need to be applied in the prediction stage in order to be sure that the class has been predicted correctly. Here, three approaches to determine the correct class are proposed:

- 1) Cover all the test data, by calculating the prediction value for all the rules.
- 2) Gather all the predicted values in order to determine all possible classes for each attribute.

- 3) Select the final class based on the highest prediction value.

This strategy has further assisted by the following measures. The True Positive (TP) which is the records or datasets that have been covered by the rules and these rules have predicted their class correctly, and the rule coverage percentage is calculated as given below:

$$\text{Coverage Percentage} = \frac{TP}{N} \quad (4-4)$$

Where N represents the total value of the predicted class by the rules.

The function for the calculation of Prediction Value (PV) for each rule is computed by the equation below [157]:

$$\text{Prediction Value} = (\alpha \times rfv) + (\beta \times rcp) \quad (4-5)$$

$$0 < \text{Quality-weight} < 1, 0 < \text{Coverage-weight} < 1$$

Where rfv is the rule fitness value and rcp is the rule coverage percentage. While α ($\alpha \in [0, 1]$) represents the quality-weight and β ($\beta = (1-\alpha)$) represents the coverage-weight, are associated with rule fitness value and rule cover percentage respectively. These two values (α and β) applied on the discovered rules from the dataset to avoid any ambiguous situations during the prediction phase and making it suitable for any classification problem.

The main purpose of the prediction strategy is to balance the influence of coverage percentage and fitness value with respect to the prediction value, which determines the final predicted class. Furthermore, the value of α and β should be chosen carefully, because they have a big impact on the predicted classification accuracy. The proposed approach presented in this study is the development of a mechanism for data classification based on the swarm based optimization algorithm, which is the BA.

Figure 4-4 demonstrates a new classification procedure based on the BA. The first stage is data pre-processing, which includes deletion of all non-numerical and missing data. Step two, involves calculating the maximum and minimum values for each attribute and category followed by the evaluation of the fitness function for the rules. Then BA is applied to search for the best values (food sources). The BA will run iteratively forming new populations so that it will keep searching for the best data until it reaches the near optimum solution. After convergence, rules are generated for output data and are assigned to their class in order to cover all data instances. Finally, all instances which are not covered by the rules are removed and checked to see if any other classes are covered by the rules. In the following chapter, the proposed B4M will be tested on five different UCI datasets in order to examine its overall performance.

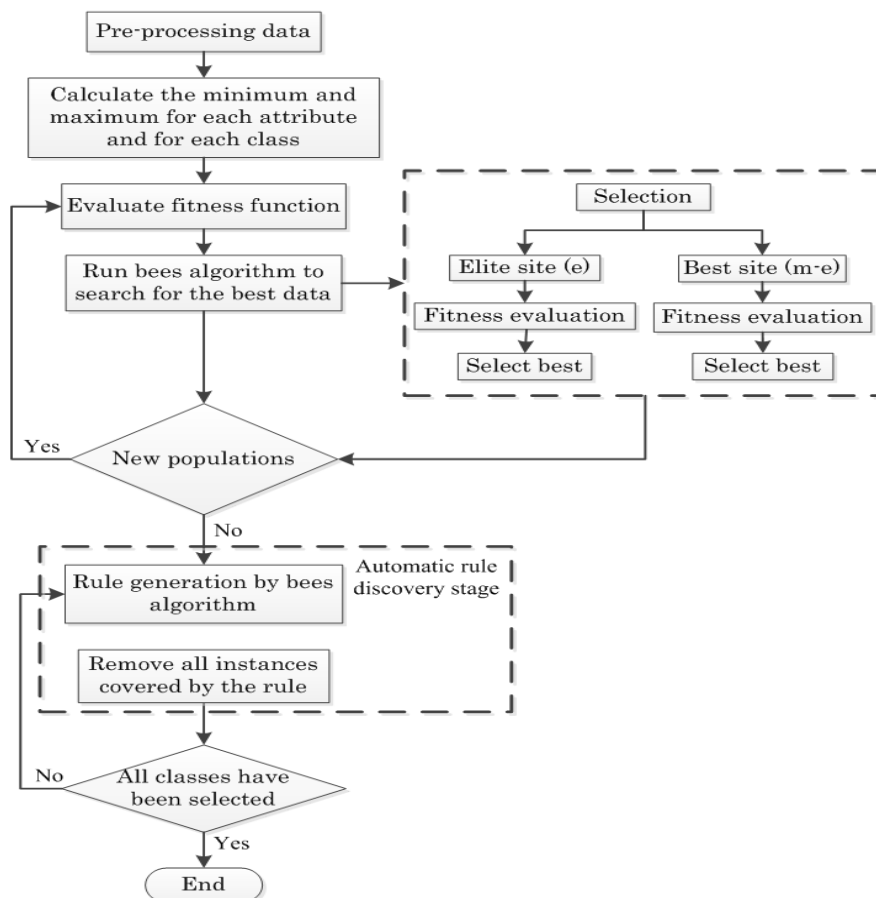


Figure 4-4: Classification procedure of proposed B4M.

4.3 Testing of B4M Performance on selected UCI Datasets

This section presents the test results obtained to show the performance of the proposed B4M algorithm on five selected UCI datasets in terms of its classification accuracy and its ability for rule discovery. Further, the proposed B4M has been compared with other classifiers such as C5.0, C4.5, Jrip and other evolutionary algorithms in order to show its strengths and weaknesses. The description of the datasets used in the test is given below.

4.3.1 Description of Datasets

The UCI datasets were used to evaluate and compare the performance of the proposed B4M algorithm. The UCI machine learning repository has about 351 datasets on its machine learning research group web page [158]. In this study, five datasets have been used namely Iris, Wine, Soybean, Breast Tissue and Image Segmentation in order to evaluate B4M performance[159]. The reason for choosing them is that all five datasets have different characteristics. For example, one has integer and real attributes, three have only real attributes, and one has categorical attributes with varying sample sizes and number of classes. This allows the proposed B4M to be tested if it is capable of dealing with different types of feature attributes similar to the real world datasets. Table 4-3 shows the characteristics of the five selected UCI datasets that were used to evaluate the B4M performance. In the following section the parameter values used in the B4M algorithm in three different trials and the test results are given.

Table 4-3: Five selected UCI dataset characteristics.

Dataset name	No. of samples	No. of attributes	Attribute type	No. of classes
Iris	150	4	Real	3
Wine	178	13	Integer, Real	3
Soybean	47	35	Categorical	4
Breast Tissue	106	10	Real	6
Image Segmentation	2310	19	Real	7

4.3.2 The B4M Parameters

The eight parameters used to study the performance of the proposed B4M algorithm are shown in table 4-4.

Table 4-4: B4M parameters.

Parameter	Value
n	500
m	20
e	10
n1	15
n2	30
Ngh	0.0234
Quality-weight	0.5
Coverage-weight	0.5

The tests were repeated three times by changing only the number of iterations from 500 to 1500 in steps of 500 (500: trial 1, 1000: trial 2, 1500: trial 3) in order to study their convergence. The number of iterations could be made higher than 1500 but this will have an effect on the processing time. Therefore, T-test and P-value were calculated between the three trials based on the overall classification accuracy achieved by the B4M. The three trials were compared statistically by evaluating each

pair 1-2, 1-3 and 2-3 respectively based on the average classification accuracy, as shown in table 4-5. In the T-test, all datasets have been chosen because they have different types of attributes and number of classes. The T-test results point out that there are statistically significant differences between these comparisons for some of the datasets. The results show that trial 3 outperformed trial 2 for the iris and soybean datasets because the P-values are lower than 0.05, while trial 2 outperformed trial 1 for the iris dataset, and trial 3 outperformed trial 1 for the soybean dataset only. Therefore, trial 3 has been selected for testing B4M on UCI datasets because it has two values lower than the threshold value (0.05).

Table 4-5: P-value for B4M parameters based on T-test.

Dataset	Trial 1-2	Trial 1-3	Trial 2-3
Iris	0.04	0.41	0.01
Wine	0.47	0.21	0.24
Soybean	0.32	0.05	0.04
Breast Tissue	0.34	0.41	0.30
Image Segmentation	0.31	0.46	0.31

4.3.3 The B4M Test Results

In testing the proposed B4M, 10-fold cross-validations have been used for each dataset to evaluate the performance by validating the predicted class. Two parameters namely quality-weight (α) and coverage-weight (β) required for class prediction should be set after generating the final rule set. During the B4M tests, these parameters were set to 0.5 empirically because it has been found that this value is the best for rule prediction, as explained in section 4.2.6. In addition, the ngh value was chosen in such a way to minimise the overlapping regions of the search space between the bees.

The proposed B4M method has been applied on five UCI datasets containing different numbers of classes (3, 3, 4, 6 and 7) to see its capability on handling multiple classes and its ability in assigning the unseen data to the correct class. After running 10-fold cross-validation, the test results were analysed statistically by calculating the average (mean) and standard deviation for the classification and validation accuracy. Table 4-6 shows the Classification Accuracy (CA) on the training data and Validation Accuracy (VA) on the unseen data with 10-fold cross-validation for all datasets. According to the results in table 4-6, the proposed B4M classification method was able to classify the data with an average classification accuracy (CA) ranging between 88.83% and 99.10%. In terms of validation, since the performance of the B4M not only depends on how well it can perform on the training dataset but also on the test dataset, the proposed B4M achieved an accuracy of 88.66% the highest for Iris dataset and 68.57% the lowest for the Image segmentation dataset. The results were assessed based on the classification accuracy on the training set and their validation accuracy on the test set. These results indicate that the proposed B4M was operating efficiently to predict the classes for the unseen data. In addition, table 4-6 shows that the B4M performance in terms of the average (mean) validation accuracy is the highest for Iris dataset and worst for the Image Segmentation. In terms of standard deviation obtained for validation accuracy the performance of B4M was the best for Soybean dataset and worst for Image Segmentation dataset because the Image Segmentation dataset was unclear and has unrecognized features between its classes.

Table 4-6: Classification and Validation Accuracy with 10-fold cross-validation using B4M.

No. of iteration	Iris		Wine		Soybean		Breast Tissue		Image Segmentation	
	CA%	VA%	CA%	VA%	CA%	VA%	CA%	VA%	CA%	VA%
1	97.67	93.33	99.26	61.11	98.55	75.00	91.38	58.33	98.97	33.33
2	98.44	100.00	98.54	77.77	99.63	75.00	89.66	66.66	96.06	76.19
3	98.45	73.33	99.25	83.33	99.85	75.00	88.14	58.33	97.83	71.42
4	97.69	80.00	98.41	88.88	98.61	87.50	89.47	75.00	98.94	90.47
5	97.67	86.66	99.25	61.11	99.65	75.00	87.93	75.00	97.89	85.71
6	99.22	86.66	99.90	83.33	97.79	87.50	92.25	91.66	94.61	66.66
7	98.45	93.33	98.51	61.11	98.85	75.00	89.66	58.33	93.48	66.66
8	96.18	93.33	98.51	72.22	98.69	62.50	86.21	91.66	94.74	42.86
9	96.92	93.33	99.92	100.00	99.61	75.00	88.33	58.33	97.89	80.95
10	96.92	86.66	99.24	55.55	99.74	75.00	85.25	75.00	93.99	71.42
Average	97.76	88.66	99.08	74.44	99.10	76.25	88.83	70.83	96.44	68.57
STD	0.91	7.73	0.57	14.63	0.69	7.10	2.14	13.18	2.11	17.98

CA = Classification Accuracy VA = Validation Accuracy

After applying the proposed B4M for all UCI datasets, the validation accuracy has been compared with and without quality-weight (α) and coverage-weight (β) as shown in figure 4-5. It can be seen that the inclusion of quality-weight and coverage-weight resulted in an increase in the validation accuracy because it produced accurate rules to predict the correct class for new unseen data.

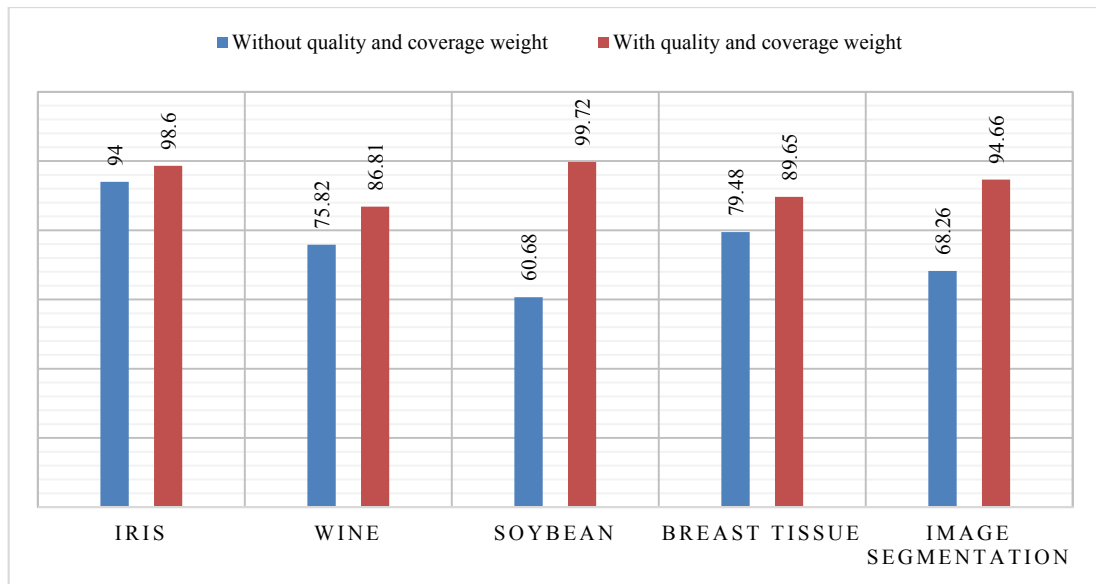


Figure 4-5: Comparison of classification accuracy (X - different methods; Y - % classification accuracy) achieved by B4M with other methods for five UCI datasets.

4.4 Comparison of B4M with Other Algorithms

A comparison was carried out between the B4M performance and other classification methods such as C5.0, C4.5, Jrip, REGAL, PART, ATM, cAnt-Miner, BEE-Miner, CART and CN2 based on the average classification accuracy (given as a %) and the average number of rules (given as a real number). The average classification accuracy and the average number of rules discovered by different classification methods for the five UCI datasets are presented in table 4-7. All the algorithms including B4M have been tested using 10-fold cross-validation method. It is clear from the table that the proposed B4M classification accuracy is better than other classification algorithms for four out of five UCI benchmark datasets. In addition, the proposed B4M classification achieved higher accuracy for Wine, Soybean, Breast Tissue and Image Segmentation in terms of classification accuracy and number of rules. However, the performance of B4M is lower than REGAL [160] and it is in the second place in terms of classification accuracy for the Iris dataset, but in terms of the number of rules, it was higher than

REGAL and others. The results show that B4M has the ability to generate less number of rules with higher classification accuracy.

Table 4-7: Comparison the results of B4M with other classification algorithms.

Compared algorithms	Iris		Wine		Soybean		Breast Tissue		Image Segmentation	
	CA%	No.of rules	CA%	No.of rules	CA%	No.of rules	CA%	No.of rules	CA%	No. of rules
C5.0 [161]	92.00	5.00	*	*	93.40	32.00	*	*	96.3	10.05
C4.5 [162], [163]	95.32	6.20	91.03	8.90	85.60	55.90	66.16	19.40	*	*
Jrip [162], [164]	96.00	3.00	92.68	5.40	*	*	60.18	7.50	94.58	17.20
REGAL[160]	99.00	11.00	97.00	60.00	*	*	*	*	*	*
PART [162], [164]	93.33	3.80	91.54	5.20	91.40	20.60	64.36	21.80	95.61	27.90
ATM [163]	96.20	4.20	95.15	5.60	87.40	50.00	65.20	12.00	*	*
cAnt-Miner _{PB} [162]	93.24	4.92	93.57	4.75	80.00	22.30	67.10	6.55	*	*
cAnt-Miner [164]	94.21	4.00	91.38	4.10	*	*	*	*	93.72	12.22
μ cAnt-Miner [164]	95.65	8.40	93.82	4.07	*	*	*	*	94.64	16.13
BEE-Miner [146]	90.22	5.76	96.08	3.13	*	*	*	*	*	*
CART [163]	93.90	4.40	93.30	5.50	87.60	35.40	64.70	7.80	*	*
CN2 [162], [165]	94.66	9.50	94.96	7.90	97.30	18.80	75.35	23.60	*	*
PSO/ACO [166]	94.67	3.00	*	*	87.01	24.20	*	*	*	*
B4M	97.76	3.00	99.08	3.10	99.10	4.60	88.83	6.10	96.44	7.60

CA = Classification Accuracy VA = Validation Accuracy

*: Data is not available.

Figure 4-6 and figure 4-7 show the average classification accuracy and average number of rules achieved by different methods for the five UCI datasets. It can be clearly seen that the proposed B4M has above average performance in terms of classification accuracy and the number of rules in four out of five datasets. However,

the processing time for all the applied algorithms have been not considered as the other algorithms have been taken from the references and it is difficult to be calculated, but the proposed algorithms have taken less than 60 seconds to detect the motor faults which is also depends on the how large is the dataset. Consequently, the results have proved that the proposed B4M is able to handle the classification data successfully and obtain equally good results if not better when compared with other classification algorithms.

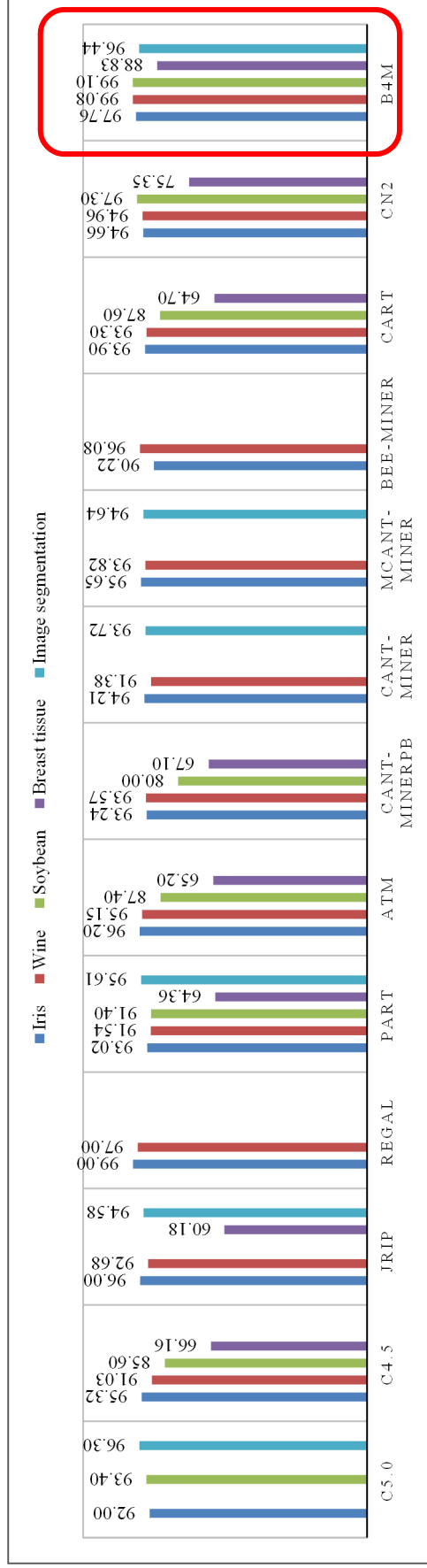


Figure 4-6: Comparison of classification accuracy (%) for five UCI datasets.

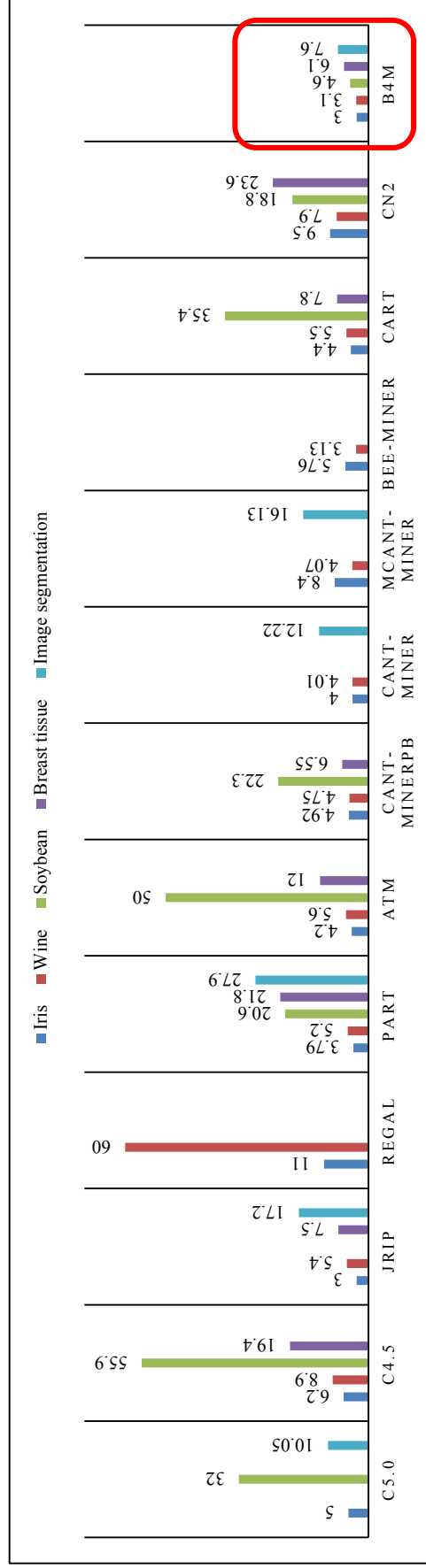


Figure 4-7: Compression of average rules number for five UCI datasets.

CHAPTER 5

PROPOSED METHODS FOR DATA PRE-PROCESSING AND FEATURE SELECTION

“In this chapter, the proposed methods of induction motor data pre-processing have been described and explained in detail. The proposed feature extraction methods from the thermal image have been described. Afterward, Wavelet Transform has been also explained and how it is applied to the thermal image, current and vibration signals. Finally, the feature selection methods have also been described and explained in detail. These methods have been translated as a software code or toolbox package using MATLAB software version “R2015a””.

5.1 HSV Colour Model

The Hue-Saturation-Value (HSV) colour model is defined as how the human eyes senses colours. It also known as Hue-Saturation-Brightness (HSB), Hue-Saturation-Lightness/luminance (HSL), and Hue-Saturation-Intensity (HSI). The following formulae have been used to convert RGB image into HSV colour model in terms of three components as stated below:

❖ In Terms of Hue:

It represents the colour types. Hue value could be calculated from the red, green and blue colours by measuring the distance from its arise. The colour was described as angle degree between ($0^\circ - 360^\circ$) in Hue. As shown in table 5-1, $0^\circ - 60^\circ$ for red colour, $60^\circ - 120^\circ$ for yellow and $120^\circ - 180^\circ$ for green, and so on. Hue region is very helpful for detection the hottest region because it works opposite with saturation as it is less meaningful when the saturation is 0 or when intensity is 0 or 1, and more meaningful when the saturation is 1. Consequently, Hue region has been used for further processing for motor fault detection.

Table 5-1: HSV colour space distribution.

Angle	$0^\circ - 60^\circ$	$60^\circ - 120^\circ$	$120^\circ - 180^\circ$	$180^\circ - 240^\circ$	$240^\circ - 300^\circ$	$300^\circ - 360^\circ$
Colour	Red	Yellow	Green	Cyan	Blue	Magenta

The formula of calculating the Hue value is explained below:

$$H = \begin{cases} 0 & \text{if } B \leq G \\ 360 - \theta & \text{if } B > G \end{cases}$$

R: Red, G: Green, B: Blue

$$\theta = \cos^{-1} \left\{ \frac{\frac{1}{2}[(R-G) + (R-B)]}{\sqrt{[(R-G)^2 + (R-B)(G-B)]^2}} \right\} \quad (5-1)$$

❖ In Terms of Saturation:

The colour range is from 0 to 100%. It also known as purity. The faded colour and greyness have been appeared when the saturation value is low. Thus, the range of the greyness is from 0 to 1, if the value is '0' the colour is grey, while the colour is primary colour (white colour) if the value is '1'. In addition, the higher the faded the greyer colour based on the following formula (S : saturation):

$$S = 1 - \frac{3}{(R+G+B)} [\min(R, G, B)] \quad (5-2)$$

❖ In Terms of Value:

The value represents the color brightness, which varies based on the saturation. The value ranges are between 0 - 100%. The colour is black when the value is '0', and the colour brightness will be change and show varies color when the value increases based on the following formula:

$$I = \frac{1}{3} (R + G + B) \quad (5-3)$$

Generally, RGB colour has been widely used in the optical instruments and digital images. However, RGB is not sensitive and helpful to statistical analysis and human visual. Consequently, the non-linear transformation of HSV or HSI from RGB colour provides important information with more accuracy than the RGB colour. As results, it has been decided to use it for processing and analyzing the thermal image of

induction motors in order to extract the best and accurate colour information for fault classification.

5.2 Image Segmentation

Image segmentation is a process of partitioning image into several or multiple segments (sets of pixels). Basically, the result of image segmentation are set of pixels that may have similar characteristics such as texture, colour, or intensity. It has three different approaches for image segmentation:

- a) Finding the thresholds based on the pixel properties distribution, which is counted as a simplest way for image segmentation. This technique has been applied onto the image pixel intensity value. Thus, it converts the digital image into binary image for further processing.
- b) Finding the boundaries between all the regions by relying on the discontinuities in intensity level. The image has been divided into sub-regions based on the method rules such as all the image pixels must have the same gray level if it is in one region. Furthermore, it relies on the neighbouring pixels clustering, which sometimes referred as region according to their functional and anatomical roles.
- c) Finding the regions directly for any abrupt changes in the intensity value. It is known as edge or boundary based method. Generally, edge detection methods have been used for finding the discontinuities in gray level.

Accordingly, image segmentation technique should be chosen based on the problem that needs to be segmented. The next section will discuss most common edge detection techniques that have been used in this research for image segmentation.

5.2.1 Image Segmentation based on Edge Detection

The edge detection methods of an image reduce the image data quantity to be processed and contain essential information regarding the object shape in the scene. They have been able to extract the exact edge line for all object in the image with good orientation as well as more literature about these techniques are available and applied in many applications such as biometrics, medical image processing, security, monitoring the electrical devices and many others. However, there is no study indicates and judges the performance of these techniques because all the judgment that have been done by authors are always separately based on their applications.

Several methods such as “Sobel”, “Prewitte”, “Roberts”, “Canny”, “LoG” and “Otsu” have been used for finding and extracting the hottest region from the thermal images by calculating the gradient based edge detection. The following sub-sections will review these techniques briefly.

5.2.1.1 Sobel Edge Detection

The Sobel edge detection method was introduced by Sobel in 1970 [167]. It proceeds the edge at those points where the gradients are higher. The gradient (∇f) is the differences between the columns and rows of neighbourhood 3x3 which is calculated by Sobel operators, table 5-2 below shows the center pixel in each column and raw [168].

Table 5-2: Image neighbourhood (center pixel).

Z1	Z2	Z3
Z4	Z5	Z6
Z7	Z8	Z9

$$\nabla f = \sqrt{S_x^2 + S_y^2} \quad (5-4)$$

Where S_x & S_y are Sobel operators in the X and Y- axis respectively.

Masks for S_x and S_y direction in Sobel operators as shown in table 5-3 and table 5-4

Table 5-3: Masks for S_x direction.

-1	-2	-1
0	0	0
1	2	1

Table 5-4: Masks for S_y direction.

-1	0	1
-2	0	2
-1	0	1

5.2.1.2 Prewitt Edge Detection

The Prewitt edge detection has proposed by Prewitt in 1970 as well [167]. It estimates the magnitude and orientation of image object edge. It is limited to eight possible directions. Nevertheless, the result shows that the most direction estimates are not perfect than the first 8. The gradient-based edge detector is estimated in the 3*3 neighbourhood for 8 directions as shown in table 5-5 and table 5-6. Thus, if all the eight convolution masks are calculated, one of the masks will be selected for data processing.

Table 5-5: Masks for S_x direction.

-1	-1	-1
0	0	0
1	1	1

Table 5-6: Masks for S_y direction.

-1	0	1
-1	0	1
-1	0	1

Prewitt edge detection technique is slightly simple to implement than the Sobel detection, but it tends to produce somewhat noisier results.

5.2.1.3 Roberts Edge Detection

Lawrence Roberts introduced the Roberts edge detection method in 1965 [169]. It performs a simple, quick to compute, 2-D spatial gradient measurements to the image. Each point of the output image represents the estimated absolute magnitude of the spatial gradient of the input image at that point. In case of 2*2 gradient operator as shown in table 5-7 and table 5-8, Roberts operator has been used for calculating the difference between adjacent pixels.

Table 5-7: Masks for S_x direction in Roberts operators.

-1	0
0	1

Table 5-8: Masks for S_y direction in Robert's operators.

0	-1
1	0

5.2.1.4 Canny Edge Detection

Canny edge detection is considered as multi-step method that can detect all object edge in the image with noise reduction [170], as shown in the following steps:

5.2.1.4.1 Noise Reduction

Gaussian filter has been applied to reduce the noise and unwanted details in the image based on the following equation:

$$g(m,n) = G_{\sigma}(m,n) * f(m,n) \quad (5-5)$$

Where $g(m, n)$ is the gradient operators, $G_\sigma(m, n)$ is the Gaussian filter, σ is the standard deviation and $f(m, n)$ is the adaptive filter.

Where the G_σ is computed by:

$$G_\sigma = \frac{1}{\sqrt{2\pi\sigma^2}} \exp\left(-\frac{m^2+n^2}{2\sigma^2}\right) \quad (5-6)$$

5.2.1.4.2 The Gradient Computation

The gradient magnitude and direction have been calculated at every single point based on the Sobel kernel for both directions vertical (G_y) and horizontal (G_x). The gradient can be calculated for each pixel from two images as follows:

$$\text{Edge Gradient } (G) = \sqrt{G_x^2 + G_y^2} \quad (5-7)$$

$$\text{Angle } (\theta) = \tan^{-1}\left(\frac{G_y}{G_x}\right) \quad (5-8)$$

Where G_x and G_y are the derivatives directions of X and Y points.

In this step, two cases have been considered for gradient: the first is high gradient, which means that there is a significant change in the colour (implying edge), and the second is low gradient, which means that there is no substantial change (no edge). It is rounded into four angles, which are two diagonal directions, horizontal and vertical.

5.2.1.4.3 Non-Maximum Suppression

In this step, full scanning for the image will be done to remove any unwanted pixels that may not constitute as edge. Every pixel will be checked, whether it is a local maximum or not. If it is not a local maximum, the pixel will be set to zero, otherwise it will be considered as edge. Consequently, at the end, the results will be a binary image with a thin edge. As illustrated in the following example in figure 5-1:

The edge on the point A is in a vertical direction and the gradient direction as normal, which is point B. Therefore, point A will be checked, if it is in local maximum, it will be considered as edge, otherwise, it will be considered as suppressed and set to zero.

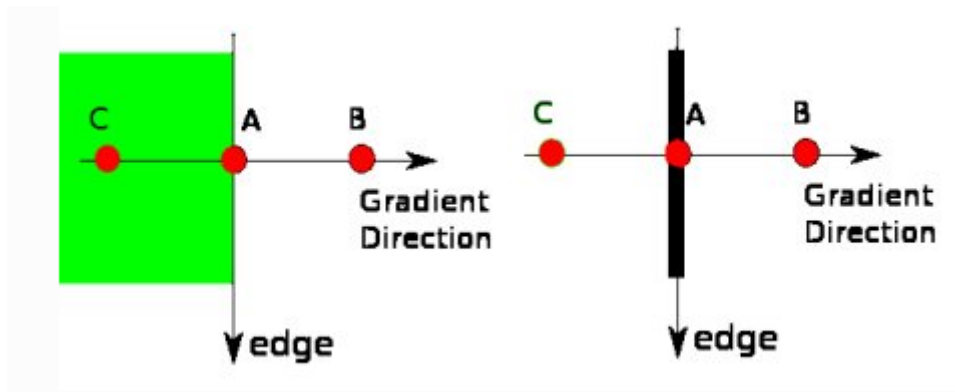


Figure 5-1: How to detect the edge by non-maximum suppression.

5.2.1.4.4 Hysteresis Thresholding

In this stage, the decision will be made to all pixels to be really edge or not. In this case, two values for thresholding is needed, \maxVal and \minVal . Any values of edges with the intensity gradient less than \minVal are non-edge (discarded) and those with more than \maxVal are edge. The values that are lie between these two values, they will be checked based on the connectivity to decide either it is an edge or not. If they are connected to non-edge pixels, they will be considered as not edge. Otherwise, they will be considered as edge.

Unlike Sobel and Roberts, the Canny edge detection is not very susceptible to noise, if Canny detector worked well it would be superior.

5.2.1.5 LoG Edge Detection

Laplacian of Gaussian (LoG) has been proposed by Marr (1982) [171]. It is a second order of derivative. LoG has two important effects; it smooths the image and computes

the laplacian, which yields a double edge image and locates the edges and finding the zero crossings between the double edges. The following masks have been used for implementing the laplacian function as shown in table 5-9 and table 5-10.

Table 5-9: Masks for G_x direction in Log.

0	-1	0
-1	4	-1
0	-1	0

Table 5-10: Masks for G_y direction in LoG.

-1	-1	-1
-1	8	-1
-1	-1	-1

The LoG has been used for finding the pixel of an edge whether it is on dark or on light side.

5.2.1.6 Otsu Method

This method has been widely applied for thermal image processing in order to detect the hot regions. It is automatically perform clustering based on image threshold. Every image has two classes of pixels, and then it separates these classes by calculating the optimum threshold with the aim of minimal into the intra-class variance. Four important steps need to be followed in this method to obtain the Otsu image, which are explained below [172]:

- 1) Select average value of image intensity (estimated threshold).
- 2) Divide the image into two regions R_1 and R_2 , and then calculate the mean μ_1 and μ_2 values for each region.

- 3) Select a new threshold

$$T = \frac{1}{2} (\mu_1 + \mu_2) \quad (5-9)$$

- 4) Repeat steps 2-4 until μ_1 and μ_2 values do not change.

All the proposed edges detection methods above have been used for extracting the hottest region from the thermal image in order to have the exact and best hotspot in the induction motor thermal image. In addition, the results that are obtained from the edge detection methods have been used for extracting the best image metrics such as mean, mean square error and peak signal to noise ratio, variance, standard deviation, skewness and kurtosis with the purpose of using them in classification algorithms by assigning them to proper class. The following section describes and discusses the image metrics based on the edge detection results.

5.3 Image Metrics

After implementing all edge detection techniques for thermal images, the most common image metrics have been applied in order to extract the best features that could be used for distinguishing between the motor faults. The most common and widely image metrics used is Mean (μ), Mean Square Error (MSE) and Peak Signal to Noise Ratio (PSNR), Variance (V), Standard Deviation (SD), Skewness (S) and Kurtosis (K). as described below [173][174]:

a) Mean (μ)

The mean is a most basic of all statistical measures. The mean has been widely used in geometry and analysis, a wide range of means have been developed for these purposes. In context of image processing filtering using mean is classified as spatial filtering and used for noise reduction. It also calculates the average

values and extract the brightness information from the image. Many types of means have been discussed in [171] such as arithmetic mean, geometric mean, harmonic mean and contra-harmonic mean. All these previous means have been relied on the arithmetic mean for reducing the image noise, which could be calculated by the equation below [171]:

$$\mu = \frac{1}{mn} \sum_{(r,c) \in W} g(r, c) \quad (5-10)$$

Where g is the noisy image, r, c is the row and column coordinates respectively, within the size of $m * n$ of image (W).

b) Mean Square Error (MSE) & Peak Signal to Noise Ratio (PSNR),

MSR is measure the differences between the reference image pixel and threshold image based on the average of the square intensity. PSNR value is relying on the MSE value as shown in the following formulae:

$$MSE = \frac{1}{MN} \sum_{i=1}^N \sum_{j=1}^M (x(i, j) - y(i, j))^2 \quad (5-11)$$

Where $x(i, j)$ is the reference image, $y(i, j)$ is the threshold image, N and M is the height and width of reference image respectively.

$$PSNR = 10 \log_{10} \frac{(2^n - 1)^2}{\sqrt{MSE}} \quad (5-12)$$

c) Variance

It measures of how far a set of numbers is spread out [175]. It is one of the several descriptors of a probability distribution, which describes how far the numbers lie from the mean. Particularly, the variance is one of the distribution moments and it is part of systematic approach to distinguish between

probability distributions. In image processing, it can be utilized to determine the edge position. Mathematically variance is given by:

$$\sigma^2 = \frac{1}{mn-1} \sum_{(r,c) \in W} \left(g(r,c) - \frac{1}{mn-1} \sum_{(r,c) \in W} g(r,c) \right)^2 \quad (5-13)$$

d) Standard Deviation (SD)

It has been widely used statistically for measuring variability or diversity. In terms of image processing, it shows how much variation/disruption exists from the average (mean). In case of low standard deviation the data point tend to be very close to the mean, while in case of high standard deviation, the data points spread out over the range of values. Consequently, the standard deviation could be mathematically calculated by using the following formula:

$$\sigma_g = \sqrt{\frac{1}{mn-1} \sum_{(r,c) \in W} \left(g(r,c) - \frac{1}{mn-1} \sum_{(r,c) \in W} g(r,c) \right)^2} \quad (5-14)$$

By using standard deviation filter, it may be able to recognize some important patterns. Therefore, this study will apply the standard deviation for induction motor thermal image for extracting the best image features.

e) Skewness

It measures the asymmetry, or more precisely, the lack of symmetry. A distribution, or data set, is symmetric if it looks the same to the right and left of the centre [176]. It can be positive, negative or undefined [177]. Qualitatively, a positive value indicates that the tail on the right side is longer than the left side and the bulk of the values lie to the left of the mean. However, a negative value indicates that the tail on the left side of the probability density function is longer than the right side and the bulk of the values lies to right of

the mean, and the zero value (undefined) indicates that the values have been distributed on both sides of the mean, which is defined as:

$$S = \frac{\frac{1}{mn-1} \sum_{(r,c) \in W} \left(\frac{1}{mn-1} \sum_{(r,c) \in W} (g(r,c) - \frac{1}{mn-1} \sum_{(r,c) \in W} g(r,c)) \right)^3}{\left(\frac{1}{mn-1} \sum_{(r,c) \in W} \left(\frac{1}{mn-1} \sum_{(r,c) \in W} (g(r,c) - \frac{1}{mn-1} \sum_{(r,c) \in W} g(r,c)) \right)^2 \right)^{\frac{3}{2}}} \quad (5-15)$$

In image processing, the darker and the glossier surfaces tend to be more positively skewed than the lighter and matt surfaces. Thus, the skewness have been used for making judgments between the image surfaces.

f) Kurtosis

It calculates ratio of the four central moment of distribution. In other word, it measures whether the data are heavy or light tailed relative to the distribution [176], [178]. Thus, the data set with high Kurtosis tend to have heavy tails, or outliers, and if the data with low kurtosis tend to have light tails or lack of outliers as defend below:

$$K = \frac{\frac{1}{mn-1} \sum_{(r,c) \in W} \left(\frac{1}{mn-1} \sum_{(r,c) \in W} (g(r,c) - \frac{1}{mn-1} \sum_{(r,c) \in W} g(r,c)) \right)^4}{\left(\frac{1}{mn-1} \sum_{(r,c) \in W} \left(\frac{1}{mn-1} \sum_{(r,c) \in W} (g(r,c) - \frac{1}{mn-1} \sum_{(r,c) \in W} g(r,c)) \right)^2 \right)^2} \quad (5-16)$$

In digital image processing, Kurtosis are interpreted in combination with noise and resolution measurement. High Kurtosis goes hand in hand with low noise and resolution.

The previous sections have discussed that the image metrics are very important for extracting the important image features, and they are very helpful for distinguishing the important differences between the images (healthy thermal image and faulty thermal image). Thus, these metrics have been adopted in this research for classifying

the IM faults, as they are easy and fast to be calculated by using “MATLAB R2015b” software for coding and organise them as “Excel” file sheet in order to be used as input data for the classification algorithms. Figure 5-2 illustrates the procedure of thermal image processing.

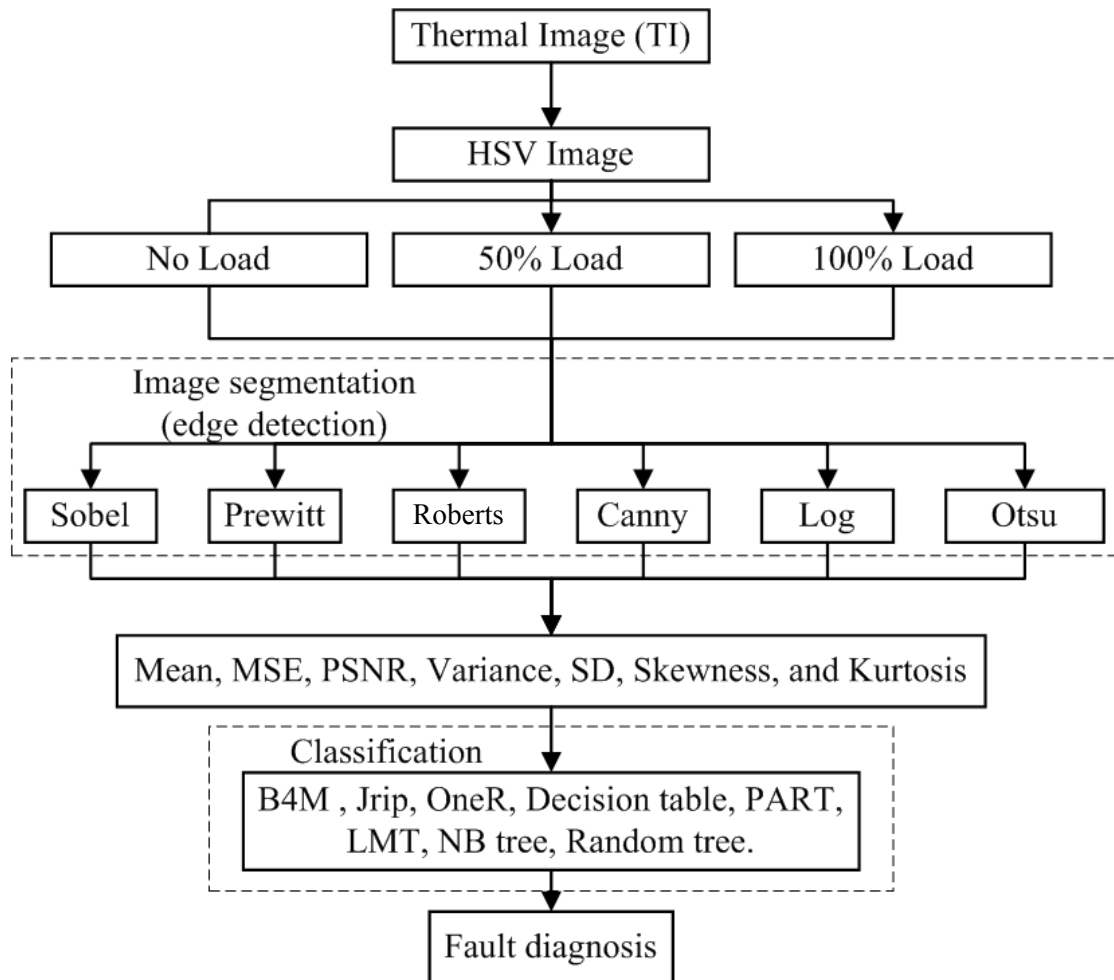


Figure 5-2: Thermal image processing diagram.

The structure and functions of Wavelet Transform (WT) will be explained in the following section, which has been also adopted as an image and signal processing for all induction motor thermal images in addition with the image metrics and for processing the current and vibration signals.

5.4 Wavelet Transform for Thermal Image, Current and Vibration Signals

Over the past ten years, there has been a significant increase in the use of wavelet transform for signal decomposition. The novel concept of wavelet was first put forward by Morlet in 1984. However, at that time, Morlet faced much criticism from his colleagues. Later, with the help of Grossman, Morlet has formalised the Continuous Wavelet Transform (CWT). In 1985, Meyer constructed a beautiful orthogonal wavelet base with good time and frequency localization properties. The year after, Meyer and Mallat have developed the idea of multiresolution analysis (MRA), which makes it easy for constructing other orthogonal wavelet basis. Before long, Daubechies proposed an orthogonal wavelet bases in a simple and ingenious way. Furthermore, he has done many researches based on the wavelet analysis frames in order to allow more liberty in the choice of wavelet basis at a little expenses of some redundancy.

In the wavelet transformation there are number of basis functions that can be used as a wavelet mother (wavelet function). It determines the wavelet transform results because it produces all wavelet functions that are used for translating and scaling the signals. It could be classified into two fundamental classes: orthogonal and bi-orthogonal as explained briefly below:

a) Orthogonal Wavelet

The coefficient of this filter are real numbers. It has the same length and not symmetric. The low pass filter, G_0 and the high pass filter H_0 are related to each other. These filters are alternated flip of each other. It automatically gives double shift orthogonality between the low and high pass filters. The possibility of obtaining perfect reconstruction could be done by alternating

flip. In addition, orthogonal filters offer high number of vanishing moments, which make them useful for signal and image processing applications.

b) Bi-orthogonal Wavelet

In this case, the low and high pass filters do not have the same length as in the orthogonal filters. The low pass filter is always symmetric, while the high pass filter could be either symmetric or asymmetric. It produces two kinds of coefficient either integer or real numbers. Furthermore, for obtaining perfect reconstruction from the signal, the bi-orthogonal filter bank has all odd length or all even length filters. These two analysis filters could be one symmetric and other one asymmetric with even length, and only symmetric with odd length.

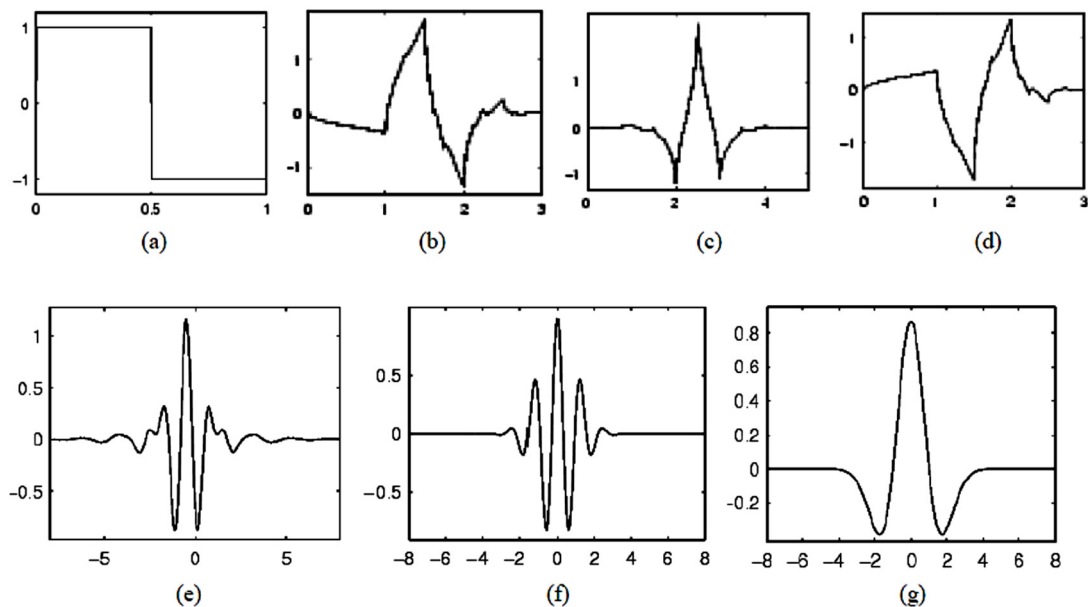


Figure 5-3: Wavelet families (a) Harr, (b) Daubechies, (c) Coiflet, (d) Symlet, (e) Meyer, (f) Morlet, (g) Mexican Hat [179].

Consequently, the details of particular application should be taken into account and choose the appropriate wavelet mother for translating the signal effectively. Figure 5-3 illustrates the most common wavelet functions.

Haar wavelet is one of the oldest and simplest wavelets. Daubechies wavelets are the most popular wavelets among both digital signal processing and image processing. The Haar, Daubechies, Coiflet, and Symlet have used in orthogonal wavelet bank filters.

These wavelets together with the Meyer wavelets have been able to obtain perfect signal reconstruction. Moreover, the Meyer, Morlet and Mexican Hat wavelets are considered as symmetric in shape. In addition, the wavelets have been chosen based on their shapes and abilities for analysing signals in some particular applications.

On the other hand, the wavelet transform provides a multiresolution decomposition of a signal or image in a bi-orthogonal bank filter, which results in a non-redundant signal or image representation. There are many functions could be generated by wavelet from one single function, which is called wavelet mother, based on translations and dilations.

Another significant aspect of the wavelet transform is that it uses for multi-scale of signal through translation and dilation in both time and frequency domains, rather than FFT, STFT and other transformation functions [180]. It has been able to analyse the non-stationary signals. Thus, recently, the WT have obtained great success in machine fault diagnosis as it is not only having the ability in analysing the non-stationary signals but also has distinct advantages. Afterwards, Daubechies and Mallat have been credited with the development of wavelet from the Continuous Wavelet Transform

(CWT) to Discrete Wavelet Transform (DWT) [181] as described in the following subsections.

5.4.1 Continuous Wavelet Transform (CWT)

The same as the Fourier Transform (FT), which obtains the correlation coefficients between the analysed and sinusoidal one. The WT obtains the correlation coefficients between the signal and an orthonormal function, which is called “wavelet function”.

The CWT allows the signals to be analysed through the correlation coefficients of that signals instead of using the whole signal information. The mathematical formula for determining CWT is shown below [179]:

$$W_x(a, b; \psi) = a^{-\frac{1}{2}} \int x(t) \bar{\psi} * \left(\frac{t-b}{a}\right) dt \quad (5-17)$$

Where a is the scale parameter, b is the time parameter, $\psi(t)$ is an analysing wavelet, and $\bar{\psi}$ is the complex conjugate of ψ .

CWT is known as one of the best tools available to detect signal singularity, which is carried out with the local maxima lines [179]. It has been applied for diagnosing the notched rotor [182], where it has been demonstrated that both CWT and changes in the second harmonics could be used as robust indicators. Furthermore, the CWT coefficient has been used as input into the Artificial Neural Network (ANN), and it has been investigated to show that their system has been able to detect combined faults shaft crack and unbalance [183]. CWT has been adopted in most of engineering applications for machine fault detection in the form of scalogram. The scalogram is known as the square of CWT modulus. However, currently, the use of CWT for diagnosis the faults in the rotating machinery is still relatively rare, this is due to the fact that the visual interpretation of wavelet results is often difficult. Thus, more efforts

have been made for extracting the best signal features for analysing the residual wavelet scalogram [184].

5.4.2 Discrete Wavelet Transform (DWT)

The most important part of DWT is that it uses the discrete data as a scale parameter. In the DWT, the scale a and the time b as described in the last equation above are discretised as follow [181]:

$$a = a_0^m, b = na_0^m b_0 \quad (5-18)$$

Where m and n are integers, thus the CWT function $\psi_{a,b}(t)$ in the equation above converted to the DWT by the following formula:

$$\psi_{m,n}(t) = a_0^{-\frac{m}{2}} \psi(a_0^{-m}t - nb_0) \quad (5-19)$$

The discretisation of the scale parameter and time parameter leads to the discrete wavelet transform, which defined as:

$$W_x(m, n; \psi) = a_0^{-\frac{m}{2}} \int x(t) \psi^*(a_0^{-m}t - nb_0) dt \quad (5-20)$$

The DWT has two important approaches to discrete the signal at different scale and position (resolution levels and different frequency), which are decomposing the signal into approximations (A) and details (D). The approximation information could be obtained from the low pass filter, while the detail information could be obtained from the high pass filter as explained in figure 5-4.

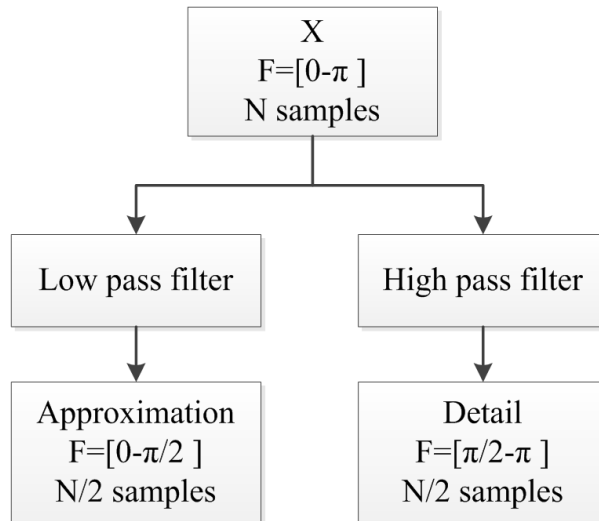


Figure 5-4: DWT decomposition signal to approximation and detail using filters [181].

Figure 5-5 shows how to analyse and synthesis the signal, the input signal goes through two one-dimensional filters, one for high pass filter (H_0), and one for low pass filter (H_1). These filters have filtering operation and followed by subsampling by factor of 2. Then, the signal will be reconstructed by first up sampling, after that, filtering and summing the sub bands will be followed.

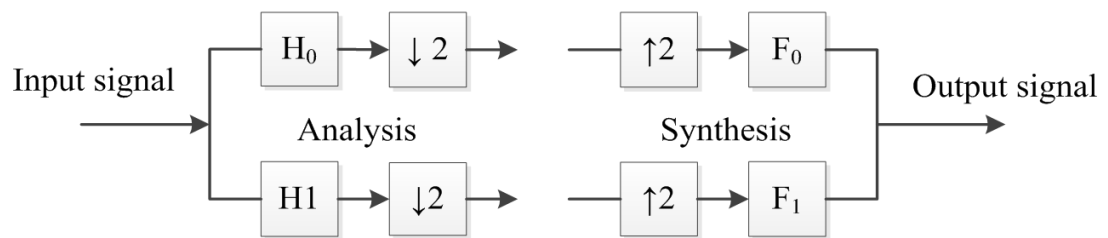


Figure 5-5: DWT two channel filters [185].

The synthesis filters F_0 and F_1 have to be adapted for analysing the H_0 and H_1 filters in order to achieve perfect reconstruction. It is very easy to obtain satisfying relationship between the 2-channel filters by considering Z-transform function. After analysis, the two sub bands will be as follows [186]:

$$\frac{1}{2} \left[H_0 \left(z^{\frac{1}{2}} \right) X \left(z^{\frac{1}{2}} \right) + H_0 \left(-z^{\frac{1}{2}} \right) X \left(-z^{\frac{1}{2}} \right) \right] \quad (5-21)$$

$$\frac{1}{2} \left[H_1 \left(z^{\frac{1}{2}} \right) X \left(z^{\frac{1}{2}} \right) + H_1 \left(-z^{\frac{1}{2}} \right) X \left(-z^{\frac{1}{2}} \right) \right] \quad (5-22)$$

The combination of these filters are:

$$\hat{X}(z) = \frac{1}{2}[F_0(z)H_0(z) + F_1(z)H_1(z)]X(z) + \frac{1}{2}[F_0(z)H_0(-z) + F_1(z)H_1(-z)]X(-z) \quad (5-23)$$

In order to overcome the problem of aliasing and distortion, the following conditions should be considered [186]:

$$F_0(z) = H_1(-z) \quad \& \quad F_1(z) = -H_0(-z)$$

The multiscale pyramid decomposition and reconstruction of an image or signal with high and low pass filters has been illustrated in figure 5-6 and figure 5-7 below.

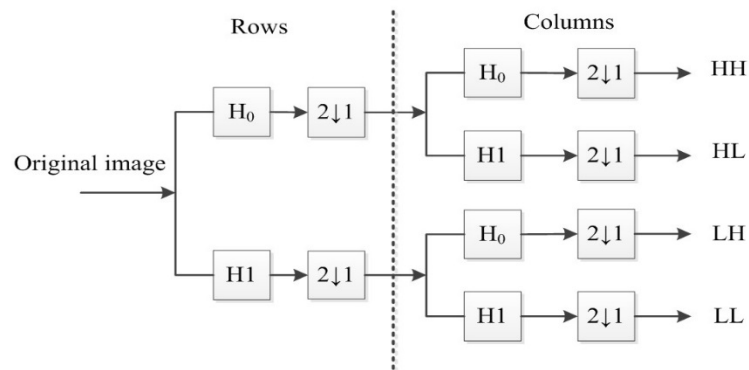


Figure 5-6: Filter bank structure of the DWT analysis [185].

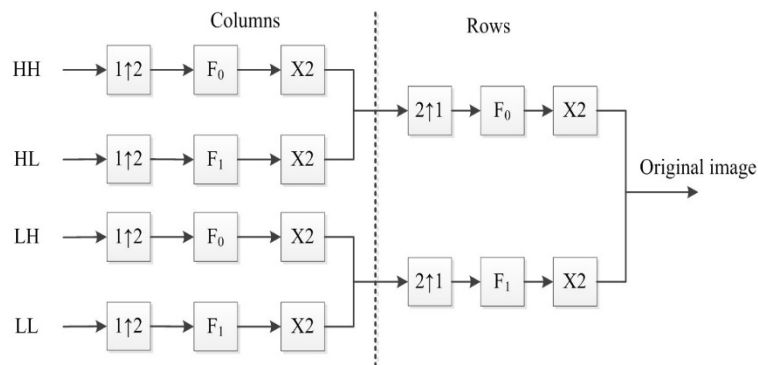


Figure 5-7: Filter bank structure of the reverse DWT synthesis [185].

After one level of decomposition, there will be four frequency bands, which are Low-Low (LL), Low-High (LH), High-Low (HL), and High-High (HH). The next decomposition level will be applied to the LL band, which forms a recursive

Chapter 5: Proposed Methods for Data Pre-Processing and Feature Selection

decomposition procedure. Consequently, an N-level of decomposition will have $3N+1$ different frequency bands, which includes $3N$ high frequency and one LL bands. Table 5-11 illustrates a brief comparison between the performance of CWT and DWT.

Table 5-11: Comparison of the performance of CWT and DWT [187].

CWT	DWT
a) It uses exponential scales with a base smaller than 2.	a) It uses exponential scales with the base equal to 2.
b) Large computational resources required to compute the CWT.	b) Less computational resources required to compute the DWT.
c) It is a shift-invariant.	c) It not shift-invariant.
d) It is highly redundant transform.	d) Is also redundant but less than the CWT.
e) It is orthonormal transform.	e) It is orthonormal vector.
f) The outputs are not down sample but not better than DWT.	f) The outputs are down sampled, but better than CWT.
g) The inverse of CWT could be implemented but usually the signal reconstruction is not perfect.	g) It provides perfect signal reconstruction upon inversion, which means that the DWT of signal coefficients could be used to synthesise and exact reproduction of the signal with numerical precision.

The DWT has been widely used for analysing the induction motor signal (thermal image, current and vibration signals) due to its excellent decorrelation property, it has been used as a transform stage in many modern image and video compression systems [188]. Image compression is one of the most important visible applications of wavelets.

Chapter 5: Proposed Methods for Data Pre-Processing and Feature Selection

Traditionally, in the field of image processing a Discrete Wavelet Transform (DWT) has been adopted for image compression due to its simplicity and practicality. It has been applied for many different types of images such as JPEG, MPEGZ, PNG, etc.

In this work, the DWT technique has been adopted for extracting the best features from the IM thermal image. Among the various DWT techniques, Daubechies wavelet is considered for analysing the thermal image, as it is multilevel decomposition wavelet. The names of the Daubechies family wavelets are written as dbN, where N is the order, and db is the “surname” of the wavelet. The db1 wavelet is the same as the Haar wavelet, which is one of the wavelet functions as mentioned above.

Figure 5-8 illustrates the nine members of the db family [189].

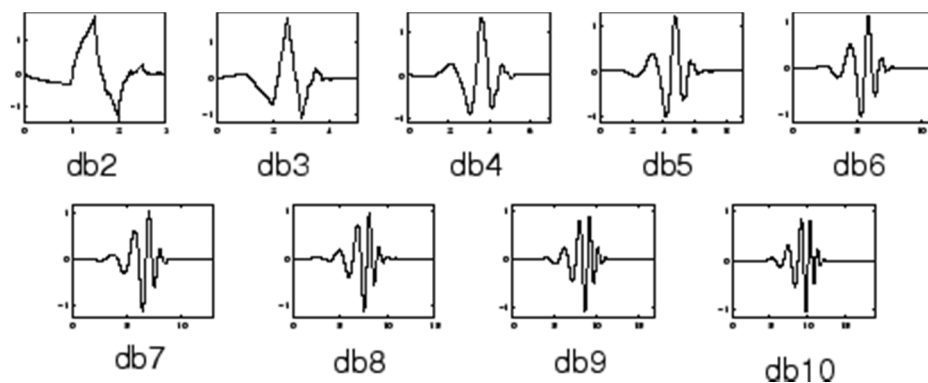


Figure 5-8: Daubechies wavelet families [189].

The wavelet toolbox in MATLAB software (version R2015a) has been used for analysing the thermal image, current signature and vibration signal.

Two-dimensional discrete wavelet analysis tool based on the Daubechies wavelet (db7) with 7 vanishing moments and 3 levels, db73 has been used for analysing the thermal images.

Procedure for thermal image analysis using DWT are below and explained in figure 5-9 :

- a) Read the thermal image and convert it to the HSV colour in order to obtain the discrete pixel values.
- b) Transformation: apply two-dimensional DWT using db7 with level 3.
- c) Save the extracted features from the image to the MATLAB workspace for further processing.
- d) Calculate the histogram for the approximation and the details coefficients.
- e) Save the data of the histogram.
- f) Repeat the same process for other images.

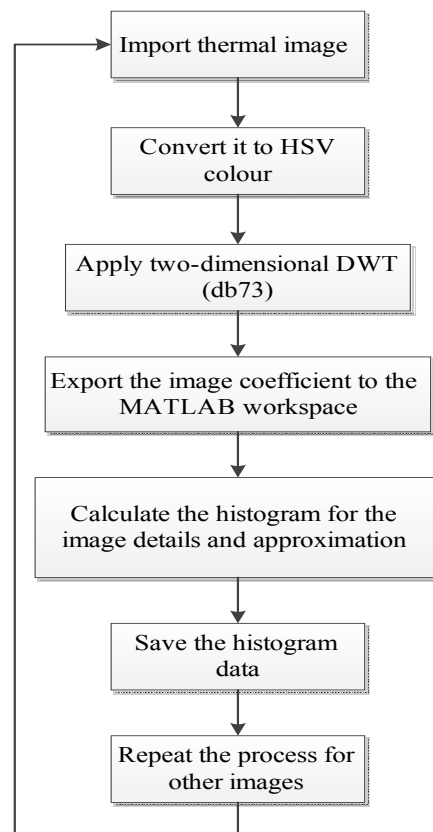


Figure 5-9: Procedure for thermal image analysis in MATLAB using wavelet toolbox.

One-dimensional discrete wavelet analysis tool has been used for analysing the current and vibration signals, the procedure of analysing these signals are as follows:

- a) Import the current/vibration signals.

- b) Apply the DWT to extract the signal features.
- c) Save the extracted features for further processing.
- d) Repeat the process for all faulty signals.

In terms of current/vibration signal, figure 5-10 illustrates the procedure of the signal analysis for the current and vibration in more details.

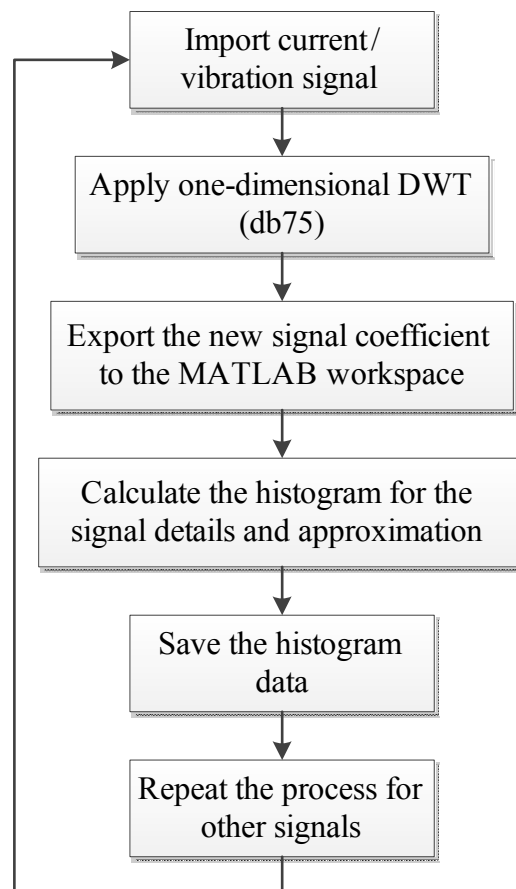


Figure 5-10: Current and vibration signals processing procedure.

Moving on now to consider feature selection method, because it plays a vital role in the field of classification. It has the ability to choose the best features among all dataset. Two important reasons for using the feature selection method: the first one is to reduce the data dimensionality, which is also reduce the processing time. The

second reason is to choose the features that increase the classification accuracy by removing the unwanted ones.

5.5 Feature Selection Methods

Feature Selection or Feature Subset Selection is an important topic in data mining especially for high dimensional datasets. It is a process commonly used in machine learning, wherein subsets of features available from the data are selected for application of a learning algorithm [190]–[192]. The best subset contains the least number of dimensions that most contribute to accuracy, whereas discard the remaining [193]. It is counted as a main stage in data pre-processing, which is used for avoiding the curse of data dimensionality. Feature selection could be decomposed into three search classes: filter, wrapper and embedded as explained in table 5-12 [194].

Chapter 5: Proposed Methods for Data Pre-Processing and Feature Selection

Table 5-12: Taxonomy of feature selection algorithms [194].

Search Class	Advantages	Disadvantages	Example
Univariate	Fast, scalable, and independent of the classifier	Ignores feature dependencies, and ignores interaction with the classifier	X^2 , Euclidian distance, and t-test.
Filter	Model feature dependencies, independent of the classifier, and better computational complexity than wrapper method	Slower than univariate technique, less scalable than univariate technique, and ignores interaction with the classifier	Correlation based Feature Selection (CFS), Markov Blanket Filter (MBF), and Fast Correlation-based feature selection (FCFS).
Deterministic	Simple, interacts with the classifier, model feature dependencies, and less computational intensive than randomized methods.	Risk of overfitting, more prone than randomized algorithm to obtain stuck in a local optimum (greedy search), and classifier dependent selection.	Sequential Forward Selection (SFS), Sequential Backward Selection (SBS), Plus L Minus R, and Beam search.
Wrapper	Less prone to local optima, interacts with the classifier, and model feature dependencies.	Computational intensive, classifier dependent selection, and higher risk of overfitting than deterministic algorithm.	Simulated annealing, randomized hill climbing, genetic algorithm, and estimation of distribution algorithms.
Embedded	Interacts with the classifier, better computational complexity than wrapper methods, and model feature dependencies.	Classifier dependent selection	Decision tree, weighted naïve bayes, and feature selection using weight vector of SVM.

It has been able to search in two ways forward and backward. sequential feature selection has two main components [195][196]:

- An objective function, called the criterion, which seeks to minimize over all feasible feature subsets. Common criteria are mean squared error (for regression models) and misclassification rate (for classification models).
- A sequential search algorithm, which adds or removes features from a candidate subset while evaluating the criterion. Since an exhaustive comparison of the criterion value at all 2^n subsets of an n -feature dataset is typically infeasible (depending on the size of n and the cost of objective calls), sequential searches move in only one direction, always growing or always shrinking the candidate set.

In this research, four feature selection methods based on the wrapper method have been used for reducing and improving the processing time and classification accuracy, which are Sequential Forward Selection (SFS), Sequential Backward Selection (SBS), Sequential Floating Forward Selection (SFFS), and Sequential Floating Backward Selection (SFBS). A brief description of these algorithms has been explained below:

5.5.1 Sequential Forward Selection (SFS)

SFS is classified as a simple greedy search algorithm. This method starting from empty set, sequentially add the feature x^+ that resulted in the highest objective function $J(Y_k+x^+)$ when combined with the features Y_k that have already been selected.

- **Algorithm**

1. Start with the empty set $Y_0 = \{\emptyset\}$.
2. Select the next best feature $x^+ = \operatorname{argmax} [J(Y_k + x)]; x \notin Y_k$.
3. Update $Y_{k+1} = Y_k + x^+; k = k + 1$.
4. Go to step two.

SFS performs best when the optimal subset has a small number of features. Furthermore, when the search is near the empty set, a large number of states can be potentially evaluated. Towards the fullest, the region examined by SFS is narrower since most of the features have already been selected. Thus, the search space is drawn as an ellipse to emphasize the fact that there are fewer states towards the full or empty sets. In addition, the main disadvantages of SFS is that it is unable to remove the obsoleted features after the addition of the new feature.

5.5.2 Sequential Backward Selection (SBS)

SBS works in opposite direction of SFS, which also known as Sequential Backward Elimination (SBE). It starts from a full set and sequentially remove the feature x^- that resulted in decreasing the value of the objective function $J(Y - x^-)$. Notice that the removal of feature may actually lead to an increase in the objective function $J(Y_k - x^-) > J(Y_k)$. Such functions are said to be non-monotonic.

- **Algorithm**

1. Start with the full set $Y_0 = X$.
2. Remove the worst feature $x^- = \operatorname{argmax} [J(Y_k - x)]; x \in Y_k$.
3. Update $Y_{k+1} = Y_k - x^-; k = k + 1$.
4. Go to step two.

SBS works best when the optimal feature subset has large number of features, since SBS spends most of its time visiting large subsets. Thus, the main limitation

of SBS is its inability to reevaluate the usefulness of a feature after it has been discarded.

5.5.3 Sequential Floating Selection

The floating variant, SFFS and SBFS, could be considered as extensions to the simpler SFS and SBS algorithms. The floating algorithms have an additional exclusion or inclusion step to remove features once they were included or excluded. Thus, a larger number of feature subset combinations can be sampled. It is very important to emphasise that this step is conditional and only occurs if the results of feature subset assessed as “better” by the criterion function after removal or addition of particular feature. There are two floating methods:

5.5.3.1 Sequential Floating Forward Selection (SFFS)

Starts from empty set. After each forward step, SFFS performs backward steps as long as the objective function increases.

5.5.3.2 Sequential Floating Backward Selection (SFBS)

Starts from the full set. After each backward step, SFBS performs forward steps as long as the objective function increases.

- **Sequential Floating Selection algorithm (the SFFS and the SFBS is analogous)**

1. Start with empty set $Y_0 = \{\emptyset\}$.
2. Select the best feature

$$x^+ = \operatorname{argmax} [J(Y_k + x)]; x \notin Y_k.$$

$$Y_k = Y_k + x^+; k = k + 1.$$

3. Select the worst feature

$$x^* = \operatorname{argmax} [J(Y_k - x)]; x \in Y_k.$$

4. If $J(Y_k - x^*) > J(Y_k)$ then

$$Y_{k+1} = Y_k + x; k = k + 1.$$

Go to step three.

Else

Go to step two.

Having discussed how to construct the B4M, image processing methods, wavelet transform analysis and feature selection methods, the next chapter addresses the ways of using the most popular machine-learning algorithm for feature selection, which is Genetic Algorithm (GA)

CHAPTER 6

GENETIC ALGORITHM BASED FEATURE SELECTION FOR B4M (GA-B4M)

“In this chapter, the proposed hybrid approach of Genetic Algorithm (GA) and proposed Bee for Mining (B4M) methods have been described and explained in detail. In addition to this, the new hybrid technique (GA-B4M) will be used for selecting the features, detect, classify and predict the induction motor faults at an early stage. These methods have also been translated as a software code using MATLAB software version “R2015a””.

6.1 Introduction

Volumetric features have big impact on the system density and most of the time it does not lead to higher prediction accuracy. However, they are not independent and might be correlated. A bad feature could completely disgrace the system performance. Therefore, it is very important to select the best features before use them as training data. These features are selected during or before the training phase in order to describe the training data. Consequently, two important point could be concluded in this case, the first is the smaller quantity of features are able to reduce the computational outlay, which plays vital role for real-time applications, and the second is leading to the higher classification accuracy. In this chapter, Genetic Algorithm (GA) has been used to select as few features as possible in order to gain best description for the training data. It has been also used to determine the important relationship between all different features to select the good subset of features. This system called a hybrid system of two machine-learning algorithms, Genetic Algorithm (GA) and Bee for Mining (B4M), with purpose of improving the proposed B4M classification accuracy based on the GA for feature selection.

In 1975, the Genetic Algorithm was developed by John Holland, University of Michigan, for providing an efficient technique for machine learning applications to solve all the optimization problems. The GA algorithm technique is based on the mechanics of biological evaluation for inheritance, mutation, natural selection and crossover (recombination) [197], [198]. It is also considered as a heuristic algorithm, which survive or select the best individual among all population.

6.2 Genetic Algorithm

GA algorithm is a computational model. It works on a set of candidate for finding the best solution, each candidate called “chromosome”, while all the set of candidate solution called “population”. It allows the chromosomes to move from one population to another by iterative process, these iterations called “generations“. Furthermore, GA has many forms for solving or optimizing problems, a simple version which is called static population model has been used for most of experiments [199]. In this model each chromosome has been ranked based on the fitness value. Two chromosomes (individuals) have to be selected and use them as parents for reproduction. The GA operators has been described below.

- **Genetic Algorithm Operators**

Genetic algorithm operators that are used in the Genetic Algorithm is to maintain the genetic diversity. It is analogues to the natural world: selection or survival fittest, reproduction (recombination or crossover) and mutation. The genetic diversity (level of biodiversity) refers to the total number of genetic characteristics in the genetic makeup of each species. The operations of GA as follows:

- a) Parent Population Initialization**

The population of each individual has been maintained within the search space of GA, which represent a possible solution to a given problem. The population size depends on the number of chromosomes in each generation. If the number of chromosomes are few, thus the GA will have few possibilities to perform the crossover and lead to explore small part of

search space. Each individual in the GA has been coded as a finite length vector of variables, in terms of binary alphabet {0, 1} as shown in figure 6-1. Thus, to continue the genetic analogy, all the individuals have been linked to chromosomes.

Population	Chromosomes 1	11100010
	Chromosomes 2	01111011
	Chromosomes 3	10101010
	Chromosomes 4	11001100
	Chromosomes 5	11101101

Figure 6-1: Population in GA

b) Evaluation

An ideal fitness function has been assigned to each solution representing the abilities of an individual to compete. The GA searches for each individual that has the best fitness value (score). Therefore, the GA aims to select best individual (solution) for the given problem in order to produce offspring better than parents by combining the chromosomes information.

c) Selection

In this step, all individuals (chromosomes) that have high fitness score are given more chance to be selected for reproduction. Several methods could be used in this step such as tournament selection, basic roulette wheel, elitist selection, rank selection, hierarchical selection and steady state selection.

d) Crossover / Recombination

In this stage, parent's portions could exchange with the purpose of producing or generating more adapted solution as shown in figure 6-2.

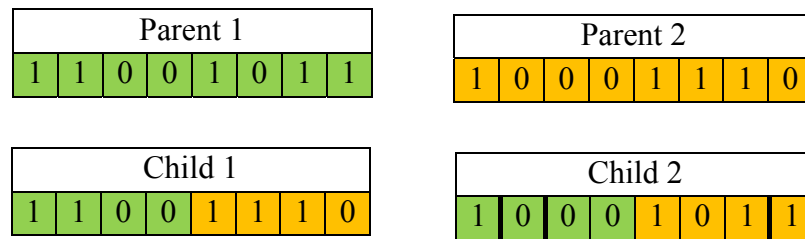
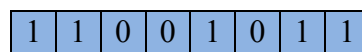


Figure 6-2: Crossover structure.

e) Mutation

This could be done by randomly selecting one chromosome from the population and change its information as illustrated in figure 6-3.



a. Before mutation



b. After mutation

Figure 6-3: Mutation changing.

The benefit of this process is to produce a new genetic (generation) by randomly change the chromosomes information to avoid the stagnation around local minima.

6.3 GA Theoretical Background

The GA works with random population for finding the optimum solutions. It evaluates the fitness of each chromosome based on specific objective function. Thus, in order to simulate the natural survival of the fittest process, the best chromosome information has been chosen to produce new offspring chromosomes. The new offspring will be involved and evaluated in the population if they provide better solutions than the weak population members. Generally, the search process will be continued for a large number of generation to obtain the best-fit value (optimum solution). Figure 6-4 illustrates the GA procedure sequence. Four important parameter have an effects on the GA performance; population size, number of generation, crossover rate and mutation rate. Therefore, the large population size and number of generations could increase the likelihood of gaining the global optimum solution, but significantly increase the processing time.

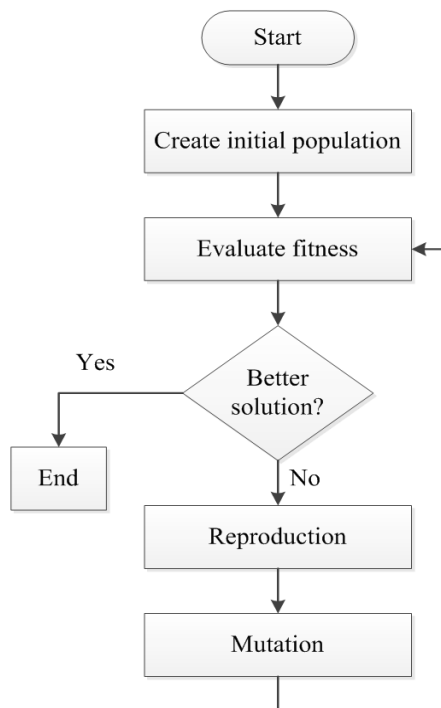


Figure 6-4: GA flow chart.

The following steps explain the GA procedure:

- a) Choose the initial population of individuals.
- b) Evaluate the fitness value of each individuals in the population.
- c) Repeat the following on the generation until the termination: (sufficient fitness achieved, etc.)
 - i. Select the best fit of individuals for reproduction.
 - ii. Breed the new individuals through crossover and mutation operations to give birth offspring.
 - iii. Evaluate the fitness value of new individuals.
 - iv. Replace fit population with new individuals.

First, define the representation of the chromosomes for a given problem because each chromosome represent a candidate solution to the problem. The most common form that define the chromosome is binary form. Then choose the specific objective function to find the optimal solution (fitness function).

Generate an initial population for the chromosomes. In general, the initialization could be done randomly, but most cases this initialization has been done by the chromosomes that are already known in order to have better performance. In case of using random initialization, each chromosome will be set to 0's or 1's randomly based on the probability (initialization probability). Then, the evaluation of fitness function will be carried out to find the most appropriate chromosome based on the higher fitness value. Two individuals have been selected from the individual population relying on the fitness function value, which are called, parents.

Eventually, the crossover operation will be applied on the selected chromosomes as explained above. Each chromosome will be divided into two segments. These segment

are exchanged in order to create two new chromosomes (two children). The second segment of parent 1 will be the second segment of child 2 and vice versa. This operation has been performed with the purpose of creating new generation that could be adapted better than the selected one. The crossover operation is very important because it makes the feature space exploration bigger to find a near optimal solution. In case of all the individuals are identical, the crossover operation will generate the same chromosome, which means that this operator unable to generate new chromosomes.

Consequently, the population diversity could be performed by applying the mutation operator. The mutation of two chromosomes are randomly changing the altering value of each element in the chromosomes based on the mutation probability. For example, if the component value is binary, the mutation converting the value from 0 to 1 or inverse. Then, evaluate the fitness value of the new created chromosomes and replacing the less adapted chromosomes by the new highest value. Go back and stop the algorithm when the maximum number of generation has reached.

6.4 GA based Feature Selection

As stated above, GA can be defined as population based and algorithmic search heuristic methods that mimics natural evolution process of man [197], [200]. Table 6-1 illustrates the comparative terminology to human genetics [201].

Table 6-1: Comparative terminology to human genetics [201].

SN	Human Genetics	GA Terminology
1	Chromosomes	Bit strings
2	Genes	Features
3	Allele	Feature value
4	Locus	Bit position
5	Genotype	Encoded string
6	Phenotype	Decoded genotype

The values of each chromosome are evaluated using a special function, which commonly referred to fitness function or objective function. In other word, the fitness function returns numerical values of each chromosome that are used to rank the chromosomes in the population. Thus, five issues in the GA should be considered, which are encoding the chromosome, population initialization, evaluate the fitness value, selection (genetic operators) and criteria to stop GA as shown in figure 6-6.

In the GA, the chromosomes are a bit strings because the GA works with binary search space. To begin with, the initial population has been created (randomly) and evaluated by using the fitness function. The binary chromosomes have been used in this research, a gene value “1” represents that the particular feature indexed has been selected. Otherwise, the feature should not be selected for chromosome evaluation.

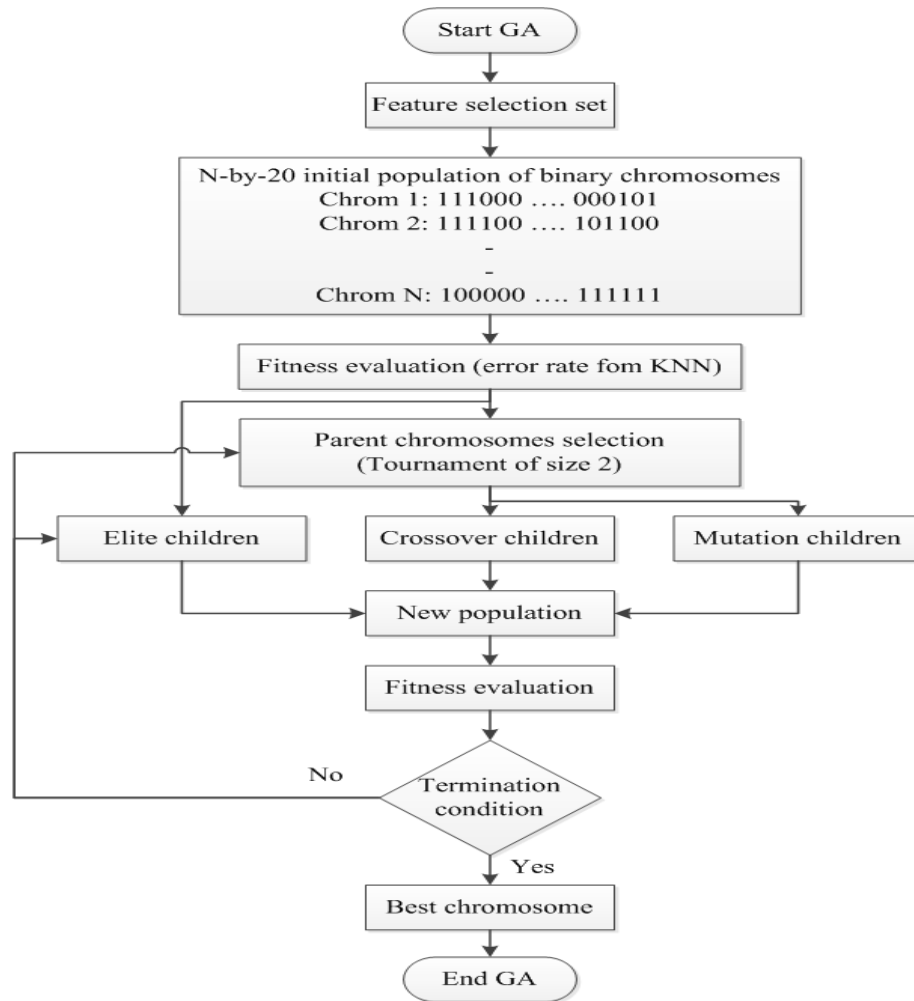


Figure 6-5: GA based feature selection.

After using the feature index (“1”), the chromosomes will be ranked and put them in the ranking index, the top fittest kids will be selected to survive the next generation. The fitness evaluation has been done by using the algorithm in figure 6-7 below. After automatically pushing the elite individuals to the next generation, the remaining individuals in the population will passes to the crossover and mutation operations in order to create new individuals. As stated above, crossover is a combination of two chromosomes (individuals) to create new chromosome, while the mutation is used for genetic perturbation of each gene in the chromosome through bits flipping based on the mutation probability as shown in figure 6-5. The configuration of the GA for this research has been explained in table 6-2.

Table 6-2: GA parameters values.

Parameter of GA	Value
Population size	100
Genomelength	100
Population type	Bitstrings
Fitness function	KNN-base classification error
Number of generations	300
Crossover	Arithmetic crossover
Crossover probability	0.8
Mutation	Uniform mutation
Mutation probability	0.1
Selection scheme	Tournament of size 2
Elitecount	2

The following steps have been considered for feature selection using genetic algorithm:

A. Initial Population Generation

In this research, the initial population is a matrix of two dimension, which are chromosome length and the population size that are containing only binary digits. The chromosome length (Genomelength) is the bit number of each chromosome, and the population size is the chromosome number in the population size. It has been recommended to make the population size equal to the value of chromosome length in order to span the search space [202]. The Pseudo code for the initial population is:

```
1- Procedure POPFUNCTION()
2- Pop Binary matrix (population size * Genomelength)
3- Return pop
4- End procedure
```

Figure 6-6: Pseudo code for creation the initial population.

B. Fitness Function

The most important part of the feature selection based on the GA is the fitness function; it has to be defined for evaluating the discriminative capability for each subset of feature. In this work, the fitness function that has been used for evaluating the chromosomes is KNN (K-Nearest Neighbour)-based fitness function. The KNN algorithm has been used for solving the classification problems by looking for the shortest distance between the training and the test data in the feature search space based on the euclidean distance ($D(x_{test}, x_i)$), as expressed in the equation below:

$$D(x_{test}, x_i) = \sqrt{\sum_{m=1}^M (x_{test} - x_i)^2} \quad (6-1)$$

The KNN has been able to count each category in the class information (as accumulated as count (x_m)) by using 3 Nearest Neighbours, after that it provides a report classification results and classification error based on the expression below:

$$argmax(count(x_m)) \quad (6-2)$$

$$\text{Subject to : } \sum_{i=1}^M count(x_m) = class \quad (6-3)$$

The position of “1” is selected for each genes, which indicates the particular feature index. Otherwise, if the genes value “id” is 0, it will not be selected for the chromosome evaluation. Thus, the current population will be evaluated and ranked based on the KNN classification error. In addition to this, the individuals that have the lower fitness value, they have a chance to be survived for the next generation. Meanwhile, the iterations that are run the GA will be part of reducing the error rate by picking up the chromosome with the lowest error rate as the error rate of each chromosome has been reported (recorded), and then the

smallest error rate will be kept or picked up by GA at the end. The expression for the fitness function is explained below:

$$fit = \frac{\alpha}{N_f} + \exp\left(\frac{-1}{N_f}\right) \quad (6-4)$$

α = KNN-based classification error.

N_f = number of selected features.

The above expression has been used for learning the GA in order to minimize the error rate and reducing the number of features. Figure 6-7 shows the Pseudo code for the above expression in the GA.

- 1- Procedure fit()
- 2- Featindex (indices of one 1's from binary chromosome)
- 3- Newdataset (dataset indexed by Featindex)
- 4- Numfeat (number of elements in Featindex)
- 5- 3 (number of neighbours)
- 6- KNNerror (classifier KNN (dataset, class information, number of neighbours KNN))
- 7- Return KNNerror
- 8- End procedure

Figure 6-7: GA fitness function based on the KNN.

C. Individual Generation for New Population

In this step, the new population has been created by using the genetic operators and elitism (mutation and crossover). In the MATLAB toolbox, GA consists three types of individuals (children): elite children, crossover children and mutation children.

a) Elite Children

These children have been automatically pushed to the next generation. In the GA MATLAB toolbox, the elitism has been identified as “Elitecount” and the default value is 2 as shown in table 6-2, which is bounded by the population size. Thus, based on the “Elitecount”, GA will pick up the best two chromosomes (the lowest fitness value) and then push them to the next generation. For example, if the number of features are 200, the remaining chromosomes are 198 that they will proceed with the crossover and mutation operators.

b) Crossover Children

This kind of operator sometimes called crossover fraction. In this search, the value of crossover is 0.8, because if it is set to 1, then the mutation operators will not be proceed in GA. Therefore, the value of this operator will be $\text{crossover} = \text{number of remaining chromosomes} * 0.8$ ($198 * 0.8 = 158$) as stated in the example above.

c) Mutation Operator

The number of mutation operator will be calculated as $\text{mutation operator} = \text{number of features} - \text{elite operator} - \text{crossover operator}$ ($198 - 158 - 2 = 38$).

d) GA Selection Mechanism

The most important part of GA is the selection mechanism because it selects the best-improved individual’s value in the population. It also

helps the GA to discard the bad individuals and keep the best one. The GA toolbox has many selection mechanisms, one is the stochastic uniform (default size is 4) and the other one is tournament. In this research, the tournament selection mechanism has been used since it is fast, simple and more efficient as stated in [203]–[205]. In addition to this, the tournament selection has been able to enforce the GA to make sure that the worst individual will not go to next generation [201], [206]–[211]. Tournament selection needs two functions to be able to apply in the GA, the first function is individual generation and the second one is picking up the best individual out of the population (the winner). The tournament selection value here is 2, which means that there are two chromosomes should be selected from the population after taken out the elite children. It keeps repeating until filling up the new population.

e) GA Termination

The GA will be stopped if it reaches to the optimal solution, which is called stopping criteria (condition). This research has two stopping conditions:

- a) Maximum number of individuals.
- b) Limit the generation stall.

The GA could be able to terminate the whole process prematurely, if the individuals are not set properly. The value of individuals has been set to 300, while the value of the genomelength has been set to 100. In this case, if the difference in the average value of the fitness function, which is

Chapter 6: Genetic Algorithm based Feature Selection for B4M (GA-B4M)

related to the genomelength, is equal to or less than 0.000001, the GA will be terminated. Consequently, this will affect the genetic homogeneity between chromosomes, then at the end the GA will produce the best chromosome.

In the previous chapters, all methods that are used in this research have been explained and how they are adapted for IM motor fault classification. The chapter follows moves on to consider the IM test rig setup in order to collect the required data for further processing.

CHAPTER 7

EXPERIMENTAL SETUP AND MEASUREMENTS

“This chapter describes all the equipment that has been used in this research to carry out the experimental tests. The test rig and the data acquisition have been also described. Furthermore, the data collection procedure has been explained. It also presents the healthy and faulty signals of the induction motor to be used to detect the IM faults using thermal image as well as current and vibration signals”.

7.1 Introduction

Previous chapters have explained the methods that will be used in this research which are proposed classification algorithm Bee for Mining (B4M), feature extraction, feature selection and the hybrid system of Genetic Algorithm based feature selection for Bee for Mining (GA-B4M). In this chapter, the equipments and experimental setup that have been used for collect the required data (thermal images, current and vibration signals) for classification process (motor protection) have been explained.

A series of experiments have been conducted and the required data have been collected to verify the proposed algorithms for induction motor fault classification. Tests have been carried out under different load conditions with different types of faults. A three-phase squirrel-cage induction motor has been used in this research. “FLIR C2” thermal imaging camera has been used for capturing the motor thermal images, stator current has been collected by using current transformers (one for each phase), and vibration levels has been collected by using laser vibrometer “OFV 303”. A general description of the experiment test rig that are used in this investigation has been explained in the following sections.

7.2 Condition Monitoring Scheme

The general condition monitoring scheme for the proposed algorithms is shown in figure 7-1. Two common phases have been adapted in this research, which are training and prediction phases as shown in figure 7-2 . The most important phase is the training phase because it prepares the data and learn the classification algorithm (train model), while the prediction phase depends on the training phase for predicting the new incoming data (unseen data). Several induction motors have been tested to check

Chapter 7: Experimental Setup and Measurements

whether they work in a healthy or faulty conditions. In case of healthy conditions, the overall signal condition should be identified by the machine learning algorithms and keep the motors running safely. However, if the machine learning indicates that the motor has fault in any parts, then the maintenance action should be taken immediately and repair or change the motor in order to prevent the catastrophic issues. Figure 7-2 illustrate the research framework and the procedure that are followed to reach the main goal, which is classifying the motor faults accurately.

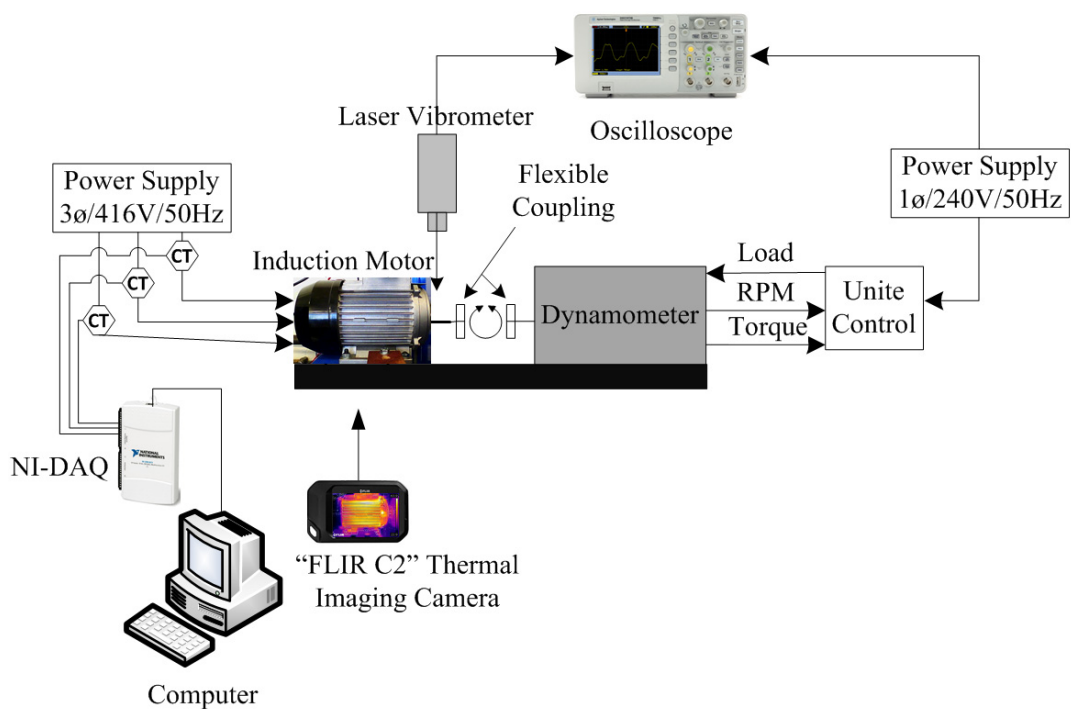


Figure 7-1: Condition monitoring scheme.

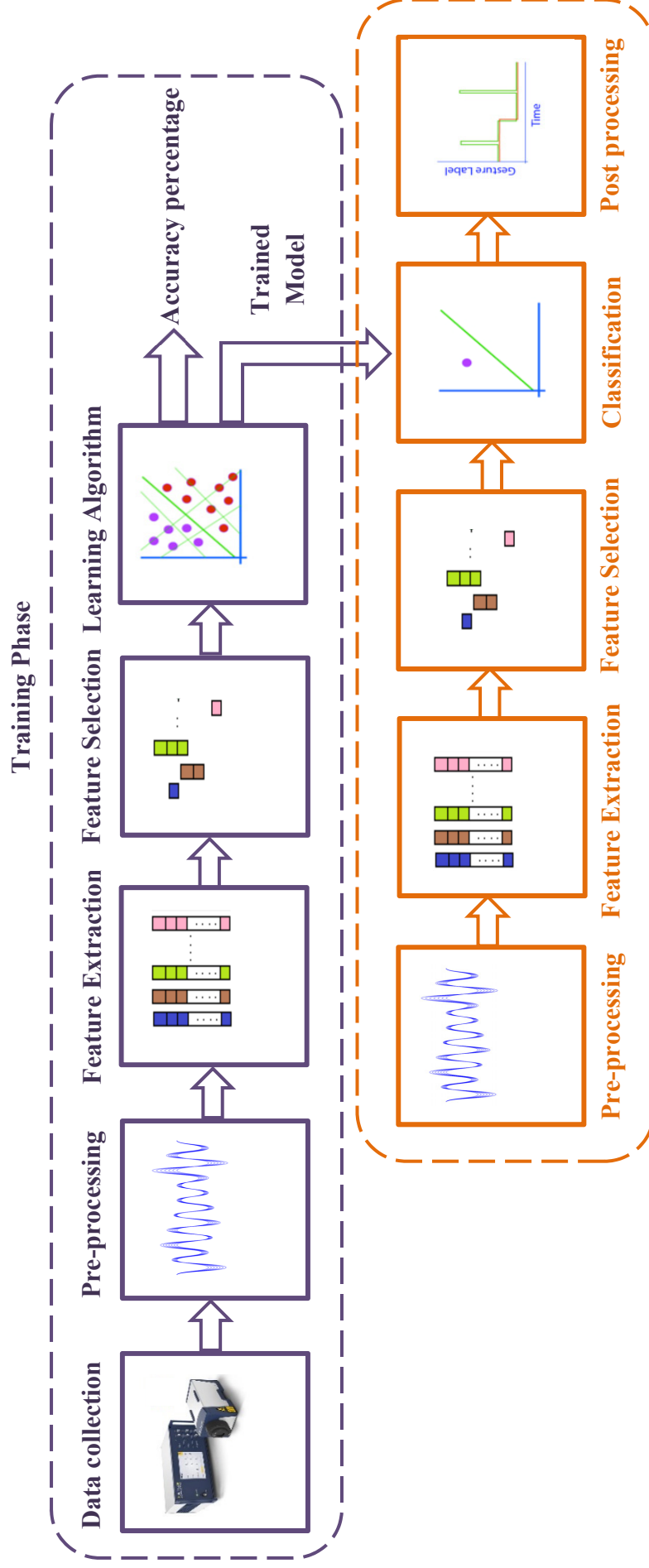


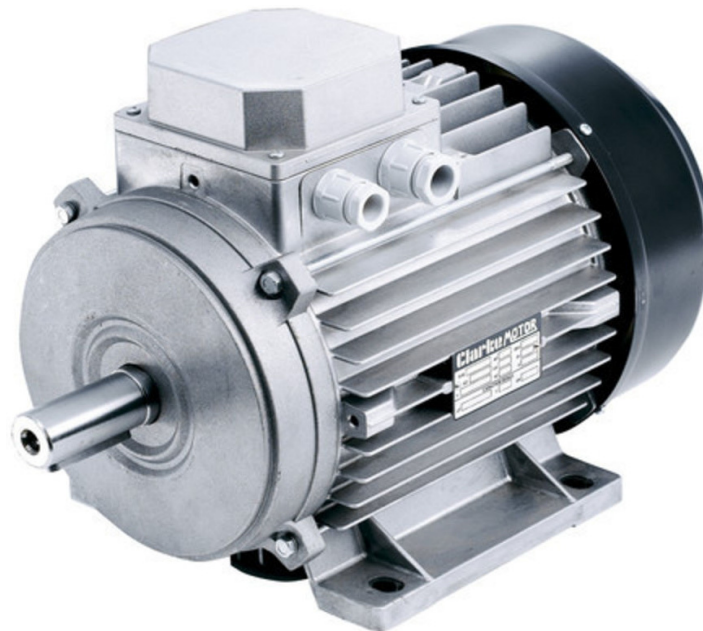
Figure 7-2: Research framework for motor fault classification.

7.3 Test Rig Equipments and Data Collection

A test bed has been built and located at Cardiff University, School of Engineering, and it has been used to perform all the experimental tests for this work. The experimental test rig in this research consists of:

a) Three-Phase Induction Motor

Three-phase squirrel cage induction motor and its specification has been illustrated in figure 7-3, which has delta connection.



Motor model	Clarke motor 80B/4
Frequency	50Hz
Output power	0.75 kW
Output horse power	1.0 hp
Speed	1480 rpm
No. of phase	3

Figure 7-3: Induction motor specification.

b) AW Dynamometer

AW dynamometer is used for creating the load to induction motor by increasing the load torque using the control panel and monitor the motor torque and speed by the dynamometer sensor panel as illustrated in figure 7-4.



Figure 7-4: Dynamometer parts: a- Electric motor dynamometer, b- Dynamometer sensor (R.P.M., torque, power, and torque rise), c- Dynamometer barker control.

c) Current Transformer

Three current transformers have been used for stator current reading (three phases) as shown in figure 7-5, the specification of current transformer has been

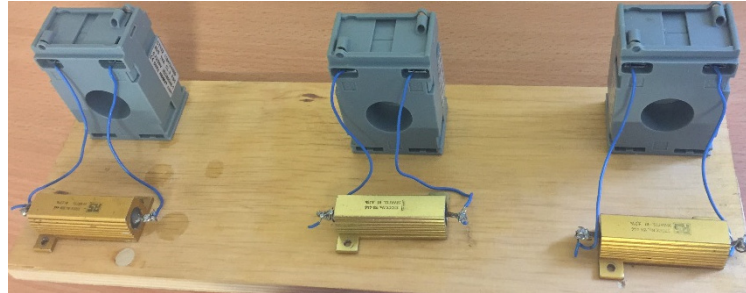


Figure 7-5: Current transformer setup for collecting the stator current.

described in table 7-1. Three 50 Watts and 1Ω resistors have inserted in series between current transformers and the DAQ in order to have the actual individual current value, through measuring voltages crossing them.

Table 7-1: Current transformer specification.

Attribute	Value
Current Ratio	40:5
Maximum Cable Diameter	21mm
Overall Height	65mm
Overall Width	45mm
Overall Depth	30mm
Minimum Temperature	-30°C
Maximum Temperature	+85°C

d) National Instrument Data Acquisition Card

The output data (signal) that are received from the current transformers will be connected to National Instrument Data Acquisition card (NI-DAQ USB-6211, 16

Chapter 7: Experimental Setup and Measurements

AI multifunction I/O). The LabView version 2015 software has been used in order to save the current data as “Excel” or “csv” file to be used for further processing. The DAQ card and the LabView circuit has been illustrated in figure 7-6 and figure 7-7 respectively.



Figure 7-6: National Instrument Data Acquisition card (NI DAQ USB-6211 16 AI multifunction I/O).

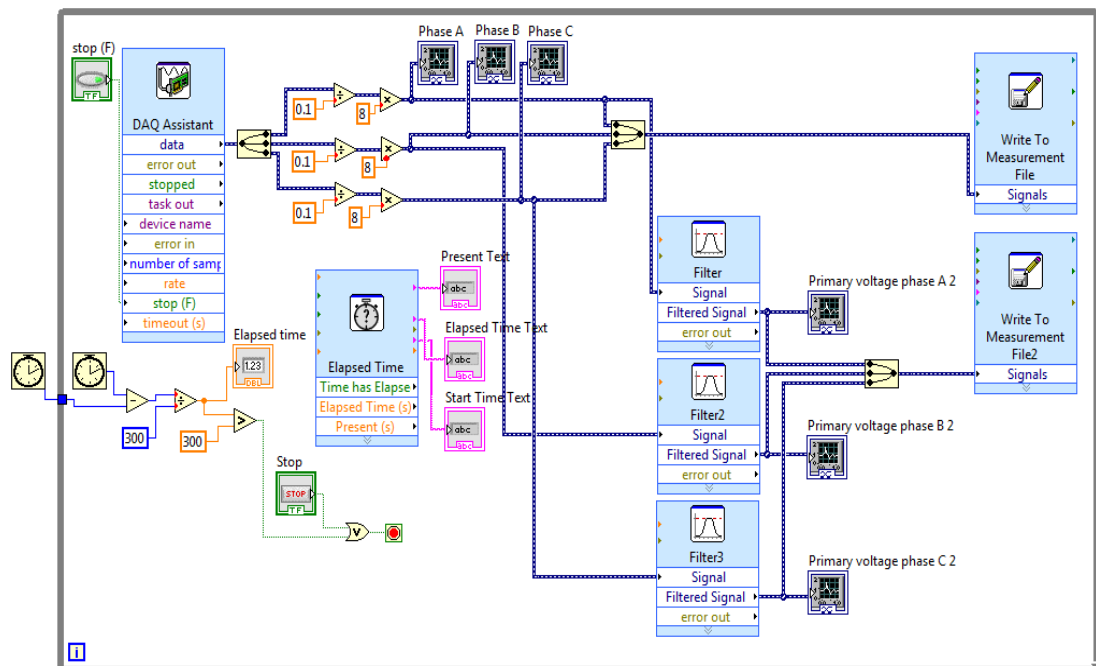


Figure 7-7: LabView circuit for collecting the stator current data.

e) Thermal Camera

FLIR C2 thermal camera has been used in this experiment in order to capture the thermal image for the healthy and faulty motor. The specification of this camera has been illustrated in the figure 7-8 below:



Focal length	1.54 mm
Size (L*W*H)	124.46*78.74*12.44 mm
IR sensor	80*60 (4,800 measurement pixel)
Operating temperature range	-10°C to +50°C
Storage temperature range	-40°C to +70°C
Digital camera	640*480 pixel
Image frequency	9 Hz
Accuracy	±2°C
Thermal sensitivity	< 0.10°C

Figure 7-8: Thermal image specifications.

f) Laser Vibrometer

The vibration signal has been collected by using the laser vibrometer “OFV-303” optical head via OFV-2200 front panel. This device uses the laser to sense the motor vibration, and then the output from the front panel has been connected to an oscilloscope in order to save the data as “Excel” or “csv” file for further processing. Figure 7-9 shows the laser vibrometer optical head, front panel and the oscilloscope. Two important factors in this device need to be calibrated before collecting the data, which are velocity and displacement range. The first one has been set to 25 mm/s/V and the latter was set to 80 $\mu\text{m}/\text{V}$. For example if the voltage is 1.2 V the displacement range will be $1.2 \times 80 \times 10^{-6} = 0.096 \text{ mm}$.



Figure 7-9: Laser vibrometer: a: Front panel, b: Optical head and c: Oscilloscope.

7.4 Rig Setup

All devices that have been described above have been connected together in the Wolfson Centre for Magnetics at Cardiff University Queens building (school of engineering) in the UK as shown in figure 7-10.

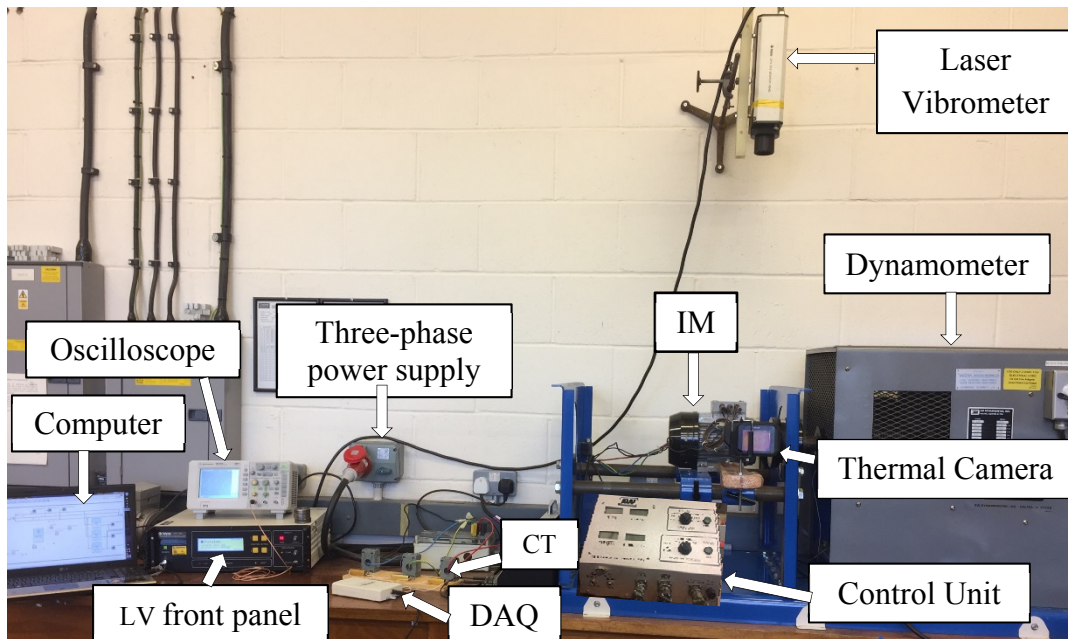


Figure 7-10: The experimental test rig.

7.5 Fault Generation

Two types of faults have been deliberately made on several induction motors. The first one is rotor fault and the second one is bearing fault. Each type of fault has a three kinds of fault. For the rotor, the faults are, one bar, four bars and eight bars; while for the bearing, the faults outer race, ball bearing and inner race as illustrated in figure 7-11. The thermal image, current and vibration signals have been collected for all the IM faults to be used for classification system. Faults description have been explained in the following sections.

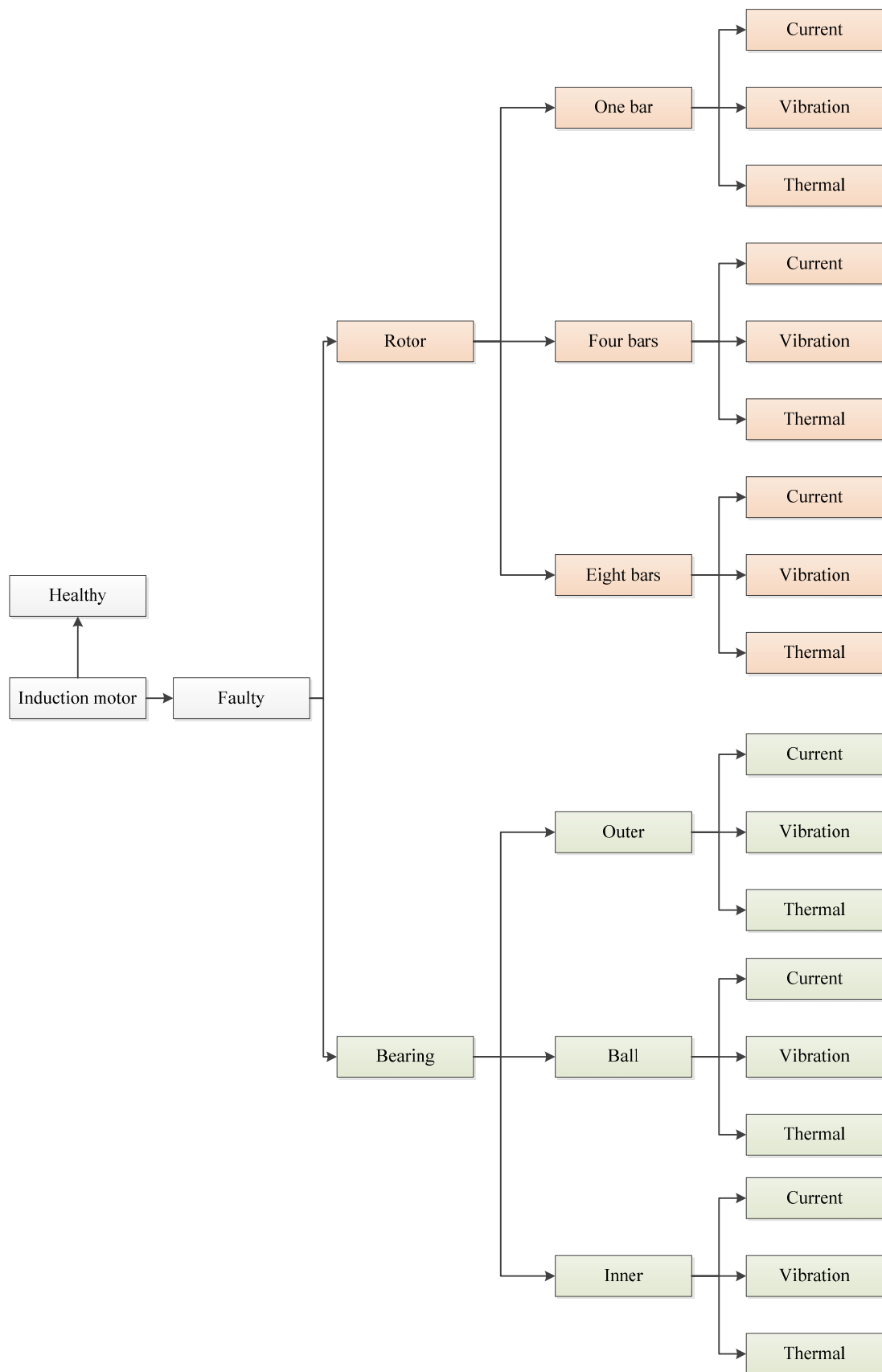


Figure 7-11: IM faults scheme.

7.6 Healthy Motor

This test were carried out in order to save the reference signal for further processing as shown in figure 7-12. Three types of loads have been applied for the motor, which are no load, 50% load and 100% load, by using an eddy current brake within the dynamometer. The motor under test was operating at steady state with load about 50% of full load at speed 750 rpm.

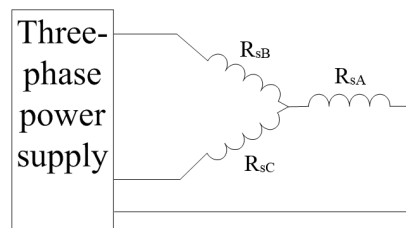


Figure 7-12: Healthy condition.

The thermal mages; current and vibration signals have been collected from this machine at three load conditions, as illustrated in figure 7-13 and figure 7-14.

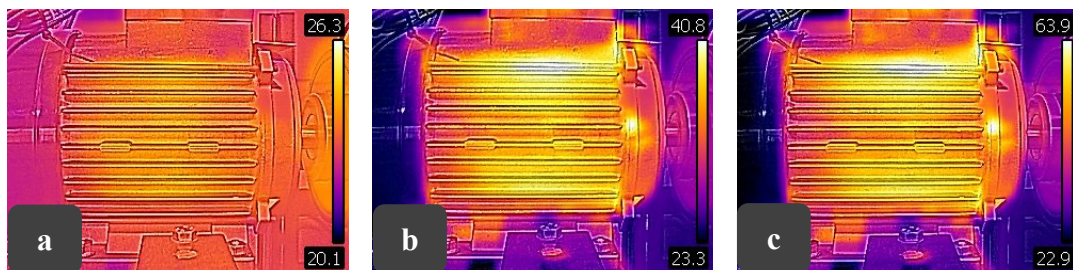


Figure 7-13: Thermal image for healthy motor, a: No load, b: 50% load c: 100% load.

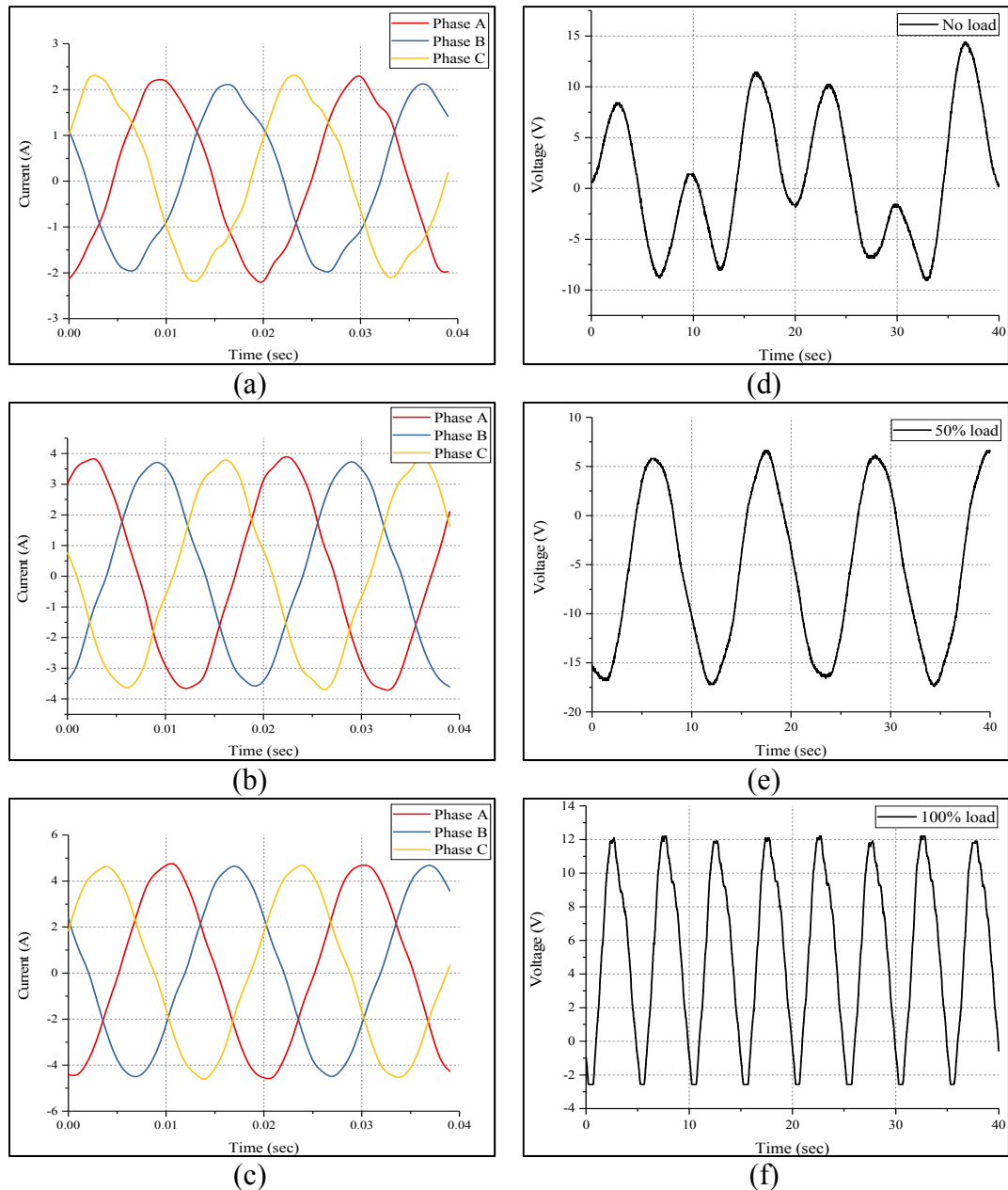


Figure 7-14: The current and vibration signals of healthy IM, a, b, and c represent the current signals at (a) no load, (b) 50% load and (c) 100% load respectively, while d, e and f represent the vibration signal at different load conditions.

7.7 Faulty Rotor

Induction motor failure through broken rotor bars, initiated by cracking in the rotor conductor, are common in many industrial applications. One of the most common reason for this kind of fault to be happened is that the large starting current occur when the motor is relatively cold, which causes a mechanical and thermal stress (maximum).

Chapter 7: Experimental Setup and Measurements

Thus, the inductance of this failure mode is greatest when the start-up time is relatively long especially for frequent starts that are required as a part of heavy duty-cycle. Figure 7-15 presents how the circuit of the rotor cage are composed of the potential of the bars inside the rotor core [212] (R_b and L_b represent the resistance and leakage inductance of each bar respectively, while R_e and L_e represent the resistance and leakage inductance of each end ring segment between adjacent part respectively). In this research, these bars has been artificially cut by using 4mm drilling holes in order to see its effect on the motor temperature, current and vibration signals. Rotor faults description have been illustrated in the following sections.

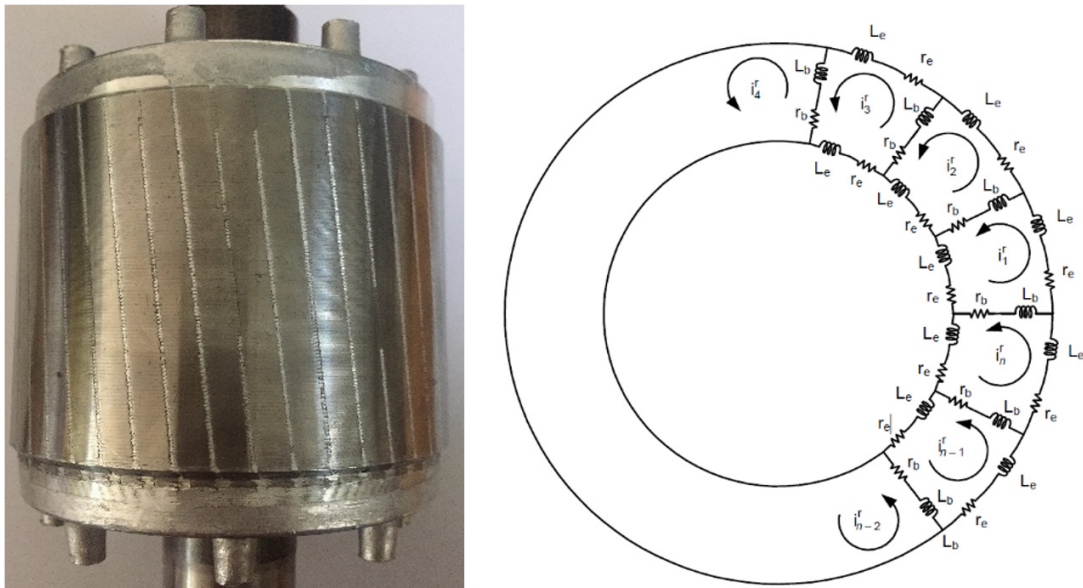


Figure 7-15: IM rotor circuit diagram.

7.7.1 One Bar Rotor Fault

One of the rotor bars has been removed from the rotor. This rotor has been tested in three different load conditions (no load, 50% load and 100% load) as mentioned above. During the measurements, three types of data have been collected, which are thermal image, current and vibration signals at the same time as illustrated in the following figures.

Chapter 7: Experimental Setup and Measurements

Figure 7-16 demonstrates the faulty rotor circuit and the faulty IM rotor (one bar). The fault has been created by using drill holes with 4mm wide and 14mm depth dimensions in order to cut the bar resistance.

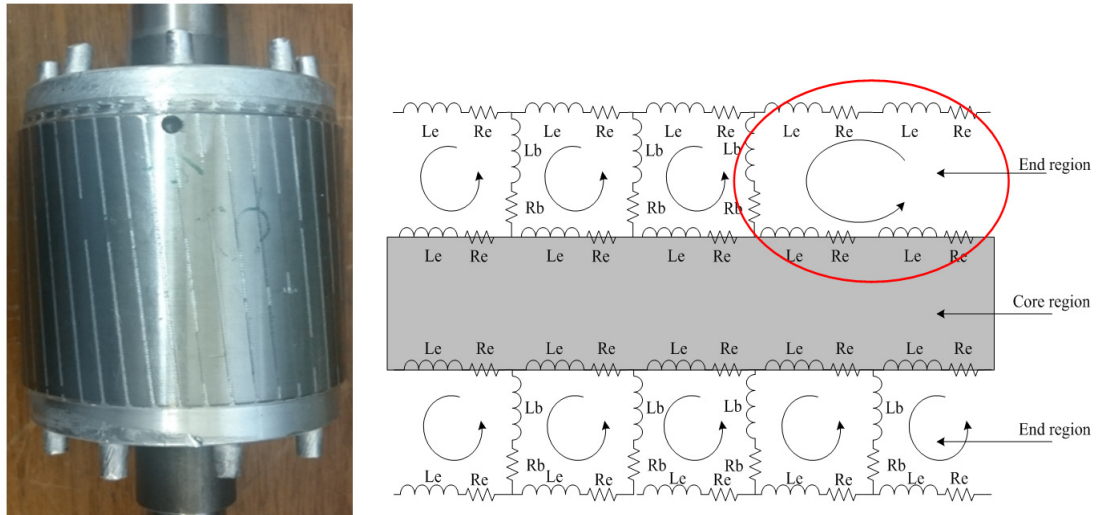


Figure 7-16: One bar fault in the experiment (left figure) and description of the rotor cage-related faults in circuit diagram (right figure).

Figure 7-17 illustrates the thermal images, which are captured in three different load condition, while figure 7-18 represents the signal of one rotor bar fault, current and vibration signals in three different load conditions.

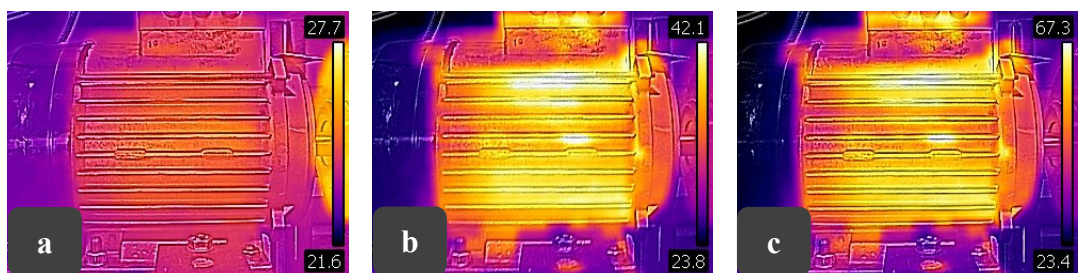


Figure 7-17: Thermal images of one bar rotor fault: a: No load, b: 50% load and c: 100% load.

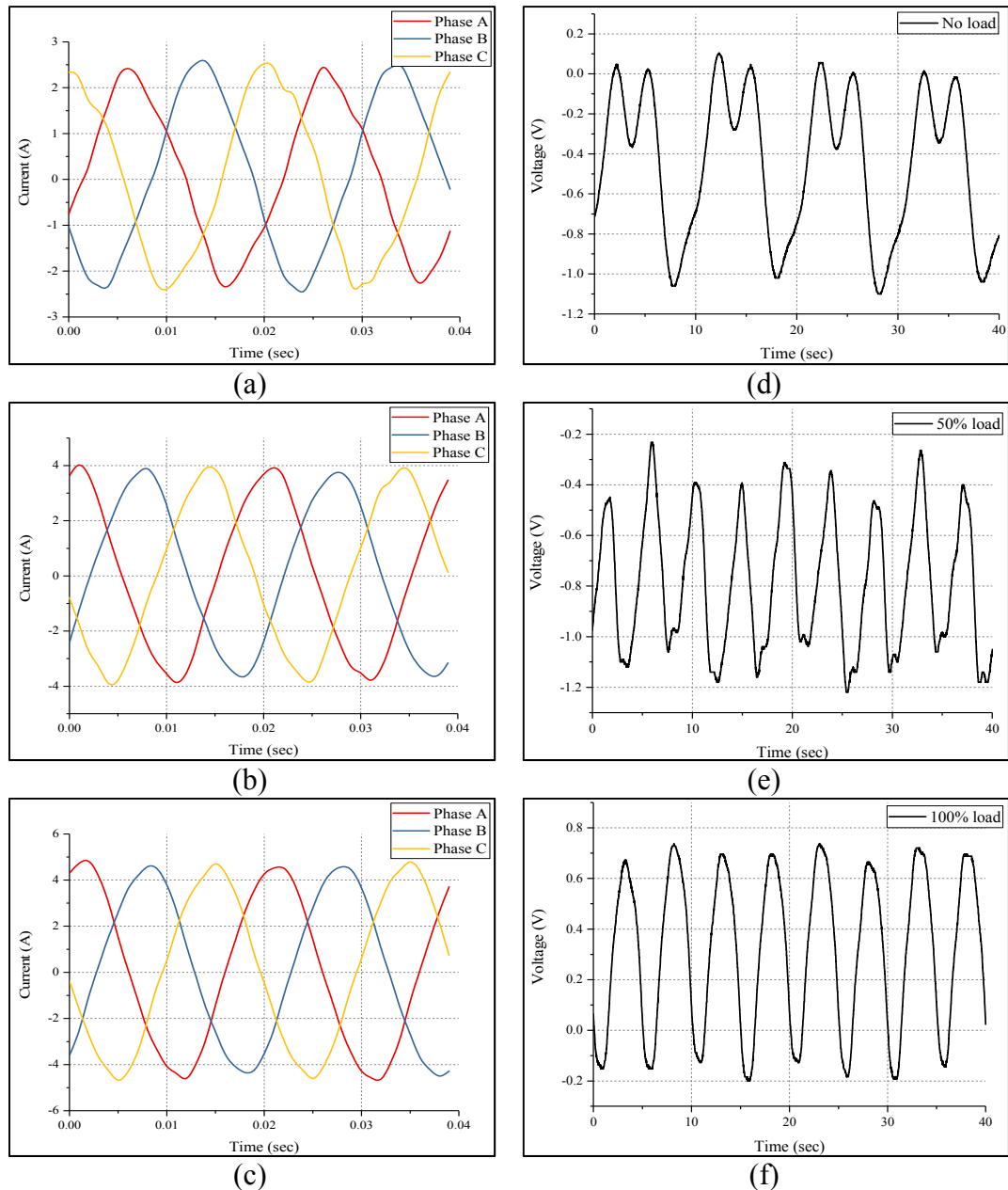


Figure 7-18: The current and vibration signals for one bar fault, a, b, and c represent the three-phase current signal at (a) no load, (b) 50% load and (c) 100% load respectively, while d, e and f represent the vibration signal at different load conditions.

7.7.2 Four Bars Rotor Fault

Four of the rotor bars have been disconnected from the rotor cage of the induction motor. This rotor has been tested in three different load conditions (no load, 50% load

Chapter 7: Experimental Setup and Measurements

and 100% load) as mentioned above. During the measurements, three types of data have been collected, which are thermal image, current and vibration signals.

Figure 7-19 demonstrates the faulty rotor (four faulty bars) circuit. The fault dimensions were the same as the one bar fault.

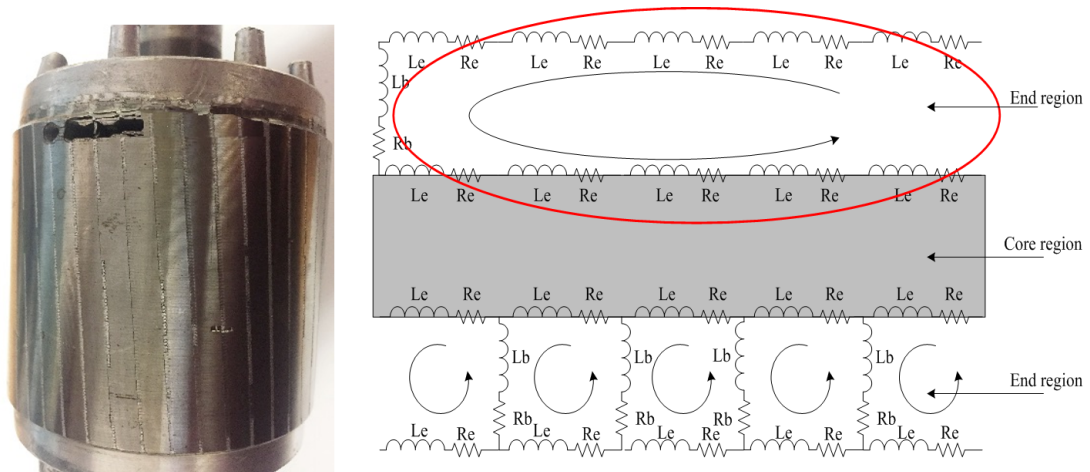


Figure 7-19: Four bars fault in the experiment (left figure) and description of the rotor cage-related faults in circuit diagram (right figure).

Figure 7-20 illustrates the thermal images, which are captured with three different load conditions, while figure 7-21 represents a portion of current and vibration signals for four bars rotor faults at three different load conditions.

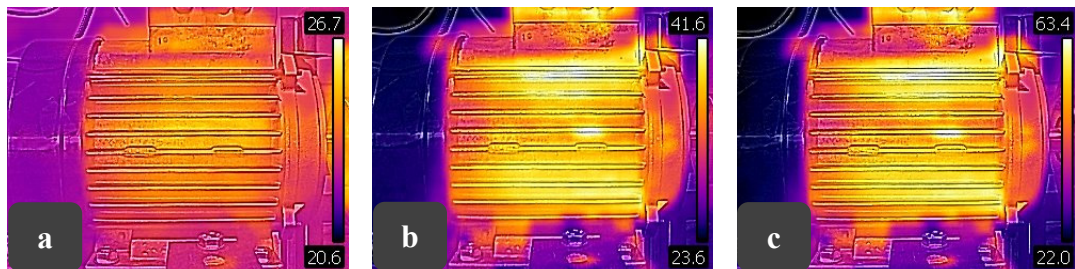


Figure 7-20: Thermal images of four rotor bars fault: a: No load, b: 50% load and c: 100% load.

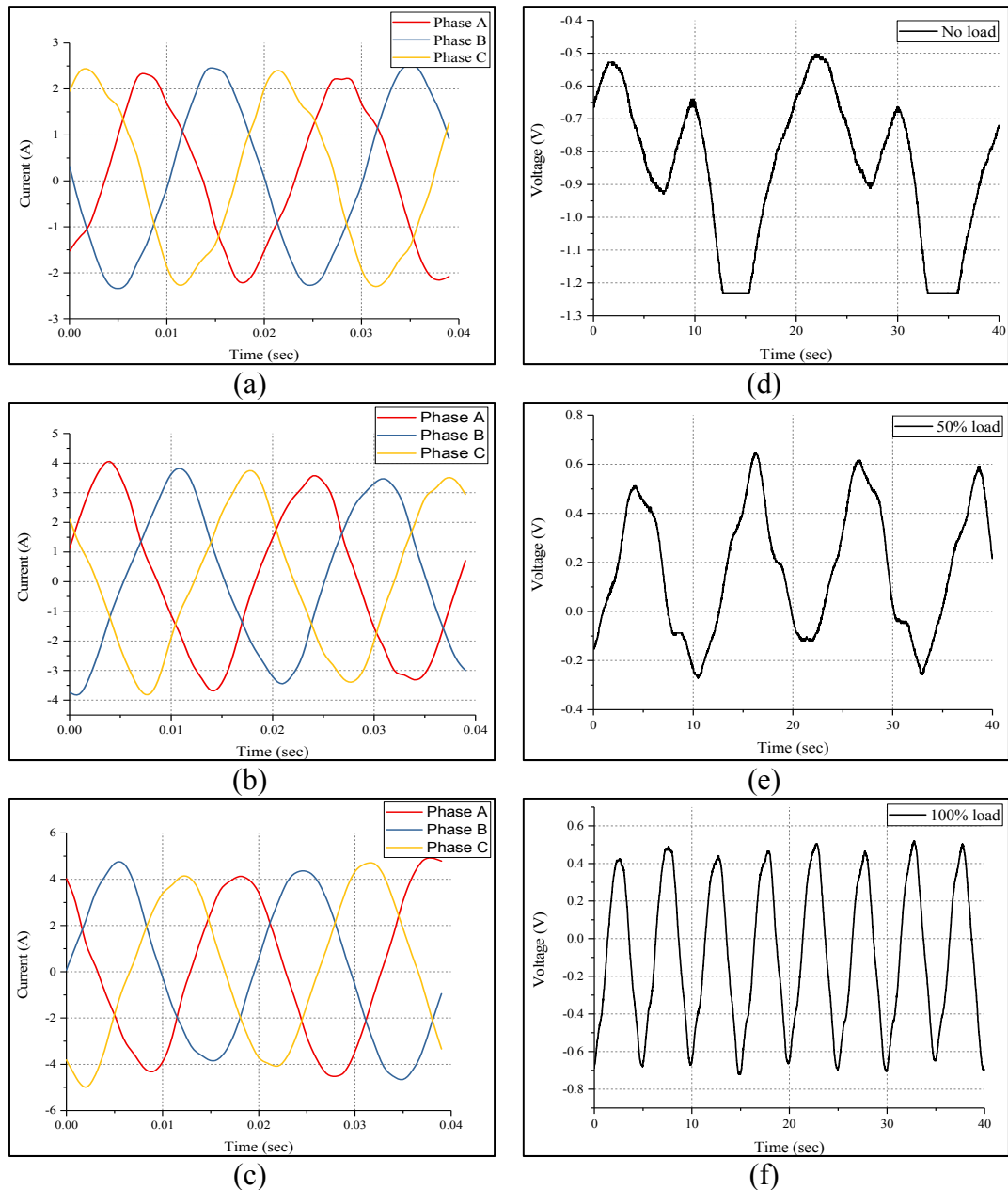


Figure 7-21: The current and vibration signals for four bars rotor faults, a, b, and c represent the three phase current signal at (a) no load, (b) 50% load and (c) 100% load respectively, while d, e and f represent the vibration signal at different load conditions.

7.7.3 Eight Bars Rotor faults

Eight of the rotor bars have been disconnected from the rotor cage. This rotor has been tested with three different load conditions (no load, 50% load and 100% load). During the measurements, three types of data have been collected, which are thermal image,

Chapter 7: Experimental Setup and Measurements

current and vibration signals. Figure 7-22 demonstrates the faulty rotor circuit and the faulty rotor (eight bars). The same hole dimensions have been used for all rotor bars faults.

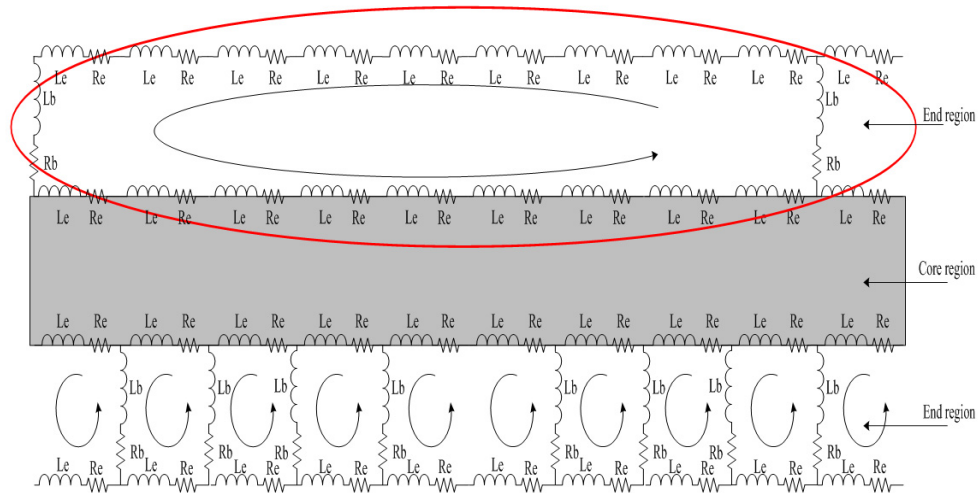


Figure 7-22: IM rotor circuit diagram with eight bars rotor fault and eight rotor bar faults has been created artificially in the experiment.

Figure 7-23 illustrates the thermal images, which are captured in three different load conditions, while figure 7-24 represents a part of current and vibration signals for eight bars rotor faults at three different load conditions.

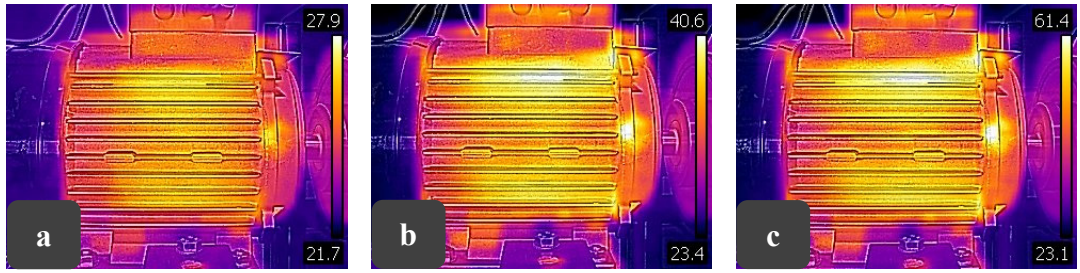


Figure 7-23: Thermal images of eight rotor bars fault: a: No load, b: 50% load and c: 100% load.

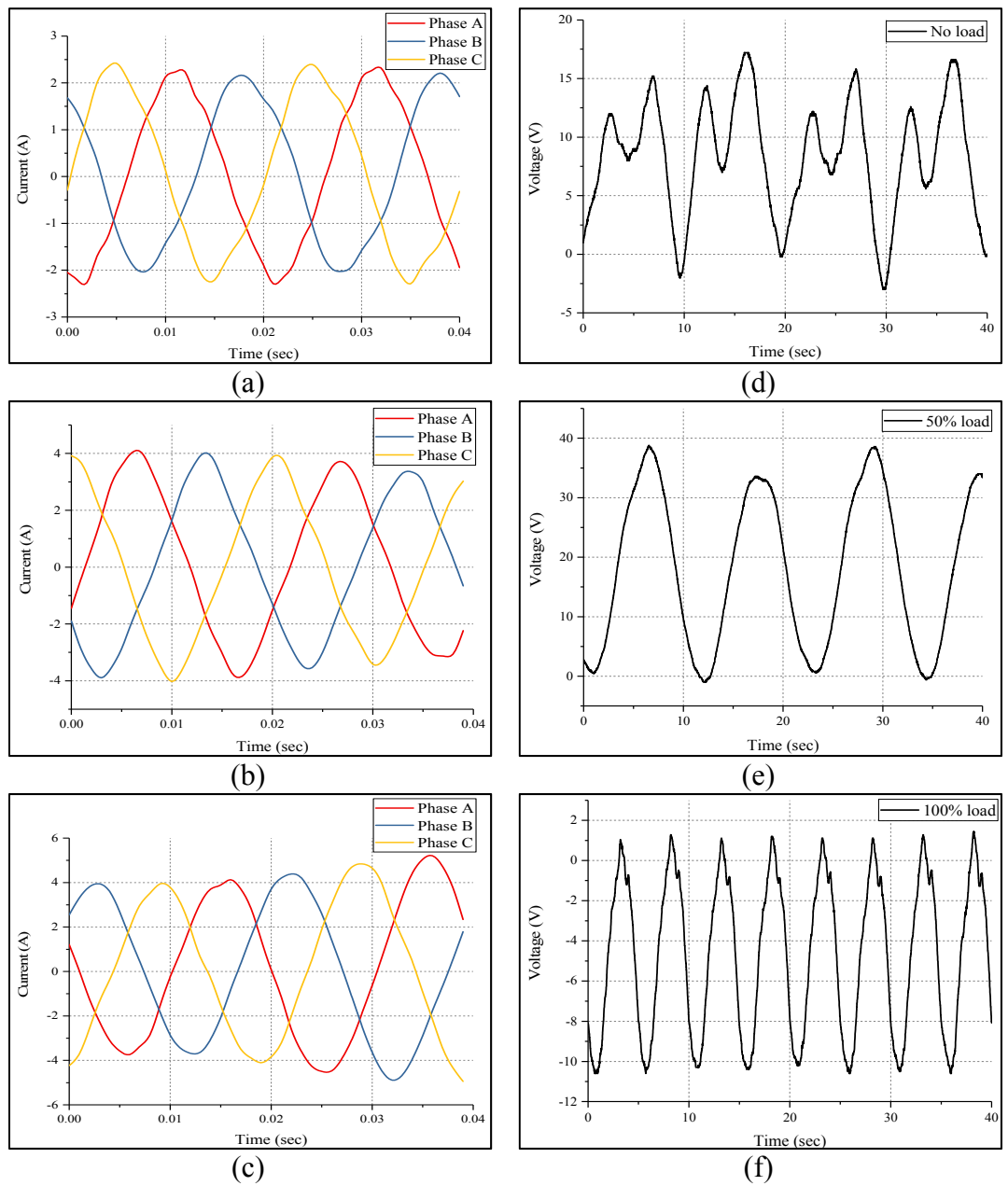


Figure 7-24: The current and vibration signals for eight rotor bars fault, a, b, and c represent the three-phase current signal at (a) no load, (b) 50% load and (c) 100%

load respectively, while d, e and f represent the vibration signal at different load conditions.

7.8 Faulty Bearings

Bearing faults are widespread in industry. The bearing faults have been categorized into two types, generalized roughness fault and single point fault. The generalized roughness fault could be caused by lack or loss of lubricant, contamination and misalignment, while the single point fault usually caused by overloading during operation, which may lead to fatigue crack in the bearing surface until piece of metal drops off. The deep groove ball bearings (6204-Z) have been used in the tests as specified in table 7-2. The tests were focusing on three faulty bearings (outer race, ball bearing and inner race) as described in the following sections. The first step was collecting the data for the healthy bearing in order to acquire base line measurements. Then, three types of bearing faults were tested and the data collected.

Table 7-2: Bearing specifications.

Attribute	Value
Inside diameter	20mm
Outside diameter	47mm
Ball bearing type	Deep groove
Race width	14mm
Number of rows	1
Static load rating	6.55kN
Material	Steel
Ball material	Steel
Cage material	Steel
Race material	Steel
Race type	Plain
Dynamic load rating	13.5kN
Bore type	Parallel

7.8.1 Outer Race Bearing Fault

In the experiment, the faulty bearing has been created by drilling a 0.2 cm hole into outer race as shown in figure 7-25.

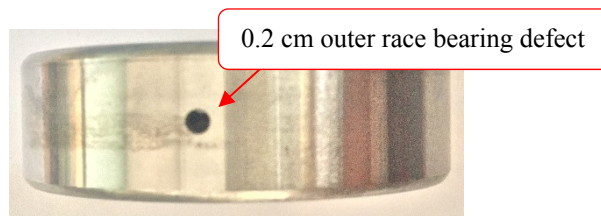


Figure 7-25: Bearing with outer race defect.

This fault has an effect on three important parameters of IM such as temperature, unbalance rotor and vibration behaviour than the healthy one. Figure 7-26 and figure 7-27 demonstrate the thermal images that have been captured from the experimental tests with outer race bearing fault, the current and vibration signals by applying three types of load (no load, 50% load and 100% load) respectively.

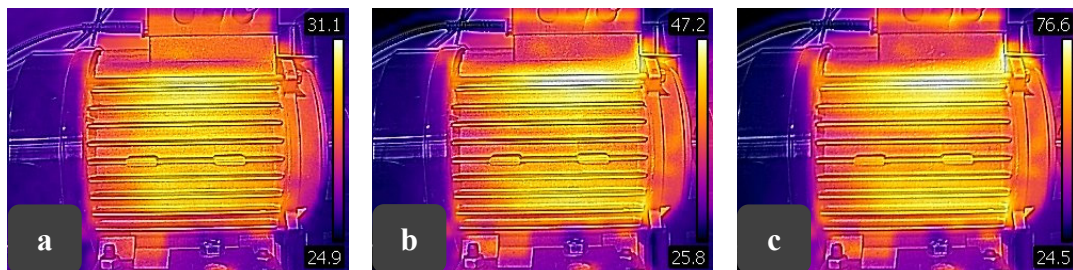
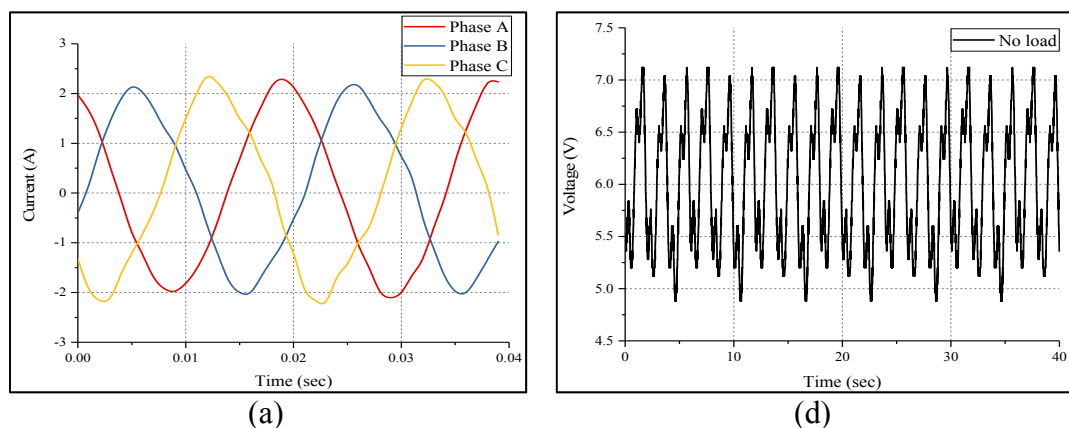


Figure 7-26: Thermal images of outer race bearing defect: a: No load, b: 50% load, and c: 100% load.



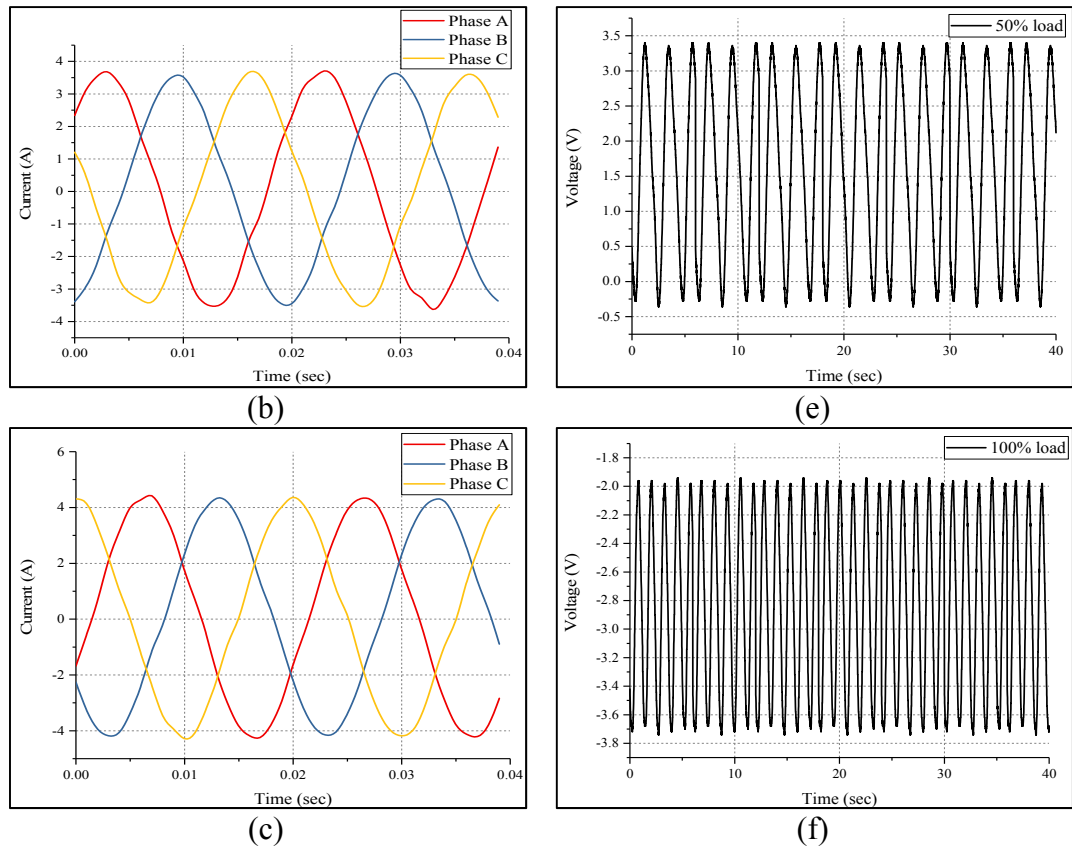


Figure 7-27: The current and vibration signals for outer race bearing defect, a, b, and c represent the three phase current signal at (a) no load, (b) 50% load and (c) 100% load respectively, while d, e and f represent the vibration signal at different load conditions.

7.8.2 Ball Bearing Fault

One ball with its cage has been removed from the bearing in order to investigate the most popular bearing faults, which is ball crashing during the load operation. Figure 7-28 shows the bearing ball defect. In addition, figure 7-29 and figure 7-30 illustrate the thermal images, current and vibration signals with ball bearing defect and three load conditions.

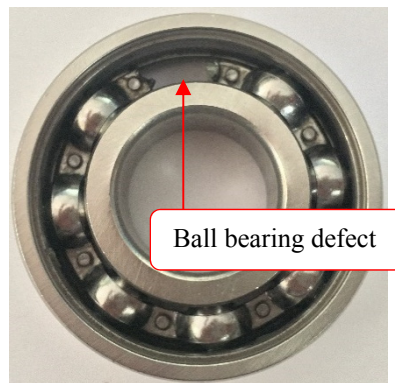


Figure 7-28: Bearing with ball defect.

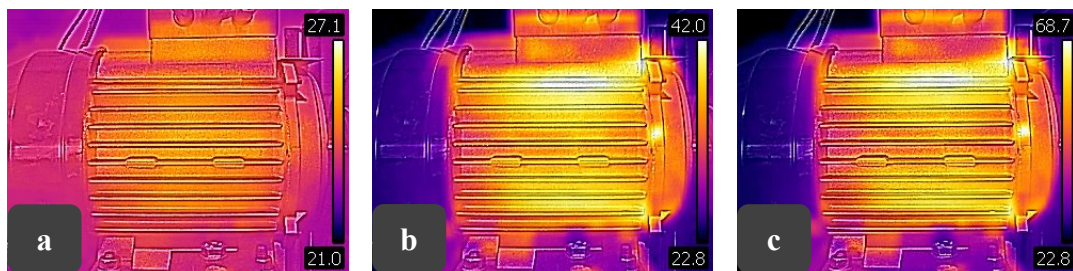
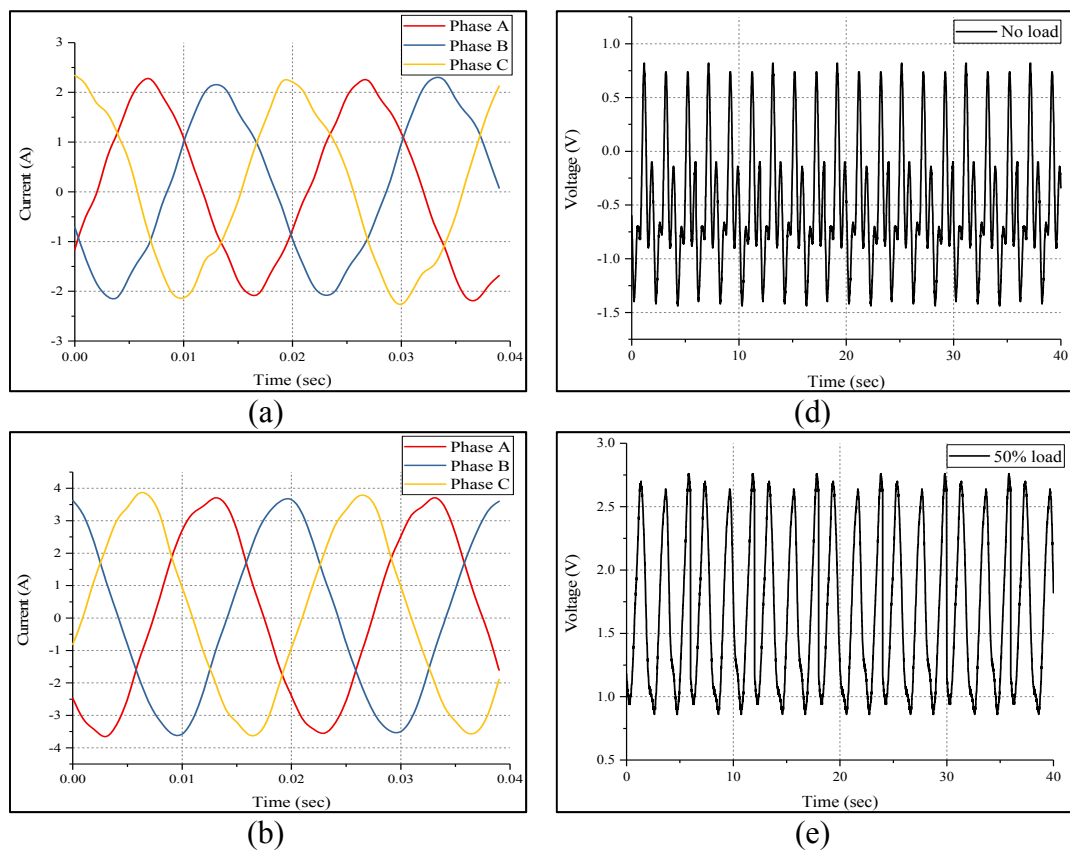


Figure 7-29: Thermal images of ball bearing defect: a: No load, b: 50% load and c: 100% load.



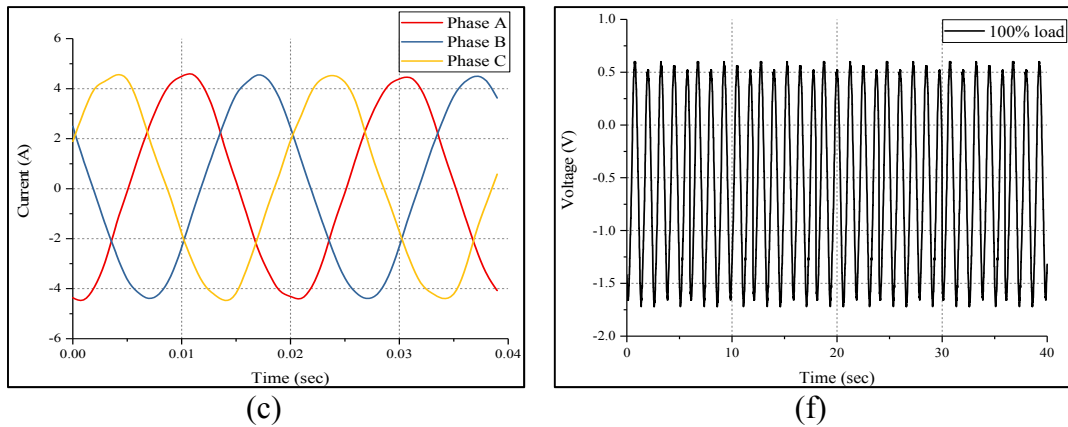


Figure 7-30: The current and vibration signals for ball bearing defect, a, b, and c represent the three-phase current signal at (a) no load, (b) 50% load and (c) 100% load respectively, while d, e and f represent the vibration signal at different load conditions.

7.8.3 Inner Race Bearing Fault

This fault has been also created by drilling a 0.2 cm hole into inner race as shown in figure 7-31. This fault has the same effects on the three parameters of IM as mentioned earlier. Figure 7-32 and figure 7-33 demonstrate the thermal images that have been captured from the experiment tests with outer race bearing fault and the current and vibration signals by applying three types of load (no load, 50% load and 100% load) respectively.



Figure 7-31: Bearing with inner race defect.

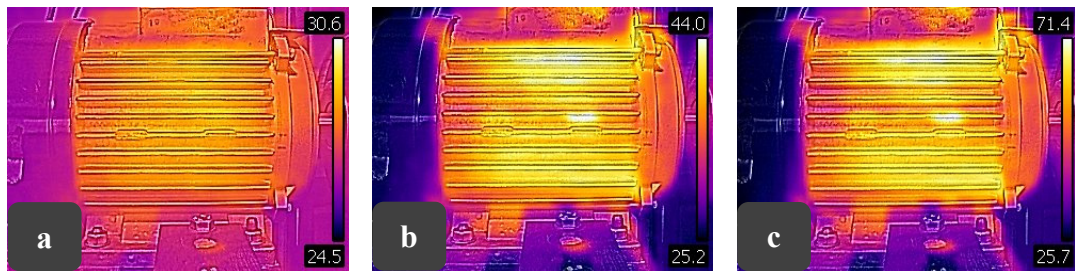


Figure 7-32: Thermal images of inner race defect: a: No load, b: 50% load and c: 100% load.

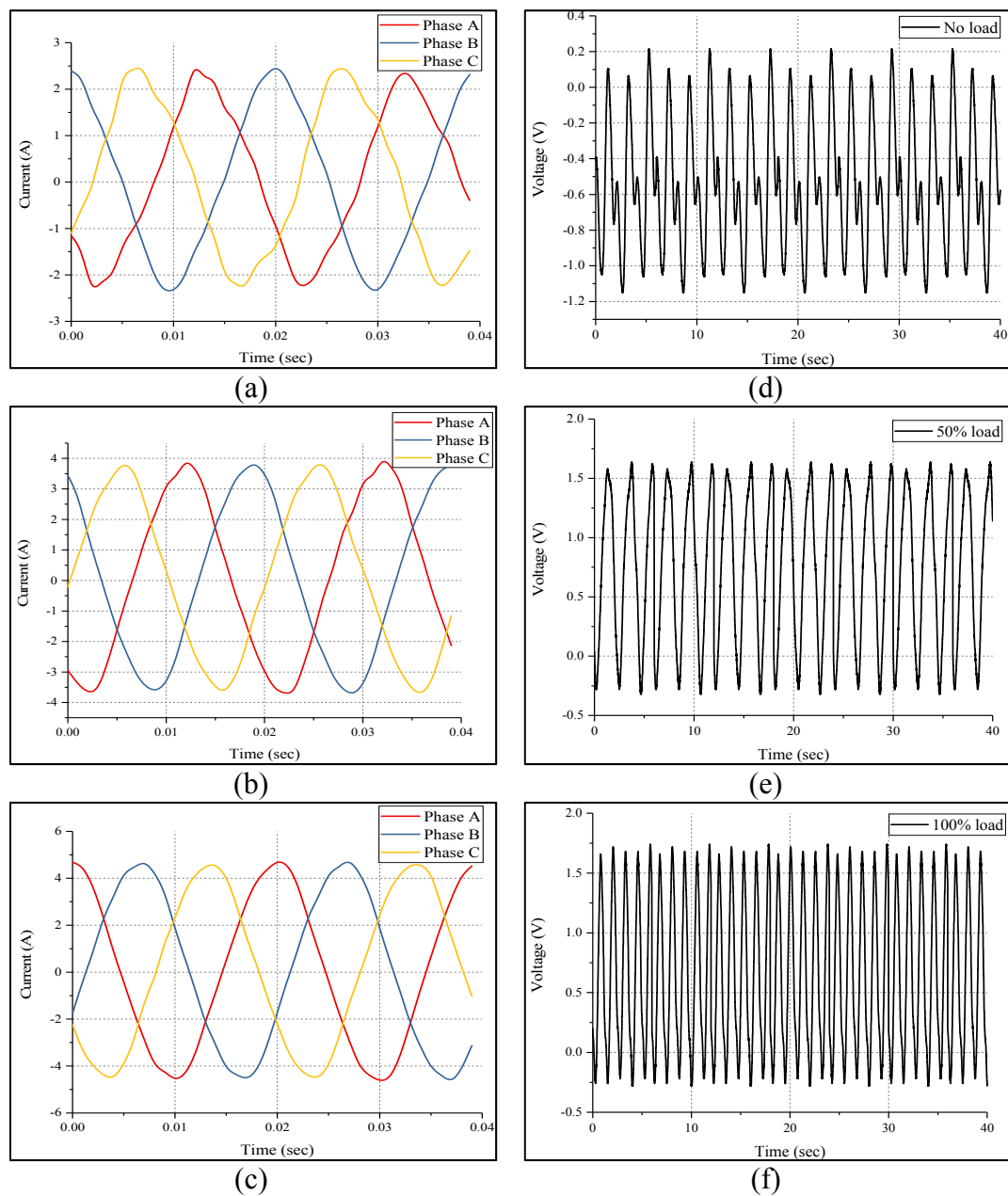


Figure 7-33: The current and vibration signals for inner race defect, a, b, and c represent the three-phase current signal at (a) no load, (b) 50% load and (c) 100%

load respectively, while d, e and f represent the vibration signal at different load conditions.

The analytical procedure and the results obtained from the IM faults are described in the next chapter.

CHAPTER 8

DATA AND SIGNAL ANALYSIS

“This chapter reports the collected data for the faulty induction motors for a range of loads. This database is used to provide the baseline representing the motor behaviour for different faults and load conditions in order to detect and classify the fault correctly. Then, the data has analysed to provide a number of statistical parameters for the healthy and faulty motors with purpose of detecting, diagnosing and assessing the severity of the seeded faults: one bar, four bars and eight bars rotor faults, outer race, ball bearing and inner race bearing fault”.

8.1 Thermal Image Analysis

First of all, the IM motor should be checked and the images have been captured when it is run in the normal condition (healthy). The normal condition data has been collected in order to be used as base line measurements (reference signal). The captured images have been used for both troubleshooting motor problems and condition monitoring because it is very useful tool for this kind of tasks. Thermography images of the induction motors reveal their operation conditions as reflected by their surface temperature, capturing infrared temperature measurements of motor temperature profile as a two-dimensional image. The infrared camera has been able to capture the object temperature at thousands of points instantaneously for all of the critical components of a motor. As discussed above in the previous chapter, two faulty cases have been created for the induction motor, which are the rotor and the bearing faults, and each of these faults have different kind of fault. The following sections discuss one faulty case for the induction motor at different load conditions, while the other cases have been placed in the appendixes in order to reduce the pictures in this chapter and prevent the repetition of each graph.

8.2 Thermal Images Analysis for Rotor Faults

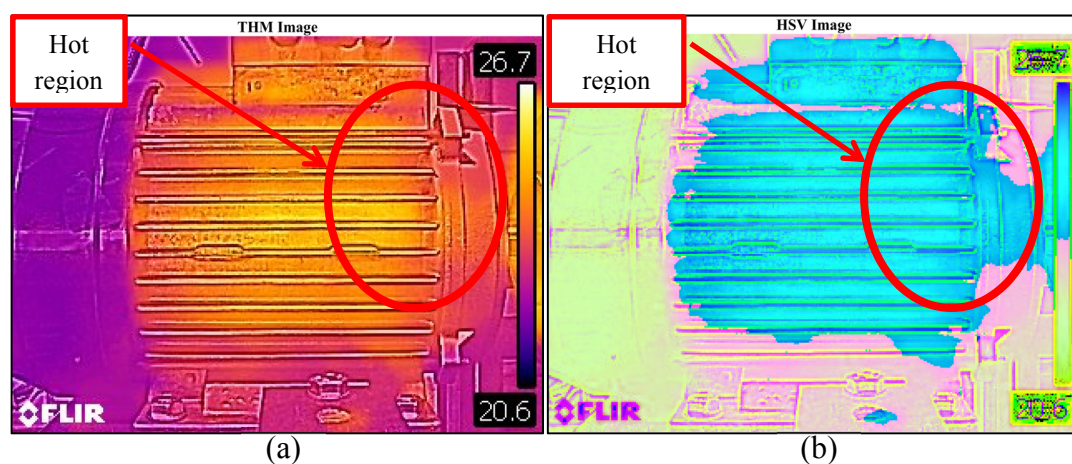
The thermal images have been captured for the rotor bar (one bar, four bars and eight bars) faults with different load conditions. The thermal camera has been placed in a fix position in order to capture the same image dimensions for all motor as it has effects on the pixel values.

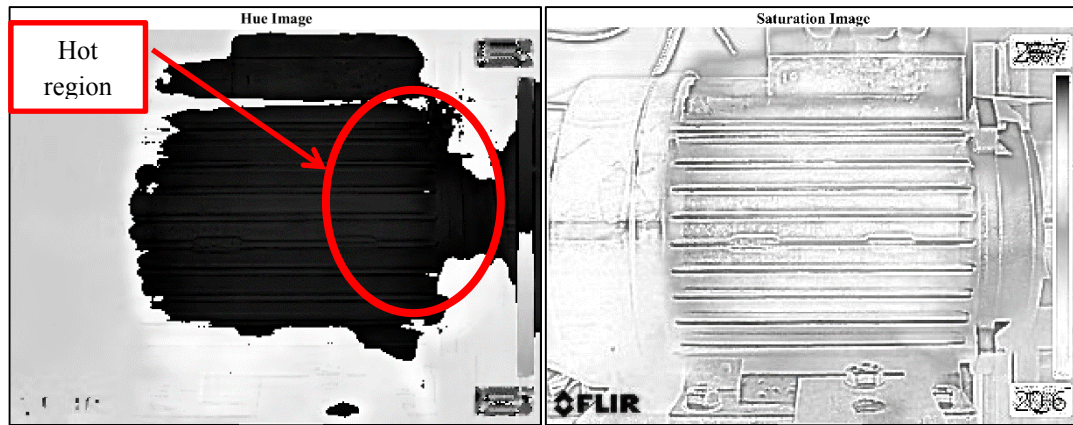
After capturing the thermal images, the next stage is to analyze these images in order to extract the best information to be used for classification system. As explained in the

chapter four section 5.2, different image-processing methods have been used for extracting the best data features from the thermal images (Hue, Sobel, Prewitt, Roberts, Canny, LoG and Otsu) as described before. MATLAB “R2015b” software has been used for applying these methods and calculating the image matrices.

8.2.1 Thermal Image Analysis for Four Bars Rotor Fault

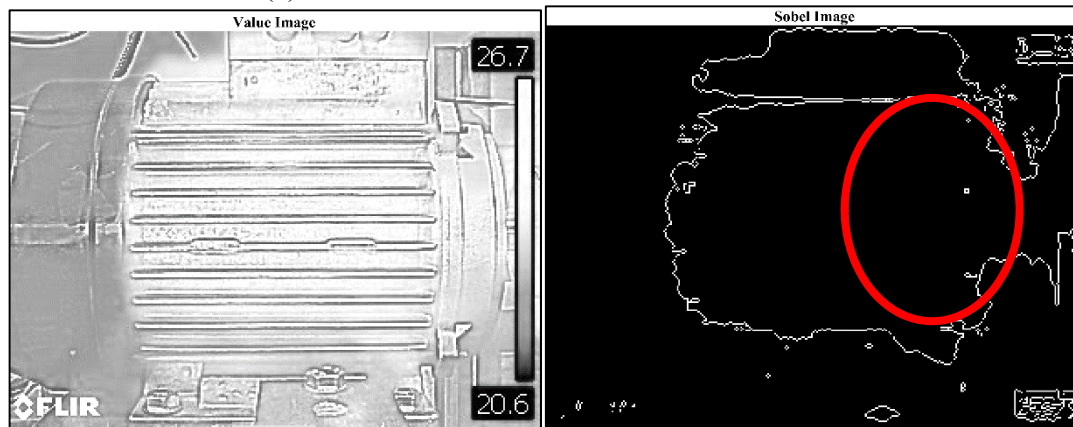
Figure 8-1 illustrates the thermal images for four bars rotor fault with no load condition, and the analyzed images have also been explained based on the proposed method HSV image. It was noticed that the Hue method technique shows the hottest region in the induction motor at temperature 26.7°C , which is a little bit higher than the room temperature. Hence, the value and saturation images have been considered but it appears that they are less helpful than the Hue image for distinguishing between the motor faults. Thus, the other proposed segmentation methods (Sobel, Prewitt, Roberts, Canny, LoG and Otsu) have been applied for the Hue image to extract the best and most useful features from the faulty raw thermal image, which are clearly illustrated in the same figure.





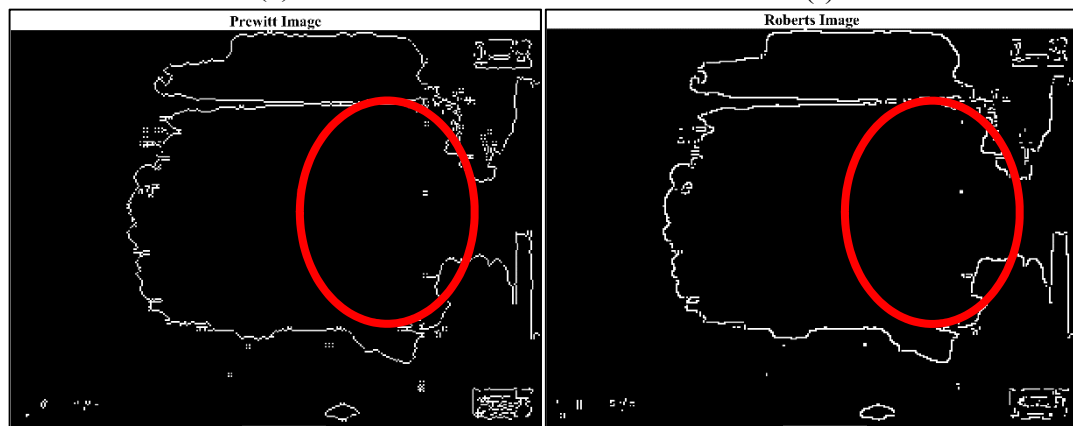
(c)

(d)



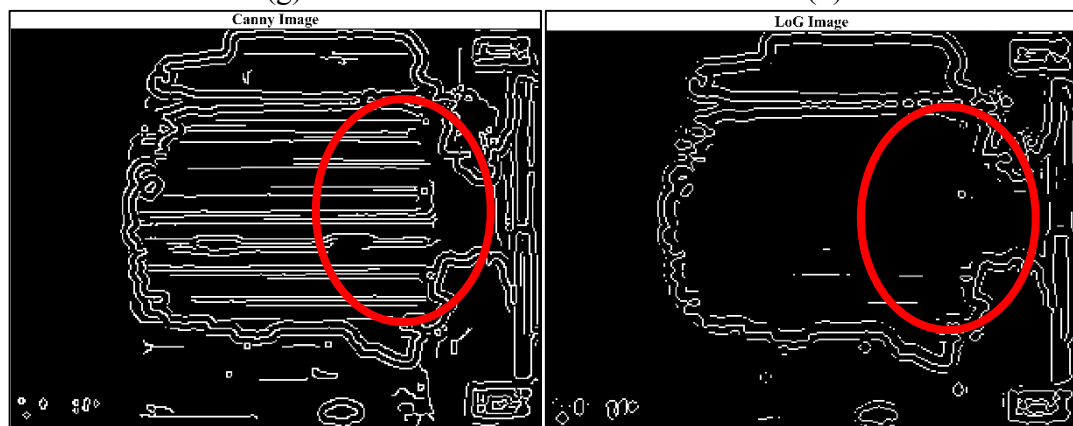
(e)

(f)



(g)

(h)



(i)

(j)

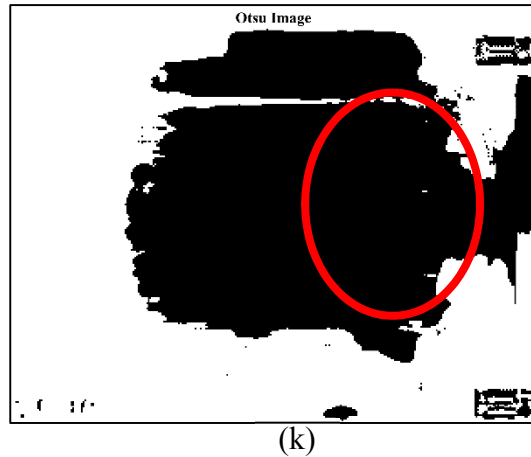
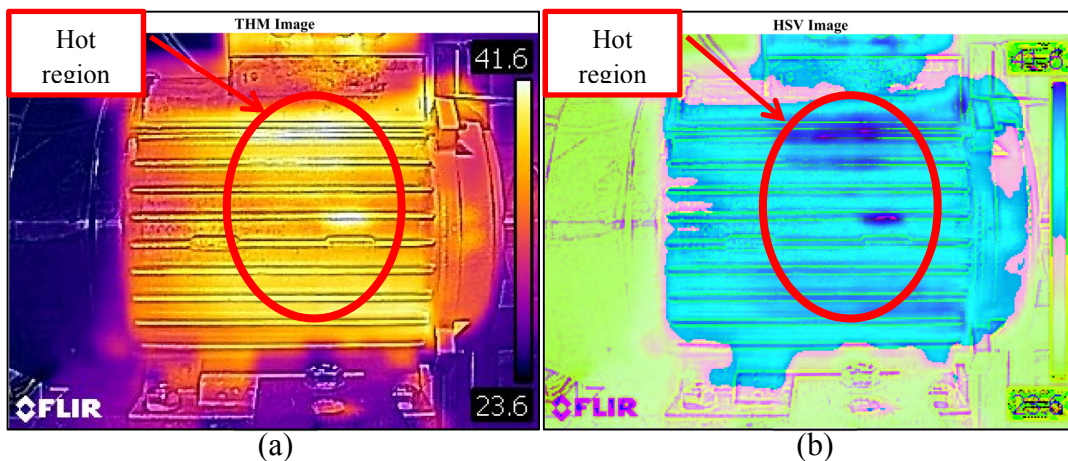
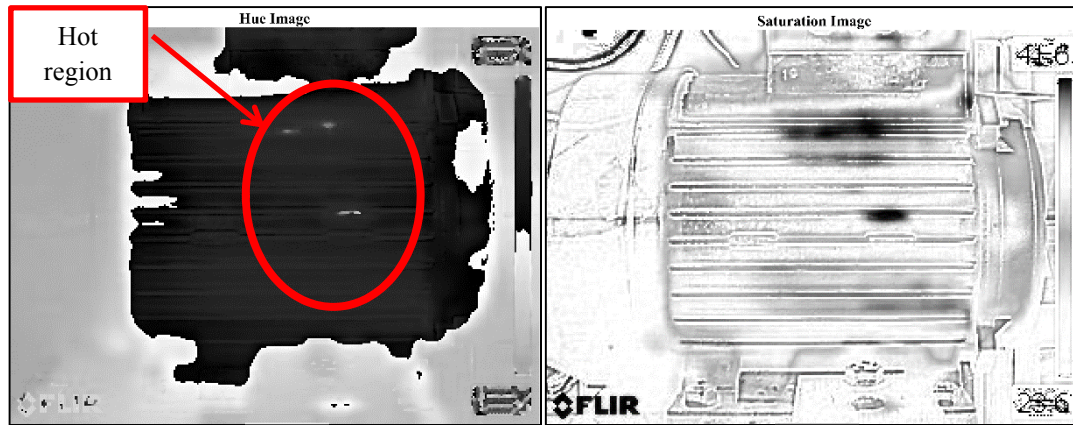


Figure 8-1: Thermal image analysis for four bars rotor fault with no load condition a) original image, b) HSV image, c) Hue image, d) Saturation image, e) Value image, f) Sobel image for Hue, g) Prewitt image for Hue, h) Roberts image for Hue, i) Canny image for Hue, j) LoG image for Hue, k) Otsu image for Hue.

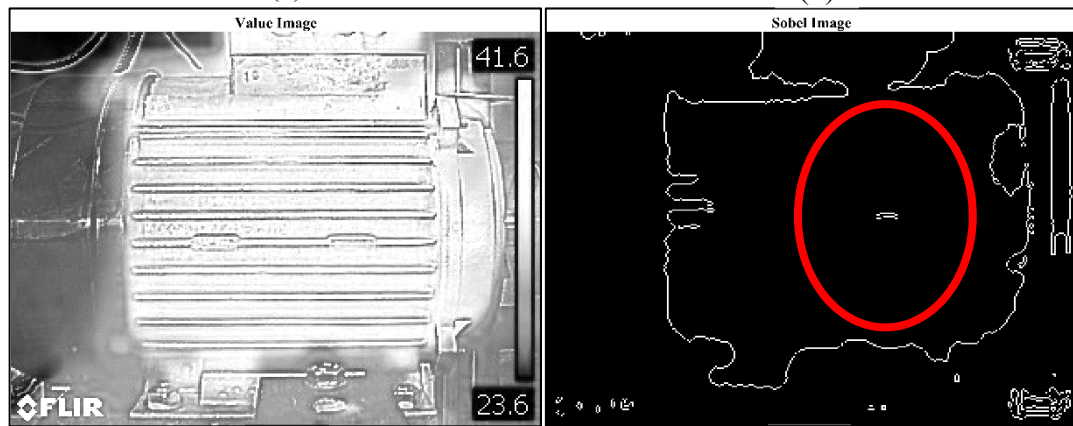
Figure 8-2 shows the induction motor thermal image for rotor fault (four bars) with 50% load condition at temperature 41.6°C , which is very clear that the motor temperature has been raised and became much bigger than the no load condition. Furthermore, the Hue image and other segmentation methods have been extended based on the temperature profile. This figure indicates that the proposed segmentation methods have been worked successfully and could be more useful for discriminating between the IM faults, and will be very helpful for the classification system to have better accuracy.





(c)

(d)



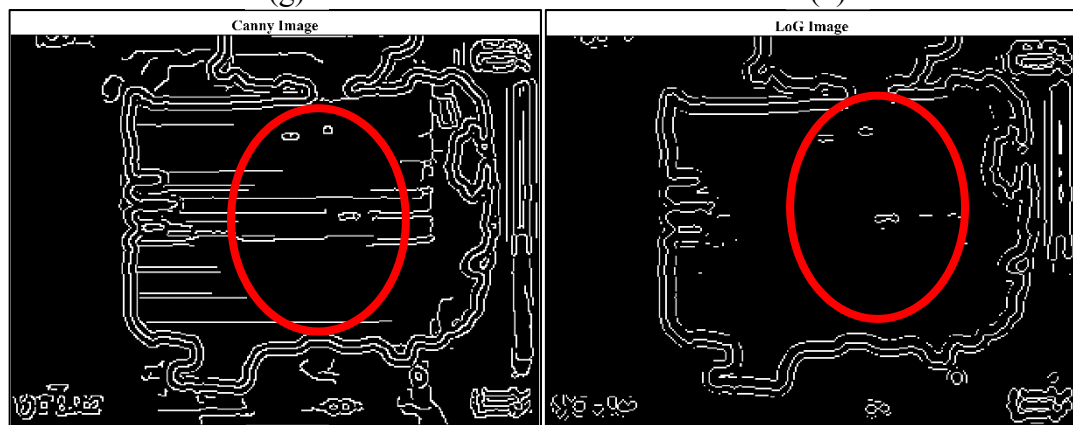
(e)

(f)



(g)

(h)



(i)

(j)

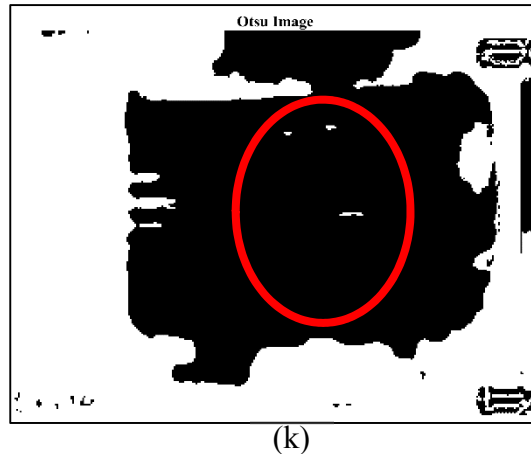
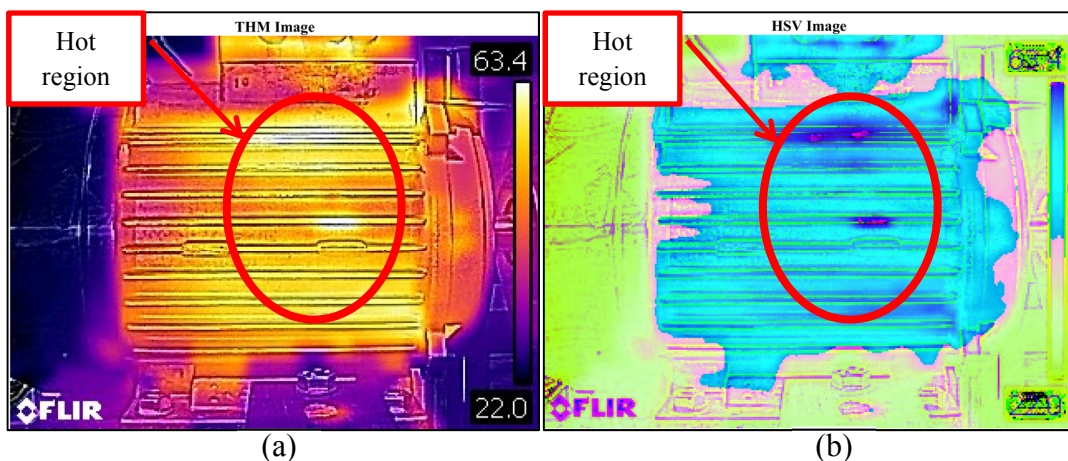
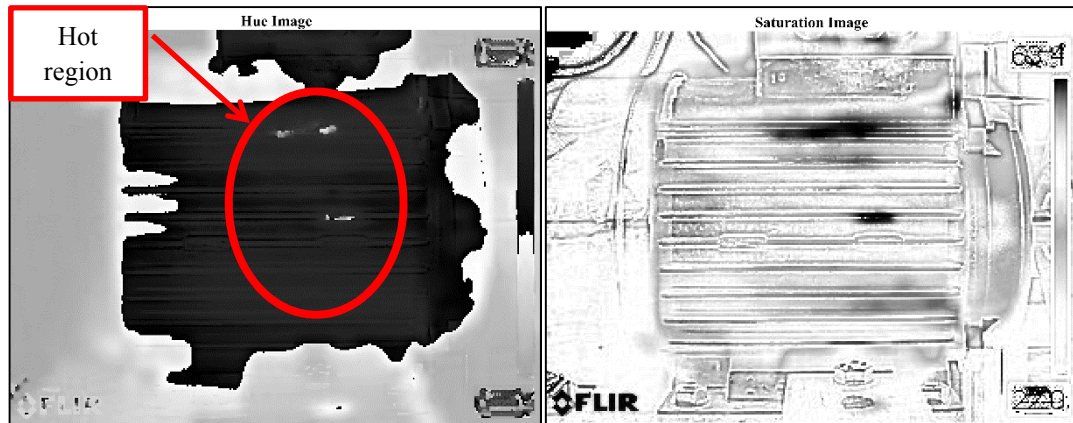


Figure 8-2: Thermal image analysis for four bars rotor fault with 50% load condition
 a) Original image, b) HSV image, c) Hue image, d) Saturation image, e) Value image, f) Sobel image for Hue, g) Prewitt image for Hue, h) Roberts image for Hue, i) canny image for Hue, j) LoG image for Hue, k) Otsu image for Hue.

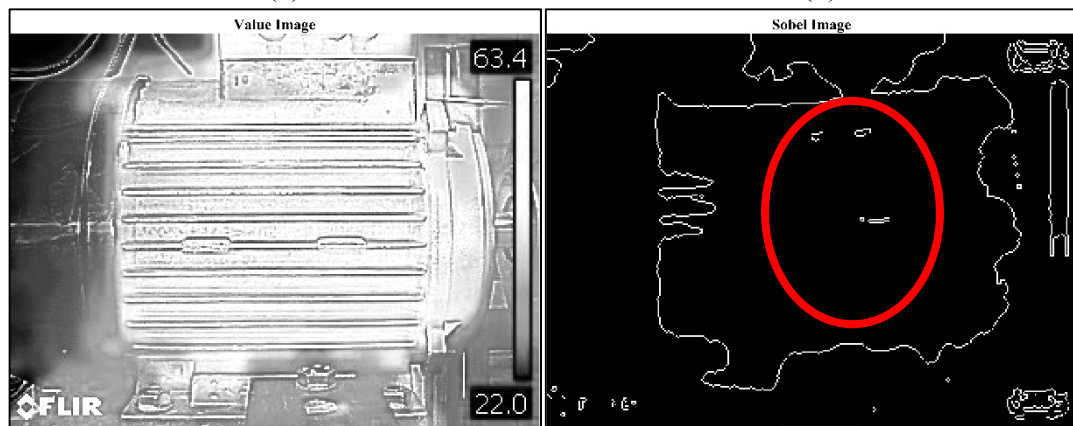
In addition to this, the 100% load condition thermal image for four rotor bars fault have been captured and segmented based on the proposed method (Hue image), as shown in figure 8-3 the hottest spot was 63.4°C temperature. It was clearly that the induction motor temperature has been raised and concentrated at some points of the image. All three induction motor thermal images have different temperature profile because of the faulty rotor; it increases the stator current in the motor by increasing the load, which is lead to increasing the temperature. In this case, the pixel values will be a little different from each other except the hotspot in the image will be more affected.





(c)

(d)



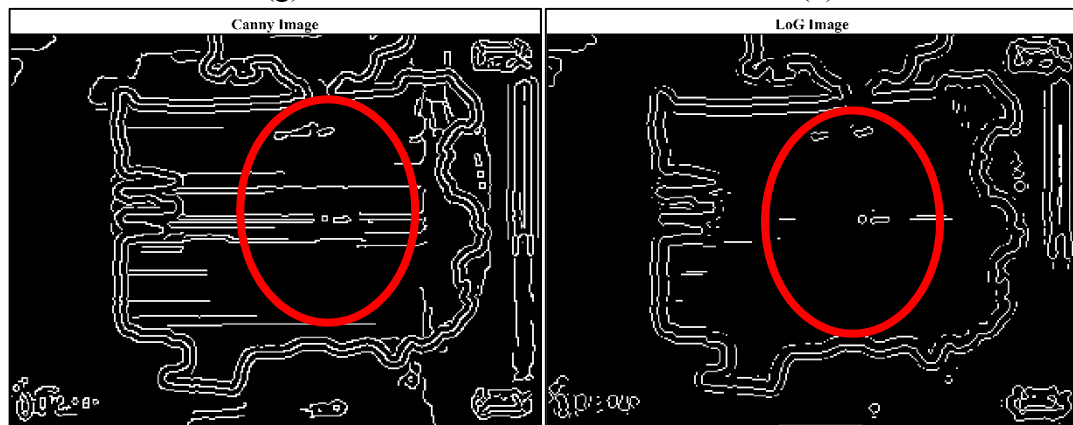
(e)

(f)



(g)

(h)



(i)

(j)

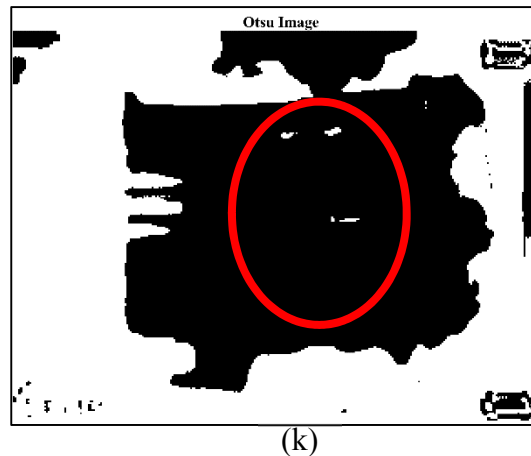


Figure 8-3: Thermal image analysis for four bars fault with 100% load condition a) Original image, b) HSV image, c) Hue image, d) Saturation image, e) Value image, f) Sobel image for Hue, g) Prewitt image for Hue, h) Roberts image for Hue, i) Canny image for Hue, j) LoG image for Hue, k) Otsu image for Hue.

After applying all the proposed image segmentation methods for all healthy and faulty thermal images, the following step is calculating the image matrices (MSE, PSNR, Variance, Mean, Standard Deviation, Skew and Kurtosis) as mentioned in chapter 5-section 5.3. Figure 8-4a shows the MSE values for six different segmentation methods (Sobel, Prewitt, Roberts, Canny, LoG, Otsu), it was clearly that the MSE values of no-load condition is much bigger than the other two load conditions (50%, 100%). Besides, the Otsu values with no-load condition has lower values than the other load conditions. In addition to this, figure 8-4b illustrates the PSNR values, which are also plays vital role in the motor fault detection, here the values having opposite trend to those of figure 8.4a. The no-load condition values are lower than all segmentation methods, whereas the Otsu values with no-load is larger than other Otsu values (50% and 100% load conditions). Thus, these values will be very helpful for the classification system for detecting the fault severity.

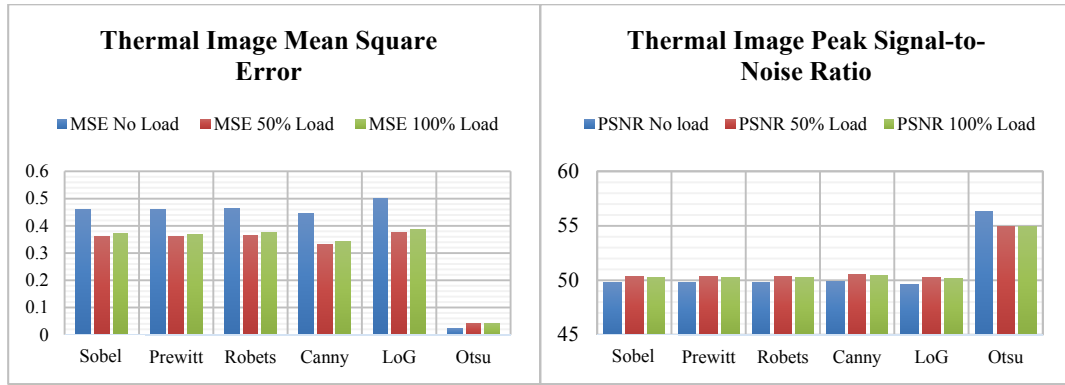


Figure 8-4: a) The MSE values, and b) The PSNR values for three different load conditions.

Figure 8-5 a and b, illustrate two important features that may help the classification system for detecting the motor faults correctly, which are the variance and mean. It was obvious that these two values have the same behaviour for all load conditions but the differences were approximately in the range of (0 - 0.25) and (0 – 0.55) for the variance and mean respectively. In general, the variance and mean in this case have almost the same value in all segmentation methods, hence, for that reason the feature selection methods have been applied for selecting the best feature to avoid overlapping problems. The feature selection methods have their own decision for selecting the most suitable feature in order to have more accurate classification system.

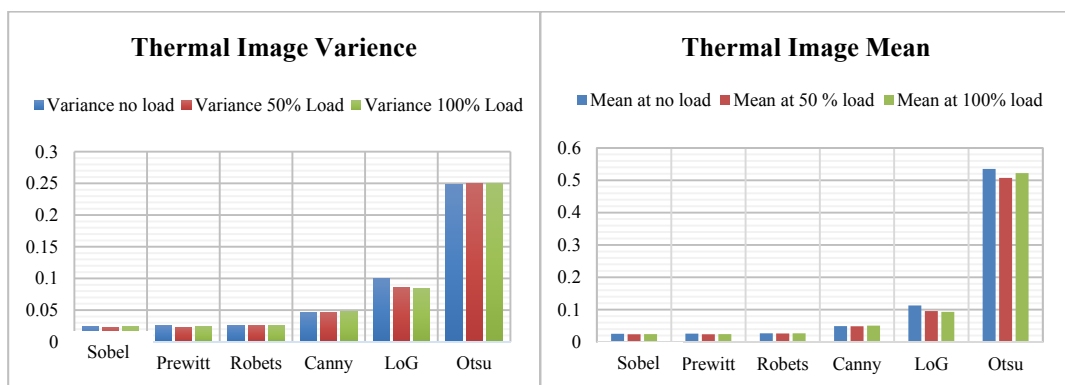


Figure 8-5: a) The variance value, and b) The mean values for different load conditions.

On other hand, figure 8-6, demonstrate the Skew and the Kurtosis values. These values have been calculated using MATLAB “R2015b” based on the formulae as mentioned in chapter 5-section 5.3. Figure 8-6 a shows that the values of Skew has a slight change in the first three segmentation methods (Sobel, Prewitt and Roberts) among three load conditions, but has large difference between the Canny, LoG and other methods, which makes it helpful for recognizing the faults in an early stage.

Furthermore, figure 8-6b illustrates the values of the Kurtosis, which almost the same as the Skew values but its range is far different from the Skew. The Sobel, Prewitt, Roberts and LoG have different values in three load conditions, while Otsu values in both Skew and Kurtosis are very low in all load conditions based on the pixels values. Nevertheless, they are still need to be taken into account for the classification system as it has negative values in the case of Skew and positive values in the case of Kurtosis. Therefore, every single point or value in the thermal image should be considered in order to classify the IM motor faults correctly.

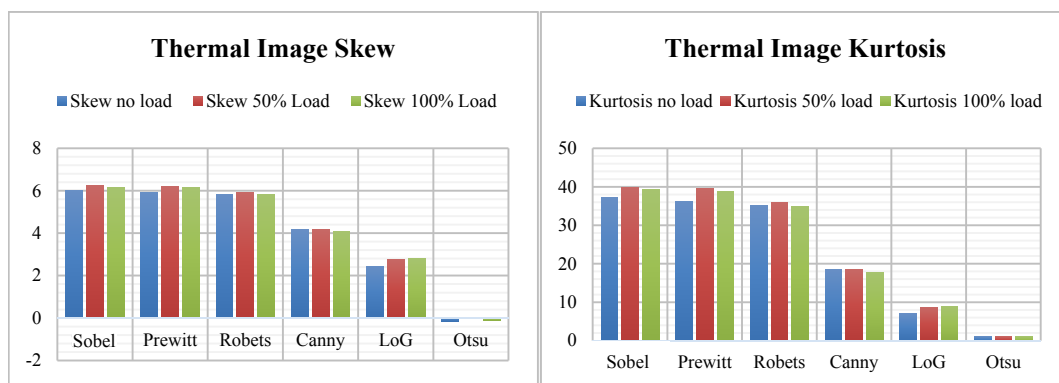


Figure 8-6: a) The thermal image Skew values and b) Thermal image Kurtosis values for different load conditions.

8.2.2 Thermal Image Wavelet Analysis for Rotor Bars Fault

Thermal image analysis based on 2D wavelet transform analysis has been widely used because it has been able to extract the most useful features by using more than one level for different types of wavelet such as Haar, Daubechies (db), Sym, etc. as mentioned in chapter 5-section 5.4. In this research, the Discrete Wavelet Transform (DWT) analysis has been included in the IM fault investigation in order to have variety of feature for detecting the motor faults in a correct way.

Initially, the N level and the wavelets types should be selected, after that, the thermal image coefficients have been determined by using 2D DWT. To do image decomposition, it is very important to decide over many selections, such as the types of mother wavelet, the decomposition level, types of coefficients and etc.. In this research, the Daubechies (db) seven mother wavelet has been applied and the decomposition level was three. The wavelet type and decomposition level are the same for all the wavelet thermal image analysis in order to obtain the same features for all faulty thermal images, which are db7 and 3 levels. Due to the thermal image data dimension, the level 3 has been chosen because there is no data for decomposition after the selected level and the image will lose most of its features. Having performed the mother wavelet and the decomposition level, two kinds of wavelet coefficients are very important to find from each class of machine conditions data. These coefficients are Approximation (a) and Details (d). Approximation coefficients that are passes through the low pass filter are considered for feature extraction as the low pass frequency signal contain most important parts of original signal. On the other hand, other wavelet coefficient except approximation could be useful for monitoring the machine fault diagnosis.

The wavelet analysis and its coefficients have been demonstrated in figure 8-7, the wavelet type was db7 using 3 levels. The purpose of using the Discrete Wavelet Transform (DWT) for analysing the thermal image is to decompose the image and extract the best coefficients that are helpful to be used for further processing. It has been clearly shown that the reconstructed image after 3 levels of decomposition was able to detect the hottest region and calculate the pixels value.

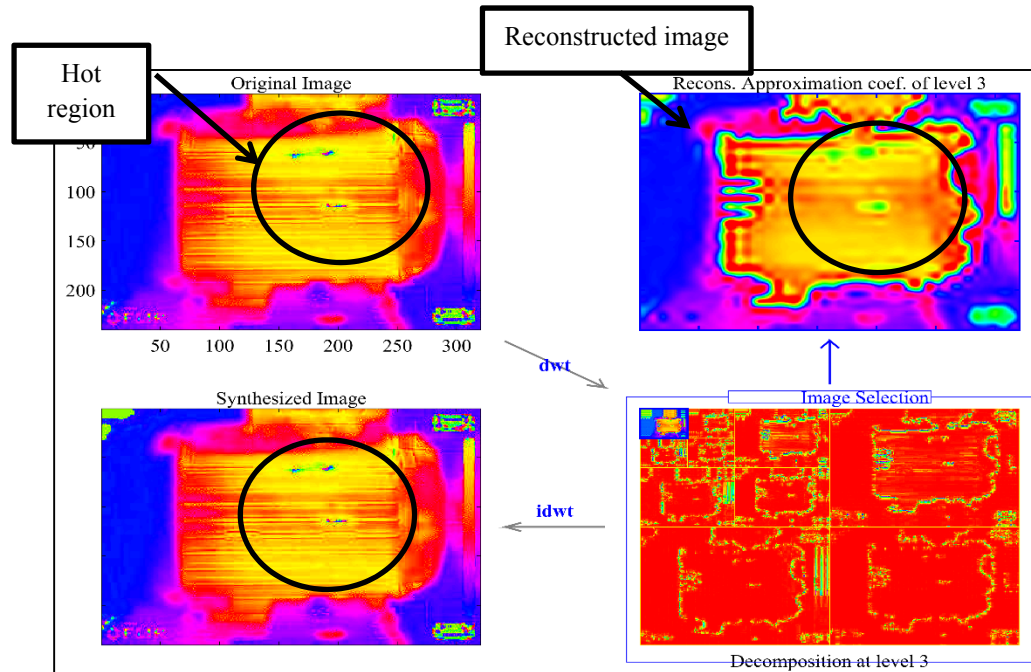


Figure 8-7: Thermal image wavelet analysis for four bars rotor fault with no load condition.

The 50% load condition thermal image has been captured for the induction motor as shown in figure 8-8. This figure shows the wavelet analysis for four bars rotor faults with 50% load and its decomposition level. Furthermore, the difference between the thermal image analysis with no-load condition and the thermal image with 50% load condition have been visibly appeared by simply looking for the hottest region in the reconstructed image.

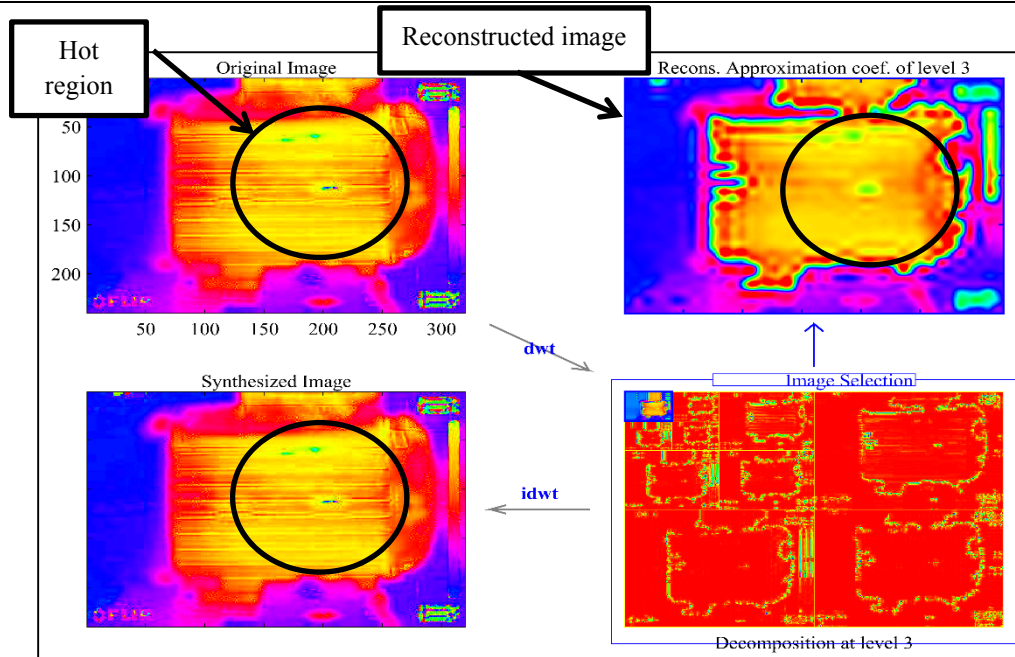


Figure 8-8: Thermal image wavelet analysis for four bars rotor faults with 50% load condition.

Figure 8-9 illustrates the four bars rotor fault with 100% load condition, the wavelet has been applied same as the above figures. It was obvious that the motor temperature in the reconstructed image became more focused than the other load conditions (no-load and 50% load). Wavelet analysis has been applied successfully for the faulty rotor thermal images. Consequently, all thermal images based on wavelet analysis have been adapted to extract more and best features to achieve good classification accuracy.

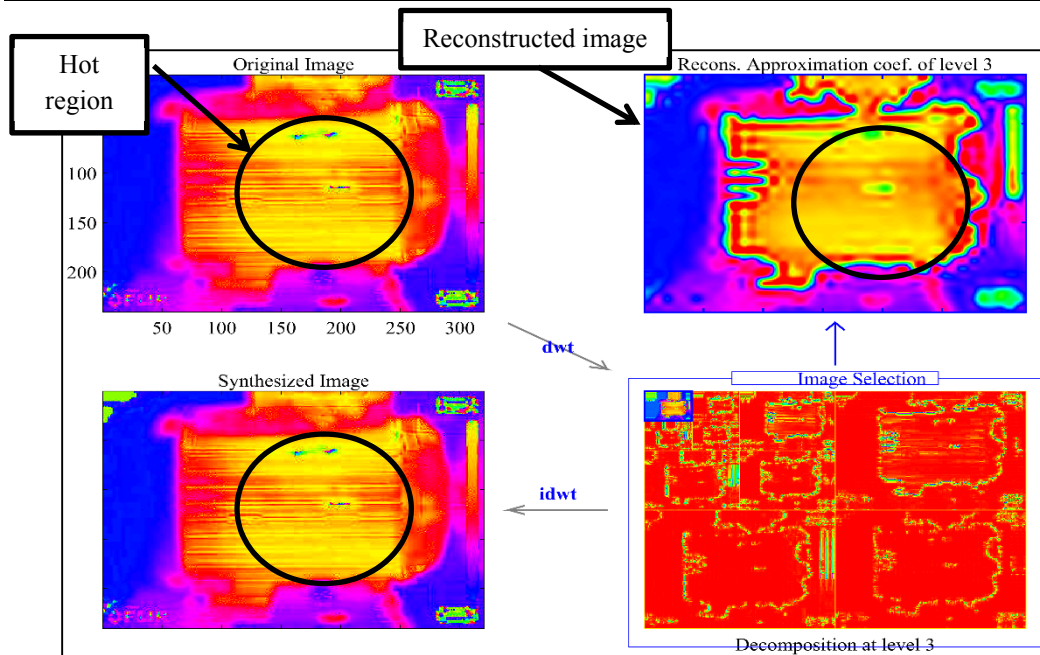


Figure 8-9: Thermal image wavelet analysis for four bars rotor faults with 100% load condition.

The comparison of the thermal image approximation coefficients of the same class with different load conditions at the same level have been shown in figures below. The histogram of approximation coefficients are shown at the same conditions and the difference is either in ranges of histogram or amplitude. Figure 8-10 demonstrates the histogram of approximation coefficients at level 1 for four bars rotor fault with different load conditions. It is noticeably clear that the coefficient level at no-load condition, 50% load and 100% load, could be categorized by ranges. The histogram peaks of these conditions for the machine lie in different ranges, which could be used to distinguish between different machine faults.

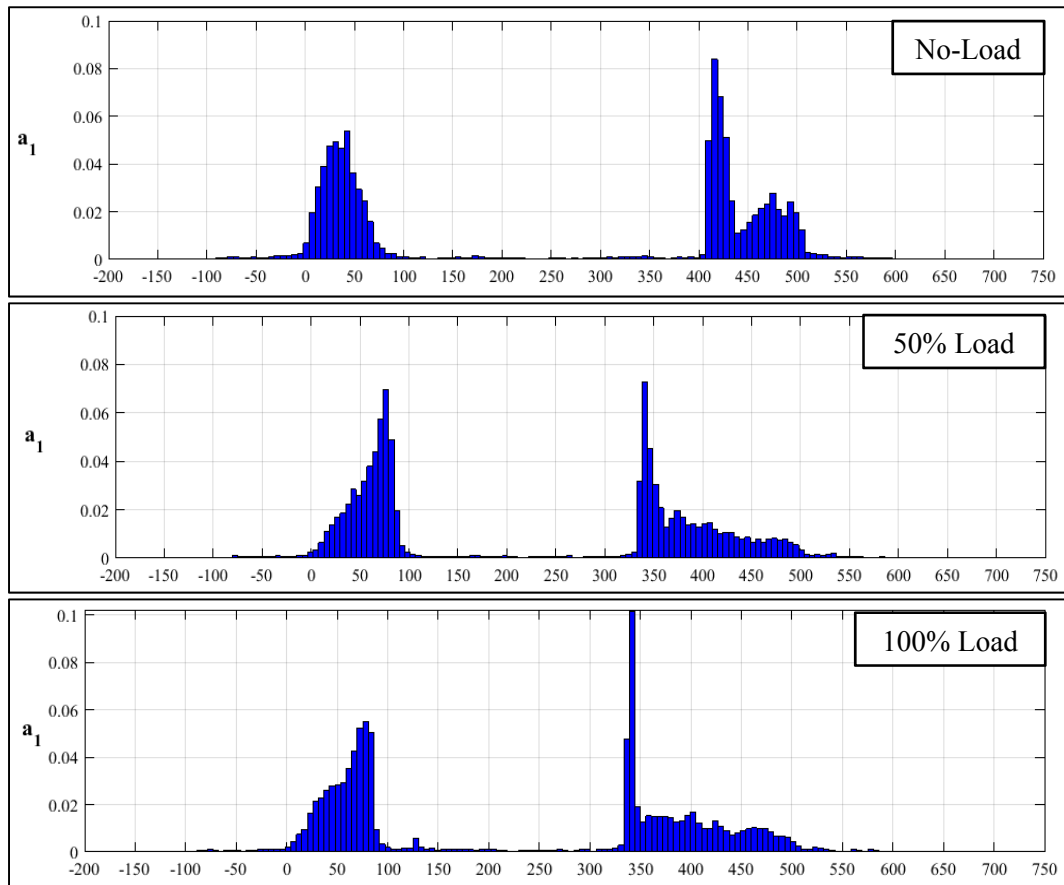


Figure 8-10: Approximation coefficients level (a_1) for four bars rotor fault at different load conditions.

Approximation coefficients at level 2 are illustrated in figure 8-11, they also have different ranges and are counted as very important features for discriminating between the IM faults detection. In case of no-load condition two-approximation coefficients peaks have been extracted from the image. The first approximation coefficient peak range was approximately between “35-170” at the peak of 0.055, while the second one lies between “800-1000” at a peak of 0.12. However, in case of 50% and 100% load conditions, both have almost the same approximation ranges, which were between about (670-900), but their peaks are different in both 50% and 100% load conditions at 0.11 and 0.17 respectively.

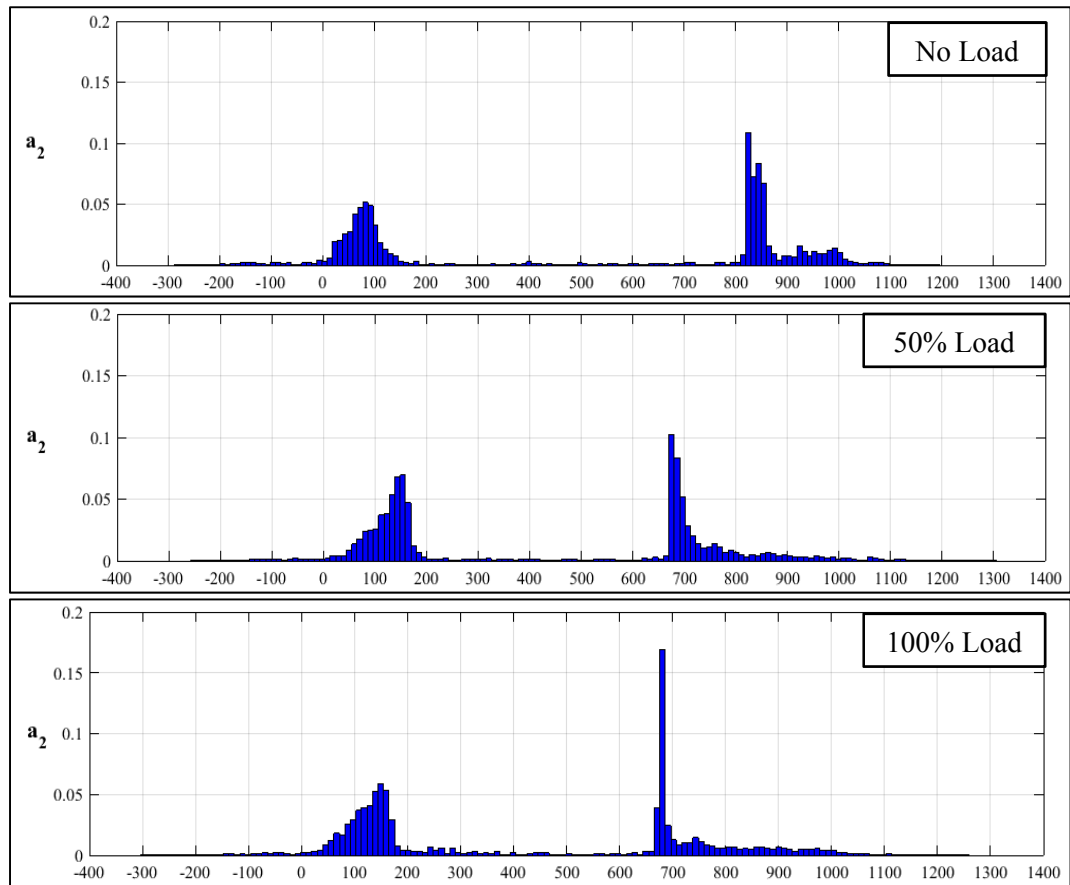


Figure 8-11: Approximation coefficients level (a_2) for four bars rotor fault at different load conditions.

In figure 8-12, the level 3 of approximation coefficients for all load conditions have been illustrated. The different between all the load conditions were obvious, which could be easily useful for classification system to distinguish between the faults severities of induction motor.

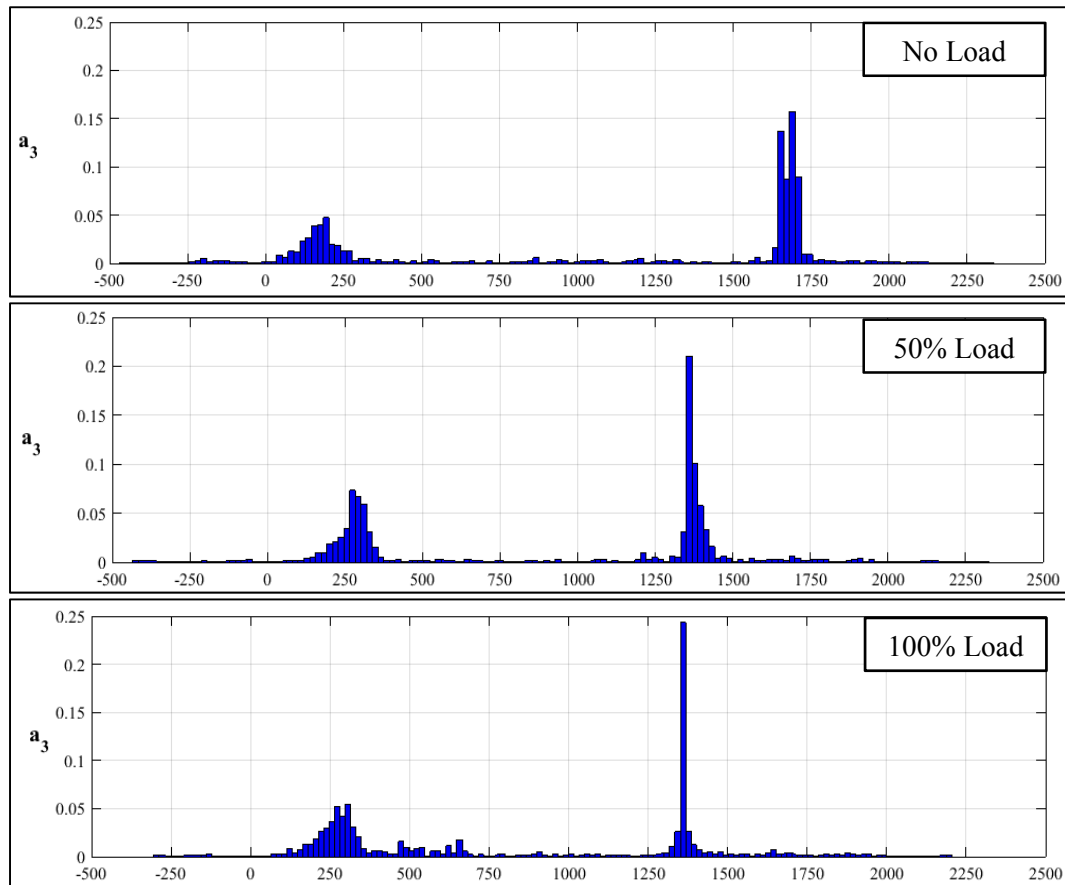


Figure 8-12: Approximation coefficients level a_3 for four bars rotor fault at different load conditions.

In other words, the entire approximation coefficients that have been described earlier have their own signatures for each fault, which will be very good features for the machine learning algorithms to discriminate between the IM faults. Moreover, these features will be combined with the features of the image segmentation methods in order to have a very strong attributes for each fault. The stronger the features, the more accurate classification system can be achieved.

In this section, the approximation coefficients for one sample of induction motor fault have been presented, because the extracted features for other faults have been done in the same procedure. The results that are obtained have been used for feeding the classification system (see appendix A).

Having discussed how to extract the rotor features based on the thermal images, the next section of this chapter addresses ways of extracting the features from the stator current and vibration signals based on the wavelet transform.

8.3 Current and Vibration Signals Analysis based on DWT

It is well known that induction machines play a dominate role in the field of electromechanical energy conversion. Induction machines are widely adopted in a variety of diverse industries product line, ranging from mining industry, process manufacturing, automation applications, heating and air conditioning, transportation, aerospace and marine propulsion applications to the health care industry [1]. Although induction machines are usually well designed and constructed to be robust, however, the possibility of incipient fault is inherent in the machine due to the stress involved in the conversion of electrical energy to mechanical energy and vice versa.

Recently, the motor current signature analysis has been widely applied in condition monitoring in order to monitor the induction machine behaviour in both online and offline. The digital signal processing have been applied for extracting the signal information, as the signal itself is not helpful for recognizing the fault. Discrete Wavelet Transform (DWT) is one of the most popular signal processing technique that has been adopted for extracting the most important features from the signal in order to be used for fault classification as mentioned in the chapter 5-section 5.4.2 . Provided a certain sampled of signal S , the DWT decomposes it onto several wavelet signals (an approximation signal a_n and n details signals d_j) [213][214]. The decomposition coefficients can be determined through convolution and implemented by using a filter [185]. LPF represents the Low Pass Filter and HPF represents the High Pass Filter. The decomposition process can be iterated with successive approximation being

decomposed in turn, so that one signal is broken down into many resolution components. Moreover, due to the automatic filtering performed by the wavelet transform, this tool provides a very attractive flexibility for the simultaneous analysis of the transient evolution of different frequency components present in the same signal. At the same time, in comparison with other tool, the computational requirements are low. Thus, the DWT is available in standard commercial software packages, so no special or complex algorithm is required for its application

In this research, MATLAB Wavelet Toolbox has been used to analyse the current and vibration signals. Prior to the application of the DWT, some considerations have to be done regarding the different parameters of the DWT decomposition, such as the type of mother wavelet, the order of the mother wavelet or the level of decomposition levels.

The first step in the DWT is selecting the mother wavelet to carry out the signal analysis. The selected mother wavelet is related to the coefficients of the filters used in the filtering process inherent to the DWT [214]. Many wavelet families have been proposed in the last decades but some families have shown better results for particular applications. Nevertheless, regarding the transient extraction of fault components, the experience achieved after the development of multiple tests shows that a wide variety of wavelet families can lead to satisfactory results.

Once the wavelet family is selected, it is advisable to carry out the DWT using high-order mother wavelet, this is, a wavelet with associated filter with a large number of coefficients. If a low-order wavelet is used, the frequency response get worse, and the overlap between the adjacent frequency bands increases. Daubechies or any other mother wavelet with high orders has shown satisfactory results.

Consequently, Daubechies 7 has been selected as the mother wavelets used for DWT analysis as mentioned in chapter 5-section 5.4.2.

The second step is to select the number of decomposition levels, which are determined by the low frequency components to trace. The lower the frequency components to be extracted, the higher the number of decomposition levels of DWT [185]. Typically, for the extraction of the frequency components caused by rotor asymmetries, the number of decomposition levels should be equal or higher than that of the detail signal containing the fundamental frequency.

Finally, the number of decomposition levels n_d is related to the sampling frequency of the signal being analysed, in this research the decomposition level is 5. This parameter has to be chosen in such a way that the DWT supplies at least three high-level signals (i.e., two details and one approximation) with frequency bands below the supply frequency [213].

Additionally, due to the non-ideal filtering carried out by the wavelet signals, it is advisable not to set the limits of the band of the wavelet signal containing the fundamental frequency very close to this frequency. Otherwise, this component could partially be filtered within the adjacent bands, masking the evolution of other components within these bands due to its much higher amplitude. Sampling frequency of 1024 sample/s, enables good resolution analysis. Table 8-1 illustrates the frequency levels of the wavelet function coefficients.

Table 8-1: Frequency levels of wavelet coefficients.

Wavelet analysis	Frequency components (Hz)
A5	0-18.75
D5	18.75-37.5
D4	37.5-75
D3	75-150
D2	150-300
D1	300-600

Once the mother wavelet and the number of decomposition level have been selected, it is possible to carry out the DWT of the signal; the obtained results of the analysed signals have been described in the following sections.

8.3.1 Current Signal Analysis

After preparing and selecting the DWT parameters, the DWT is now ready for analysing the IM current signal for extracting the information to discriminate between the motor faults.

8.3.1.1 Current Signal Analysis of Healthy and Faulty Motor

Figure 8-13 illustrates the motor healthy rotor details coefficients based on db7 at 5 levels. The wavelet coefficients d_1 - d_5 represents the detail coefficients for healthy motor (current signal) with different load conditions (No-load, 50% load and 100% load).

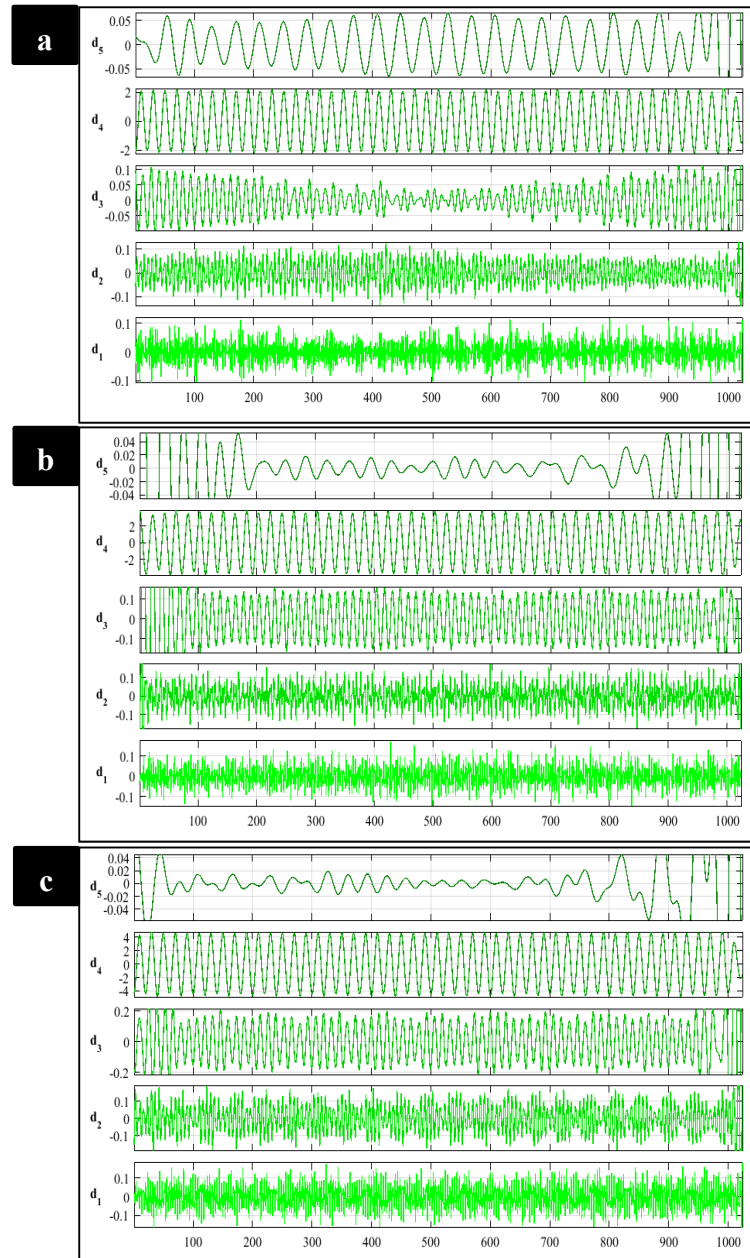


Figure 8-13: Wavelet analysis for healthy current signal with three different load conditions a) No-load, b) 50 % load, c) 100% load.

Figure 8-14 demonstrates the wavelet coefficients (current signal) for four bars with different load conditions. This level of wavelet has very helpful data for distinguishing between the motor faults even if it has too small difference. This is because in the motor environment every single change in the signal of the motor means that the motor has something wrong except the applied load may increase the amplitude of the current, which is normal. The difference between the wavelet coefficients were

obvious in all the details levels between the healthy and four bars faulty rotor. The difference has been happened in the signal amplitude (± 4) and the signal shape, which could be easier for the classification system to classify the fault severity and diagnose it correctly. This difference has been occurred because the faulty rotor need more current to be rotated as some of its bars missing, and by increasing the load; the current will rise dramatically. Thus, the more missing bars the more current needs to rotate the rotor.

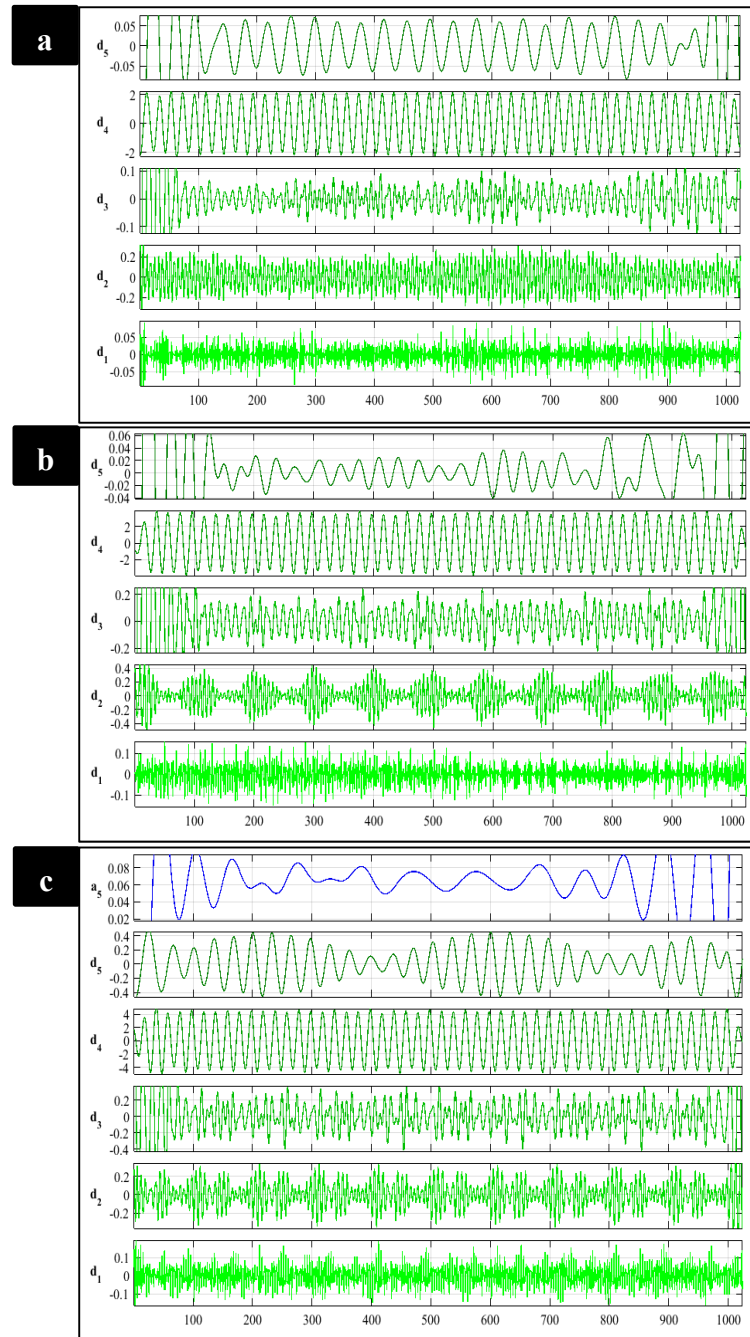


Figure 8-14: Wavelet analysis for four bars faulty rotor based on current signal for with three different load conditions a) No-load, b) 50 % load, c) 100% load.

The healthy rotor current signal is different from the faulty rotor current signal in a number of respects as shown in following figures. Two different details coefficients have been extracted to explain the differences between the healthy and faulty rotor. Figure 8-15 illustrates the d_5 , d_3 for the healthy and faulty rotors (four bars) with no load condition. The difference between these signals have been detected by red oval

shape. The healthy d_5 and faulty d_5 has the same range approximately between (± 0.05) but the shape of the signal has different points, while the difference is very clear between the healthy d_3 and the faulty d_3 as the magnitude has been reduced significantly comparing to the healthy signal.

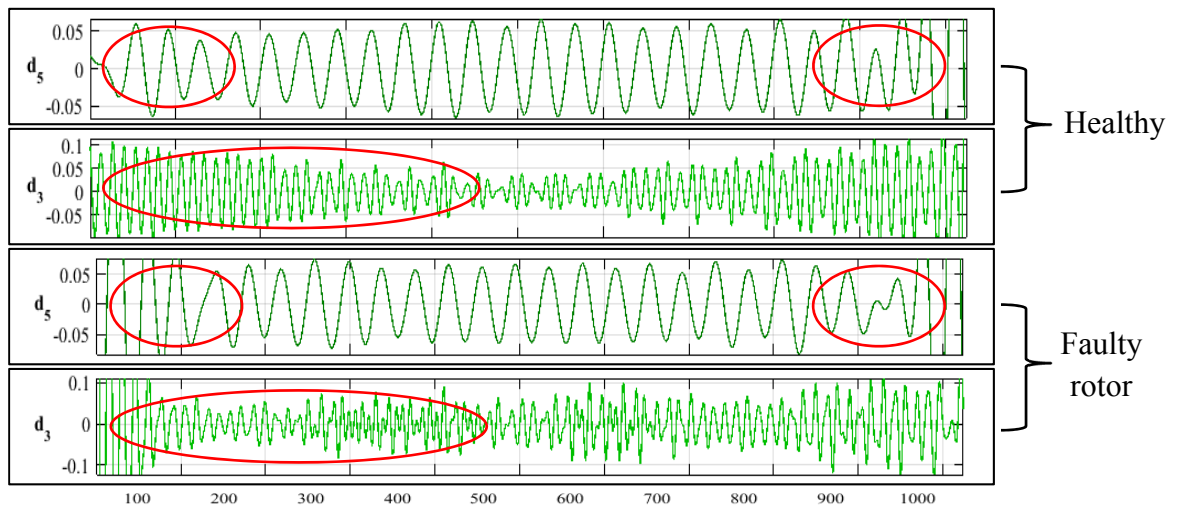


Figure 8-15: The d_5 and d_3 wavelet analysis coefficients for healthy and faulty rotor based on the current signal with no load condition.

Additionally, figure 8-16 demonstrates the d_5 and d_2 for the healthy and faulty rotor (four bars) current signals with 50% load condition. By looking to this figure, the difference between the healthy and faulty signals are obvious and the behaviour of the current signal are completely different in the shape and the range of the signal. Thus, the coefficients will be very strong for classification system to distinguish between the induction motor faults.

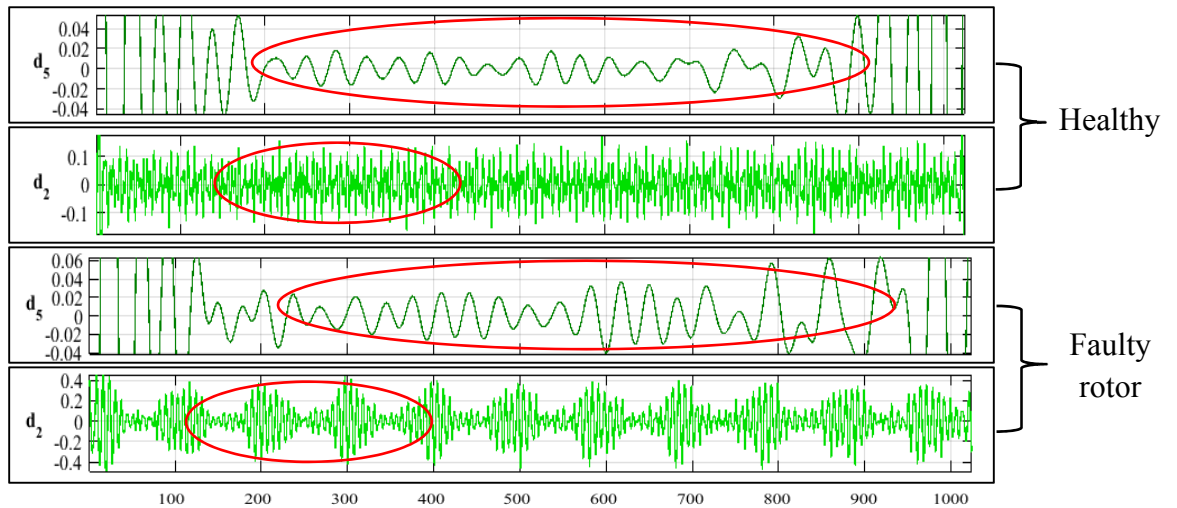


Figure 8-16: The d_5 and d_2 wavelet coefficients for healthy and faulty (four bars) rotor current signal with 50% load condition.

Similarly, figure 8-17 shows the d_5 and d_3 wavelet coefficients for healthy and faulty (four bars) with 100% load condition. The signals are totally changed. It is clearly that the rotor current has been able to be used for IM fault detection as it has very helpful coefficients. Therefore, the extracted features will be robust for classifying the motor faults.

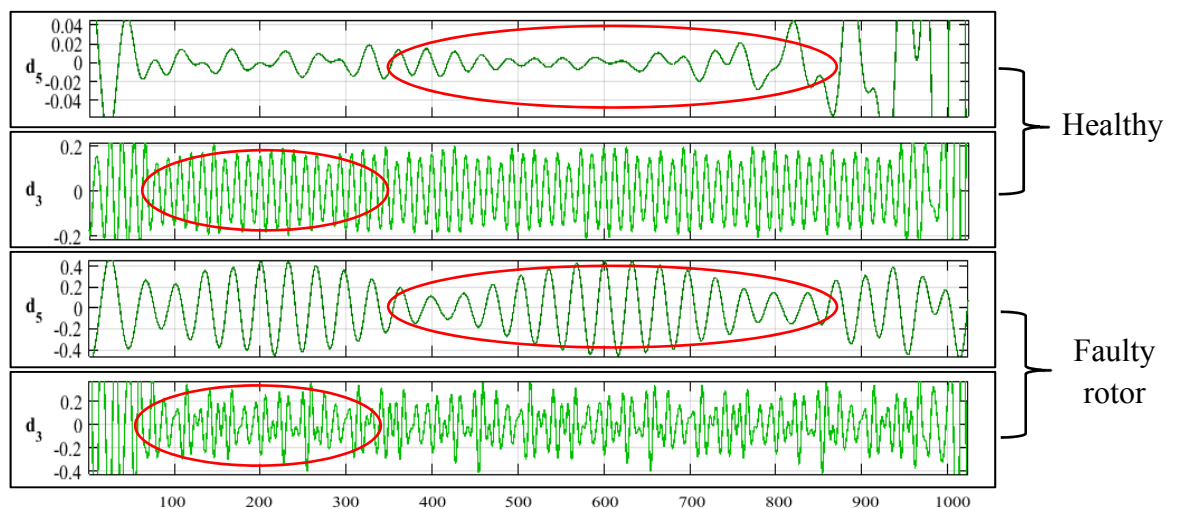


Figure 8-17: The d_5 and d_3 wavelet coefficients for healthy and faulty rotor (four bars) current signal with 100% load condition.

8.3.2 Vibration Signal Analysis

The measurements of vibration signals have been collected from two different faults condition in addition to the healthy condition, which are rotor fault (one bar, four bars and eight bars) and bearing fault (outer, inner and ball). These faulty signals have been collected with different load conditions (no load, 50% load and 100% load).

8.3.2.1 Vibration Signal Analysis of Healthy and Faulty Motor

The following describes two IM cases, which are healthy and four bars faulty rotor, based on vibration signal. As mentioned in chapter 7- section 7.1, the vibration signals have been collected by using laser vibrometer with the same displacement for all healthy and faulty conditions.

The faulty rotor has a big impact on the motor balance, which may effects on the motor vibration performance. The vibration signal of healthy machine has been demonstrated in figure 8-18. It shows the details coefficients of DWT analysis. The same decomposition levels have been applied as in the current signal in order to reduce the data dimensionality and time consumption. It is clear from the figure below that the vibration signal of healthy motor has almost the same behaviour in three different load conditions. As its healthy machine, the vibration signal will be the same and it may vary in the range (d5 (± 0.2), d4 (± 0.1), d3 (± 0.1), d2 (± 0.1), d1 (± 0.2)) based on the applied load. Therefore, this signal contains important data to be used for further processing.

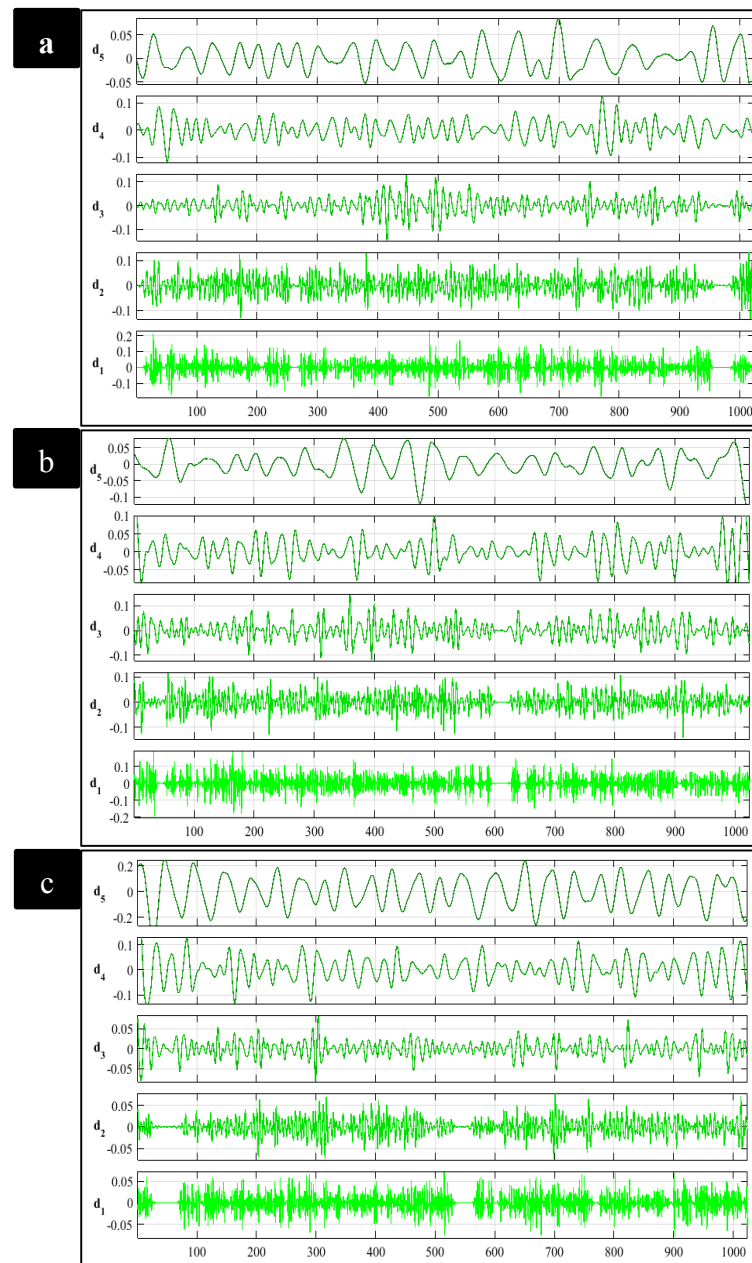


Figure 8-18: Wavelet analysis for healthy vibration signal of induction motor with three different load conditions a) No-load, b) 50% load and c) 100% load.

The detailed coefficients of DWT for IM four bars rotor fault have been illustrated in figure 8-19. The range of faulty signal are far less than the healthy signal in all decomposition levels ($d_5(\pm 0.005)$, $d_4(\pm 0.005)$, $d_3(\pm 0.005)$, $d_2(\pm 0.005)$, $d_1(\pm 0.05)$). By adapting the vibration signal for induction motor faults detection, the classification system will classify the bearing and unbalanced rotor fault correctly.

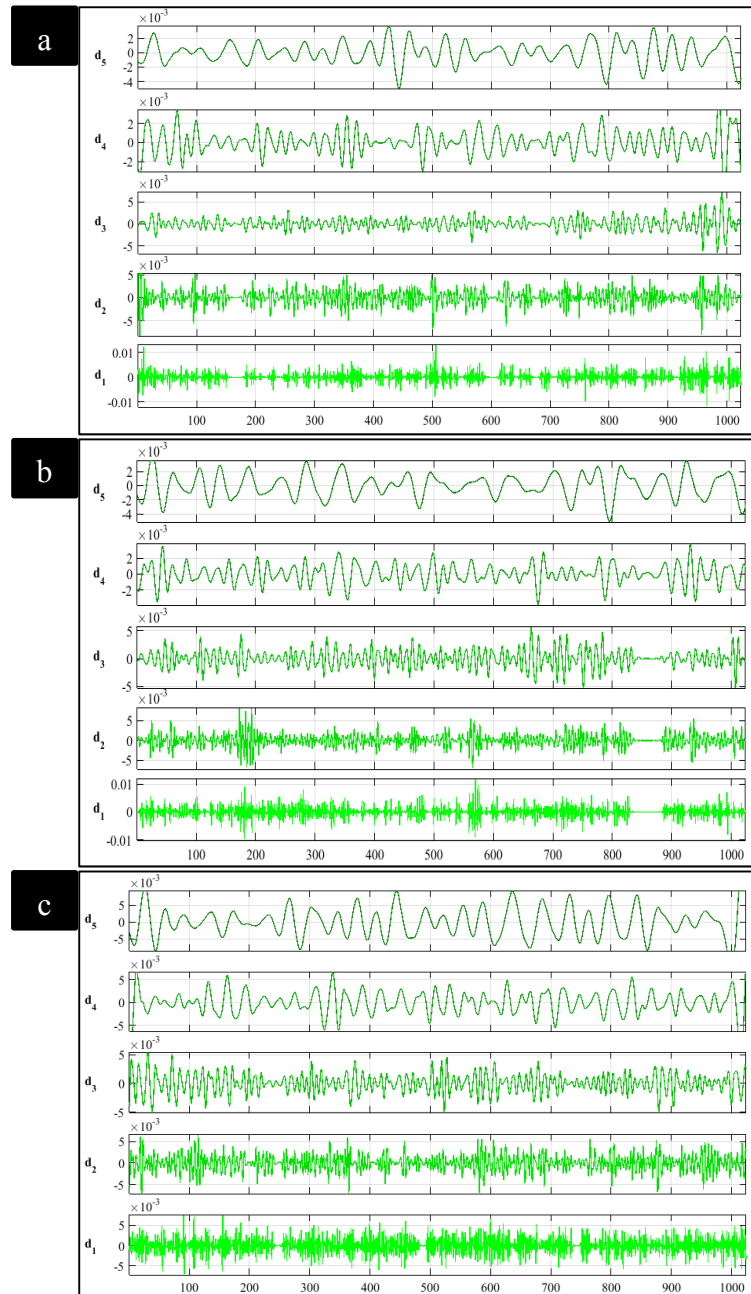


Figure 8-19: Wavelet analysis for faulty rotor (four bars) vibration signal of with three different load conditions a) No-load, b) 50% load and c) 100% load.

The comparison between the healthy and faulty vibration signal is shown in the following figures. Figure 8-20 demonstrates d_5 and d_3 wavelet coefficients of the vibration signal for healthy rotor and faulty rotor (four bars) with no-load condition. It is obvious that both signals has very good attitude to distinguish between the IM

faults. The healthy rotor vibration signal in d_5 and d_3 have a very high displacement than the faulty rotor (four bars), which have low displacement by (10^{-3}) .

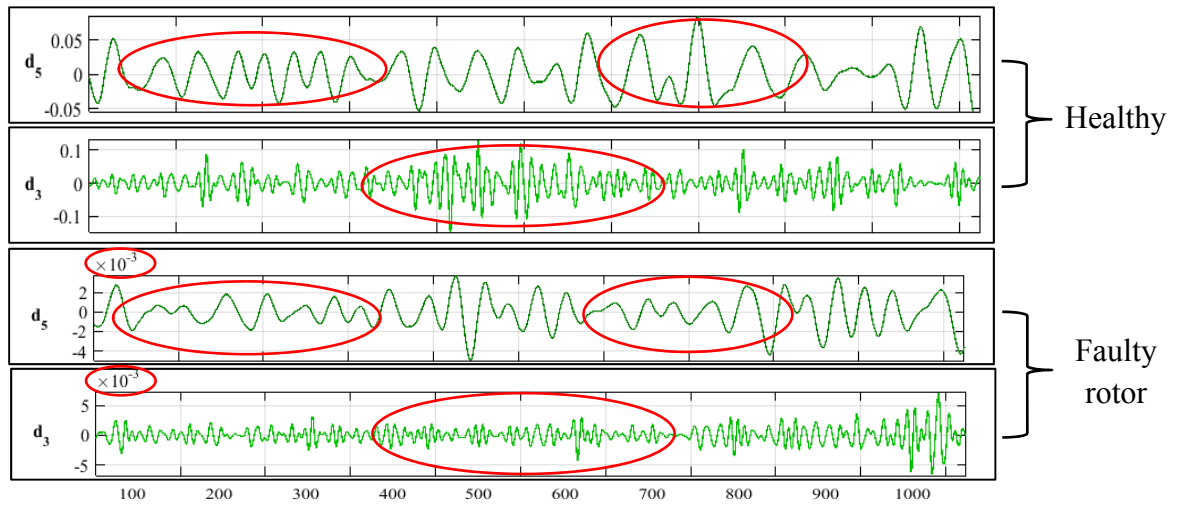


Figure 8-20: The d_5 and d_3 wavelet coefficients for healthy and faulty rotor (four bars) based on the vibration signal with no-load condition.

The vibration signal for the healthy and faulty rotor (four bars) with 50% load condition have been illustrated in figure 8-21. A comparison has been carried out with d_5 and d_2 wavelet coefficients. These four signals are completely different in every single point. Thus, by using this kind of signal, it will be possible to detect the fault straight away only by looking at its curve.

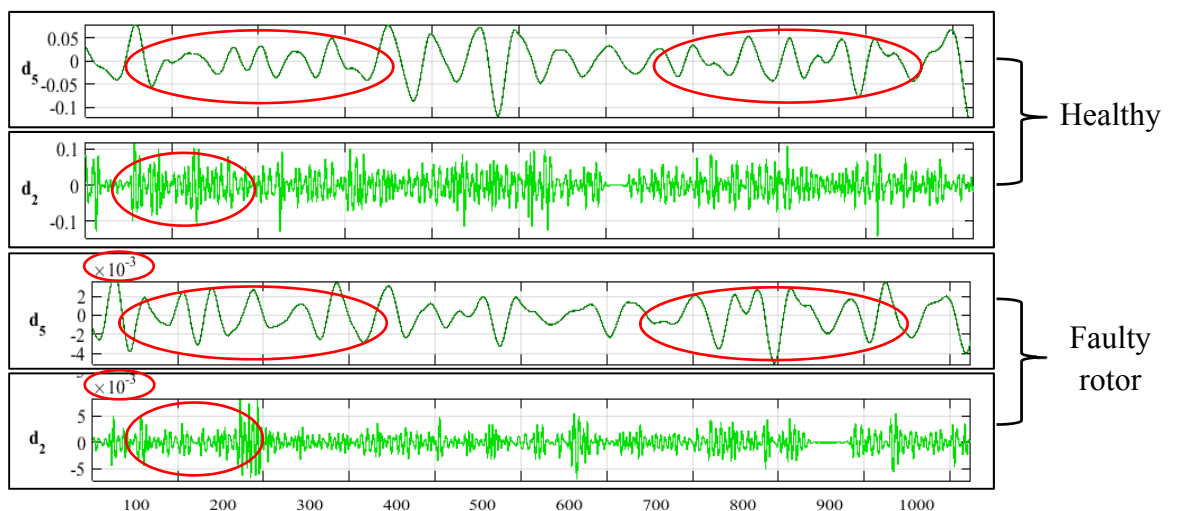


Figure 8-21: The d_5 and d_2 wavelet coefficients for healthy and faulty rotor (four bars) based on the vibration signal with 50% load condition.

Chapter 8: Data and Signal Analysis

In figure 8-22, the d_5 and d_3 wavelet coefficients for the healthy and faulty rotor (four bars) with 100% load condition have been demonstrated and it was very appropriate for motor faults detection to pick up these two coefficient because they are considerably different from each other.

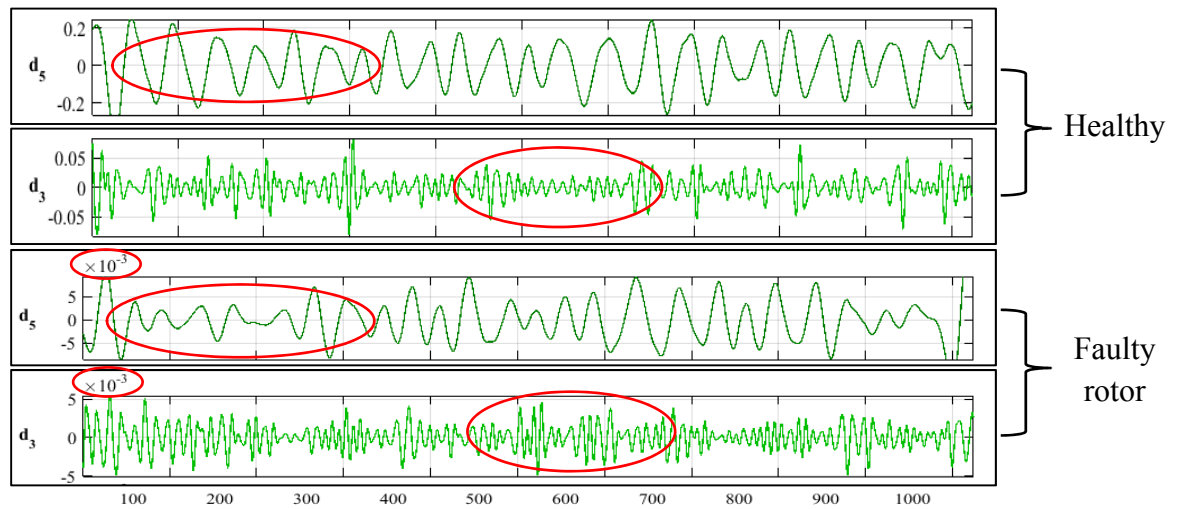


Figure 8-22: The d_5 and d_3 wavelet coefficients for healthy and faulty rotor (four bars) based on the vibration signal with 100% load condition.

CHAPTER 9

RESULTS AND DISCUSSION

“This chapter presents the results and discussion on innovative, non-instructive, accurate and reliable methods for the early detection and diagnosis of faults in an induction motor (IM) using the proposed B4M classification algorithm. The proposed B4M and other proposed algorithm have achieved very good results for detecting the induction motor faults. It also discuss the limitations of the proposed algorithms. The confusion matrix for all condition monitoring classification have been also presented”.

9.1 B4M Classification based on Thermal Image for Fault Detection

9.1.1 Feature Extraction

The acquired raw thermal image consists of information that specifies the induction motor faults as described in chapter 5. After applying 2D-DWT for 7th induction motor conditions (healthy, one bar rotor fault, four bars rotor faults, eight bars rotor faults, outer race bearing fault, ball bearing fault and inner race bearing fault) with different load conditions, three features have been extracted from the decomposition level in addition to 7 features of image matrices, as discussed in chapter 5 - section 5.2. Overall, 10 features have been extracted from the thermal image and each feature contains 250 samples. These features have been labelled correctly in order to be recognized by the classification system. Table 9-1 illustrates sample of the induction motor extracted features with no-load condition from the thermal images, for the all thermal image processing see Appendix A.

In this research, induction motor fault data for all load conditions have been combined together as the load level is not as important as the motor fault. For example, if the motor has ball bearing fault, it does not need to be loaded to indicate that the motor has fault by the classification system because it does not matter if it loaded or not, the important thing is to detect the motor fault at an early stage. For that reason, the features and the samples contain all the three load conditions are presented as one package.

Table 9-1: Sample of thermal image dataset features.

MSE	PSNR	Mean	Variance	SD	Skew	Kurtosis	DWT-L1	DWT-L2	DWT-L3	Class
0.35544	50.37697	0.033294	0.032186	0.179405	5.202815	28.06927	7374.418	5755.196	5698.162	THI_Healthy
0.355061	50.37929	0.033047	0.031955	0.17876	5.224353	28.29386	7371.491	5758.126	5712.633	THI_Healthy
0.356839	50.36844	0.033906	0.032757	0.180989	5.150518	27.52783	7392.745	5794.468	5743.5	THI_Healthy
0.327645	50.55379	0.048177	0.045857	0.214142	4.219851	18.80713	7377.146	5768.278	5723.003	THI_Healthy
0.390395	50.17328	0.110638	0.098399	0.313685	2.4825	7.162792	7377.632	5767.941	5717.903	THI_Healthy
1.115213	47.89401	0.056194	0.034037	0.184491	4.447897	22.35044	7377.38	5764.134	5707.82	THI_Healthy
0.529472	49.51159	0.026107	0.025426	0.159454	5.943954	36.33057	6814.463	2706.993	2060.024	THI_Ball
0.528401	49.51598	0.026706	0.025993	0.161223	5.871298	35.47213	6813.795	2693.899	2040.216	THI_Ball
0.532611	49.49875	0.026615	0.025907	0.160955	5.8822	35.60026	6813.861	2578.934	2042.111	THI_Ball
0.499385	49.63863	0.048307	0.045974	0.214416	4.213234	18.75132	6813.848	2664.022	2042.314	THI_Ball
0.557119	49.40106	0.103151	0.092512	0.304158	2.609492	7.809435	6813.76	2660.433	2039.408	THI_Ball
1.023253	48.08089	0.044909	0.025965	0.161137	5.195361	30.20926	6813.597	2661.292	2033.908	THI_Ball
0.429967	49.96363	0.021224	0.020774	0.144131	6.643619	45.13766	6692.17	4875.692	5601.464	THI_Inner
0.429461	49.96618	0.022396	0.021895	0.147968	6.455504	42.67352	6688.247	4920.295	5602.509	THI_Inner
0.434157	49.94257	0.022878	0.022355	0.149514	6.3823	41.73374	6682.724	4761.425	5624.128	THI_Inner
0.408121	50.07686	0.047878	0.045586	0.213509	4.235168	18.93663	6686.429	4884.199	5608.071	THI_Inner
0.460576	49.8143	0.098945	0.089156	0.298591	2.686319	8.216297	6687.071	4872.795	5608.182	THI_Inner
0.817972	48.56711	0.041137	0.022291	0.149301	5.534342	34.57538	6689.066	4848.259	5608.071	THI_Inner
0.373017	50.27216	0.02401	0.023434	0.153082	6.218737	39.67267	6065.826	3831.969	3053.98	THI_Outer
0.373109	50.27162	0.024583	0.023979	0.154853	6.140251	38.70267	6063.761	3734.959	2999.285	THI_Outer
0.374113	50.26579	0.025964	0.02529	0.159028	5.961689	36.54173	6069.003	3720.587	2911.754	THI_Outer
0.347152	50.4282	0.050951	0.048355	0.219898	4.084159	17.68034	6064.922	3721.488	2976.198	THI_Outer
0.388041	50.18642	0.095794	0.086619	0.294311	2.746795	8.544869	6065.356	3743.7	2982.747	THI_Outer
0.778282	48.67512	0.044808	0.024792	0.157456	5.274818	31.21595	6066.338	3799.011	2981.655	THI_Outer
0.614847	49.18697	0.026771	0.026054	0.161414	5.863544	35.38113	6000.446	5589.383	2179.712	THI_One Bar
0.614134	49.18949	0.027904	0.027125	0.164698	5.732878	33.86587	5997.884	5597.897	2158.793	THI_One Bar
0.613881	49.19038	0.025482	0.024833	0.157584	6.02241	37.2694	5994.098	5590.324	2158.671	THI_One Bar
0.583517	49.30054	0.049023	0.046621	0.215918	4.177287	18.44972	5996.962	5596.833	2159.391	THI_One Bar
0.597334	49.24972	0.081042	0.074475	0.272901	3.070407	10.42738	5997.032	5595.281	2157.883	THI_One Bar

Chapter 9: Results and Discussions

1.146763	47.83344	0.039478	0.024328	0.155974	5.541718	33.55016	5996.591	5590.627	2155.486	THI_One Bar
0.461924	49.80795	0.025508	0.024857	0.157663	6.019085	37.22937	6774.535	5447.211	2401.727	THI_Four Bar
0.46213	49.80698	0.026133	0.02545	0.159531	5.940744	36.29243	6773.504	5450.199	2262.051	THI_Four Bar
0.464033	49.79806	0.02694	0.026215	0.161909	5.843511	35.14661	6768.262	5444.712	2317.648	THI_Four Bar
0.444115	49.89333	0.049036	0.046632	0.215946	4.176641	18.44431	6771.848	5449.253	2258.909	THI_Four Bar
0.500314	49.63459	0.113216	0.1004	0.316859	2.441363	6.960242	6772.072	5448.475	2298.591	THI_Four Bar
0.974684	48.18649	0.046206	0.02684	0.163828	5.046564	28.68837	6773.364	5446.273	2405.489	THI_Four Bar
0.435604	49.93534	0.024622	0.024016	0.154972	6.134997	38.63817	5890.516	3127.84	3262.712	THI_Eight Bar
0.434861	49.93905	0.025664	0.025006	0.158132	5.999239	36.99085	5888.15	3049.997	3074.364	THI_Eight Bar
0.437517	49.92583	0.026732	0.026018	0.161299	5.868193	35.43567	5888.931	2904.768	3214.26	THI_Eight Bar
0.408709	50.07373	0.04875	0.046374	0.215346	4.190924	18.56383	5888.136	2995.282	3090.578	THI_Eight Bar
0.449218	49.86852	0.107253	0.095751	0.309436	2.538471	7.443824	5888.699	3014.085	3133.662	THI_Eight Bar
0.913147	48.3281	0.045972	0.025513	0.159729	5.182312	30.20803	5889.927	3093.372	3247.034	THI_Eight Bar

*THI: Thermal Image.

9.1.2 Feature Selection

All features contribute to the classification system and there is a need for selecting the best feature before classification. Researchers have been carried out studies to select the best feature selection technique that makes them more robust across various classifiers. The classification accuracy increased by approximately 3-5% across a wide range of classifiers using feature selection methods [215]. Four feature selection methods have been used in this research (as described in chapter 5-section 5.5) in order to select and compare which feature selection technique is suitable for motor fault detection based on B4M classification algorithm. These methods are Sequential Forward Selection (SFS), Sequential Backward Selection (SBS), Sequential Floating Forward Selection (SFFS) and Sequential Floating Backward Selection (SFBS).

The feature selection methods have been ran using MATLAB “R2015a” feature selection package, which is created by [216]. The feature selection approach is employed to choose the most robust feature among the whole dataset which showed increase in classification accuracy of about 10% higher for all classifiers when compared with previous results as stated in [217].

After applying the feature selection methods, the selected features have been illustrated in table 9-2. It was clearly that few features have been selected in all feature selection algorithm, which means that these features have strong data that make the classifier to discriminate between the motor faults.

Table 9-2: The selected features for the thermal image dataset.

Feature Selection Method							
SFS		SBS		SFFS		SFBS	
MSE	√	MSE	x	MSE	√	MSE	√
PSNR	√	PSNR	x	PSNR	√	PSNR	√
Mean	x	Mean	√	Mean	x	Mean	x
Variance	x	Variance	√	Variance	x	Variance	x
SD	√	SD	x	SD	x	SD	√
Skew	x	Skew	x	Skew	√	Skew	√
Kurtosis	x	Kurtosis	x	Kurtosis	x	Kurtosis	√
DWT-L1	√	DWT-L1	√	DWT-L1	√	DWT-L1	x
DWT-L2	√	DWT-L2	√	DWT-L2	√	DWT-L2	√
DWT-L3	√	DWT-L3	√	DWT-L3	√	DWT-L3	√

9.1.3 Classification Results

The classification process splits the data points depending on the percentage level of data given for training and testing sets. Training set means learning the data points to perform the correlation tasks, which is storing the data by giving set of rule to perform further operations. Testing set helps to find the classification accuracy of the trained data points. Furthermore, a cross validation technique is used to evaluate the predictive models by partitioning the original samples into training set to train the model and testing set to evaluate the model. The data sets were given as an input to the algorithm for training and testing which gives out the rules, classification accuracy and confusion matrix. The features have been extracted and selected, the induction motor faults data are ready to be fed for the most classification system, especially the classification systems that are accepting the categorical attributes. In this research, 10-folds cross validation have been used for training and testing the system. Moreover, all the data

Chapter 9: Results and Discussions

have been labelled from 1 to 7 to be defined as motor faults for the B4M classification algorithm as shown in table 9-3.

Table 9-3: Thermal image dataset description.

Machine Condition	Class Label	No. of samples	No. of Training Samples	No. of Testing Samples
Healthy	1	250	240	10
Ball bearing fault	2	250	240	10
Bearing Inner race fault	3	250	240	10
Bearing outer race fault	4	250	240	10
One bar rotor fault	5	250	240	10
Four bars rotor fault	6	250	240	10
Eight bars rotor fault	7	250	240	10
Total Samples		1750	1680	70

Before applying the proposed B4M classification method, some parameters need to be defined, which are already chosen as described in (chapter 4 - section 4.3.2). The B4M has been applied for five different datasets:

- Datasets without feature selection (Full).
- Datasets with Sequential Forward Selection (SFS).
- Datasets with Sequential Backward Selection (SBS).
- Datasets with Sequential Floating Forward Selection (SFFS).
- Datasets with Sequential Floating Backward Selection (SFBS)

All the above datasets have been used as input for B4M classification algorithm with 10-folds cross validation. By applying the B4M classification method, the efficiency of 10 given features, which are obtained from feature extraction for seven conditions, are illustrated in table 9-4.

Table 9-4: The proposed B4M classification results.

Dataset type	No. of rules	Classification accuracy (%)
Full	15	80.93
SFS	10	98.97
SBS	7	96.16
FFFS	7	92.04
SFBS	7	94.23

As can be seen in table 9-4, the results were satisfactory because they have achieved more than 90% for all the four feature selection methods rather than the full datasets (without feature selection). This indicates that the B4M classification algorithm is well trained and could be applied for diagnosing the motor faults. In other words, the lowest classification accuracy and higher number of rules were obtained by using the full datasets, while the highest classification accuracy has been recorded by using Sequential Feature Selection (SFS) method with less number of rules. Furthermore, the other feature selection methods have obtained slightly less classification accuracy than each other but the number of rules was lower than the full and the SFS datasets. In this case the number of rules are very important to be very low as they have an effects on the classification system for detecting the motor faults at an early stage by reducing the checking time (time consuming). Thus, the SBS feature selection method is considered as the best because it has gained more than 96% of classification accuracy and lower number of rules as shown in figure 9-1.

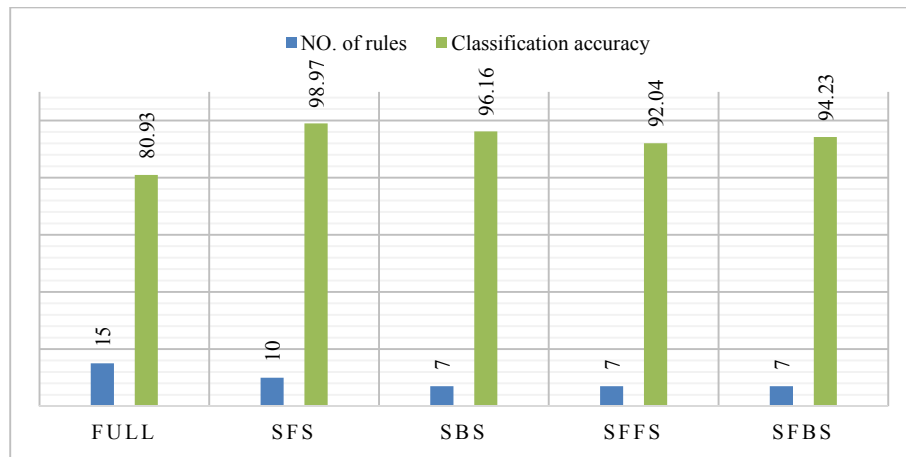


Figure 9-1: The proposed B4M classification accuracy and number of rules based on thermal image dataset.

Table 9-5 shows the confusion matrix for the proposed B4M based on the SBS feature selection method.

Table 9-5: Confusion matrix of the proposed B4M for the thermal image dataset.

True Class	Predicted Class						
	Healthy	Ball bearing	Inner race	Outer race	One bar	Four bars	Eight bars
Healthy	239	0	0	0	1	0	0
Ball bearing	2	230	3	3	0	2	0
Inner race	4	5	228	0	0	3	0
Outer race	1	1	4	232	2	0	0
One bar	8	0	0	4	226	2	0
Four bars	0	0	0	0	0	240	0
Eight bars	0	0	0	0	0	0	240

The interpretation of confusion matrix is as follows:

- The diagonal elements in the confusion matrix show the correctly classified instances. The first row is belong to “healthy motor” good class with only one misclassification, which is 239 correct out of 240 samples. The ball bearing fault obtained 230 correct class out of 240 (10 samples are misclassified).

While, 228 out of 240 instances were correctly classified in class “inner race bearing fault”, which means only 12 instances have been misclassified. In addition, 232 out of 240 have been classified correctly for “outer race bearing fault”, which is slightly lower than other bearing faults.

- In terms of rotor fault, 226 out 240 were correctly classified as they depend on the signal compared with the healthy condition. All the instances from class “four bars rotor fault” and “eight bars rotor fault” were classified correctly 240 out 240, which means that the B4M have good discrimination between the motor faults.

The results indicate that the proposed B4M classification algorithm has been applied successfully for detecting the induction motor faults; the results were very acceptable as the misclassification instances for the motor faults are very low. Even though the classification accuracy was about 96.16% but the rules that produces by the B4M were very good to save the time and cost. Many reasons that prevent the B4M from achieving the 99% classification accuracy and lower number of rules, the most important one is the overlapping between the dataset attributes, which may enforce the algorithm to misclassify some classes. Consequently, dominant and discriminatory fault characteristics in seven fault of induction motor conditions could be extracted from the thermal image matrices, approximation and details coefficients by DWT was very helpful features for motor fault detection without touching the motor (contactless).

9.1.4 Comparison of B4M Performance with other Classification Algorithms

The accuracy of the proposed B4M classification algorithm has been compared with other eight well-known classification algorithms (Decision Table (DT), RIPPER

(Repeated Incremental Pruning to Produce Error Reduction), OneR (One Rule), PART (Projective Adaptive Resonance Theory), J48, LMT (Logistic Model Tree), Naïve Bayes tree and Random Tree). All these methods have been ran using the most popular software, which is called “WEKA” (Waikato Environment for Knowledge Analysis). The WEKA software is a machine learning software written in Java. It has been developed at the University of Waikato in New Zealand. It contains a collection of visualization tools and algorithms for data analysis and predictive modelling, together with graphical use interfaces for easy access to these functions. It has been created to support several standard data mining tasks, more specifically, data pre-processing, clustering, classification, regression, visualization and feature selection.

In order to obtain statistically significant results and to prove the performance of the proposed diagnosis methodology, the other classification algorithm have been trained and tested under 10-folds cross validation scheme. Thus, considering all the conditions, the same dataset has been used to be applied for these algorithms with purpose of comparing the classification performance with the proposed B4M at same conditions. The same selected features have been used for classifying the induction motor faults.

In terms of classification accuracy, the proposed classification algorithm (B4M) has a compaitive results compairing to other classification algorithm as shown in figure 9-2. Figure 9-2 illustrates the classification accuracy results for different classification and feature selection methods including the proposed B4M. Clearly from the figure that there are two classificaiton algorithms have obtained 100% accuracy which is counted in the machine learning field as an excellent classifies because they have achived 100% with no missclassified data. However, the problem of these classifies have

Chapter 9: Results and Discussions

produced too many rules for predicting the new incoming data. Thus, this problem will have an effect on the fault detection process as it will take long time to go through all the rule set to decide whether the new data is faulty or not. It can be seen that the feature selection methods have positive and negative impacts on all classifiers. For instance, in “Naïve Bayes” classifier the full dataset (without feature selection) has been ranked as the highest among all other feature selection algorithm, while in other classifiers has ranked the lowest. Besides, SFS feature selection method has achieved the highest accuracy in the proposed B4M 98.97% among other classifiers, but also got lower accuracy in Naïve Bayes classifier. This is the most significant reason of using feature selection methods as it is good to reduce the data dimensionality and may rise or decline the classifier accuracy.

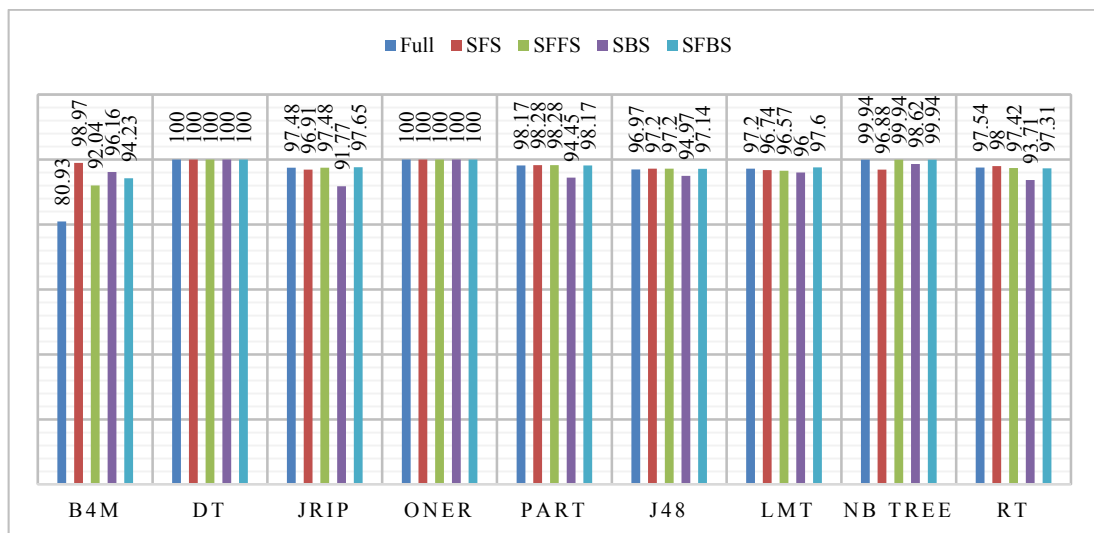


Figure 9-2: Comparison of the classification accuracy for different feature selection and classification algorithms based on the thermal image dataset.

Overall, the proposed B4M classification algorithm has acquired very good and competitive results comparing to other classification algorithms, since it is counted as new released classification algorithm. The obtained results were good enough to detect the induction motor faults at an early stage. All the classification algorithms have achieved good results depending on the dataset, if the dataset has overlapping

Chapter 9: Results and Discussions

between its features the classification accuracy will be affected directly. The more clear dataset the more accurate classification system. The B4M result were not the higher classification accuracy. A possible explanation for this might be that the proposed B4M need more improvements for its parameters or objective function to be considered as classification system with high accuracy. Another possible explanation for this is that the proposed B4M has limited local and global searches and it may prevent it from finding the best value for each class. Another possible explanation for these results may be the lack of adequate iterations for the proposed B4M. All classification methods are different from the proposed B4M in a number of respects. The proposed B4M is a combination between optimization algorithm (Bees Algorithm) and data mining rule discovery as the main job for the BA is providing the optimal solutions for many engineering problems as mentioned in the literature. The challenging part here is how to convert the work of BA from optimization to classification, while the other classification methods have been designed for classifying the data.

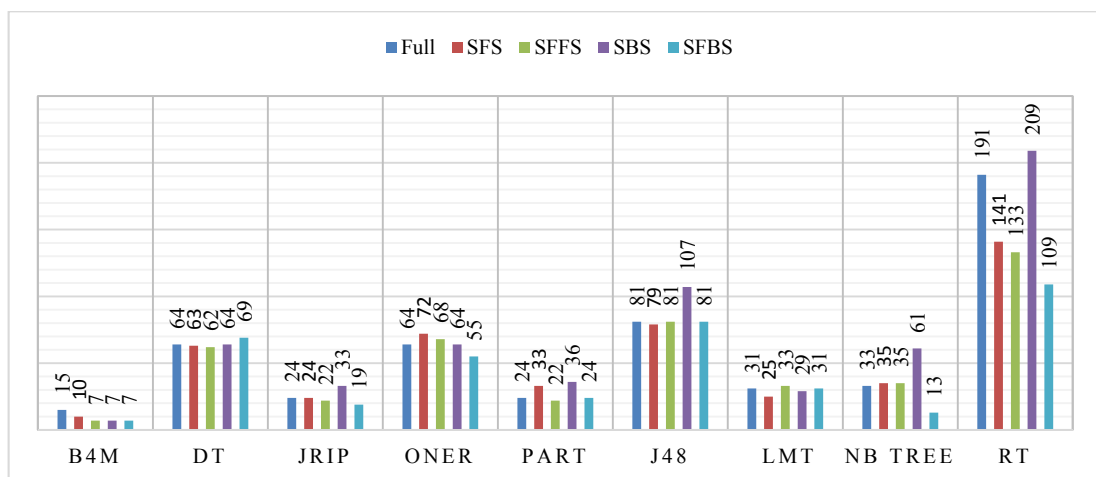


Figure 9-3: Comparison of the number of rules for different feature selection and classification algorithms based on the thermal image dataset.

In terms of number of rules, the proposed B4M obtained the best and lower number of rules among all other classification algorithms as shown in figure 9-3. This is owing to the rule pruning strategy that are adopted in the proposed B4M, which removes the unrelated rules and keep the better rules in order to classify the data correctly.

The number of rules are the most important factor in the machine learning algorithms as it shows the strength of the classification algorithm. When the number of rules are low, it means that the classification system has been focused on the best values among all the dataset features. The higher number of rules, the more time needed to decide the best class for the new data. In figure 9-3, most of the classification algorithms have fallen to produce rules lower than the proposed algorithm. The other classifiers have obtained a satisfactory result for producing the lower number of rules. In the meantime, the proposed B4M has shown its ability to focus on both the classification accuracy and the number of rules, as some classifiers produce far different number of rules with the same dataset, but this has not happened with the proposed B4M. The proposed B4M keeps holding the best values for each class while it searches for the other best one. This advantage makes it the best from other classifiers and produce lower number of rules.

The induction motor fault detection based on the thermal image using proposed B4M classification algorithm has been discussed and the next section will describe the induction motor fault detection based on the motor current signature analysis.

9.2 B4M Classification based on Current Signal for Fault Detection

9.2.1 Feature Extraction

The database includes seven different faults and three load conditions (no load, 50% load and 100% load). There are three distinct recordings, each of which belong to one

phase of the motor for each load condition. The number of raw data vector and the dimension are the same for the current signal in each phase. Hence, only one phase signal has been selected for further processing in order to exploit in the experimental stage. The wavelet coefficients have been extracted from the raw current signals contains large amount of information about the motor status. The 1D DWT have been applied for 6 fault conditions in addition to healthy condition (one bar rotor fault, four bars rotor faults, eight bars rotor faults, outer race bearing fault, ball bearing fault and inner race bearing fault) with different load conditions in order to extract the best fault information from the current signal. Ten features have been extracted from the raw current signal, five features belong to DWT details coefficients and five features are belong to DWT approximation coefficients with the aim of having all possibilities for induction motor faults detection as explained in chapter 5 - section 5.4. The data belong to each class in the database consists of 10 attributes, each of which has 750 samples as each fault consists of 250 samples for no load, 250 samples for 50% load and 250 samples for 100% load. Therefore, 10 features vectors with the size of 750 samples for seven faults (5250 samples) were obtained for each class in the dataset. All these features have been labelled properly for their class with the purpose of recognising by the classification system. Table 9-6 shows sample of extracted features from the current signal based on DWT. For full signal, see Appendix B.

As stated in the previous section, the induction motor faults data for all load conditions have been combined together as the load level is not important than the motor fault.

Table 9-6: Sample of current signal dataset features.

	Details Coefficients										Approximation Coefficient										Class
	DWT-L1	DWT-L2	DWT-L3	DWT-L4	DWT-L5	DWT-L1	DWT-L2	DWT-L3	DWT-L4	DWT-L5	DWT-L1	DWT-L2	DWT-L3	DWT-L4	DWT-L5						
0.026568	-0.03872	-0.55671	-1.65528	0.073444	-1.9992	-1.96048	-1.40377	0.251508	0.178063	C_Healthy											
-0.0316	-0.01178	-0.24011	-1.73073	0.056357	-1.75704	-1.74525	-1.50514	0.225591	0.169234	C_Healthy											
0.036752	0.052294	0.108902	-1.65977	0.038454	-1.29968	-1.35197	-1.46087	0.198901	0.160447	C_Healthy											
-0.0149	0.036014	0.359069	-1.36945	0.021487	-0.80117	-0.83718	-1.19625	0.173199	0.151712	C_Healthy											
-0.06501	-0.03566	0.462156	-0.85336	0.005882	-0.27791	-0.24226	-0.70441	0.148953	0.143071	C_Healthy											
0.061824	-0.06226	0.521777	-0.22816	-0.00849	0.357533	0.41979	-0.10199	0.126173	0.134661	C_Healthy											
0.035594	0.074226	0.491038	1.680431	-0.03719	2.223757	2.149531	1.658493	-0.02194	0.015255	C_Ball											
-0.06565	0.054567	0.168955	1.764551	-0.02508	1.983288	1.928721	1.759766	-0.00478	0.02029	C_Ball											
-0.02633	-0.01647	-0.17331	1.700394	-0.01254	1.523403	1.539873	1.713179	0.012785	0.025323	C_Ball											
0.080624	-0.05353	-0.39404	1.414034	-0.00091	0.995874	1.049399	1.443438	0.029404	0.030314	C_Ball											
-0.03278	-0.04243	-0.4492	0.899032	0.009499	0.452135	0.494563	0.943766	0.044733	0.035234	C_Ball											
0.009306	0.010055	-0.45609	0.27168	0.018693	-0.11566	-0.12572	0.330368	0.058688	0.039995	C_Ball											
0.109274	0.208875	-0.29167	-2.26282	-0.12272	-2.68648	-2.89535	-2.60368	-0.34086	-0.21814	C_Inner											
-0.24774	0.070465	-0.00852	-2.43225	-0.09379	-2.67118	-2.74165	-2.73312	-0.30087	-0.20708	C_Inner											
0.093193	-0.23384	0.283239	-2.40744	-0.06375	-2.61783	-2.38398	-2.66722	-0.25979	-0.19603	C_Inner											
0.020801	-0.15631	0.418091	-2.08878	-0.03417	-2.04601	-1.88969	-2.30778	-0.219	-0.18483	C_Inner											
0.025788	0.164504	0.375752	-1.46568	-0.0058	-1.10471	-1.26922	-1.64497	-0.17928	-0.17349	C_Inner											
-0.08015	0.185862	0.270392	-0.68377	0.021662	-0.36792	-0.55378	-0.82417	-0.1404	-0.16206	C_Inner											
-0.16348	-0.67363	-1.89961	0.803657	0.676142	0.241125	0.914758	2.81437	2.010712	1.334571	C_Outter											
0.348243	-0.60929	-1.16396	1.047503	0.507336	1.043682	1.652967	2.816926	1.769423	1.262088	C_Outter											
-0.07823	0.084278	-0.37872	1.241553	0.33197	2.469007	2.384729	2.763444	1.521891	1.189921	C_Outter											
-0.10674	0.374101	0.381625	1.354934	0.163026	3.391229	3.017128	2.635503	1.280569	1.117543	C_Outter											
0.023752	0.335007	0.917248	1.378931	0.004941	3.681308	3.346301	2.429053	1.050121	1.045181	C_Outter											
0.058038	0.274137	1.511951	1.320732	-0.14427	3.936164	3.662028	2.150077	0.829345	0.973613	C_Outter											
0.013535	-0.10701	-0.46992	-1.78669	0.024095	-2.3016	-2.19459	-1.72468	0.062019	0.037924	C_One Bar											
-0.02882	-0.03291	-0.15783	-1.88186	0.015826	-2.02267	-1.98976	-1.83193	0.049932	0.034106	C_One Bar											
0.057816	0.099749	0.178946	-1.8209	0.007095	-1.50474	-1.60449	-1.78343	0.037466	0.03037	C_One Bar											

Chapter 9: Results and Discussions

-0.05888	0.087226	0.392617	-1.52555	-0.0011	-1.02005	-1.10727	-1.49989	0.025659	0.026763	C_One Bar
0.02353	-0.04801	0.444836	-0.98828	-0.0086	-0.57674	-0.52874	-0.97357	0.014712	0.023315	C_One Bar
0.011513	-0.10462	0.445287	-0.33189	-0.01534	0.013559	0.118176	-0.32711	0.004784	0.020124	C_One Bar
0.115213	0.34138	0.335142	-1.55628	-0.29653	-1.66728	-2.00866	-2.3438	-0.78752	-0.49098	C_4 Bars
-0.26357	0.15895	0.342516	-1.72721	-0.23215	-1.91935	-2.0783	-2.42082	-0.6936	-0.46146	C_4 Bars
0.041771	-0.3154	0.324662	-1.76848	-0.16486	-2.35612	-2.04072	-2.36539	-0.59691	-0.43205	C_4 Bars
0.09425	-0.24875	0.190513	-1.61205	-0.09926	-2.17203	-1.92328	-2.11379	-0.50174	-0.40249	C_4 Bars
0.004343	0.177805	-0.02221	-1.2496	-0.03698	-1.50384	-1.68164	-1.65943	-0.40984	-0.37286	C_4 Bars
-0.07309	0.239191	-0.28726	-0.76847	0.022717	-1.13726	-1.37645	-1.08919	-0.32072	-0.34344	C_4 Bars
0.092636	0.441992	0.904231	-0.96073	-0.37632	-0.64585	-1.08784	-1.99207	-1.03134	-0.65502	C_8 Bars
-0.16806	0.376576	0.580003	-1.12468	-0.28442	-1.06858	-1.44516	-2.02516	-0.90047	-0.61605	C_8 Bars
0.019995	-0.06377	0.234902	-1.21367	-0.18888	-1.80863	-1.74486	-1.97976	-0.76609	-0.57721	C_8 Bars
0.094363	-0.28216	-0.12114	-1.18665	-0.09656	-2.22471	-1.94255	-1.82141	-0.63476	-0.5382	C_8 Bars
-0.09392	-0.25652	-0.39162	-1.03702	-0.00985	-2.19414	-1.93762	-1.546	-0.50898	-0.49913	C_8 Bars
0.05171	-0.10011	-0.70497	-0.80482	0.072227	-1.99806	-1.89795	-1.19299	-0.38817	-0.4604	C_8 Bars

*C: Current signal.

9.2.2 Feature Selection

The feature selection method is the next stage. Generally, the number and type of input features affect the precision performance and computation efficiency of the machine learning algorithms. Therefore, it is essential to select the best features to acquire good results. Here the feature selection methods play vital role to reduce the data dimensionality as the dataset have more than 5000 samples. The bigger the dataset size, the more time needed for classification process. Similarly, four most common feature selection methods (Sequential Forward Selection (SFS), Sequential Backward Selection (SBS), Sequential Floating Forward Selection (SFFS) and Sequential Floating Backward Selection (SFBS)) have been used in this part (as described in chapter 5 - section 5.5) to select and compare which is the best and more helpful feature for motor fault diagnosis based on B4M classification algorithm. MATLAB “R2015a” has been used for running all the feature selection methods.

After applying feature selection methods, the selected features of DWT-based current signal have been illustrated in table 9-7.

Table 9-7: The selected features for the current signal dataset.

		Feature Selection Method							
		SFS	SBS	SFFS	SFBS				
Details	Coefficients	DWT-L1	√	DWT-L1	√	DWT-L1	x	DWT-L1	√
		DWT-L2	x	DWT-L2	x	DWT-L2	√	DWT-L2	x
		DWT-L3	√	DWT-L3	√	DWT-L3	√	DWT-L3	x
		DWT-L4	√	DWT-L4	√	DWT-L4	√	DWT-L4	√
		DWT-L5	√	DWT-L5	x	DWT-L5	√	DWT-L5	x
Approximation	Coefficient	DWT-L1	√	DWT-L1	√	DWT-L1	x	DWT-L1	√
		DWT-L2	x	DWT-L2	x	DWT-L2	√	DWT-L2	x
		DWT-L3	√	DWT-L3	√	DWT-L3	x	DWT-L3	√
		DWT-L4	x	DWT-L4	√	DWT-L4	√	DWT-L4	x
		DWT-L5	x	DWT-L5	x	DWT-L5	√	DWT-L5	√

Chapter 9: Results and Discussions

It can be seen from table 9-7 that the feature selection methods have neglected some features and kept some others, as these features may have big impact on the classification accuracy, which lead to have too many misclassified data. The selected features have been used as input data for the proposed B4M classification method in order to classify induction motor faults.

9.2.3 Classification Results

The DWT-based current signal are ready for classification task. The dataset should split into two sets, training and testing sets. 100-folds cross validation has been also used for splitting this data in order to validate the system and check the time consumption as these are very important targets to be improved. The data have been labelled from 1 to 7 to be recognized by the proposed B4M and other classification systems. The datasets descriptions have been illustrated in table 9-8.

Table 9-8: Current signal dataset description.

Machine Condition	Class Label	No. of samples	No. of Training	No. of Testing
Healthy	1	750	650	100
Ball bearing fault	2	750	650	100
Bearing Inner race fault	3	750	650	100
Bearing outer race fault	4	750	650	100
One bar rotor fault	5	750	650	100
Four bars rotor fault	6	750	650	100
Eight bars rotor fault	7	750	650	100
Total Samples		5250	4550	700

Chapter 9: Results and Discussions

The proposed B4M classification algorithm have been applied with the same parameters, which are already chosen as described in (chapter 4 - section 4.3.2). Five different datasets have been fed to the B4M as stated below:

- Datasets without feature selection (Full).
- Datasets with Sequential Forward Selection (SFS).
- Datasets with Sequential Backward Selection (SBS).
- Datasets with Sequential Floating Forward Selection (SFFS).
- Datasets with Sequential Floating Backward Selection (SFBS)

All the above dataset have been used as input for B4M classification algorithm with 100-folds cross validation. By applying the proposed classification method, the system efficiency of 10 given features that are obtained from feature extraction has been illustrated in table 9-9.

Table 9-9: The proposed B4M classification results.

Dataset type	No. of rules	Classification Accuracy (%)
Full	7	75.44
SFS	8	79.62
SBS	7	74.36
SFFS	7	77.05
SFBS	10	77.81

The result that is obtained by the proposed B4M classification algorithm was very good as it exceeds 70%. In addition to this, all possible induction motor faults have been recognized by the proposed B4M because the more faults occurred the more complex data for the classification system to discriminate between the fault correctly. Furthermore, most of various studies about fault diagnosis were generally concerned about only one or few faults using current signal, but this study defeats a gap in fault

diagnosis literature by diagnosing all possible induction motor faults with new proposed classification algorithm. In other word, the current signal was very helpful for diagnosing either electrical or mechanical motor faults by proposed B4M, which could prevent the motor from failure by detecting the faults at an early stage. As can be seen in table 9-9, the classification percentage is varying based on the selected features, which means that some features have affected critically on the classification accuracy.

In terms of number of rules, the proposed B4M produces very small number of rules for diagnosing the motor fault. This is another advantage that the B4M has low number of rules. To put it simply, the lower the number of rules, the less time consumption to detect the fault for new incoming data (unseen data). Moreover, the sequential feature selection (SFS) method has been adopted for motor fault diagnosis as it has the highest classification accuracy with low number of rules but not the lower.

Consequently, the proposed B4M has been successfully applied for detecting the induction motor faults based on the current signal. All extracted features from the current signal by DWT have very helpful information for sensing the faults by the classification system as shown in table 9-9.

Table 9-10 shows the confusion matrix of the proposed B4M based on current signal using the SFS feature selection method.

Chapter 9: Results and Discussions

Table 9-10: Confusion matrix of the proposed B4M for the current signal dataset.

True Class	Predicted Class						
	Healthy	Ball bearing	Inner race	Outer race	One bar	Four bars	Eight bars
Healthy	600	10	16	0	20	4	0
Ball bearing	32	520	40	40	10	8	0
Inner race	55	38	407	95	45	10	0
Outer race	10	95	120	408	17	0	0
One bar	27	0	10	18	580	15	0
Four bars	0	0	5	5	35	585	20
Eight bars	0	0	0	28	48	52	522

The confusion matrix describes the way of how the B4M classifying the data:

- The most important part of the confusion matrix is the diagonal elements, because all the elements that are classified correctly have been placed in the diagonal. The healthy motor class has been classified correctly by diagnosing 600 elements out of 650, which indicates that the B4M has been able to classify more than 90% of all healthy features. However, the misclassified instances have been spread in all other motor faults but the highest was with one bar fault since its current signal was very similar to the healthy signal.
- For the bearing faults, the ball bearing fault achieved 520 correct sample out of 650 (only 130 samples have been misclassified), which is the lowest comparing to other bearing faults. While 234 samples have been misclassified for the inner race bearing fault (407 correct out of 650 samples). Furthermore, 408 samples out of 650 have been classified correctly for the outer race bearing fault. Consequently, the results show that the proposed classification system has been able to detect and discriminate between the induction motor faults correctly. Additionally, the induction motor bearing faults have been obtained

the lowest correct sample out of 650 samples since the current signals for these faults (ball, inner race, outer race) have been overlapped in some elements and it may effect on the classification accuracy.

- The classifications results for the rotor faults were very good as can be seen in table 9-10. In this case, the correctly classified elements have been the higher than bearing faults. For one rotor bar fault, 580 elements out of 650 elements have been classified correctly, which means only 70 elements have been misclassified and most of them have been recorded as healthy. As stated earlier the reason was the signal similarity between the healthy and one bar fault. Besides, for four bars rotor fault, 585 elements out 650 elements have been classified correctly, which is slightly more than one rotor bar faults. Furthermore, the eight bars rotor fault have obtained 522 correct sample out of 650, which is the lowest among all the rotor bar faults due to mentioned reasons.

Accordingly, the proposed classification system (B4M) has been successfully applied for diagnosing the induction motor faults based on current signal with the help of DWT and feature selection methods. The extracted features by DWT were very supportive to make the raw current signal clearer to be distinguished among all the motor faults. In addition to this, the feature selection methods have been played a crucial role in the classification process by selecting the most strongest features to be used as input for the classification system, as some features have negative impact on the system fault diagnosis.

Most studies in the field of condition monitoring have only focused on the current signal for detecting either rotor or bearing faults, while in this research the current

signal has been adopted for detecting both the rotor and bearing faults together with different types of faults and conditions. Since the current signal having much more information about the behaviour the motor rotor, it is also helpful for bearing faults as it changes the motor balance during heavy load. The classification accuracies of the proposed B4M were reasonable, as the dataset were very large and complex. As mentioned earlier that in the field of the machine learning, these classification accuracy are acceptable because they are obtained 80% approximately, which is good for new released classification system without any improvements. One reason why the proposed B4M has classification accuracy less than 90% is that the dataset has overlapped in some elements, which may lead the B4M to misclassify some classes. Furthermore, the proposed B4M produces low number of rules, which is another advantage as the number of rules could effect on the processing time for classifying a new incoming data. Consequently, the proposed B4M classification algorithm has been able to detect the induction motor faults based on the current signal and produced satisfactory results.

9.2.4 Comparison of B4M Performance with other Classification Algorithms

The current dataset have been used with other eight classification algorithms (Decision Table, JRIP, OneR (One Rule), PART (Projective Adaptive Resonance Theory), J48, LMT (Logistic Model Tree), Naïve Bayes tree and Random Tree) with the purpose of comparing their performances with the proposed classification method (B4M) performance. Similarly, the WEKA software has been used to run all the mentioned classification systems. 100-fold cross validation was used for all classifiers in order to compare their performances at same conditions. In addition, the selected features have been used for these eight classifiers.

Chapter 9: Results and Discussions

Most of the classification algorithms have been applied successfully as shown in figure 9-4. The proposed classification algorithm has been recorded as the higher in two-feature selection algorithms among all other classifiers, 79.62% and 77.81% for the sequential forward selection and sequential floating backward selection respectively. Thus, the proposed B4M classification algorithm has been used for motor fault detection successfully with very impressive results. Few classification systems have obtained very low classification accuracy, while some others acquired very acceptable results. For example, OneR classifier has achieved the lower accuracy, whereas the NB tree has reasonable results in most of dataset. The reason is that all classifiers depend on the dataset. If the dataset have clear and distinguishable features, the classification accuracy will be very high. Therefore, if the OneR obtained low classification accuracy, it does not mean that the classifier is not good, because it may obtain very accurate results by applying other dataset. So forth, the proposed classification algorithm, it may has very high classification accuracy based on the dataset itself.

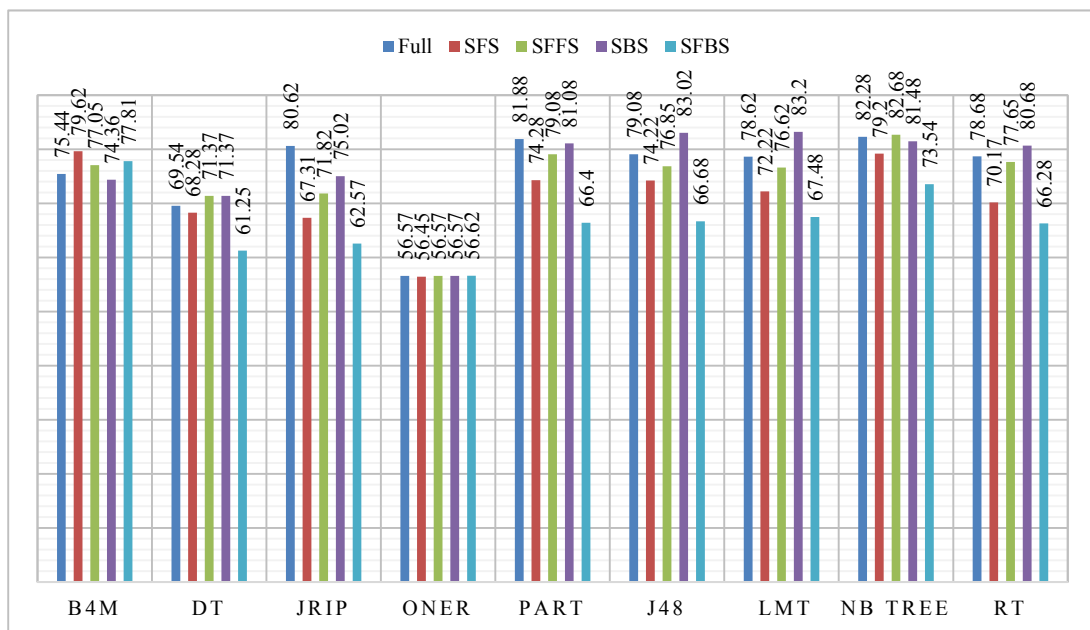


Figure 9-4: Comparison of the classification accuracy for different feature selection and classification algorithms based on current signal dataset.

Chapter 9: Results and Discussions

In terms of rules, figure 9-5 shows the number of rules that are produced from all the applied classification systems. It can be seen that the proposed B4M has the lower number of rules among all the other classifiers. This advantage makes the proposed classification system more robust and less time consumer as the lower number of rules the less time consumption for classifying the new data as explained earlier. The number of rules has been varied for all other classifiers, some have many rules such as RT system and some have low rules such as JRIP system. The number of rules are also relying on system calculations and the dataset dimensionality because the complex and large samples of dataset could lead to produce more rules. Here the rule pruning is needed to reduce the number of rules and choose the most powerful rule for classifying the new data with less error as happened with the proposed B4M. The proposed B4M has a rule pruning strategy to remove all the unrelated rules from the rule set as explained in chapter 4 section 4.2.5.

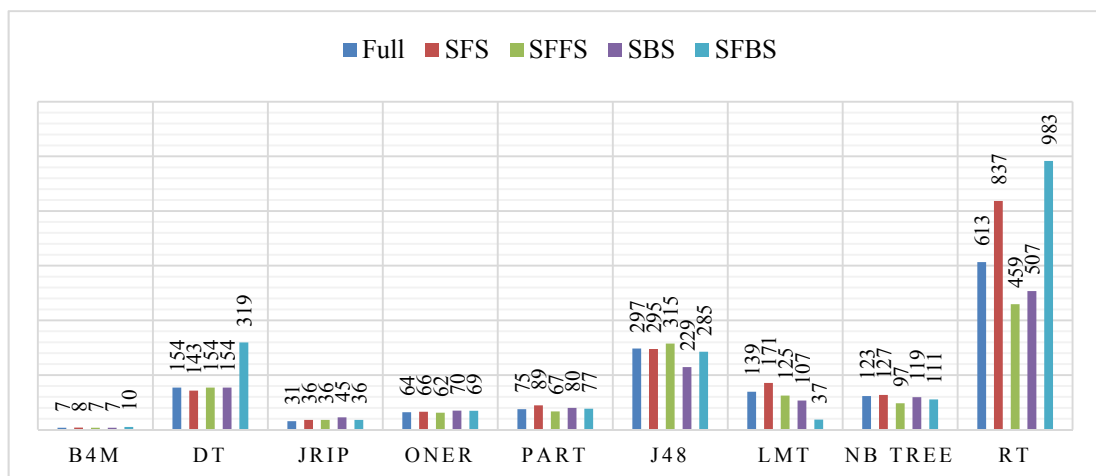


Figure 9-5: Comparison of the number of rules for different feature selection and classification algorithms based on current signal dataset.

The induction motor fault detection based on the current signal using the proposed B4M classification algorithm has been discussed and the next section will describe the induction motor fault detection based on the motor vibration signal analysis.

9.3 B4M Classification based on Vibration Signal for Fault Detection

9.3.1 Feature Extraction

Similarly, the feature extraction procedure for the vibration signal is the same as in the current signal. The datasets consist of three load conditions (no-load, 50% load and 100% load) with seven different faults (one bar rotor fault, four bars rotor faults, eight bars rotor faults, outer race bearing fault, ball bearing fault and inner race bearing fault). The 1-Dimensional DWT has been also applied for healthy and faulty conditions with same mother wavelet and decomposition level to extract the best features from the vibration signal. 10 features have been extracted from the raw vibration signal as the vibration signal itself are not clear enough for diagnosing the motor faults. These features have been splitted to 5 for DWT details coefficients and 5 for the DWT approximation coefficients. Thus, the dataset consists of 10 features for healthy and faulty conditions. Each fault has 750 samples for each feature. All datasets have been labelled accurately for each class to make them easy for the classification system to recognise the fault. Table 9-11 illustrates sample of the vibration dataset to be used for further processing. For full vibration signal, see Appendix B.

Table 9-11: Sample of vibration signal dataset features.

	Details Coefficients					Approximation Coefficient					Class
	DWT-L1	DWT-L2	DWT-L3	DWT-L4	DWT-L5	DWT-L1	DWT-L2	DWT-L3	DWT-L4	DWT-L5	
6.01E-15	0.001132	-0.00787	0.020654	0.020654	-0.00542	0.6	0.598868	0.606738	0.586084	0.5915	V_Healthy
-6.01E-15	0.0012	-0.00813	0.023238	0.023238	-0.01118	0.6	0.5988	0.606928	0.58369	0.594868	V_Healthy
-5.51E-06	0.000479	-0.00636	0.02397	0.02397	-0.01693	0.600006	0.599527	0.605885	0.581915	0.598845	V_Healthy
-2.81E-05	-0.00157	-0.0015	0.022004	0.022004	-0.02233	0.600028	0.6016	0.6031	0.581095	0.603427	V_Healthy
-3.57E-05	-0.00442	0.005651	0.017383	0.017383	-0.02723	0.600036	0.60446	0.598809	0.581426	0.608654	V_Healthy
4.75E-05	-0.00627	0.012386	0.01082	0.01082	-0.03158	0.599952	0.606225	0.593839	0.583019	0.614603	V_Healthy
0.010729	0.017512	0.040957	0.140128	0.140128	0.197773	-0.61073	-0.62824	-0.6692	-0.80933	-1.0071	V_Ball
-0.02461	0.01153	0.012935	0.160674	0.160674	0.198333	-0.63539	-0.64692	-0.65986	-0.82053	-1.01886	V_Ball
0.021083	-0.00362	-0.01711	0.172738	0.172738	0.19712	-0.68108	-0.67746	-0.66035	-0.83309	-1.03021	V_Ball
-0.01705	-0.01052	-0.03641	0.170932	0.170932	0.194293	-0.72295	-0.71243	-0.67602	-0.84695	-1.04124	V_Ball
0.018221	-0.00845	-0.04144	0.153822	0.153822	0.189739	-0.75822	-0.74977	-0.70833	-0.86215	-1.05189	V_Ball
-0.02018	-0.00749	-0.042	0.128529	0.128529	0.183123	-0.79982	-0.79234	-0.75034	-0.87887	-1.06199	V_Ball
-0.0011	-0.00353	-0.00352	-0.00732	-0.00732	-0.01553	-0.4069	-0.40338	-0.39986	-0.39254	-0.37701	V_Inner
0.00343	-0.00232	-0.00122	-0.00847	-0.00847	-0.01272	-0.40343	-0.40111	-0.39989	-0.39142	-0.3787	V_Inner
-0.00287	0.001648	0.000857	-0.009	-0.00975	-0.00975	-0.39713	-0.39878	-0.39964	-0.39063	-0.38088	V_Inner
0.002594	0.00224	0.002114	-0.0086	-0.0068	-0.0068	-0.39459	-0.39683	-0.39895	-0.39034	-0.38354	V_Inner
-0.00444	0.000227	0.002124	-0.00725	-0.00394	-0.00394	-0.39556	-0.39579	-0.39791	-0.39066	-0.38672	V_Inner
0.003215	-0.0005	0.002158	-0.00524	-0.00114	-0.00114	-0.39522	-0.39472	-0.39688	-0.39164	-0.3905	V_Inner
0.023078	0.007002	0.011155	0.037118	0.037118	-0.07911	5.496922	5.48992	5.478765	5.441648	5.520759	V_Outter
-0.04683	-0.0005	0.007242	0.042955	0.042955	-0.0873	5.486828	5.487327	5.480085	5.43713	5.524431	V_Outter
0.049938	-0.01154	0.001644	0.046762	0.046762	-0.09486	5.470062	5.481599	5.479955	5.433192	5.528052	V_Outter
-0.02245	-0.01106	-0.00409	0.047331	0.047331	-0.10137	5.462447	5.473511	5.4776	5.43027	5.531639	V_Outter
-0.02675	0.00306	-0.00924	0.044335	0.044335	-0.10658	5.466754	5.463694	5.472934	5.428599	5.535177	V_Outter
0.047443	0.018839	-0.01373	0.039162	0.039162	-0.11035	5.472557	5.453718	5.467444	5.428283	5.53863	V_Outter
0.000208	0.000785	-0.00047	-0.00626	0.000421	0.000421	-0.71221	-0.71299	-0.71253	-0.70627	-0.70669	V_One Bar
-0.00027	0.001852	-0.00063	-0.00707	0.000308	0.000308	-0.71173	-0.71358	-0.71295	-0.70588	-0.70619	V_One Bar
-0.00089	0.002265	-0.00046	-0.0075	0.000191	0.000191	-0.71111	-0.71337	-0.71291	-0.70541	-0.7056	V_One Bar
0.000564	-0.00033	-5.86E-05	-0.00731	7.99E-05	7.99E-05	-0.71256	-0.71223	-0.71218	-0.70486	-0.70494	V_One Bar

Chapter 9: Results and Discussions

0.00201	-0.00397	0.000633	-0.00645	-2.21E-05	-0.71401	-0.71004	-0.71067	-0.70422	-0.70419	V_One Bar
-0.00197	-0.0025	0.001189	-0.00525	-0.00012	-0.71003	-0.70753	-0.70872	-0.70347	-0.70336	V_One Bar
0.003108	0.006806	-0.00045	-0.00281	-0.00131	-0.65111	-0.65791	-0.65747	-0.65466	-0.65335	V_4 Bars
-0.00682	0.000628	-9.39E-05	-0.00326	-0.00138	-0.65718	-0.6578	-0.65771	-0.65445	-0.65307	V_4 Bars
0.003706	-0.01023	0.000279	-0.00354	-0.00143	-0.66771	-0.65747	-0.65775	-0.65421	-0.65278	V_4 Bars
-0.00129	-0.00571	0.000479	-0.00355	-0.00147	-0.66271	-0.657	-0.65748	-0.65392	-0.65246	V_4 Bars
-0.00022	0.008598	0.000486	-0.00326	-0.00149	-0.64778	-0.65637	-0.65686	-0.6536	-0.65211	V_4 Bars
-0.00111	0.008675	0.000463	-0.00281	-0.00149	-0.64689	-0.65557	-0.65603	-0.65322	-0.65173	V_4 Bars
0.009792	0.005494	-0.10998	-0.1861	-0.05997	0.990208	0.984714	1.094695	1.2808	1.340768	V_8 Bars
-0.00687	-0.01812	-0.05514	-0.20562	-0.06744	1.006866	1.024987	1.080126	1.285751	1.353192	V_8 Bars
-0.03779	-0.04668	0.005452	-0.21347	-0.07437	1.037791	1.084469	1.079017	1.292484	1.366855	V_8 Bars
0.064302	-0.01495	0.05159	-0.20244	-0.0803	1.135698	1.150647	1.099057	1.301497	1.381798	V_8 Bars
-0.06974	0.052562	0.074781	-0.1707	-0.085	1.269742	1.21718	1.142399	1.313096	1.398095	V_8 Bars
0.047583	0.059288	0.095177	-0.12956	-0.08834	1.352417	1.293129	1.197952	1.327517	1.415853	V_8 Bars

*V: Vibration signal.

9.3.2 Feature Selection

Four feature selection methods (Sequential Forward Selection (SFS), Sequential Backward Selection (SBS), Sequential Floating Forward Selection (SFFS) and Sequential Floating Backward Selection (SFBS)) have been used for selecting the most helpful features, as the feature selection have been used for reducing the data dimensionality to increase the classification system accuracy (as mentioned earlier). MATLAB “R2015a” has been used for running the feature selection methods. After applying feature selection methods, the selected features of DWT-based vibration signal have been illustrated in table 9-12.

Table 9-12: The selected features for the vibration signal dataset.

		Feature Selection Method							
		SFS		SBS		SFFS		SFBS	
Details	Coefficients	DWT-L1	x	DWT-L1	x	DWT-L1	x	DWT-L1	√
		DWT-L2	x	DWT-L2	√	DWT-L2	√	DWT-L2	√
		DWT-L3	√	DWT-L3	√	DWT-L3	x	DWT-L3	x
		DWT-L4	x	DWT-L4	√	DWT-L4	x	DWT-L4	x
		DWT-L5	x	DWT-L5	√	DWT-L5	√	DWT-L5	x
Approximation	Coefficient	DWT-L1	√	DWT-L1	x	DWT-L1	√	DWT-L1	√
		DWT-L2	√	DWT-L2	x	DWT-L2	√	DWT-L2	√
		DWT-L3	√	DWT-L3	√	DWT-L3	√	DWT-L3	√
		DWT-L4	x	DWT-L4	√	DWT-L4	x	DWT-L4	x
		DWT-L5	x	DWT-L5	x	DWT-L5	√	DWT-L5	√

It can be seen from table 9-12 that the feature selection methods have disregard some features and kept some others, as these features may overlapped with each other, which may lead to have many misclassified data. The selected features have been used as input data for the proposed B4M classification method in order to classify induction motor faults.

9.3.3 Classification Results

The vibration dataset is ready to be used as input for the proposed B4M classification algorithm. The dataset has been divided into training and testing sets. 100-folds cross validations have been applied for this dataset to check the classification system performance. Similarly, the dataset has been labelled from 1 to 7 to be used for the proposed and other classification systems. Table 9-13 shows the vibration dataset description for all induction motor faults.

Table 9-13: Vibration signal dataset description.

Machine Condition	Class Label	No. of samples	No. of Training	No. of Testing
Healthy	1	750	650	100
Ball bearing	2	750	650	100
Bearing Inner race	3	750	650	100
Bearing outer race	4	750	650	100
One bar rotor	5	750	650	100
Four bars rotor	6	750	650	100
Eight bars rotor	7	750	650	100
Total Samples		5250	4550	700

The proposed B4M classification algorithm have been applied with the same parameters, which are already chosen as described in (chapter 4 - section 4.3.2). Five different datasets have been fed to the B4M as stated below:

- Datasets without feature selection (Full).
- Datasets with Sequential Forward Selection (SFS).
- Datasets with Sequential Backward Selection (SBS).
- Datasets with Sequential Floating Forward Selection (SFFS).
- Datasets with Sequential Floating Backward Selection (SFBS)

Chapter 9: Results and Discussions

All the above datasets have been used as input for B4M classification algorithm with 100-folds cross validation. By applying the B4M classification method, the proposed system accuracy of 10 given features has been demonstrated in table 9-14.

Table 9-14: The proposed B4M classification results.

Dataset type	No. of rules	Classification accuracy (%)
Full	9	60.00
SFS	7	80.50
SBS	7	45.75
SFFS	12	48.75
SFBS	7	70.68

The proposed B4M classification algorithm has obtained good outcomes in some datasets and poor in others. Perhaps the most serious disadvantage of this classification is that it needs to reset its parameters (by increasing or reducing the number of iterations or number of bees, etc.) or needs more than one run to obtain the best results. In this research, the parameters of the proposed B4M have been kept the same for all the motor condition in order to be compared with other condition monitoring approaches and check the strength and the weakness of the proposed classification algorithm. As a result, all the results will be compared based on two main things, either on the feature selection method or on the dataset. Here the proposed B4M has obtained very good results by relying on the SFS and SFBS feature selection methods with very low number of rules, while it has obtained very poor results with other feature selection methods. Thus, the DWT features that are obtained from the vibration signal have been very cooperative for detecting the induction motor faults correctly and the proposed B4M has been successfully applied for the detecting induction motor faults based on the vibration signal.

Chapter 9: Results and Discussions

Table 9-15 shows the confusion matrix for the proposed B4M based on vibration signal using the SFS feature selection method.

Table 9-15: Confusion matrix of the proposed B4M for the vibration signal dataset.

True Class	Predicted Class						
	Healthy	Ball bearing	Inner race	Outer race	One bar	Four bars	Eight bars
Healthy	543	4	23	78	2	0	0
Ball bearing	6	596	20	28	0	0	0
Inner race	20	25	556	42	3	4	0
Outer race	19	20	38	545	20	8	0
One bar	52	12	12	32	522	20	0
Four bars	23	0	0	33	64	487	43
Eight bars	0	62	12	34	41	88	413

The confusion matrix describes the way of how the B4M classifying the vibration dataset:

- As stated previously, the diagonal elements are the most important part in the confusion matrix because they show the correct classification elements among all the features that are belong to specific class or correctly classified.
- In terms of the healthy conditions, the proposed B4M has classified 543 samples out of 650 (only 107 samples are misclassified), which means that the B4M has recognized the healthy motor among six fault conditions.
- In terms of bearing fault, the proposed B4M has obtained the highest correct elements in ball bearing defect than all other faults (596 out of 650), while the inner race fault has achieved the second highest than other bearing faults (556 out of 650). In addition, the outer race-bearing fault has obtained about 545 correct samples. Consequently, despite of the classification accuracy and the

number of misclassification samples, the proposed B4M has good attitude to classify the bearing faults correctly without any further implementation or improving in the objective function.

- In terms of rotor bars fault, the correct classification elements were lower than the bearing faults as the vibration signal is more suitable for the bearing faults than the rotor faults. Thus, 522 samples of one rotor bar fault out of 650 have been classified correctly by the proposed B4M, whereas 487 samples have been classified correctly to detect the four bars rotor fault. In addition, 413 correct samples have been classified as eight rotor bars fault by the proposed B4M. Since the dataset has very large number of data in each class, there is no doubt that the misclassification could be happened in such dataset. Many reasons for the misclassification or low classification accuracy that might be happened. First, the complex the dataset is, the higher possibility of misclassification samples can occurred. Second, the dataset overlapped with each other, which may lead the classification system to miss the correct class for these data.

In view of that, the proposed classification algorithm (B4M) has obtained good results for discriminating and detecting the motor faults in an early stage based on the vibration signal. The DWT features have positive outcome as they have extracted the important information from the raw vibration signal, as well as the feature selection methods that have been used for reducing the data dimensionality and select the best features.

As mentioned earlier that most studies have focused on current signal for detecting either the rotor or bearing faults, while in the vibration signal also has concentrated

for detecting the mechanical faults only, whereas in this research the vibration signal has been used for detecting the mechanical and electrical fault simultaneously. Moreover, the results show that the vibration signal could also be used for detecting the rotor faults as the rotor fault has negative impact on the motor balance, which may lead to change the motor vibration behaviour. The number of rules that are produced from the B4M are very acceptable comparing to the dataset size because the higher number of rules, the longer time for classification system needed to classify the new data. Therefore, the proposed classification algorithm is capable to detect the induction motor faults.

9.3.4 Comparison of B4M Performance with other Classification Algorithms

Similarly, eight classification algorithms (Decision Table, JRIP (Repeated Incremental Pruning), One R (One Rule), PART (Projective Adaptive Resonance Theory), J48, LMT (Logistic Model Tree), Naïve Bayes tree and Random Tree) have been applied for the vibration dataset in order to compare the performance of the proposed B4M classification algorithm. The same dataset has been used for all these classifiers. The dataset has been divided into training and testing sets as mentioned above. In order to validate the classification performance 100-folds cross validation have been applied for these classifiers.

The classification systems have been successfully applied for all different datasets (full, SFS, SFFS, SBS and SFBS). The proposed B4M have obtained good results in two datasets (SFS and SFBS) with 80.5% and 70.68% classification accuracy respectively as shown in figure 9-6. Figure 9-6 shows that the proposed B4M has ranked the first among all the classification algorithms with sequential feature

selection method, while it classified as the second after random tree algorithm with the sequential floating backward feature selection method.

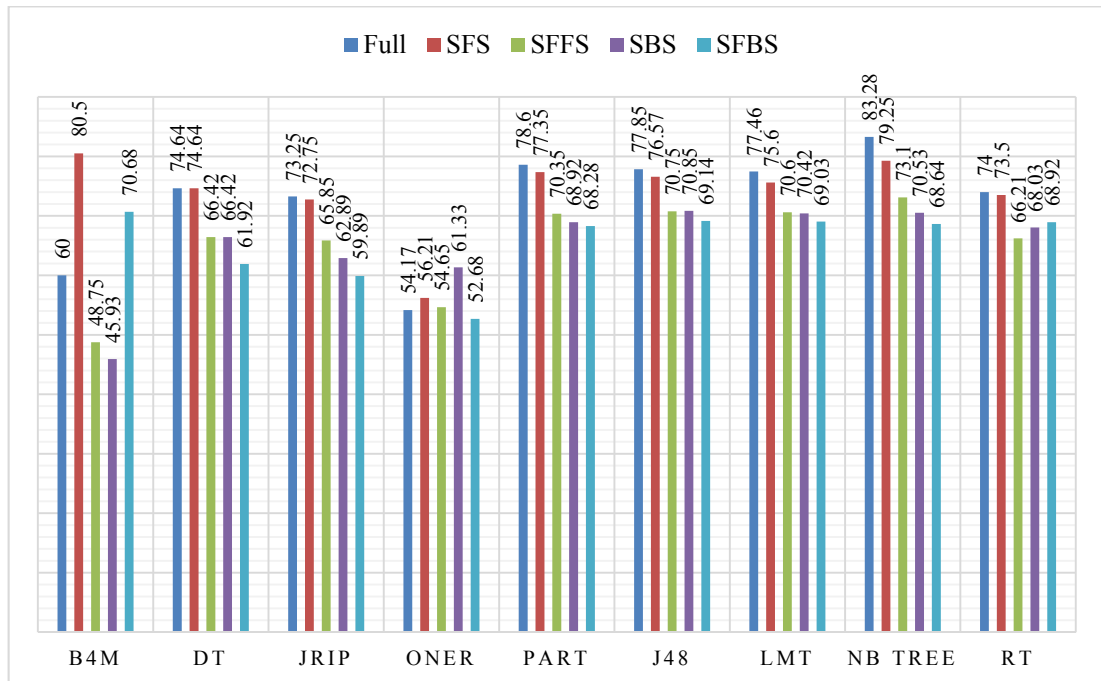


Figure 9-6: Comparison of the classification accuracy for different feature selection and classification algorithms based on the vibration signal dataset.

On the other hand, the proposed B4M has achieved less than 50% accuracy in both the sequential floating forward selection and sequential backward selection algorithms by 48.75% and 45.93% accuracy respectively. There are several possible explanation for this result. This inconsistency may due to the vast overlapping between the features or the attributes, as the vibration signal was very sensitive and sometimes the classification systems have difficulties to discriminate between the data classes. The other contradictory result may be due to the feature selection algorithm, as the feature selection method may fails to choose the best features since the feature selection methods play a vital role in classification accuracy results.

Additionally, figure 9-7 illustrates the number of rules for all classification algorithms. As shown in figure 9-7, the proposed B4M obtained the lower number of rules among

all 8 classification algorithms. As mentioned above, the number of rules relying on the classification system calculations and the dataset dimensions. The proposed B4M has produced the lower number of rules as it has rule pruning strategy, which is different from other classifiers. The rule pruning is responsible to remove the unrelated rules from the rule set and keep the better rules that cover all data samples as explained in chapter 4 - section 4.2.5.

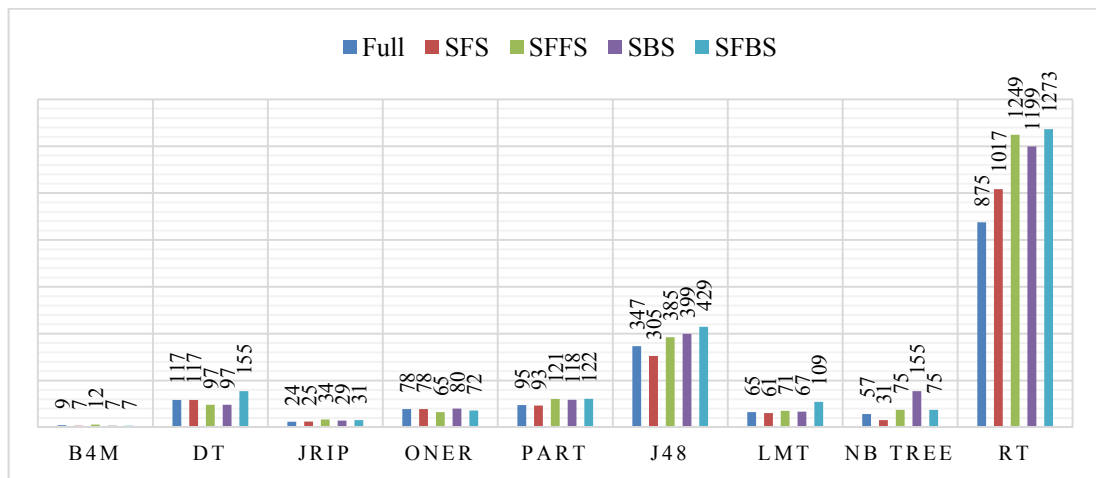


Figure 9-7: Comparison of the number of rules for different feature selection and classification methods based on the vibration signal dataset.

9.4 GA-B4M

For improving the proposed B4M classification algorithm, the GA has been adapted for selecting the best feature in addition to the previous feature selection methods. The GA has been used widely in the field of optimization, clustering, classification and feature selection. It has been successfully applied and it has positively effects on the classification accuracy for many classification algorithms.

The selected features for thermal image, current and vibration signals datasets by the GA have been illustrated in table 9-16.

Table 9-16: The selected features for all condition monitoring dataset based on GA.

Dataset Features					
Thermal		Current		Vibration	
MSE	√	DWT-L1	x	DWT-L1	√
PSNR	x	DWT-L2	x	DWT-L2	√
Mean	x	DWT-L3	x	DWT-L3	x
Variance	x	DWT-L4	x	DWT-L4	x
SD	x	DWT-L5	x	DWT-L5	√
Skew	√	DWT-L1	√	DWT-L1	x
Kurtosis	√	DWT-L2	√	DWT-L2	x
DWT-L1	√	DWT-L3	√	DWT-L3	x
DWT-L2	x	DWT-L4	x	DWT-L4	x
DWT-L3	x	DWT-L5	x	DWT-L5	x

After applying the GA for feature selection, the new selected features have been applied for the same classification algorithms (Decision Table, JRIP, OneR, PART, J48, LMT, Naïve Bayes tree and Random Tree) along with the proposed B4M method.

9.4.1 Classification Results

The classification systems have been applied with the same parameters and conditions as in the previous systems. The results were very good and there are improvements in the classification accuracy for not only the proposed B4M but also for other classification algorithms as shown in figures 9-8, 9-9 and 9-10.

In terms of thermal image features, the results of the proposed B4M have been ranked as the highest classification system among all other systems (DT, Jrip, PART, J48 and NB tree). There are two likely causes for the differences between the results with the full, SFS, SBS, SFFS, SFBS feature selection methods and the results with feature selection based on the genetic algorithm. The first one is that the features became very

few as only 4 feature out of 10 have been used for classification since some algorithms does not have the ability to classify such a dataset with small number of features, as system calculation itself has not been able to calculate the best rules or classify the dataset. The second is might be because of the dataset have overlapping in the selected features. However, eight classification algorithms have been able to classify the thermal image dataset successfully with very good classification accuracy as shown in figure 7-8.

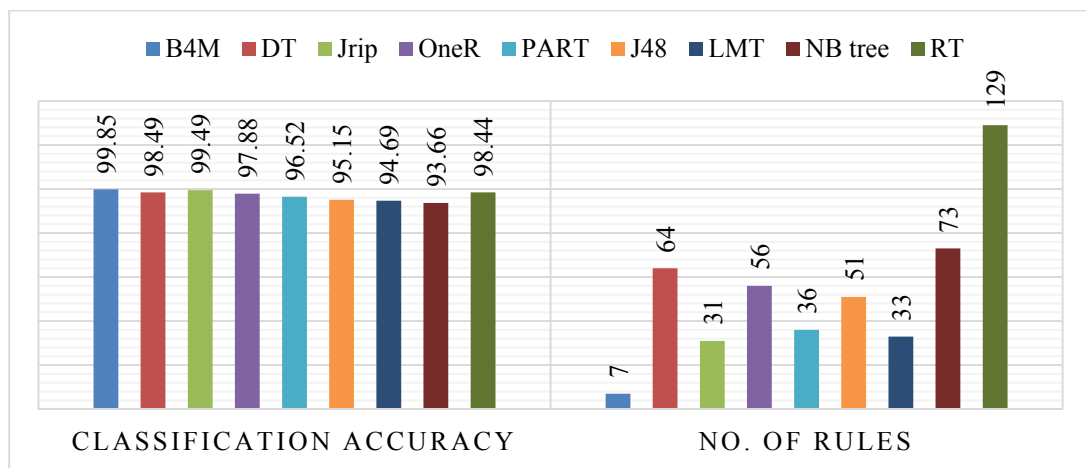


Figure 9-8: The comparison of classification and number of rules for different classification methods based on the thermal image dataset.

In terms of current signal, all the classification algorithms have been successfully applied and have obtained very good results as illustrated in figure 9-9. The classification accuracy has been raised up in some classification systems and went down for some others. Nevertheless, the proposed B4M has achieved very competitive result comparing to other classification algorithms. For example, the classification accuracy for the proposed B4M was 79.74% with 16 rules, which is ranked the 6 out of 9 classification systems. While the highest classification accuracy was recorded by the LMT algorithm (81.31%) with 47 rules. Thus, still the proposed B4M algorithms

has the lowest number of rules among all other classification algorithms as shown in figure 9-9.

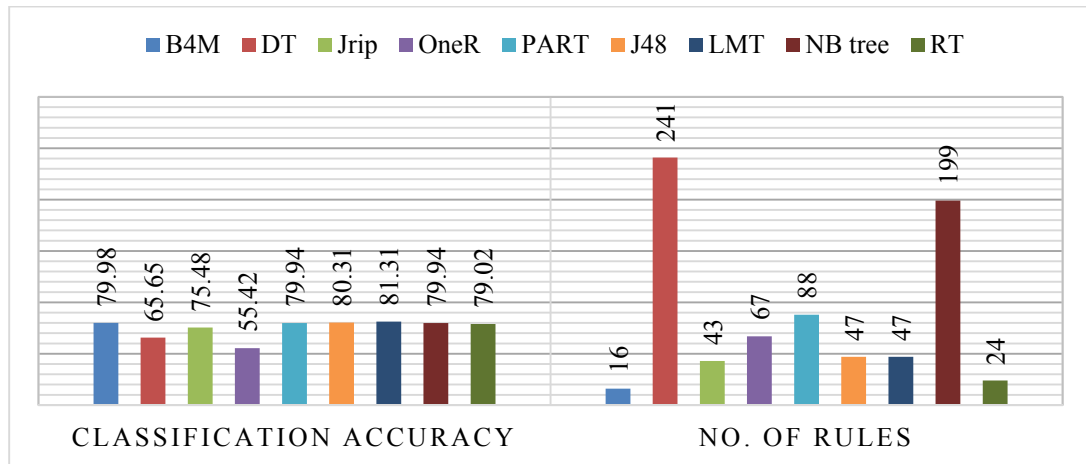


Figure 9-9: The comparison of classification accuracy and number of rules for different classification methods based on the current signal dataset.

Similarly, dealing with the vibration signal, the highest classification accuracy and the lowest number of rules have been recorded by the proposed classification algorithm (B4M), which is 98.74% and 7 rules as shown in figure 9-10.

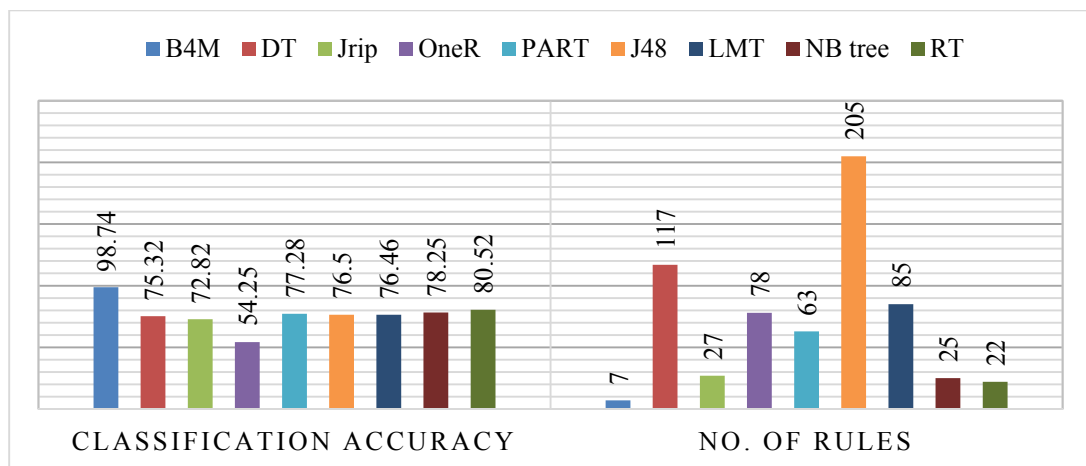


Figure 9-10: The comparison of classification accuracy and number of rules for different classification algorithms based on the vibration signal dataset.

9.5 Classification Results for Testing Dataset based on B4M

After obtaining the classification accuracy for the training dataset, the following results have explained the classification test accuracy for the test dataset based classification accuracy of training dataset relying on the SFS feature selection method. Figure 9-11 illustrates the classification test accuracy of the thermal image test dataset. It was clearly from the figure below that the proposed classification algorithm (B4M) has obtained the highest classification accuracy comparing to other classifiers. These results have indicated that the proposed algorithm has been able to detect, classify and predict the motor faults correctly better than other classifier. The reason of having good results is that the features that are extracted for the thermal images make the classifier able to discriminate between the motor faults with less misclassification percentage. Another reason is that the feature selection method has select the most helpful attributes among all other features. However, the DT and OneR classifiers have obtained 100% classification accuracy for the training dataset as mentioned above, while the classification test accuracy were the lower for both 76.36% and 52.20% respectively. One reason why these classifiers results have declined is that they may consider the new data as noisy data which make them unable to classify the data correctly, or the new data may overlapped between each other which may assigned to the incorrect class. Thus, it now understood that the dataset plays an important role in the classification accuracy.

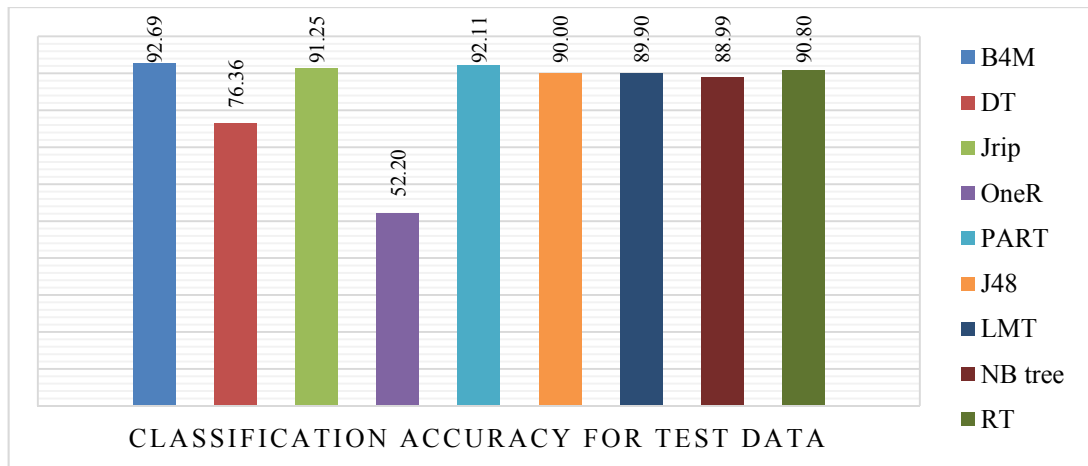


Figure 9-11: Classification accuracy for test dataset of thermal image.

In terms of current signal, the proposed B4M has achieved 76.35% classification test accuracy based on the current test dataset, which was the second highest classifier after NB tree (76.70%) as shown in

figure 9-12. The most likely causes of low classification test accuracies among all the classifiers are the data overlapping and data similarity. Furthermore, the feature selection method is an important factor for reducing or increasing the classification accuracy based on the clarity of dataset. The other classifiers have obtained similar accuracy, which were between 70.00% to 76.33%. While the DT and the OneR classifiers have obtained 63.02% and 52.20% respectively, due to the reasons above.

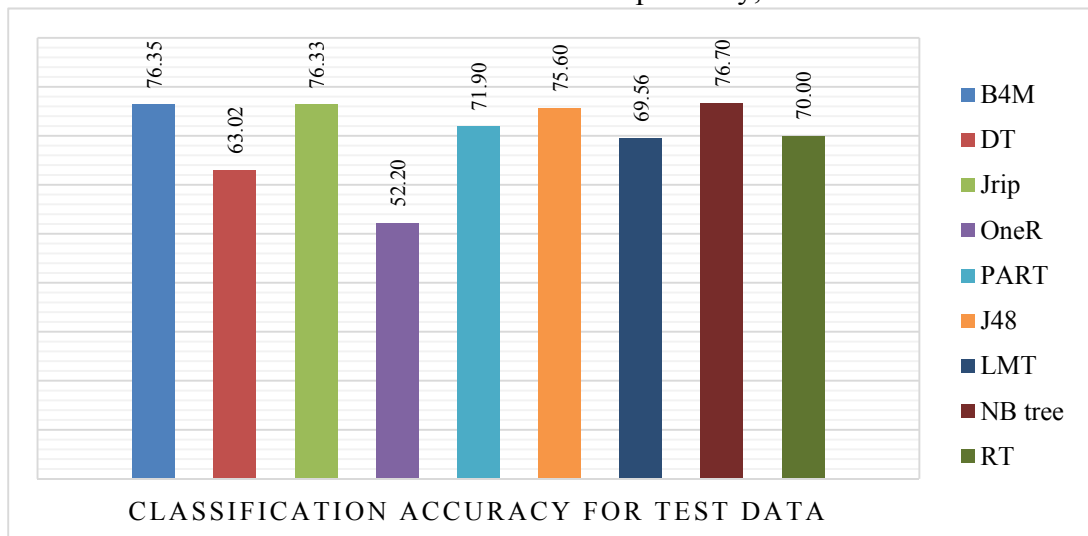


Figure 9-12: Classification accuracy for test dataset of current signal.

In terms of vibration signal, the proposed B4M has acquired 93.85% classification test accuracy based on the vibration test dataset, which was the forth-highest classifier after NB tree (95.00%), OneR (95.00%) and PART (93.99%) as illustrated in figure 9-13. As mentioned above the dataset and the feature selection method are important driving factors of reducing and increasing the classification system accuracy. The dataset is generally seen as factor strongly related to the classification accuracy as the more accurate the dataset, the more accurate classification system. The same issue for other classifiers, this is why that there is no single study exist shows that there is one best technique for all kind of classifications.

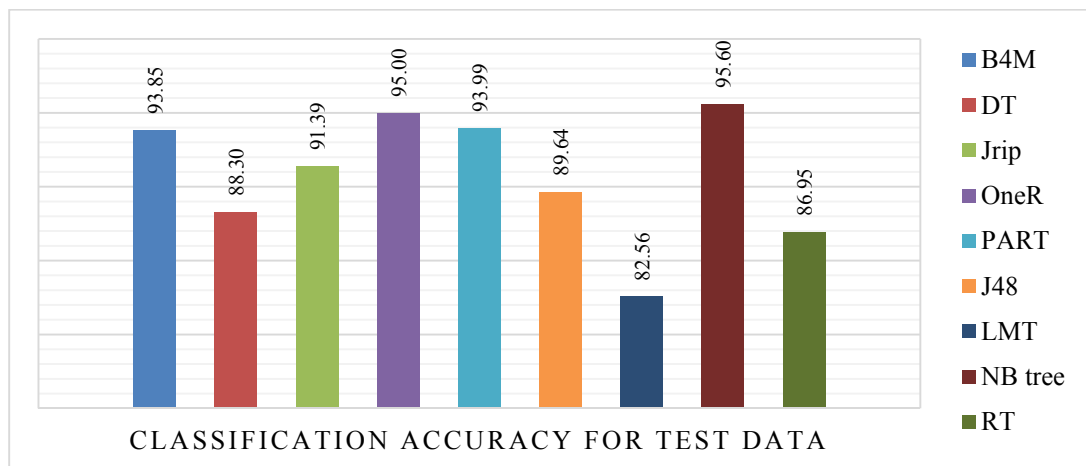


Figure 9-13: Classification accuracy for test dataset of vibration signal.

9.6 Classification Results for Testing Dataset based on GA-B4M

The proposed hybrid approach (GA-B4M) has been applied for the all condition monitoring methods in order to compare the performance of the proposed classification algorithm (B4M) with other classifiers, does the GA has improved the classification accuracy or not.

Figure 9-14 illustrates the classification test accuracy of thermal image test dataset based on the GA-B4M. The results show that the GA have a positive impact on all

classifiers as it has increased their classification accuracies better than without GA as explained above. The proposed B4M has obtained 98.92% classification accuracy, which was the highest comparing to other classifiers. In addition, the test classification accuracy of the DT and OneR classifiers have increased to 90.10% and 79.60% comparing to the test classification accuracy without GA. Consequently, the GA is a significant contributory factor to the development of classification accuracy not only for the proposed B4M but also for other well-known classifiers.

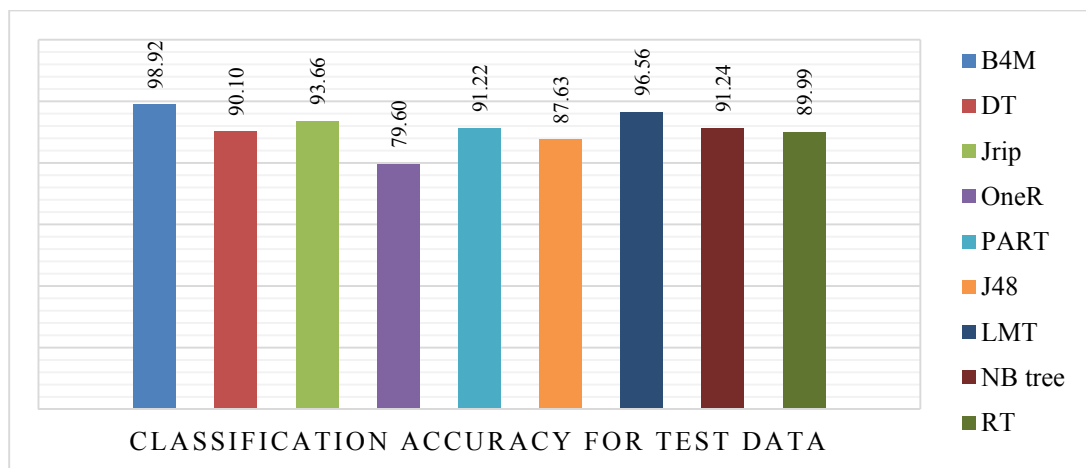


Figure 9-14: Classification accuracy of thermal image test dataset based on GA-B4M.

Figure 9-15 shows the classification test accuracy for the current dataset based on GA-B4M. The results show that the proposed classification method (B4M) has achieved 82.88% accuracy, which is counted as the third highest classifier after J48 (89.76%) and PART (85.39%). Similarly, the classification test accuracy for all classifiers has been increased based on GA as the GA has the ability to choose and reduce the data dimensionality by selecting the best features to be used to feed the classification systems.

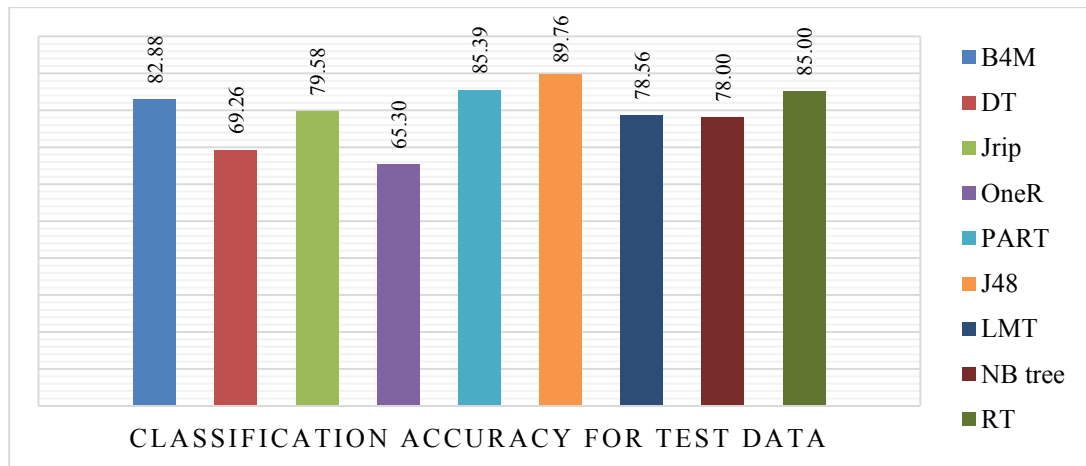


Figure 9-15: Classification accuracy of current test dataset based on GA-B4M.

In terms of vibration test dataset, figure 9-16 demonstrates the classification test accuracy based on the GA-B4M. The proposed B4M has achieved the second highest accuracy after OneR (98.56%) which is 98.36%. the results have indicated that the proposed B4M has been able to detect, classify and predict by achieving good accuracy and at the same time produce less number of rules. Furthermore, the results show that it was not only effective and more robust, but also more efficient, making it at least as good as other methods.

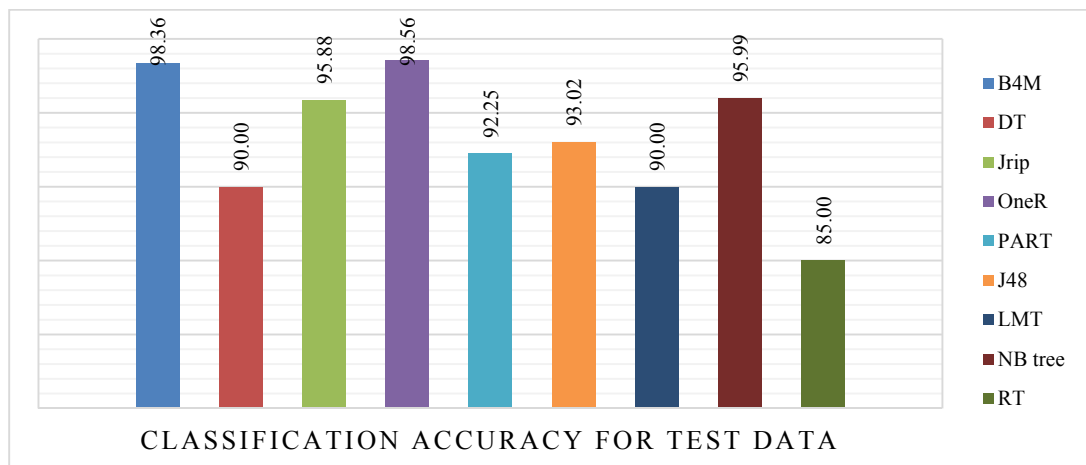


Figure 9-16: Classification accuracy of vibration test dataset based on GA-B4M.

CHAPTER 10

CONCLUSIONS AND FUTURE WORK

“This chapter illustrates contribution to knowledge. It summarises the achievements of this research and explains how the objectives stated in chapter one were achieved. The chapter concludes the study findings and suggests some aspects for future work”.

10.1 Overview

The purpose of this research was to advance the field of condition monitoring and fault diagnosis for three-phase induction motors. The wide usage of the induction motors in the industrial applications have increased the need for the condition monitoring to keep the motor working safely. The literature review has presented and summarized the state of the art for most condition monitoring techniques that are related to the proposed methods. Fault diagnosis based on the artificial intelligence is the focus of this research. Previously, the condition monitoring was relying on the traditional methods like monitoring the stator current waveform or vibration signals based on the basic devices, but due to advance in science and technology, digital signal processing based techniques and artificial intelligence approaches, which were not known before, have recently been introduced to condition monitoring for induction motor protection. These techniques provide the means to enhance the classical protection principles to be faster, more secure, low cost and reliable protection for the induction motors. In addition, the advance techniques have improved the time consumption of fault detection that have an effect on the production line. All this will change the practice for the induction motor protection.

Recently, the most common artificial intelligence techniques for the condition monitoring and fault diagnosis of induction motors are ANN, FLS, GA and many others in combination with data mining, which are used for classifying the motor faults in early stage. These techniques have been applied for a very complex and non-linear systems. However, it was possible to conclude from the review that no single approach would suffice for both classification and diagnosis. Furthermore, it is increasingly recognised that most individual artificial intelligence techniques suffer from specific

drawbacks, for that reason a new classification methods and hybrid approach are needed in most practical situations. Besides, most of the machine learning algorithms (optimization algorithms) have been converted to a classification algorithm based on data mining for the purpose of reducing the data dimensionality and make the machine learning algorithms more robust for analysing the complex (experimental data) data.

Finally, the classification algorithms based on data mining are still used in the differential condition monitoring although they have some disadvantages as mentioned in the literature. Each method mentioned in the literature was trying to overcome the disadvantages of previous methods. The proposed classification methods are also doing the same but the challenge of these methods are having simplicity in algorithm design, producing less number of rules and good classification accuracy for discriminating between the induction motor faults. This makes the proposed new methods a competitive alternative to existing methods.

10.2 Conclusions

This research has proposed a novel framework for condition monitoring and fault diagnosis of small induction motors. The DWT has been performed on the thermal image, current and vibration signals in order to extract the data (feature extraction) with more information related to the fault. In addition to this, the four feature selection methods (Sequential Forward Selection (SFS), Sequential Backward Selection (SBS), Sequential Floating Forward Selection (SFFS) and Sequential Floating Backward Selection (SFBS)) have been applied to the extracted features with purpose of choosing the most helpful features that are assisted the classification systems to obtain more accurate results for fault detection.

Additionally, this research has answered the primary aims which can be summarised as: addressing whether the Bees Algorithm based on data mining is suitable for induction motor fault diagnosis system, improving sensitivity to incipient faults in comparison to a conventional approach, implementing and evaluating a framework to condition monitoring and fault diagnosis for induction motor and accurately diagnosing results.

The research work carried out in this thesis included a number of important aspects that were novel and not previously implemented by other researchers or practitioners in a similar manner. These aspects of novelty are summarized below:

1- In Terms of Machine Learning

- a) This research proposes a novel tool known as “Bee for Mining” (B4M) for classification tasks, which enables the Bees Algorithm (BA) to discover rules automatically. In the proposed B4M, two parameters namely quality-weight and coverage-weight have been added to the BA to avoid any ambiguous situations during the prediction phase. The contributions of the proposed B4M algorithm are two-fold:
 - The first novel contribution is in the field of swarm intelligence, using a new version of BA for automatic rule discovery.
 - The second novel contribution is the formulation of a weight metric based on quality and coverage weight of the rules discovered from the dataset to carry out Meta-Pruning and making it suitable for any classification problem in the real world.

b) The proposed algorithm was implemented and tested using five different benchmark datasets: Iris, Wine, Soybean, Breast Tissue and Image Segmentation from University of California, at Irvine (UCI Machine Learning Repository) and was compared with other well-known classification algorithms. The results obtained using the proposed B4M show that it was capable of achieving better classification accuracy and at the same time reduce the number of rules in four out of five UCI datasets. Furthermore, the results show that it was not only effective and more robust, but also more efficient, making it at least as good as other methods such as C5.0, C4.5, Jrip and other evolutionary algorithms, and in some cases even better.

2- In Terms of Condition Monitoring

- a) The proposed novel method (B4M) has been successfully applied in three main induction motor faults detection scheme such as thermal, current and vibration condition monitoring.
- b) The proposed B4M classification based on the induction motor thermal images has obtained very good results for diagnosis the IM faults correctly with minimum number of rules. The thermal images have been captured from different machine conditions with different types of faults including the healthy condition (reference signal). The classification accuracy of the proposed B4M has achieved competitive results comparing to other classification algorithms with very low number of rules. Furthermore, the proposed image processing technique (Sobel, Prewitt, Roberts, Canny, LoG and Otsu) with the help of feature selection methods have

significantly assisted in improving classification accuracy of B4M for classifying the induction motor faults correctly.

- c) The new classification algorithm has been applied to induction motor faults detection based on the motor current signature analysis (MCSA). The MCSA has been collected from three different motor conditions (no load, 50% load and 100% load) with seven different types of faults (one rotor bar, four rotor bars, eight rotor bars, outer race bearing, ball bearing and inner race bearing fault) including the healthy condition (reference signal). The proposed classification algorithm has obtained very good results by using the current signal coefficients that are extracted by Discrete Wavelet Transform (DWT) and feature selection methods.
- d) The new proposed classification algorithm has been also applied to induction motor fault detection based on the vibration signal with the same condition of DWT as in the current signal. The B4M acquired very satisfying results compared to other classification algorithms.

The new proposed method is not like other methods for induction motor faults detection. For instance, some methods detect the fault based on the load conditions as they have divided the faults relying on the motor load. In this case, some faults does not appear during low load or have difficulties to be detected by the classification system. However, the proposed algorithm is not depending on the motor load condition because all the different load conditions have been combined together as one fault or one package. Therefore, there is no need to wait for the motor to be loaded to detect the faults because if the faults are happened and the motor does not loaded, the motor could be fail to run. Consequently, the motor faults detection based on B4M

have overcome this problem and become very sensitive for any changing in the motor signals behaviour to detect and diagnose the most common induction motor faults correctly.

3- In Terms of Machine Learning Hybrid System

- a) A new hybrid system has been proposed which is a combination between the Genetic Algorithm and B4M classification algorithm. The purpose of this system was to use the GA as feature selection method. Two important reasons of creating this system, the first one is to reduce the data dimensionality, and the second one is to increase the classification system accuracy. Then, the selected features were fed to the proposed B4M algorithm to detect the motor fault correctly.
- b) The proposed hybrid system has been applied to three induction motor condition approaches; thermal image, current and vibration signals. The system achieved very competitive results comparing to other classification algorithms. The Genetic Algorithm based feature selection has positive impact in supporting the classification system to gain very good classification accuracy.

In general, the research has presented a new competitive methods over those mentioned in the literature particularly classification algorithm, which is still dependable and widely used in condition monitoring up to now. The competition was based on two factors, the classification accuracy and the number of rules. Simultaneously, the improvement of these factors was not at the cost of lower reliability and security. The proposed methods have shown a very high accuracy in all

the tests performed on the induction motor. The efficiency and effectiveness of these methods were proved by both simulation in MATLAB software and practical experiments. In simulation, the proposed B4M has been validated based on the UCI datasets. While practically, the data have been collected experimentally from the induction motors with different load conditions and types of faults.

10.3 Future Work

The purpose of the work presented in this thesis was to advance the research in the two fields: machine learning and induction motor condition monitoring for faults diagnosis. After this objective has been achieved, there is generally still much work to implement this new knowledge into widespread applications. Nevertheless, there is still additional work required to apply this new classification system scheme in industry. Suggestions for future research directions are summarised below:

1- In Terms of Machine Learning

- a) Find out other optimization algorithms and study their abilities to be converted to classification algorithm based on data mining rule discovery, since each algorithm has different calculations and it may help rise the capability of the artificial intelligence to solve the real world problems properly.
- b) Develop a new hybrid classification system to obtain very high classification accuracy.
- c) Generalize the proposed classification algorithm to other types of motors, or apply it in other application such as engine, surface crack (concrete), and many others.

2- In Terms of Condition Monitoring

- a) Apply the proposed method on other induction motors (different size) to see the effect of the motor rates on the classification accuracy.
- b) Simulate and seed other types of common failure mode, for instance, stator fault, air gap eccentricity fault etc. In this research, each fault was simulated individually (one fault at a time). Future work could explore simultaneous faults and faults combining e.g. phase imbalance and rotor bar together, or two bearing faults together (outer race and ball bearing).
- c) In using a wavelet transform, different wavelets have different impacts in revealing fault features. It would be more complementary if some criteria could be established, with regard to which types of wavelets are more suitable for certain types of non-stationary events. One type of wavelet has been studied in this work. Therefore, enhancement of fault features in wavelet analysis should be investigated by using different mother wavelet analysis.
- d) Apply empirical mode decomposition level based techniques for different types of induction motor faults.
- e) Investigate the effectiveness of other image processing technique.
- f) The analysis carried out in this research was “offline” condition monitoring. Future work should be developed and concentrated on “online” condition monitoring.

REFERENCES

- [1] P. Girdhar and C. Scheffer, "Practical Machinery Vibration Analysis and Predictive Maintenance," *Newnes*, vol. 1, p. 222, 2004.
- [2] A. Davies, P. W. Prickett, and R. I. Grosvenor, "Future developments in condition monitoring techniques and systems," in *Handbook of Condition Monitoring*, pp. 541–560, 1998,.
- [3] A. Albarbar and A. Starr R. Pietruszkiewicz, *Towards the Implementation of Integrated Multi-measurand Wireless Monitoring System*. 2007.
- [4] M. N. Uddin and M. M. Rahman, "Online current and vibration signal monitoring based fault detection of bowed rotor induction motor," in *2015 IEEE Energy Conversion Congress and Exposition, ECCE 2015*, pp. 2988–2994, 2015.
- [5] E. Artigao, S. Koukoura, A. Honrubia-Escribano, J. Carroll, A. McDonald, and E. Gómez-Lázaro, "Current Signature and Vibration Analyses to Diagnose an In-Service Wind Turbine Drive Train," *Energies*, vol. 11, no. 4, p. 960, 2018.
- [6] M. Kezunovic, *A survey of neural net applications to protective relaying and fault analysis*, vol. 5. 1997.
- [7] M. Chow, R. Sharpe, and J. Hung, "On the Application and Design of Artificial Neural Networks for Motor Fault Detection Part II," *IEEE Transactions on Industrial Electronics*, vol. 40, no. 2. pp. 189–196, 1993.
- [8] B. Li, M. Y. Chow, Y. Tipsuwan, and J. C. Hung, "Neural-network-based motor rolling bearing fault diagnosis," *IEEE Trans. Ind. Electron.*, vol. 47, no. 5, pp. 1060–1069, 2000.
- [9] M. E. H. Benbouzid, "A review of induction motors signature analysis as a medium for faults detection," *IEEE Trans. Ind. Electron.*, vol. 47, no. 5, pp. 984–993, 2000.
- [10] S. Nandi, H. A. Toliyat, and X. Li, "Condition monitoring and fault diagnosis of electrical motors - A review," *IEEE Transactions on Energy Conversion*, vol. 20, no. 4. pp. 719–729, 2005.
- [11] S. Bindu and V. V. Thomas, "Diagnoses of internal faults of three phase squirrel cage induction motor - A review," in *Proceedings of the 2014*

-
- International Conference on Advances in Energy Conversion Technologies - Intelligent Energy Management: Technologies and Challenges, ICAECT 2014*, pp. 48–54, 2014.
- [12] O. C. N. Souto, J. C. de Oliveira, and L. M. Neto, “Induction motors thermal behaviour and life expectancy under non-ideal supply conditions,” *Harmonics and Quality of Power, 2000. Proceedings. Ninth International Conference on*, vol. 3. pp. 899–904 vol.3, 2000.
- [13] P. C. Krause, O. Wasynczuk, and S. D. Sudhoff, “Analysis of Electric Machinery and Drive Systems,” *Power Engineering*. pp. 1–65, 2002.
- [14] P. C. Sen, *Principles of electric machines and power electronics*. New York: John Wiley & Sons, 1997.
- [15] H. A. Toliyat, S. Nandi, S. Choi, and H. Meshgin-Kelk, *Electric Machines: Modeling, Condition Monitoring, and Fault Diagnosis*. CRC Press, 2012.
- [16] E. H. El Bouchikhi, V. Choqueuse, and M. Benbouzid, “Induction machine faults detection using stator current parametric spectral estimation,” *Mech. Syst. Signal Process.*, vol. 52–53, no. 1, pp. 447–464, 2015.
- [17] P. Krause, O. Wasynczuk, and S. Sundhoff, *Analysis of Electric Machinery*. New York: Mc-Graw Hill, 1986.
- [18] A. Sharma, S. Chatterji, L. Mathew, and M. Khan, “A Review of Fault Diagnostic and Monitoring Schemes of Induction Motors,” *Int. J. Res. Appl. Sci. Eng. Technol.*, vol. 3, no. IV, pp. 1145–1152, 2015.
- [19] A. E. Fitzgerald, *Electric machinery*, vol. 319, no. 4. 2003.
- [20] A. Bellini, F. Filippetti, C. Tassoni, and G.-A. Capolino, “Advances in diagnostic techniques for induction machines,” *IEEE Trans. Ind. Electron.*, vol. 12, no. 55, pp. 4109–4126, 2008.
- [21] K. S. Gaeid, H. W. Ping, M. Khalid, and A. L. Salih, “Fault Diagnosis of Induction Motor Using MCSA and FFT,” *Electrical and Electronic Engineering*, vol. 1, no. 2. pp. 85–92, 2011.
- [22] C. Y. Lee, “Effects of unbalanced voltage on the operation performance of a three-phase induction motor,” *IEEE Trans. Energy Convers.*, vol. 14, no. 2, pp. 202–208, 1999.
- [23] M. O. Mustafa, G. Nikolakopoulos, and T. Gustafsson, “Experimental evaluation of a broken rotor bar fault detection scheme based on Uncertainty

-
- Bounds violation,” in *IECON Proceedings (Industrial Electronics Conference)*, pp. 5543–5548, 2013.
- [24] P. J. Tavner, *Condition Monitoring of Rotating Electrical Machines*, vol. 2, no. 4. 2008.
- [25] A. H. Bonnett and G. C. Soukup, “Cause and Analysis of Stator and Rotor Failures in Three-Phase Squirrel-Cage Induction Motors,” *IEEE Trans. Ind. Appl.*, vol. 28, no. 4, pp. 921–937, 1992.
- [26] J. Milimonfared, H. M. Kelk, S. Nandi, A. Der Minassians, and H. A. Toliyat, “A novel approach for broken-rotor-bar detection in cage induction motors,” *IEEE Trans. Ind. Appl.*, vol. 35, no. 5, pp. 1000–1006, 1999.
- [27] S. Bhattacharyya, D. Sen, S. Adhvaryyu, and C. Mukherjee, “Induction Motor Fault Diagnosis by Motor Current Signature Analysis and Neural Network Techniques,” *J. Adv. Comput. Commun. Technol. (ISSN 2347 - 2804)*, vol. 3, no. 1, pp. 12–18, 2015.
- [28] E. Muljadi, R. Schiferl, and T. A. Lipo, “Induction Machine Phase Balancing by Unsymmetrical Thyristor Voltage Control,” *IEEE Transactions on Industry Applications*, vol. IA-21, no. 3. pp. 669–678, 1985.
- [29] W. T. Thomson and M. Fenger, “Current signature analysis to detect induction motor faults,” *IEEE Ind. Appl. Mag.*, vol. 7, no. 4, pp. 26–34, 2001.
- [30] P. Pillay, P. Hofmann, and M. Manyage, “Derating of induction motors operating with a combination of unbalanced voltages and over or undervoltages,” *IEEE Trans. Energy Convers.*, vol. 17, no. 4, pp. 485–491, 2002.
- [31] K. J. Hammadi, D. Ishak, and M. Kamarol, “On-line monitoring and diagnosis broken rotor bars in squirrel-cage induction motor by using LabView,” *Aust. J. Basic Appl. Sci.*, vol. 5, no. 9, pp. 1525–1528, 2011.
- [32] K. S. Gaeid, H. W. Ping, M. Khalid, and L. Salih, “Fault Diagnosis, Induction Motor, Unbalance Voltage, Broken Rotor Bar, MCSA, FFT, Vector Control; Fault Diagnosis, Induction Motor, Unbalance Voltage, Broken Rotor Bar, MCSA, FFT, Vector Control,” *Electr. Electron. Eng.*, vol. 1, no. 2, pp. 85–92, 2011.
- [33] I. Y. Önel and M. E. H. Benbouzid, “Induction motor bearing failure detection and diagnosis: Park and concordia transform approaches comparative study,” *IEEE/ASME Trans. Mechatronics*, vol. 13, no. 2, pp. 257–262, 2008.

-
- [34] K. Salloum Gaeid and H. Wooi Ping, "Wavelet fault diagnosis and tolerant of induction motor: A review," *Int. J. Phys. Sci.*, vol. 6, no. 3, pp. 358–376, 2011.
- [35] R. Puche-Panadero, M. Pineda-Sanchez, M. Riera-Guasp, J. Roger-Folch, E. Hurtado-Perez, and J. Perez-Cruz, "Improved resolution of the MCSA method via Hilbert transform, enabling the diagnosis of rotor asymmetries at very low slip," *IEEE Trans. Energy Convers.*, vol. 24, no. 1, pp. 52–59, 2009.
- [36] M. Drif and A. J. M. Cardoso, "Airgap-eccentricity fault diagnosis, in three-phase induction motors, by the complex apparent power signature analysis," *IEEE Trans. Ind. Electron.*, vol. 55, no. 3, pp. 1404–1410, 2008.
- [37] D. Miljkovic, "Brief review of motor current signature analysis," *IEEE Ind. Appl. Mag.*, vol. 5, no. 1, pp. 14–26, 2015.
- [38] O. A. Omitaomu, M. K. Jeong, A. B. Badiru, and J. W. Hines, "Online support vector regression approach for the monitoring of motor shaft misalignment and feedwater flow rate," *IEEE Trans. Syst. Man Cybern. Part C Appl. Rev.*, vol. 37, no. 5, pp. 962–970, 2007.
- [39] S. Shashidhara and D. Raju, "stator winding fault diagnosis of three-phase induction motor by park's vector approach," *ISSN Int. J. Adv. Res. Electr. Electron. Instrum. Eng.*, vol. 2, no. 7, pp. 2320–3765, 2013.
- [40] P. T. Krein, *Power Electronics Handbook*. 2011.
- [41] J. Robinson, C. D. Whelan, and N. K. Haggerty, "Trends in advanced motor protection and monitoring," *IEEE Trans. Ind. Appl.*, vol. 40, no. 3, pp. 853–860, 2004.
- [42] I. Std, P. Systems, R. Subcommittee, E. Committee, I. Industry, A. Society, and I. S. Board, "IEEE Recommended Practice for the Design of Reliable Industrial and Commercial Power Systems," *Analysis*, vol., 1997.
- [43] G. Fox, "Overload Protection For Medium Voltage Motors Controlled By Switchgear Starters," in *Record of Annual Pulp and Paper Industry Technical Conference*, pp. 82–86, 1990.
- [44] G. J. Paoletti and A. Rose, "Improving Existing Motor Protection For Medium Voltage Motors," *IEEE Trans. Ind. Appl.*, vol. 25, no. 3, pp. 456–464, 1989.
- [45] S. F. Farag, R. G. Bartheld, and T. G. Habetler, "An integrated on-line motor protection system," *IEEE Ind. Appl. Mag.*, vol. 2, no. 2, pp. 21–26, 1996.

-
- [46] T. Albers and A. H. Bonnett, "Motor temperature considerations for pulp and paper mill applications," *IEEE Trans. Ind. Appl.*, vol. 38, no. 6, pp. 1701–1713, 2002.
- [47] R. Beguenane, M. El, H. Benbouzid, M. Tadjine, A. Tayebi, S. Automatiques, U. De Picardie, and J. Veme, "Speed and Rotor Time Constant Estimation via MRAS Strategy for Induction Motor Drives Rachid," in *IEE Proc. Electr. Power Appl.*, no. 3, pp. 3–5, 1997.
- [48] T. G. Habetler, R. G. Harley, and D. J. Gritter, "A Stator and Rotor Resistance Estimation Technique for Conductor Temperature Monitoring," *Ind. Appl. Conf.*, pp. 381–387, 2000.
- [49] Z. Gao, T. G. Habetler, R. G. Harley, and R. S. Colby, "A sensorless rotor temperature estimator for induction machines based on current harmonic spectral estimation scheme," in *EPE-PEMC 2006: 12th International Power Electronics and Motion Control Conference, Proceedings*, pp. 431–437, 2007.
- [50] Z. Gao, T. G. Habetler, and R. G. Harley, "A Complex Space Vector Approach to Rotor Temperature Estimation for Line-Connected Induction Machines With Impaired Cooling," *IEEE Trans. Ind. Electron.*, vol. 56, no. 1, pp. 239–247, 2009.
- [51] Z. Gao, R. S. Colby, and L. Turner, "Induction-motor rotor temperature estimation using superheterodyne receivers," *IEEE Trans. Ind. Appl.*, vol. 48, no. 4, pp. 1267–1278, 2012.
- [52] D. Di. Reigosa, J. M. Guerrero, A. B. Diez, and F. Briz, "Rotor Temperature Estimation in Doubly-Fed Induction Machines Using Rotating High-Frequency Signal Injection," *IEEE Trans. Ind. Appl.*, vol. 53, no. 4, pp. 3652–3662, 2017.
- [53] Y. Huang and C. Gühmann, "Temperature estimation of induction machines based on wireless sensor networks," pp. 267–280, 2018.
- [54] G. Singh, T. C. Anil Kumar, and V. N. A. Naikan, "Induction motor inter turn fault detection using infrared thermographic analysis," *Infrared Phys. Technol.*, vol. 77, pp. 277–282, 2016.
- [55] G. Singh and V. N. A. Naikan, "Infrared thermography based diagnosis of inter-turn fault and cooling system failure in three phase induction motor," *Infrared Phys. Technol.*, vol. 87, pp. 134–138, 2017.

-
- [56] W. K. W. K. Wong, P. N. T. P. N. Tan, C. K. L. C. K. Loo, and W. S. L. W. S. Lim, "Machine condition monitoring using omnidirectional thermal imaging system," *Signal Image Process. Appl. (ICSIPA), 2009 IEEE Int. Conf.*, 2009.
- [57] M. Blödt, P. Granjon, B. Raison, and J. Regnier, "Mechanical fault detection in induction motor drives through stator current monitoring - Theory and application examples," in *Fault Detection*, pp. pp.451–488, 2010.
- [58] W. T. Thomson and M. Fenger, "Case histories of current signature analysis to detect faults in induction motor drives," *IEEE Int. Electr. Mach. Drives Conf. 2003. IEMDC'03.*, vol. 3, 2003.
- [59] I. M. Culbert and W. Rhodes, "Using current signature analysis technology to reliably detect cage winding defects in squirrel-cage induction motors," *IEEE Trans. Ind. Appl.*, vol. 43, no. 2, pp. 422–428, 2007.
- [60] M. E. H. Benbouzid, M. Vieira, and C. Theys, "Induction motors' faults detection and localization using stator current advanced signal processing techniques," *Power Electron. IEEE Trans.*, vol. 14, no. 1, pp. 14–22, 1999.
- [61] R. R. Schoen and T. G. Habetler, "Effects of time-varying loads on rotor fault detection in induction machines," *IEEE Trans. Ind. Appl.*, vol. 31, no. 4, pp. 900–906, 1995.
- [62] W. T. Thomson, D. Rankin, and D. G. Dorrell, "On-line current monitoring to diagnose airgap eccentricity in large three-phase induction motors - industrial case histories verify the predictions," *IEEE Trans. Energy Convers.*, vol. 14, no. 4, pp. 1372–1378, 1999.
- [63] M. Arkan, D. K. Perović, and P. Unsworth, "Online stator fault diagnosis in induction motors," *IEE Proc. - Electr. Power Appl.*, vol. 148, no. 6, p. 537, 2001.
- [64] A. Miletic and M. Cettolo, "Frequency converter influence on induction motor rotor faults detection using motor current signature analysis-experimental research," in *IEEE International Symposium on Diagnostics for Electric Machines, Power Electronics and Drives, SDEMPED 2003 - Proceedings*, pp. 124–128, 2003.
- [65] R. R. Obaid and T. G. Habetler, "Current-based algorithm for mechanical fault detection in induction motors with arbitrary load conditions," *Conf. Rec. IEEE Ind. Appl. Conf. IAS Annu. Meet.*, vol. 2, pp. 1347–1351, 2003.

-
- [66] T. M. Wolbank, P. Nussbaumer, H. Chen, and P. E. Macheiner, "Non-invasive detection of rotor cage faults in inverter fed induction machines at no load and low speed," in *Diagnostics for Electric Machines, Power Electronics and Drives, 2009. SDEMPED 2009. IEEE International Symposium on*, pp. 1–7, 2009.
- [67] J. R. Stack, T. G. Habetler, and R. G. Harley, "Bearing fault detection via autoregressive stator current modeling," *IEEE Trans. Ind. Appl.*, vol. 40, no. 3, pp. 740–746, 2004.
- [68] L. V Dimitrov and V. J. Chobanov, "Diagnosis of rotor faults of induction motors, operated in non-rated conditions," *Electronics Technology: Meeting the Challenges of Electronics Technology Progress, 2004. 27th International Spring Seminar on*, vol. 1. pp. 110–113 vol.1, 2004.
- [69] J.-H. Jung, J.-J. Lee, and B.-H. Kwon, "Online Diagnosis of Induction Motors Using MCSA," *IEEE Trans. Ind. Electron.*, vol. 53, no. 6, pp. 1842–1852, 2006.
- [70] L. Frosini, C. Harlisca, and L. Szabo, "Induction machine bearing fault detection by means of statistical processing of the stray flux measurement," *IEEE Trans. Ind. Electron.*, vol. 62, no. 3, pp. 1846–1854, 2015.
- [71] P. Zhang, Y. Du, T. G. Habetler, and B. Lu, "A survey of condition monitoring and protection methods for medium-voltage induction motors," *Ind. Appl. IEEE Trans.*, vol. 47, no. 1, pp. 34–46, 2011.
- [72] R. L. Winder and W. E. Littmann, "Bearing damage analysis," *Natl. Bur. Stand. Publ.*, 1976.
- [73] G. K. Singh and S. A. K. Sa'ad Ahmed, "Vibration signal analysis using wavelet transform for isolation and identification of electrical faults in induction machine," *Electr. Power Syst. Res.*, vol. 68, no. 2, pp. 119–136, 2003.
- [74] D. G. Dorrell, "Calculation of unbalanced magnetic pull in small cage induction motors with skewed rotors and dynamic rotor eccentricity," *IEEE Trans. Energy Convers.*, vol. 11, no. 3, pp. 483–488, 1996.
- [75] A. Belahcen, "Methods of calculating the magnetic forces for vibration and noise analysis in electrical machines," *Acta Polytech. Scand. Electr. Eng.*, no. 103, pp. 2–54, 2000.

-
- [76] D. G. Dorrell and A. C. Smith, "Calculation and measurement of unbalanced ic pull in cage induction motors with eccentric rotors . Part 2 : Experimental investigation," *IEE Proc. - Electr. Power Appl.*, vol. 143, no. 3, 1996.
- [77] W. R. Finley, M. M. Hodowanec, and W. G. Holter, "An analytical approach to solving motor vibration problems," *IEEE Trans. Ind. Appl.*, vol. 36, no. 5, pp. 217–232, 2000.
- [78] F. C. Trutt, "Detection of ac machine winding deterioration using electrically excited vibrations," *IEEE Trans. Ind. Appl.*, vol. 37, no. 1, pp. 10–14, 2001.
- [79] G. H. Müller and C. F. Landy, "A novel method to detect broken rotor bars in squirrel cage induction motors when interbar currents are present," *IEEE Trans. Energy Convers.*, vol. 18, no. 1, pp. 71–79, 2003.
- [80] F. Villada, D. Cadavid, N. Munoz, D. Valencia, and D. Parra, "Fault diagnosis in induction motors fed by PWM inverters," *4th IEEE Int. Symp. Diagnostics Electr. Mach. Power Electron. Drives, 2003. SDEMPED 2003.*, no. August, pp. 229–234, 2003.
- [81] L. Vandeveld and J. A. A. Melkebeek, "Numerical analysis of vibrations of squirrel-cage induction motors based on magnetic equivalent circuits and structural finite element models," *Conf. Rec. 2001 IEEE Ind. Appl. Conf. 36th IAS Annu. Meet. (Cat. No.01CH37248)*, vol. 4, no. 1, pp. 2288–2295, 2001.
- [82] J. Zhang, R. X. Li, P. Han, D. F. Wang, and X. C. Yin, "Wavelet packet feature extraction for vibration monitoring and fault diagnosis of turbo-generator," *2003 Int. Conf. Mach. Learn. Cybern. Vols 1-5, Proc.*, pp. 76–81, 2003.
- [83] J. R. Stack, T. G. Habetler, and R. G. Harley, "Fault-signature modeling and detection of inner-race bearing faults," *IEEE Trans. Ind. Appl.*, vol. 42, no. 1, pp. 61–68, 2006.
- [84] M. M. Rahman and M. N. Uddin, "Online Unbalanced Rotor Fault Detection of an IM Drive Based on Both Time and Frequency Domain Analyses," in *IEEE Transactions on Industry Applications*, vol. 53, no. 4, pp. 4087–4096, 2017.
- [85] L. Cristaldi, M. Faifer, L. Piegari, M. Rossi, and S. Toscani, "Rotor fault detection in field oriented controlled induction machines," *Power Electron. Electr. Drives Autom. Motion (SPEEDAM), 2010 Int. Symp.*, pp. 529–534, 2010.

-
- [86] M. Y. Chow, R. N. Sharpe, and J. C. Hung, "On the application and design of artificial neural networks for motor fault detection. II," *IEEE Transactions on Industrial Electronics*, vol. 40, no. 2, pp. 189–196, 1993.
- [87] Y. Han and Y. H. Song, "Condition Monitoring Techniques for Electrical Equipment—A Literature Survey," *IEEE Trans. Power Deliv.*, vol. 18, no. 1, pp. 4–13, 2003.
- [88] A. Abu-Siada and S. Islam, "A novel online technique to detect power transformer winding faults," *IEEE Trans. Power Deliv.*, vol. 27, no. 2, pp. 849–857, 2012.
- [89] W. L. Chan, a. T. P. So, and L. L. Lai, "Three-dimensional thermal imaging for power equipment monitoring," *IEE Proc. - Gener. Transm. Distrib.*, vol. 147, p. 355, 2000.
- [90] J. A. R. Nunez, L. M. Velazquez, L. A. M. Hernandez, R. J. R. Troncoso, and R. A. Osornio-Rios, "Low-Cost Thermographic Analysis for Bearing Fault Detection on Induction Motors," *J. Sci. Ind. Res. (India)*, vol. 75, no. July, pp. 412–415, 2016.
- [91] A. Glowacz and Z. Glowacz, "Diagnosis of the three-phase induction motor using thermal imaging," *Infrared Phys. Technol.*, vol. 81, pp. 7–16, 2017.
- [92] N. Khamisan, K. H. Ghazali, and A. H. M. Zin, "A thermograph image extraction based on color features for induction motor bearing fault diagnosis monitoring," *ARPJ. Eng. Appl. Sci.*, vol. 10, no. 22, pp. 17095–17101, 2015.
- [93] Z. Huo, Y. Zhang, R. Sath, and L. Shu, "Self-adaptive Fault Diagnosis of Roller Bearings using Infrared Thermal Images," pp. 6113–6118, 2017.
- [94] A. M. Younus, A. Widodoa, B. Yang, and S. Korea, "APPLICATION OF THERMAL IMAGE : MACHINE FAULT DIAGNOSIS USING PCA AND ICA COMBINE WITH SVM," *8th intern proc conf of ICME*, vol. 1, pp. 26–28, 2009.
- [95] G. M. Lim, D. M. Bae, and J. H. Kim, "Fault diagnosis of rotating machine by thermography method on support vector machine," *J. Mech. Sci. Technol.*, vol. 28, no. 8, pp. 2947–2952, 2014.
- [96] V. T. Tran, B. S. Yang, F. Gu, and A. Ball, "Thermal image enhancement using bi-dimensional empirical mode decomposition in combination with relevance vector machine for rotating machinery fault diagnosis," *Mech. Syst. Signal Process.*, vol. 38, no. 2, pp. 601–614, 2013.

- [97] D. K. Chaturvedi, M. S. Iqbal, and M. Pratap, "Intelligent health monitoring system for three phase induction motor using infrared thermal image," *Int. Conf. Energy Econ. Environ. - 1st IEEE Uttar Pradesh Sect. Conf. UPCON-ICEEE 2015*, pp. 0–5, 2015.
- [98] M. J. Picazo-Rodenas, R. Royo, and J. Antonino-Daviu, "A New Methodology for Complementary Diagnosis of Induction Motors Based on Infrared Thermography," *Int. J. Energy Convers.*, vol. 3, no. 2, pp. 44–52, 2015.
- [99] P. Karvelis, G. Georgoulas, C. D. Stylios, I. P. Tsoumas, J. A. Antonino-Daviu, M. J. P. Rodenas, and V. Climente-Alarcon, "An automated thermographic image segmentation method for induction motor fault diagnosis," in *IECON 2014 - 40th Annual Conference of the IEEE Industrial Electronics Society*, pp. 3396–3402, 2014.
- [100] A. Widodo, D. Satrijo, T. Prahasto, G. M. Lim, and B. K. Choi, "Confirmation of thermal images and vibration signals for intelligent machine fault diagnostics," *Int. J. Rotating Mach.*, 2012.
- [101] J. G. Fantidis, K. Karakoulidis, G. Lazidis, C. Potolias, and D. V. Bandekas, "The study of the thermal profile of a three-phase motor under different conditions," *ARPJ. Eng. Appl. Sci.*, vol. 8, no. 11, pp. 892–899, 2013.
- [102] M. Haji and H. A. Toliyat, "Pattern recognition-a technique for induction machines rotor fault detection broken bar fault," in *IEMDC 2001 - IEEE International Electric Machines and Drives Conference*, pp. 899–904, 2001.
- [103] H. Nejjari and M. E. H. Benbouzid, "Monitoring and diagnosis of induction motors electrical faults using a current Park's vector pattern learning approach," *IEEE Trans. Ind. Appl.*, vol. 36, no. 3, pp. 730–735, 2000.
- [104] M. B. K. Bouzid, G. Champenois, N. M. Bellaaj, L. Signac, and K. Jelassi, "An effective neural approach for the automatic location of stator interturn faults in induction motor," *IEEE Trans. Ind. Electron.*, vol. 55, no. 12, pp. 4277–4289, 2008.
- [105] D. M. Sonje, P. Kundu, and A. Chowdhury, "Novel Approach for Multi Class Fault Diagnosis in Induction Machine Based on Statistical Time Features and Random Forest Classifier," *Int. Conf. Mater. Alloy. Exp. Mech.*, vol. 225, 2017.
- [106] J. F. Martins, V. F. Pires, and A. J. Pires, "Unsupervised neural-network-based algorithm for an on-line diagnosis of three-phase induction motor stator fault," *IEEE Trans. Ind. Electron.*, vol. 54, no. 1, pp. 259–264, 2007.

-
- [107] F. B. Abid, S. Zgarni, and A. Braham, "Bearing fault detection of induction motor using SWPT and DAG support vector machines," in *IECON Proceedings (Industrial Electronics Conference)*, 2016.
- [108] R. H. Abiyev and O. Kaynak, "Fuzzy Wavelet Neural Networks for Identification and Control of Dynamic Plants—A Novel Structure and a Comparative Study," *IEEE Trans. Ind. Electron.*, vol. 55, pp. 3133–3140, 2008.
- [109] A. Soomro, I. Kalwar, K. Kazi, and S. Khoso, "A Hybrid Monitoring Technique for Diagnosis of Mechanical Faults in Induction Motor," *Indian J. Sci.*, vol. 9, no. December, 2016.
- [110] A. Glowacz, W. Glowacz, Z. Glowacz, J. Kozik, M. Gutten, D. Korenciak, Z. F. Khan, M. Irfan, and E. Carletti, "Fault diagnosis of three phase induction motor using current signal, MSAF-Ratio15 and selected classifiers," *Arch. Metall. Mater.*, vol. 62, no. 4, pp. 2413–2419, 2017.
- [111] J. Binfet and B. M. Wilamowski, "Implementation of fuzzy logic systems and neural networks in industry," *Comput. Ind.*, vol. 32, pp. 261–272, 1997.
- [112] H. Su and K. T. Chong, "Induction machine condition monitoring using neural network modeling," *IEEE Trans. Ind. Electron.*, vol. 54, no. 1, pp. 241–249, 2007.
- [113] L. Jack and A. Nandi, "Genetic algorithms for feature selection in machine condition monitoring with vibration signals," *Vision, Image Signal Process. IEEE Proc.*, vol. 147, no. 3, pp. 205–212, 2000.
- [114] S. Wu and T. Chow, "Induction Machine Fault Detection Using SOM-Based RBF Neural Networks," *IEEE Trans. Ind. Electron.*, vol. 51, no. 1, pp. 183–194, 2004.
- [115] S.-Y. Shao, W.-J. Sun, R.-Q. Yan, P. Wang, and R. X. Gao, "A Deep Learning Approach for Fault Diagnosis of Induction Motors in Manufacturing," *Chinese J. Mech. Eng. (English Ed.)*, vol. 30, no. 6, 2017.
- [116] R. K. Patel and V. K. Giri, "Feature selection and classification of mechanical fault of an induction motor using random forest classifier," *Perspect. Sci.*, vol. 8, pp. 334–337, 2016.
- [117] B. Samanta, "Gear fault detection using artificial neural networks and support vector machines with genetic algorithms," *Mech. Syst. Signal Process.*, vol. 18, no. 3, pp. 625–644, 2004.

-
- [118] A. Saxena and A. Saad, "Evolving an artificial neural network classifier for condition monitoring of rotating mechanical systems," *Appl. Soft Comput. J.*, vol. 7, no. 1, pp. 441–454, 2007.
- [119] B. Satish and N. D. R. Sarma, "A fuzzy BP approach for diagnosis and prognosis of bearing faults in induction motors," *IEEE Power Eng. Soc. Gen. Meet. 2005*, pp. 1–4, 2005.
- [120] M. Saimurugan, K. I. Ramachandran, V. Sugumaran, and N. R. Sakthivel, "Multi component fault diagnosis of rotational mechanical system based on decision tree and support vector machine," *Expert Syst. Appl.*, vol. 38, no. 4, pp. 3819–3826, 2011.
- [121] N. Saravanan, V. N. S. K. Siddabattuni, and K. I. Ramachandran, "Fault diagnosis of spur bevel gear box using artificial neural network (ANN), and proximal support vector machine (PSVM)," *Appl. Soft Comput. J.*, vol. 10, no. 1, pp. 344–360, 2010.
- [122] A. Purarjomandlangrudi, A. H. Ghapanchi, and M. Esmalifalak, "A data mining approach for fault diagnosis: An application of anomaly detection algorithm," *Measurement*, vol. 55, pp. 343–352, 2014.
- [123] C. Romero and S. Ventura, "Educational data mining: A survey from 1995 to 2005," *Expert Syst. Appl.*, vol. 33, no. 1, pp. 135–146, 2007.
- [124] M. Çelik, D. Karaboğa, and F. Köylü, "Artificial bee colony data miner (ABC-Miner)," in *INISTA 2011 - 2011 International Symposium on INnovations in Intelligent SysTems and Applications*, pp. 96–100, 2011.
- [125] M. B. Gorzałczany and F. Rudziński, "A multi-objective genetic optimization for fast, fuzzy rule-based credit classification with balanced accuracy and interpretability," *Appl. Soft Comput. J.*, vol. 40, pp. 206–220, 2016.
- [126] F. Rudziński, "A multi-objective genetic optimization of interpretability-oriented fuzzy rule-based classifiers," *Appl. Soft Comput. J.*, vol. 38, pp. 118–133, 2016.
- [127] J. Kennedy, R. C. Eberhart, Y. Shi, C. Jacob, J. R. Koza, F. H. B. Iii, D. Andre, and M. a Keane, *Swarm Intelligence*. 2001.
- [128] A. Colorni, M. Dorigo, and V. Maniezzo, "Distributed Optimization by Ant Colonies," *Proc. first Eur. Conf. Artif. Life*, vol. 142, no. or D, pp. 134–142, 1991.

-
- [129] J. Han and M. Kamber, *Data Mining: Concepts and Techniques*, vol. 54, no. Second Edition. 2006.
- [130] R. Sikora and S. Piramuthu, "Framework for efficient feature selection in genetic algorithm based data mining," *Eur. J. Oper. Res.*, vol. 180, no. 2, pp. 723–737, 2007.
- [131] X. Huang, F. Shi, W. Gu, and S. Chen, "SVM-based fuzzy rules acquisition system for pulsed GTAW process," *Eng. Appl. Artif. Intell.*, vol. 22, no. 8, pp. 1245–1255, 2009.
- [132] T. Sousa, A. Neves, and A. Silva, "Swarm optimisation as a new tool for data mining," in *Proceedings of the International Parallel and Distributed Processing Symposium, 2003.*, p. 6 pp, 2003.
- [133] K. N. V. D. Sarath and V. Ravi, "Association rule mining using binary particle swarm optimization," *Eng. Appl. Artif. Intell.*, vol. 26, no. 8, pp. 1832–1840, 2013.
- [134] Z. Liang, J. Sun, Q. Lin, Z. Du, J. Chen, and Z. Ming, "A novel multiple rule sets data classification algorithm based on ant colony algorithm," *Appl. Soft Comput.*, vol. 38, pp. 1000–1011, 2016.
- [135] S. N. Omkar and R. Karanth U, "Rule extraction for classification of acoustic emission signals using Ant Colony Optimisation," *Eng. Appl. Artif. Intell.*, vol. 21, no. 8, pp. 1381–1388, 2008.
- [136] M. A. Mohd Shukran, Y. Y. Chung, W.-C. Yeh, N. Wahid, and A. M. Ahmad Zaidi, "Artificial Bee Colony based Data Mining Algorithms for Classification Tasks," *Mod. Appl. Sci.*, vol. 5, no. 4, pp. 217–231, 2011.
- [137] M. Castellani, Q. T. Pham, and D. T. Pham, "Dynamic Optimisation by a Modified Bees Algorithm," *Proc. Inst. Mech. Eng. Part I J. Syst. Control Eng.*, vol. 226, no. 7, pp. 956–971, 2012.
- [138] M. S. Packianather, B. Yuce, E. Mastrocinque, F. Fruggiero, D. T. Pham, and A. Lambiase, "Novel Genetic Bees Algorithm applied to single machine scheduling problem," in *World Automation Congress Proceedings*, 2014.
- [139] a. a. Fahmy, M. Kalyoncu, and M. Castellani, "Automatic design of control systems for robot manipulators using the bees algorithm," *Proc. Inst. Mech. Eng. Part I J. Syst. Control Eng.*, vol. 226, no. 4, pp. 497–508, 2011.
- [140] D. T. Pham and a Haj Darwish, "Using the bees algorithm with Kalman filtering to train an artificial neural network for pattern classification," *Proc.*

-
- Inst. Mech. Eng. Part I J. Syst. Control Eng.*, vol. 224, no. 7, pp. 885–892, 2010.
- [141] A. Jevtić, P. Gazi, D. Andina, M. O. Jamshidi, A. Jevtic, P. Gazi, and D. Andina, “Building a Swarm of Robotic Bees,” *2010 World Autom. Congr. WAC 2010*, no. 2, pp. 1–6, 2010.
- [142] B. Yuce, D. T. Pham, M. S. Packianather, and E. Mastrocinque, “An enhancement to the Bees Algorithm with slope angle computation and Hill Climbing Algorithm and its applications on scheduling and continuous-type optimisation problem,” *Prod. Manuf. Res.*, vol. 3, no. 1, pp. 3–19, 2015.
- [143] D. T. Pham, A. J. Soroka, A. Ghanbarzadeh, E. Koc, S. Otri, and M. Packianather, “Optimising neural networks for identification of wood defects using the bees algorithm,” in *2006 IEEE International Conference on Industrial Informatics, INDIN’06*, pp. 1346–1351, 2007.
- [144] M. S. Packianather, M. Landy, and D. T. Pham, “Enhancing the speed of the bees algorithm using pheromone-based recruitment,” in *IEEE International Conference on Industrial Informatics (INDIN)*, pp. 789–794, 2009.
- [145] D. T. Pham, H. AL-Jabbouli, M. Mahmuddin, S. Otri, and A. Haj Darwish, “Application of the Bees Algorithm to Fuzzy Clustering,” *Innov. Prod. Mach. Syst.*, 2008.
- [146] P. Tapkan, L. Özbakir, S. Kulluk, and A. Baykasoglu, “A cost-sensitive classification algorithm: BEE-Miner,” *Knowledge-Based Syst.*, vol. 95, pp. 99–113, 2016.
- [147] Y. B. Koca and A. Ünsal, “A Review on Detection and Monitoring of Stator Faults of Induction Motors,” vol. 6, no. 10, pp. 70–74, 2017.
- [148] A. Gedzurs, “Temperature protection methods of induction motor,” *Res. Rural Dev.*, vol. 1, pp. 258–263, 2015.
- [149] W. Thomson and R. Gilmore, “Motor current signature analysis to detect faults in induction motor drives-fundamentals, Data interpretation, and industrial case histories,” in *Proceedings of 32nd Turbo ...*, no. 1987, pp. 145–156, 2003.
- [150] C. M. Riley, B. K. Lin, T. G. Habetier, and G. B. Kliman, “Stator current harmonics and their causal vibrations: a preliminary investigation of sensorless vibration monitoring applications,” *IEEE Trans. Ind. Appl.*, vol. 35, no. 1, pp. 94–99, 1999.

-
- [151] M. E. H. Benbouzid, M. Vieira, and C. Theys, "Induction motors' faults detection and localization using stator current advanced signal processing techniques," *IEEE Trans. Power Electron.*, vol. 14, no. 1, pp. 14–22, 1999.
- [152] M. E. H. Benbouzid and G. B. Kliman, "What stator current processing-based technique to use for induction motor rotor faults diagnosis?," *IEEE Trans. Energy Convers.*, vol. 18, no. 2, pp. 238–244, 2003.
- [153] P. A. Delgado-Arredondo, D. Morinigo-Sotelo, R. A. Osornio-Rios, J. G. Avina-Cervantes, H. Rostro-Gonzalez, and R. de J. Romero-Troncoso, "Methodology for fault detection in induction motors via sound and vibration signals," *Mech. Syst. Signal Process.*, vol. 83, pp. 568–589, 2017.
- [154] V. Fernandez-Cavero, D. Morinigo-Sotelo, O. Duque-Perez, and J. Pons-Llinares, "A Comparison of Techniques for Fault Detection in Inverter-Fed Induction Motors in Transient Regime," *IEEE Access*, vol. 5, pp. 8048–8063, 2017.
- [155] B. Corne, B. Vervisch, C. Debruyne, J. Knockaert, and J. Desmet, "Comparing MCSA with vibration analysis in order to detect bearing faults - A case study," in *Proceedings - 2015 IEEE International Electric Machines and Drives Conference, IEMDC 2015*, pp. 1366–1372, 2016.
- [156] M. Nazarian, M. Dezfouli, and A. Haronabadi, "Classification of Breast Cancer Samples Through Using the Artificial Bee Colony Algorithm," *Int. J. Comput. Appl. Technol. Res.*, vol. 2, no. 5, pp. 522–525, 2013.
- [157] D. T. Larose and C. D. Larose, *Discovering Knowledge in data An Introduction to Data Mining*, vol. 53, no. 9. 2014.
- [158] M. Lichman, "UCI Machine Learning Repository," *Irvine, CA: University of California, School of Information and Computer Science*, 2013. [Online]. Available: <http://archive.ics.uci.edu/ml/>. [Accessed: 15-Mar-2017].
- [159] K. Bache and M. Lichman, "UCI Machine Learning Repository," *University of California Irvine School of Information*, vol. 2008, no. 14/8, 2013.
- [160] A. Giordana and F. Neri, "Search-Intensive Concept Induction," *Evol. Comput.*, vol. 3, no. 4, pp. 375–416, Dec. 1995.
- [161] D. T. Pham and A. A. Afify, "RULES-6: a simple rule induction algorithm for supporting decision making," *31st Annual Conference of IEEE Industrial Electronics Society, 2005. IECON 2005*. p. 6, 2005.

-
- [162] F. E. B. Otero, A. A. Freitas, and C. G. Johnson, "A new sequential covering strategy for inducing classification rules with ant colony algorithms," *IEEE Trans. Evol. Comput.*, vol. 17, no. 1, pp. 64–76, 2013.
- [163] O. E. B. Otero, A. A. Freitas, and C. G. Johnson, "Inducing Decision Trees with an Ant Colony Optimization Algorithm," *Appl. Soft Comput.*, vol. 12, no. 11, pp. 3615–3626, 2012.
- [164] K. M. Salama, A. M. Abdelbar, F. E. B. Otero, and A. A. Freitas, "Utilizing multiple pheromones in an ant-based algorithm for continuous-attribute classification rule discovery," *Appl. Soft Comput. J.*, vol. 13, no. 1, pp. 667–675, 2013.
- [165] P. Domingos, "Unifying Instance-Based and Rule-Based Induction," *Mach. Learn.*, vol. 24, no. 2, pp. 141–168, 1996.
- [166] N. Holden and A. A. Freitas, "A Hybrid PSO/ACO Algorithm for Discovering Classification Rules in Data Mining," *J. Artif. Evol. Appl.*, vol. 2008, pp. 1–11, 2008.
- [167] R. C. Gonzalez, R. E. Woods, and S. L. Eddins, *Digital Image Processing Using MATLAB*, vol. 1. 2004.
- [168] T. Dutta, J. Sil, and P. Chottopadhyay, "Condition monitoring of electrical equipment using thermal image processing," in *2016 IEEE 1st International Conference on Control, Measurement and Instrumentation, CMI 2016*, 2016.
- [169] L. Gi. Roberts, "Machine perception of three-dimensional solids," 1965.
- [170] J. Canny, "A Computational Approach to Edge Detection," *IEEE Trans. Pattern Anal. Mach. Intell.*, vol. PAMI-8, no. 6, pp. 679–698, 1986.
- [171] R. Gonzalez and R. Woods, *Digital image processing*. 2002.
- [172] N. Otsu, "A Threshold Selection Method from Gray-Level Histograms," *IEEE Trans. Syst. Man. Cybern.*, vol. 9, no. 1, pp. 62–66, 2008.
- [173] V. Kumar and P. Gupta, "Importance of Statistical Measures in Digital Image Processing," *Int. J. Emerg. Technol. Adv. Eng.*, vol. 2, no. 8, pp. 56–62, 2012.
- [174] Ashish and Aijay, "Review on thermal image processing techniques for machine condition monitoring," *Int. J. Wirel. Commun. Netw. Technol.*, vol. 3, no. 3, pp. 49–53, 2014.
- [175] S. Aja-Fernández, R. S. J. Estépar, C. Alberola-López, and C.-F. Westin, "Image quality assessment based on local variance.," *Proc. 28th IEEE EMBS Annu. Int. Conf.*, vol. 1, pp. 4815–8, 2006.

-
- [176] D. N. Joanes and C. A. Gill, "Comparing measures of sample skewness and kurtosis," *J. R. Stat. Soc. Ser. D Stat.*, vol. 47, no. 1, pp. 183–189, 1998.
- [177] I. Motoyoshi, S. Nishida, L. Sharan, and E. H. Adelson, "Image statistics and the perception of surface qualities," *Nature*, vol. 447, no. 7141, pp. 206–209, 2007.
- [178] R. Ferzli, L. J. Karam, and J. Caviedes, "A robust image sharpness metric based on kurtosis measurement of wavelet coefficients," *Proc. Int. Work. Video Process. Qual. Metrics Consum. Electron.*, vol. 12, no. 3, 2005.
- [179] Z. K. Peng and F. L. Chu, "Application of the wavelet transform in machine condition monitoring and fault diagnostics: A review with bibliography," *Mech. Syst. Signal Process.*, vol. 18, no. 2, pp. 199–221, 2004.
- [180] J. T. Sawicki, A. K. Sen, and G. Litak, "Multiresolution wavelet analysis of the dynamics of a cracked rotor," *Int. J. Rotating Mach.*, 2009.
- [181] M. V. Wickerhauser, A. Jensen, A. la Cour-Harbo, A. Boggess, and F. J. Narcowich, "Ripples in Mathematics: The Discrete Wavelet Transform," *Am. Math. Mon.*, vol. 110, no. 2, p. 163, 2003.
- [182] J. J. Sinou, "An experimental investigation of condition monitoring for notched rotors through transient signals and wavelet transform," *Exp. Mech.*, vol. 49, no. 5, pp. 683–695, 2009.
- [183] H. K. Srinivas, K. S. Srinivasan, and K. N. Umesh, "Role of an artificial neural network and a wavelet transform for condition monitoring of the combined faults of unbalance and cracked rotors," *Int. J. Acoust. Vib.*, vol. 15, no. 3, pp. 121–127, 2010.
- [184] L. M. Hee, M. S. Leong, and K. H. Hui, "Analysis of Residual Wavelet Scalogram for Machinery Fault Diagnosis," *Adv. Mater. Res.*, vol. 845, pp. 113–117, 2013.
- [185] F. Ponci, A. Monti, L. Cristaldi, and M. Lazzaroni, "Diagnostic of a faulty induction motor drive via wavelet decomposition," *IEEE Trans. Instrum. Meas.*, vol. 56, no. 6, pp. 2606–2615, 2007.
- [186] K. C. D. Kompella, V. G. R. Mannam, and S. R. Rayapudi, "DWT based bearing fault detection in induction motor using noise cancellation," *J. Electr. Syst. Inf. Technol.*, vol. 3, no. 3, pp. 411–427, 2016.

-
- [187] P. E. T. Jorgensen and M. S. Song, "Comparison of discrete and continuous wavelet transforms," in *Computational Complexity: Theory, Techniques, and Applications*, pp. 513–526, 2012.
- [188] J. M. Shapiro, "Embedded Image Coding Using Zerotrees of Wavelet Coefficients," *IEEE Trans. Signal Process.*, vol. 41, no. 12, pp. 3445–3462, 1993.
- [189] C. Vonesch, T. Blu, and M. Unser, "Generalized daubechies wavelet families," *IEEE Trans. Signal Process.*, vol. 55, no. 9, pp. 4415–4429, 2007.
- [190] F. Song, D. Zhangs, Y. Xu, and J. Wang, "Five new feature selection metrics in text categorization," *Int. J. Pattern Recognit. Artif. Intell.*, vol. 21, no. 6, 2007.
- [191] U. R. Aparna and S. Paul, "Feature selection and extraction in data mining," in *Proceedings of 2016 Online International Conference on Green Engineering and Technologies, IC-GET 2016*, 2017.
- [192] V. Angelis, G. Felici, and G. Mancinelli, "Feature Selection for Data Mining," in *Data Mining and Knowledge Discovery Approaches Based on Rule Induction Techniques*, vol. 6, pp. 227–252, 2006.
- [193] A. Azizi and H. R. Pourreza, "Efficient IRIS Recognition through Improvement of Feature Extraction and subset Selection," *Int. J. Comput. Sci. Inf. Secur.*, vol. 2, no. 1, p. 10, 2009.
- [194] L. Ladha and T. Deepa, "Feature selection methods and algorithms," *Int. J. ...*, vol. 3, no. 5, pp. 1787–1797, 2011.
- [195] J.-H. Lee and S.-Y. Oh, "Feature selection based on geometric distance for high-dimensional data," *Electron. Lett.*, vol. 52, no. 6, pp. 473–475, 2016.
- [196] S. C. H. Hoi, J. Wang, P. Zhao, and R. Jin, "Online feature selection for mining big data," in *1st International Workshop on Big Data, Streams and Heterogeneous Source Mining: Algorithms, Systems, Programming Models and Applications, BigMine-12 - Held in Conjunction with SIGKDD Conference*, pp. 93–100, 2012.
- [197] M. Mitchell, *An Introduction to Genetic Algorithms*. 1995.
- [198] J. Carr, "An Introduction to Genetic Algorithms," *Whitman Coll. Math. Dep.*, pp. 1–40, 2014.
- [199] A. Fraser and D. Burnell, *COMPUTER MODELS IN GENETICS*. 1970.

-
- [200] J. Tian, Q. Hu, and X. Ma, "An Improved KPCA / GA-SVM Classification Model for Plant Leaf Disease Recognition Apple Leaf Disease Recognition Based on KPCA and Optimized GA-SVM," vol. 18, no. 61, pp. 7737–7745, 2012.
- [201] S. N. Sivanandam and S. N. Deepa, *Introduction to genetic algorithms*. 2008.
- [202] Mathworks, "Statistics and Machine Learning Toolbox™ User's Guide R2017a," *MatLab*, pp. 1–9214, 2017.
- [203] A. E. Eiben and J. E. Smith, *Introduction to Evolutionary Computing*, vol. 2. 2015.
- [204] P. Civicioglu, "Transforming geocentric cartesian coordinates to geodetic coordinates by using differential search algorithm," *Comput. Geosci.*, vol. 46, pp. 229–247, 2012.
- [205] B. Baudry, F. Fleurey, J. M. Jézéquel, and Y. Le Traon, "Automatic test case optimization: A bacteriologic algorithm," *IEEE Softw.*, vol. 22, no. 2, pp. 76–82, 2005.
- [206] M. Taherdangkoo, M. Paziresh, M. Yazdi, and M. H. Bagheri, "An efficient algorithm for function optimization: Modified stem cells algorithm," *Cent. Eur. J. Eng.*, vol. 3, no. 1, pp. 36–50, 2013.
- [207] J. Zhang, H. S. H. Chung, and W. L. Lo, "Clustering-based adaptive crossover and mutation probabilities for genetic algorithms," *IEEE Trans. Evol. Comput.*, vol. 11, no. 3, pp. 326–335, 2007.
- [208] D. E. Goldberg, B. Korb, and K. Deb, "Messy Genetic Algorithms : Motivation , Analysis , and First Results," 1989.
- [209] M. Mutingi and C. Mbohwa, "Fuzzy grouping genetic algorithms: Advances for real-world grouping," in *Studies in Computational Intelligence*, vol. 666, pp. 67–86, 2017.
- [210] C. R. Reeves, "Genetic algorithms and grouping problems," *IEEE Transactions on Evolutionary Computation*, vol. 5, no. 3. p. 297, 2001.
- [211] M. Srinivas and L. M. Patnaik, "Adaptive Probabilities of Crossover and Mutation in Genetic Algorithms," *IEEE Trans. Syst. Man Cybern.*, vol. 24, no. 4, pp. 656–667, 1994.
- [212] C. Pezzani, P. Donolo, G. Bossio, M. Donolo, A. Guzman, and S. E. Zocholl, "Detecting broken rotor bars with zero-setting protection," *IEEE Trans. Ind. Appl.*, vol. 50, no. 2, pp. 1373–1384, 2014.

-
- [213] J. A. Antonino-Daviu, M. Riera-Guasp, J. R. Folch, and M. P. Molina Palomares, "Validation of a new method for the diagnosis of rotor bar failures via wavelet transform in industrial induction machines," *IEEE Trans. Ind. Appl.*, vol. 42, no. 4, pp. 990–996, 2006.
- [214] C. S. Burrus, R. Gopinath, and H. Guo, "Wavelets and Wavelet Transforms," in *Introduction to Wavelets and Wavelet Transform—A Primer*, C. S. Burrus, Ed. Englewood Cliffs: Rice University, Houston, Texas, 1998.
- [215] C. Sarkar, S. Cooley, and J. Srivastava, "Robust feature selection technique using rank aggregation," *Appl. Artif. Intell.*, vol. 28, no. 3, pp. 243–257, 2014.
- [216] D. Ververidis and C. Kotropoulos, "Fast and accurate sequential floating forward feature selection with the Bayes classifier applied to speech emotion recognition," *Signal Processing*, vol. 88, no. 12, pp. 2956–2970, 2008.
- [217] K. Selvakuberan, D. Kayathiri, B. Harini, and M. I. Devi, "An efficient feature selection method for classification in health care systems using machine learning techniques," in *ICECT 2011 - 2011 3rd International Conference on Electronics Computer Technology*, vol. 4, pp. 223–226, 2011.

APPENDIX A - THERMAL IMAGE ANALYSIS

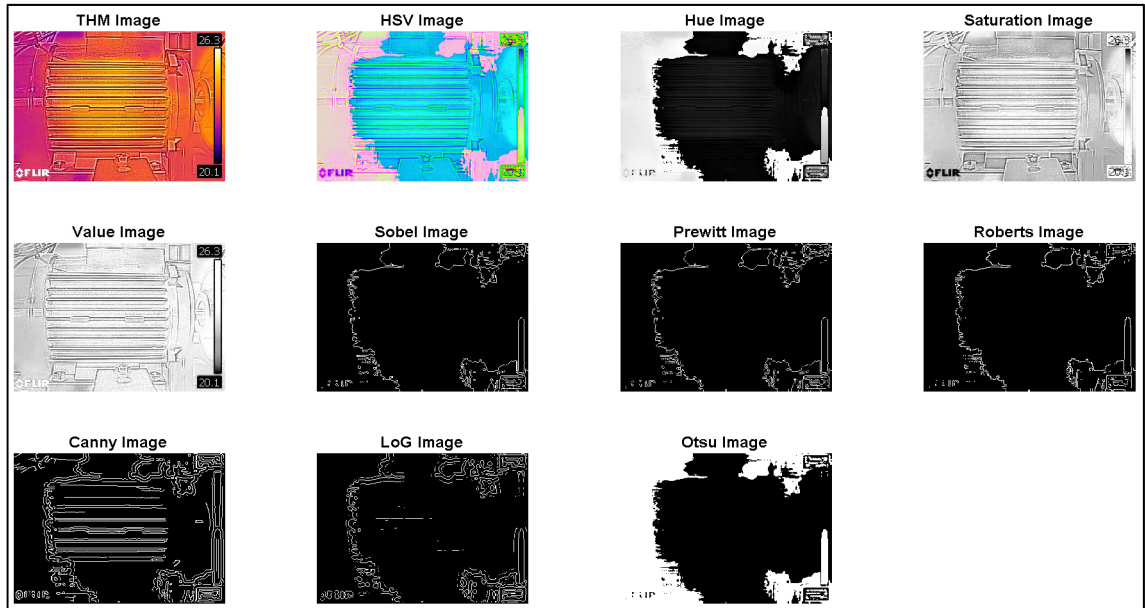


Figure A-1: Thermal image analysis for healthy motor with no load.

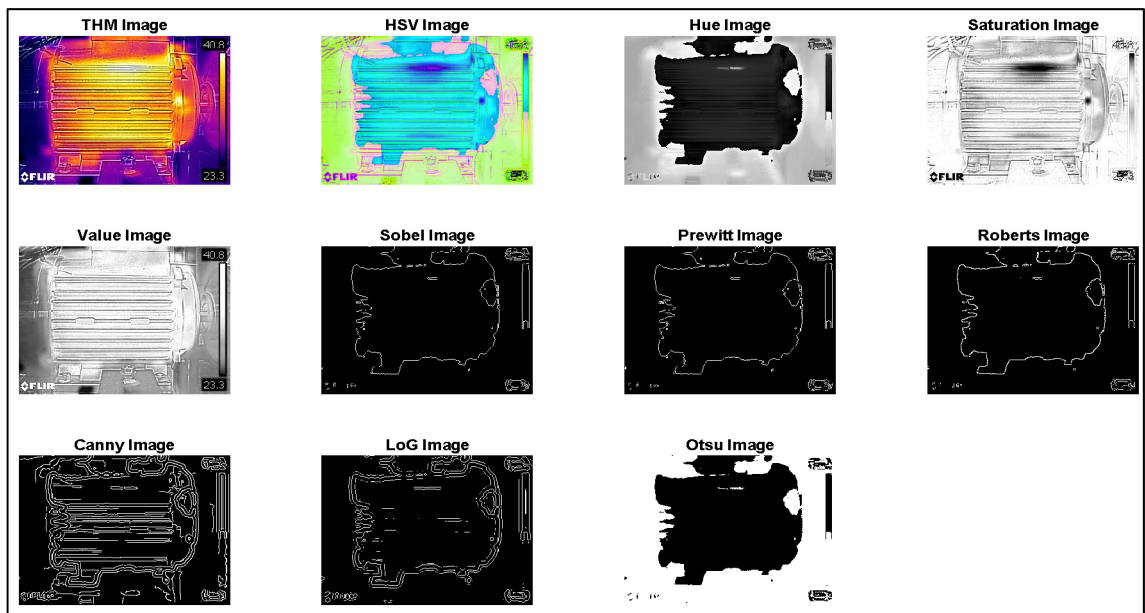


Figure A-2: Thermal image analysis for healthy motor with 50% load.

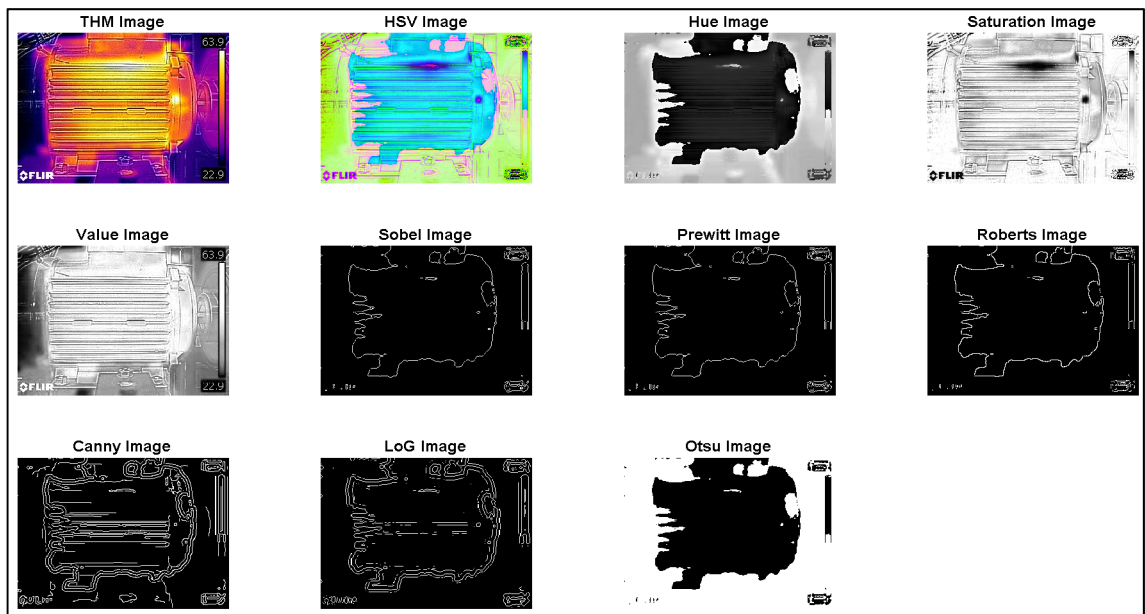


Figure A-3: Thermal image analysis for healthy motor with 100% load.

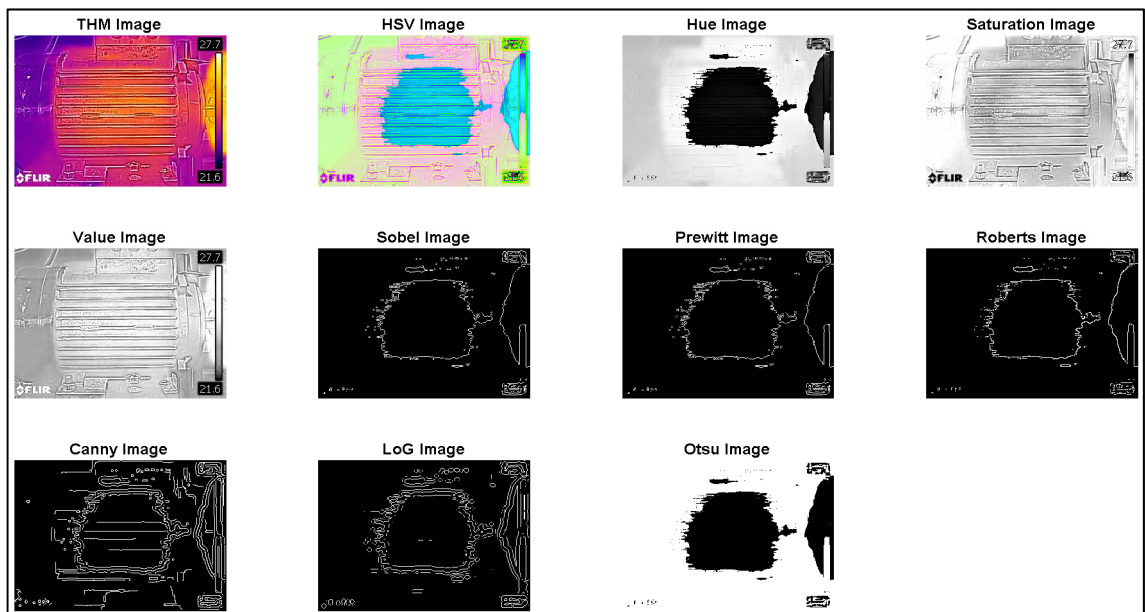


Figure A-4: Thermal image analysis for one bar fault with no load.

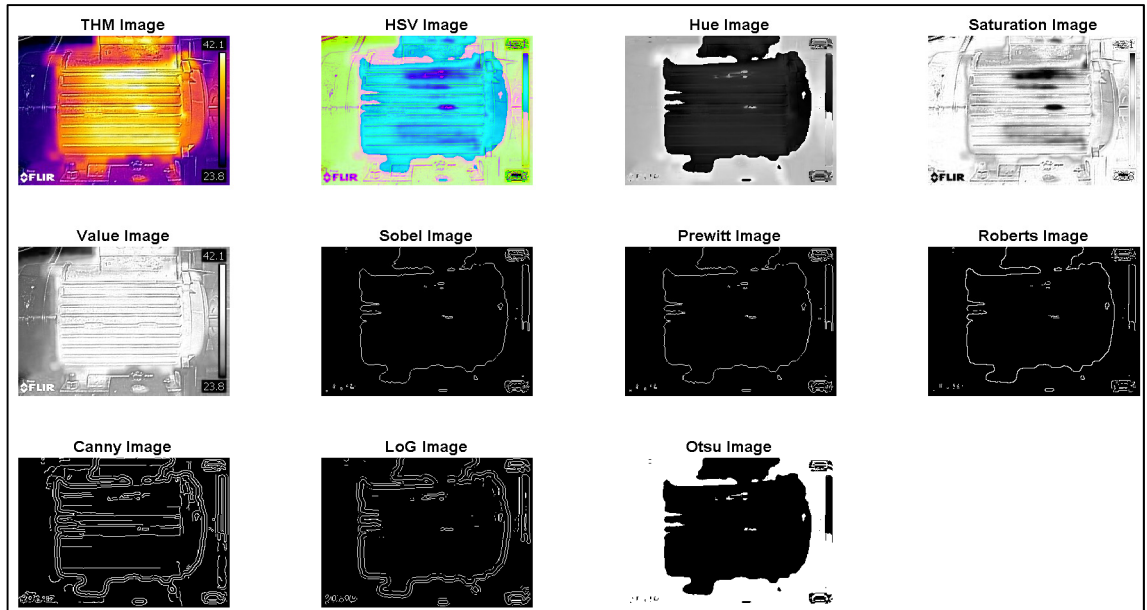


Figure A-5: Thermal image analysis for one bar fault with 50% load.

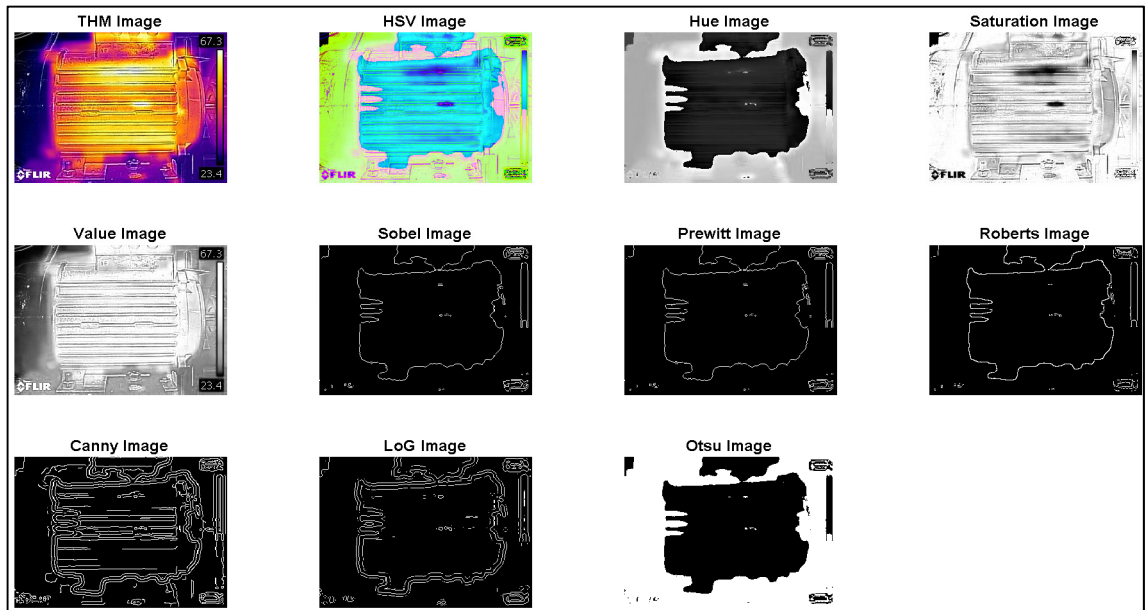


Figure A-6: Thermal image analysis for one bar fault with 100% load.

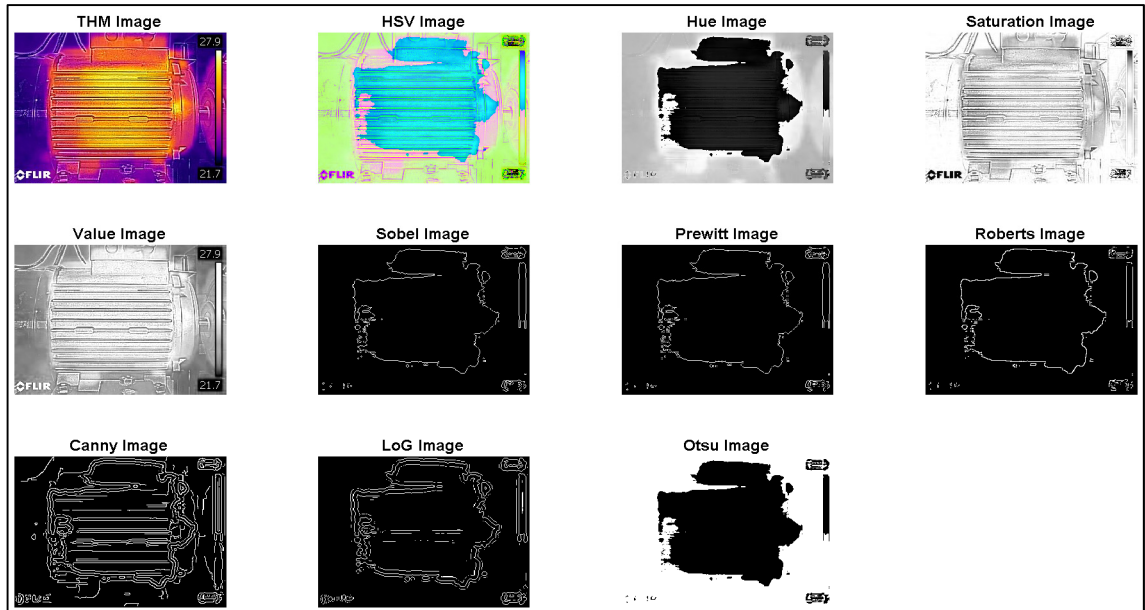


Figure A-7: Thermal image analysis for eight bars fault with no load.

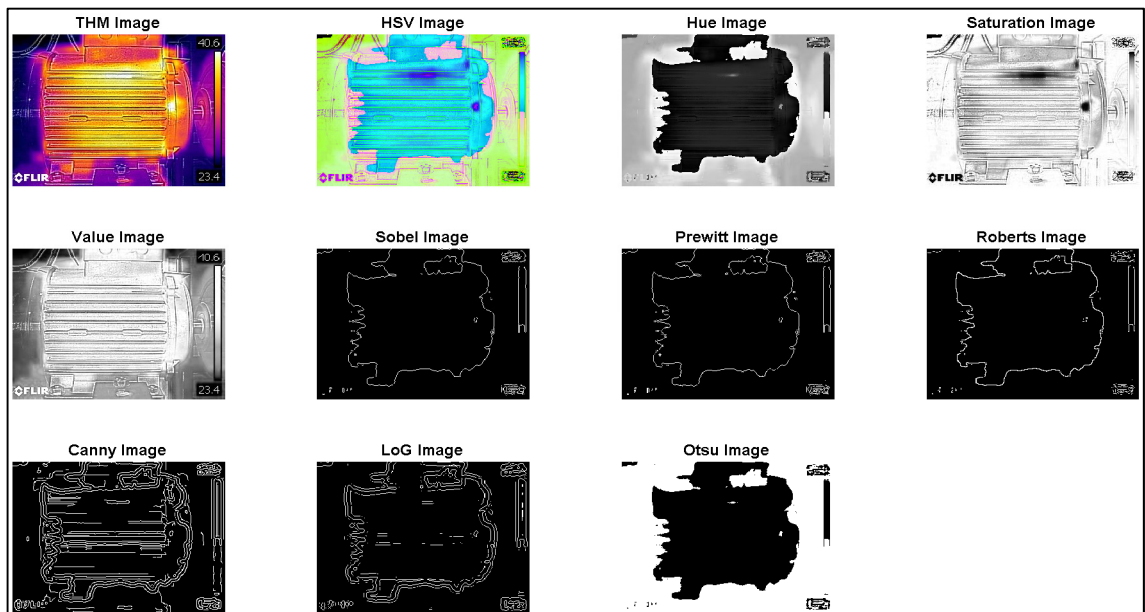


Figure A-8: Thermal image analysis for eight bars fault with 50% load.

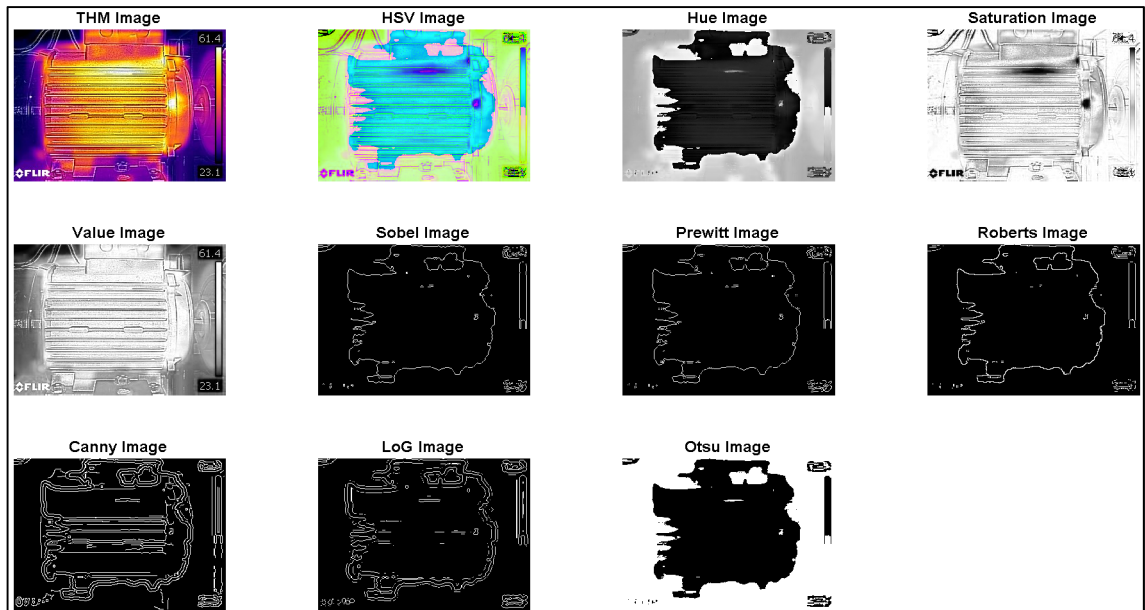


Figure A-9: Thermal image analysis for eight bars fault with 100% load.

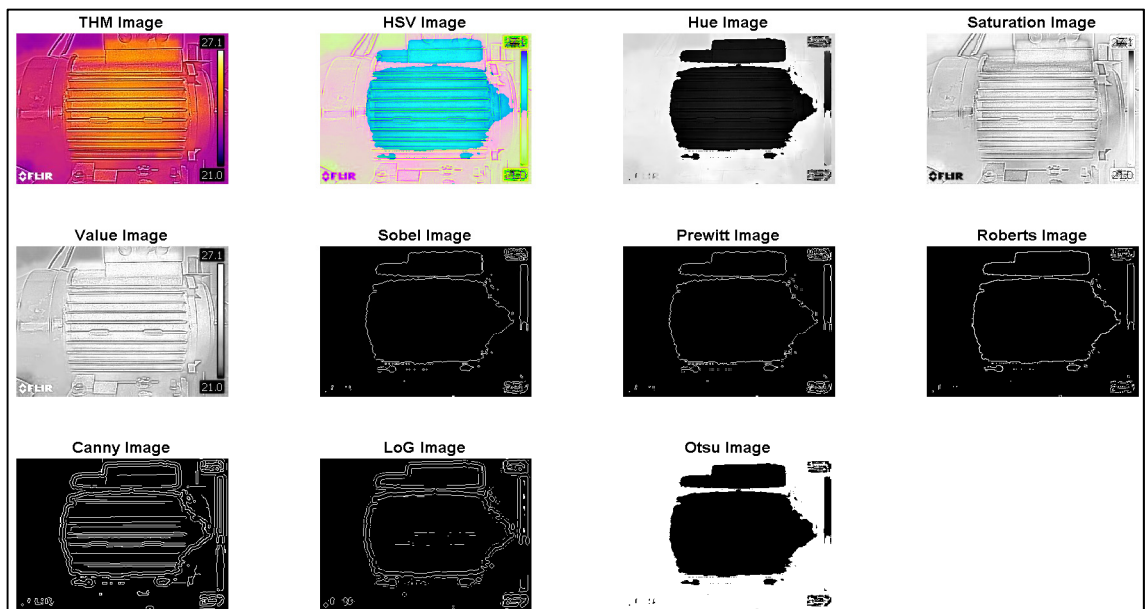


Figure A-10: Thermal image analysis for ball bearing fault with no load.

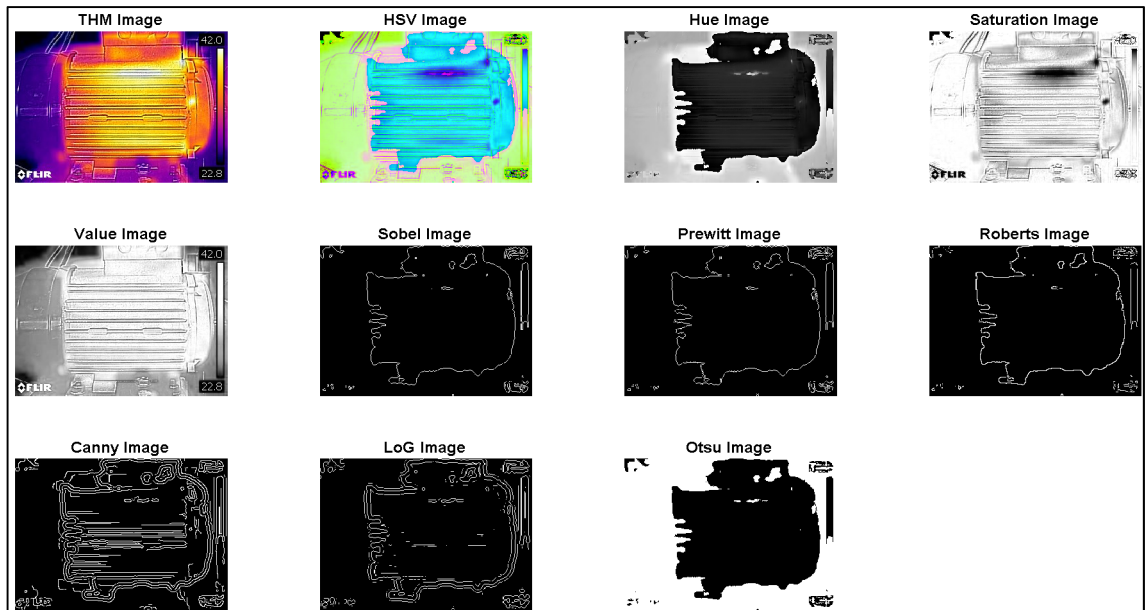


Figure A-11: Thermal image analysis for ball bearing fault with 50% load.

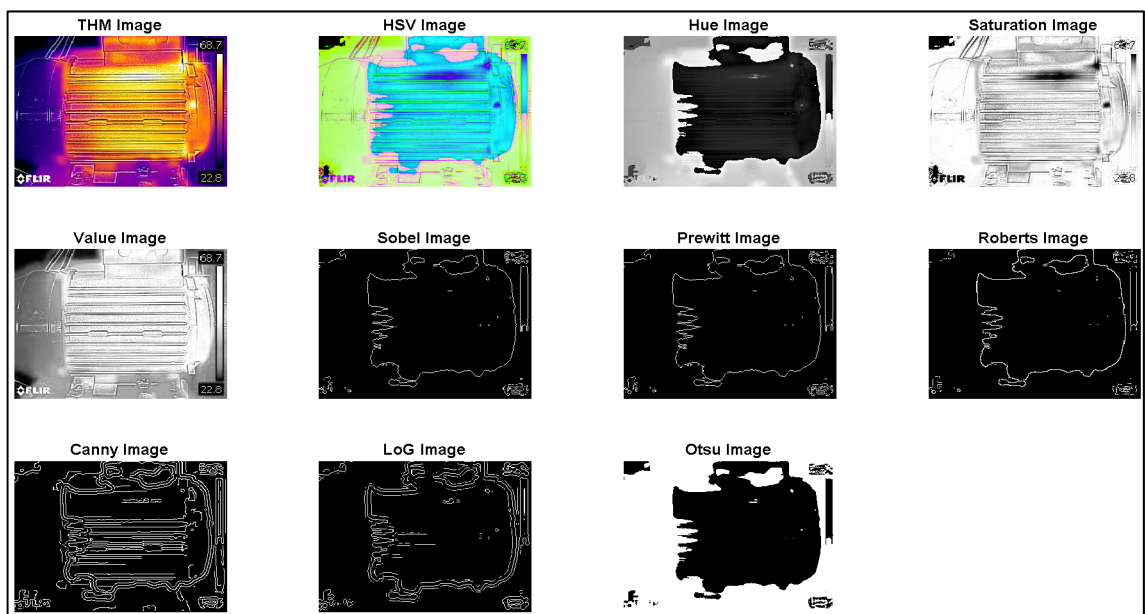


Figure A-12: Thermal image analysis for ball bearing fault with 100% load.

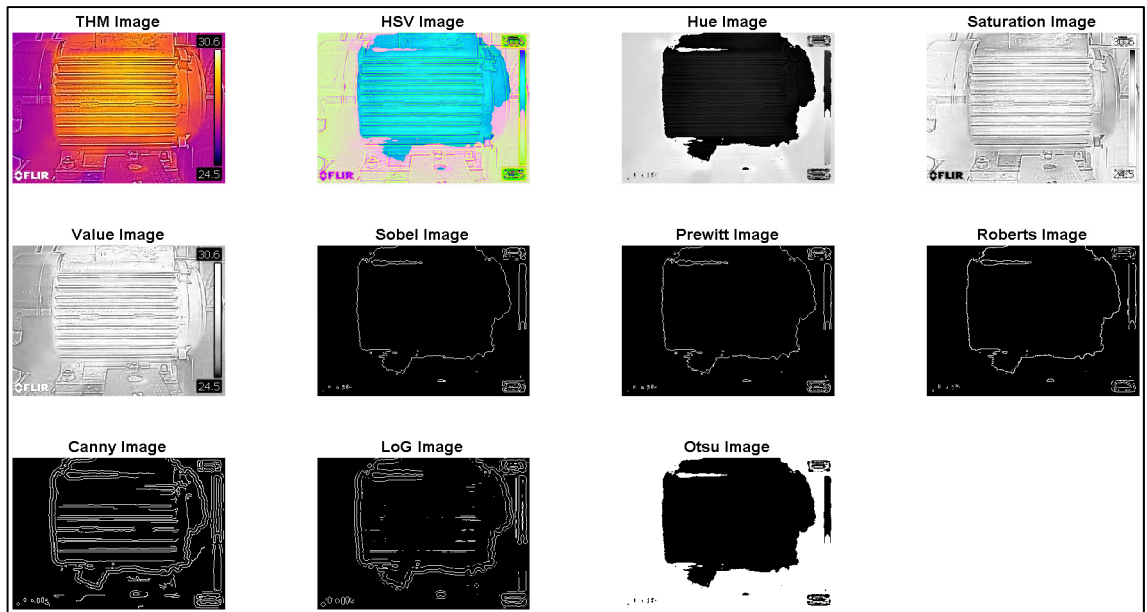


Figure A-13: Thermal image analysis for inner race bearing fault with no load.

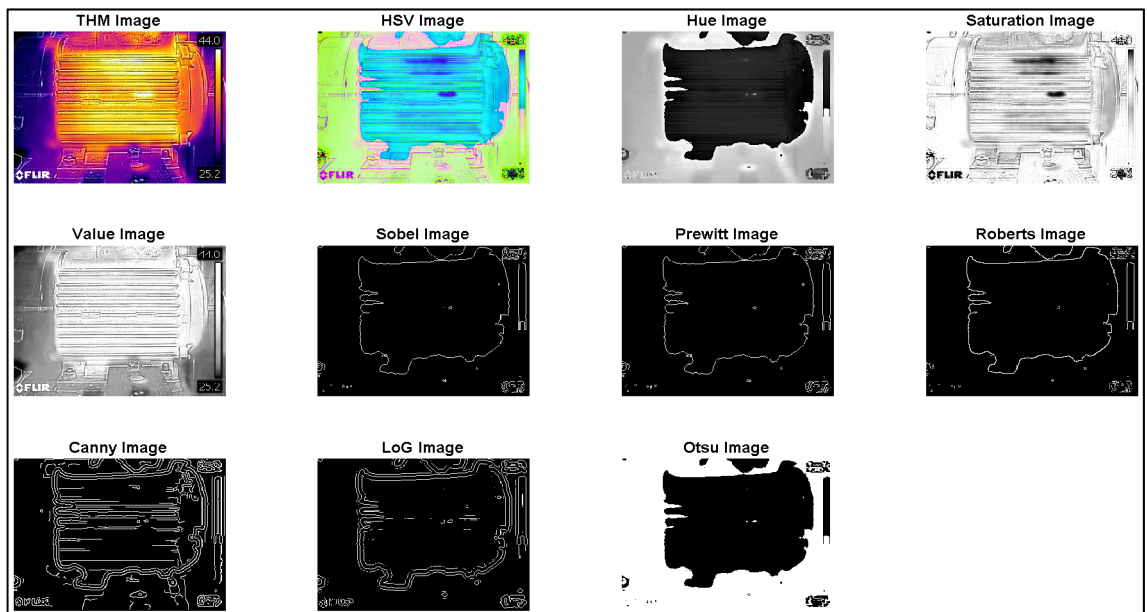


Figure A-14: Thermal image analysis for inner race bearing fault with 50% load.

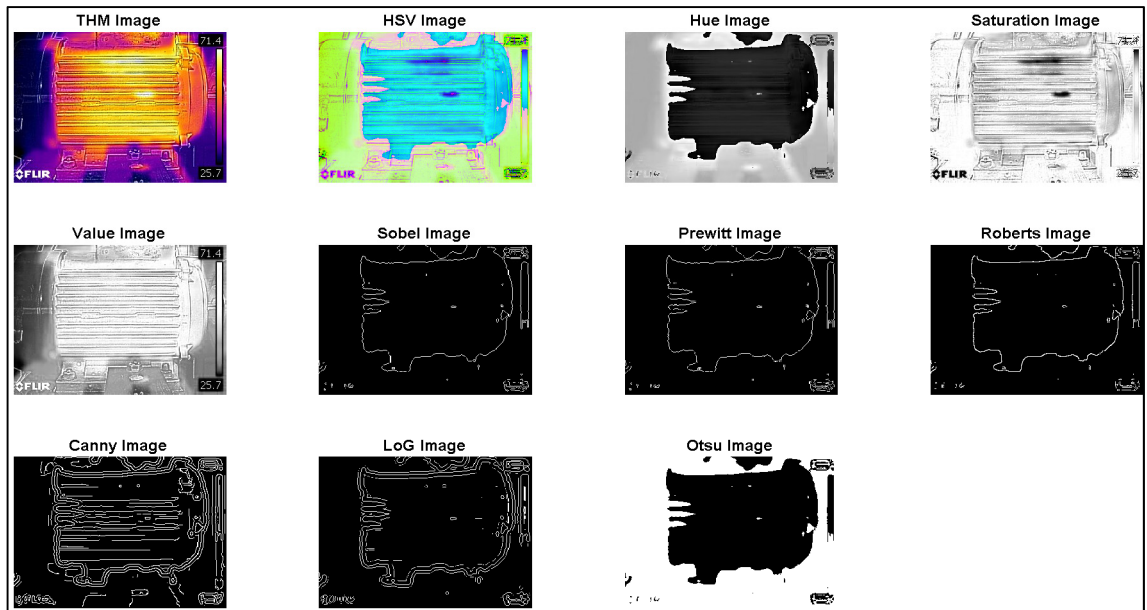


Figure A-15: Thermal image analysis for inner race bearing fault with 100% load.

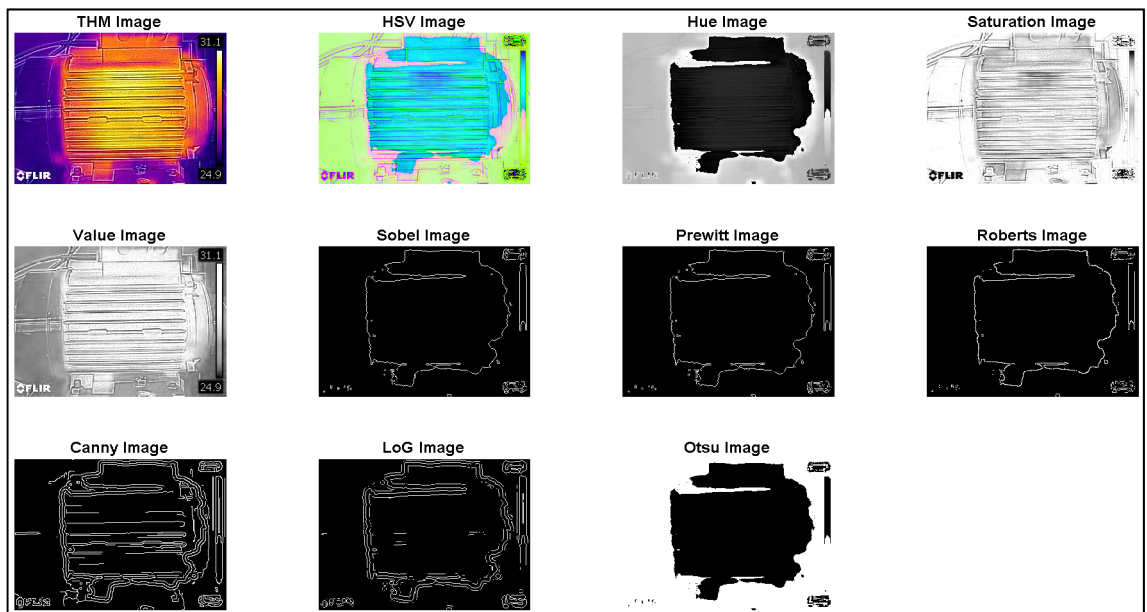


Figure A-16: Thermal image analysis for outer race bearing fault with no load.

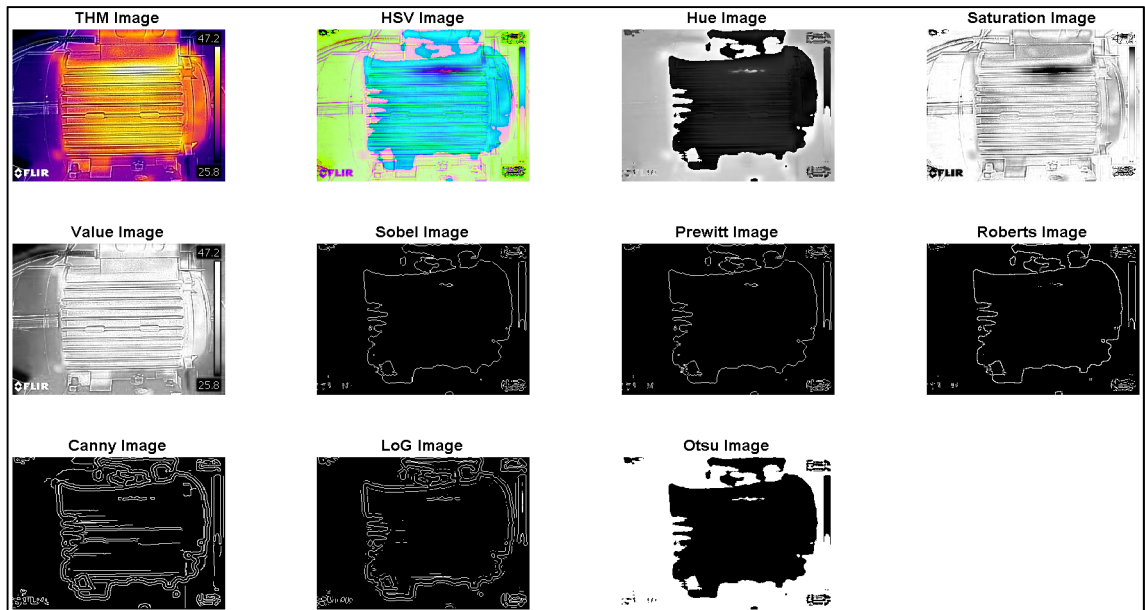


Figure A-17: Thermal image analysis for outer race bearing fault with 50% load.

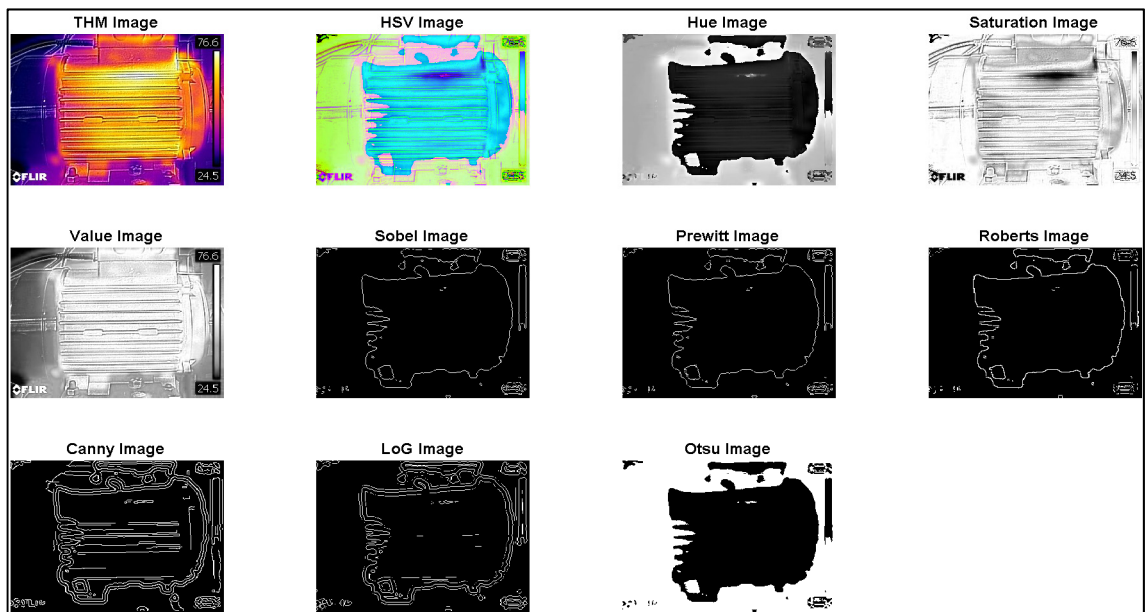


Figure A-18: Thermal image analysis for outer race bearing fault with 100% load.

APPENDIX B - CURRENT AND VIBRATION SIGNALS ANALYSIS

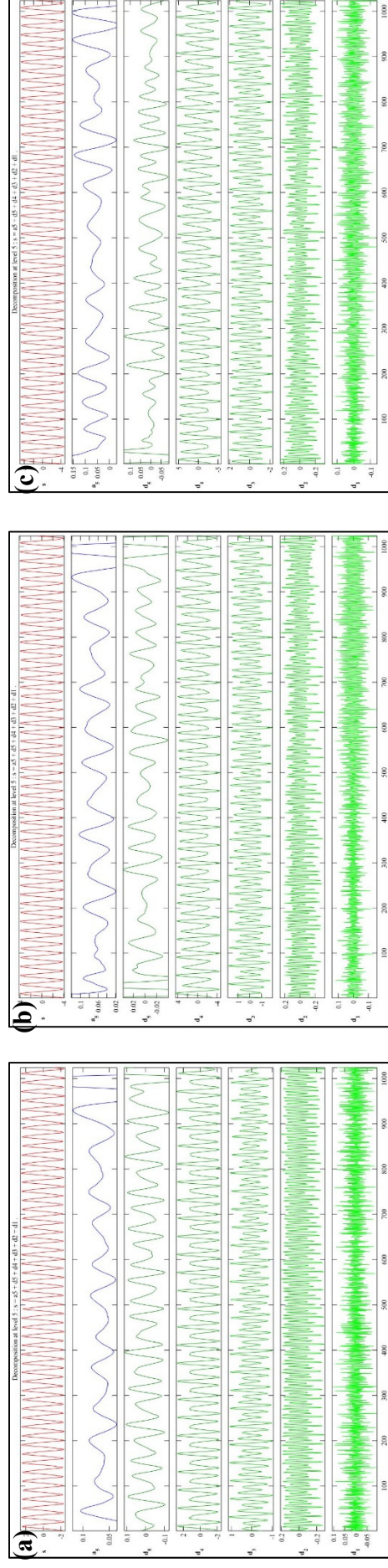


Figure B-1: Wavelet analysis for one bar rotor fault based on current signal a) No load, b) 50 % load, c) 100% load.

Appendix B – CURRENT AND VIBRATION SIGNALS ANALYSIS

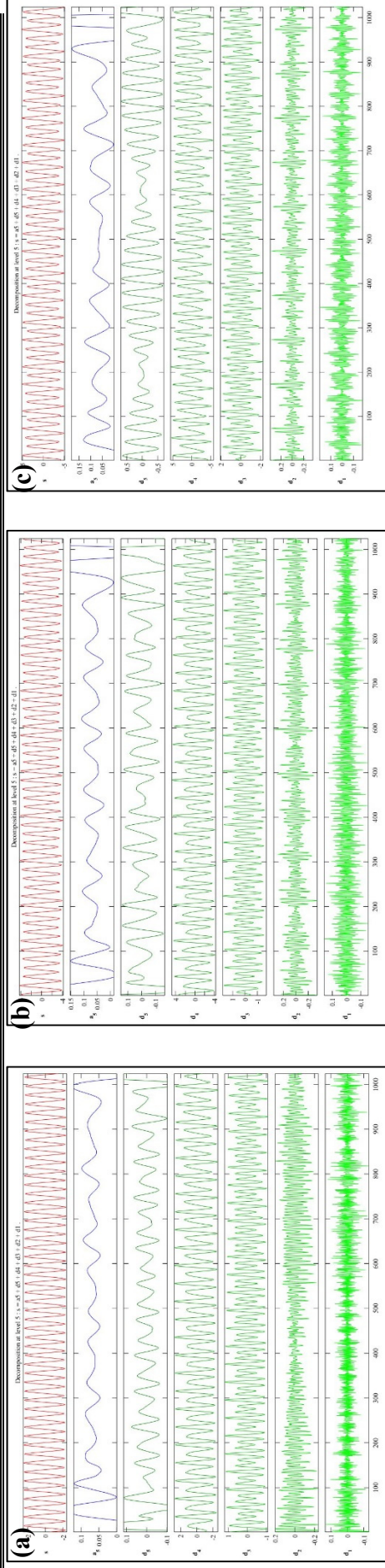


Figure B-2: Wavelet analysis for eight bars rotor fault based on current signal a) No load, b) 50 % load, c) 100% load.

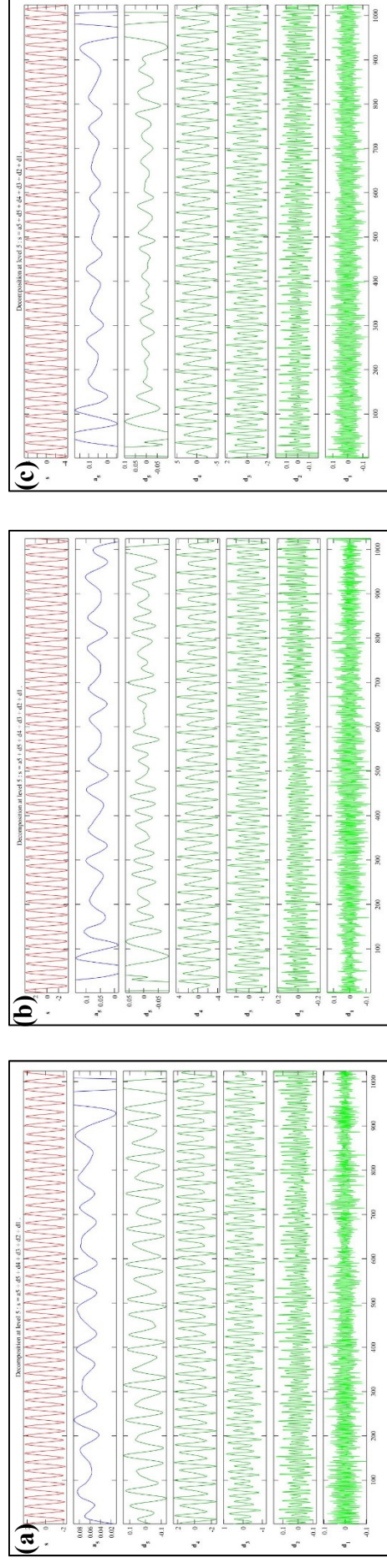


Figure B-3: Wavelet analysis for ball bearing fault based on current signal a) No load, b) 50 % load, c) 100% load.

Appendix B – CURRENT AND VIBRATION SIGNALS ANALYSIS

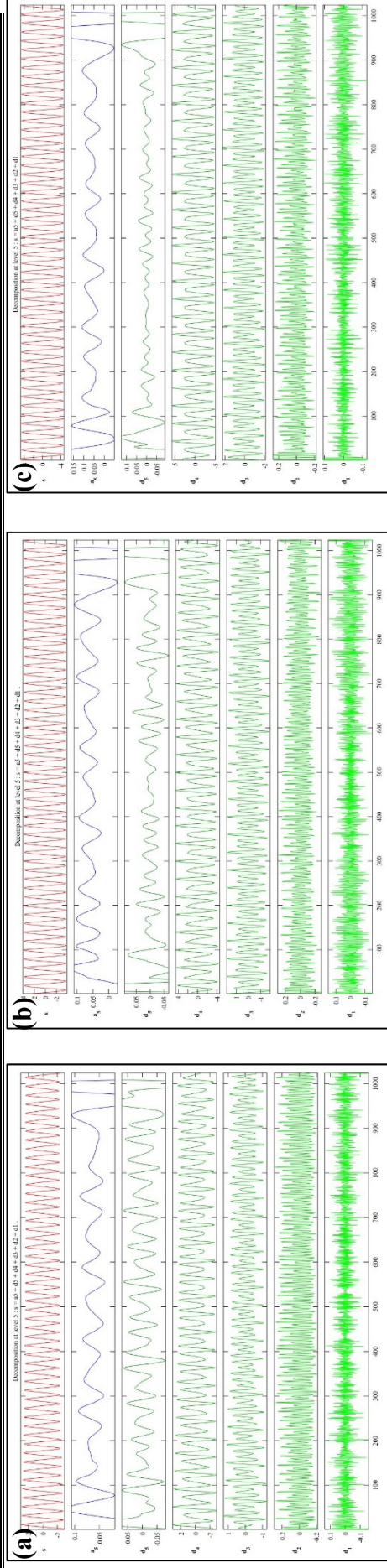


Figure B-4: Wavelet analysis for inner race bearing fault based on current signal a) No load, b) 50 % load, c) 100% load.

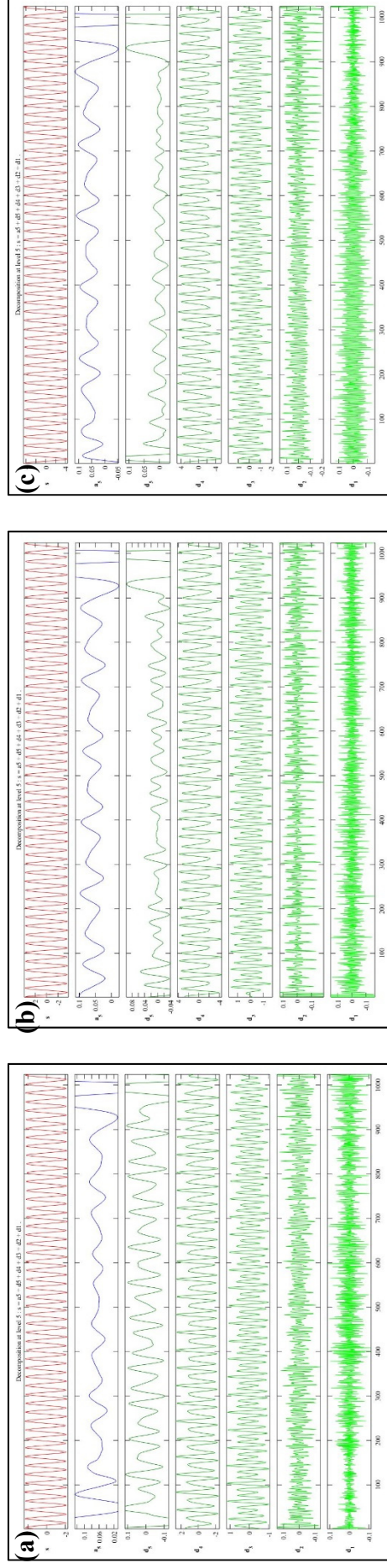


Figure B-5: Wavelet analysis for outer race bearing fault based on current signal a) No load, b) 50 % load, c) 100% load.

Appendix B - CURRENT AND VIBRATION SIGNALS ANALYSIS

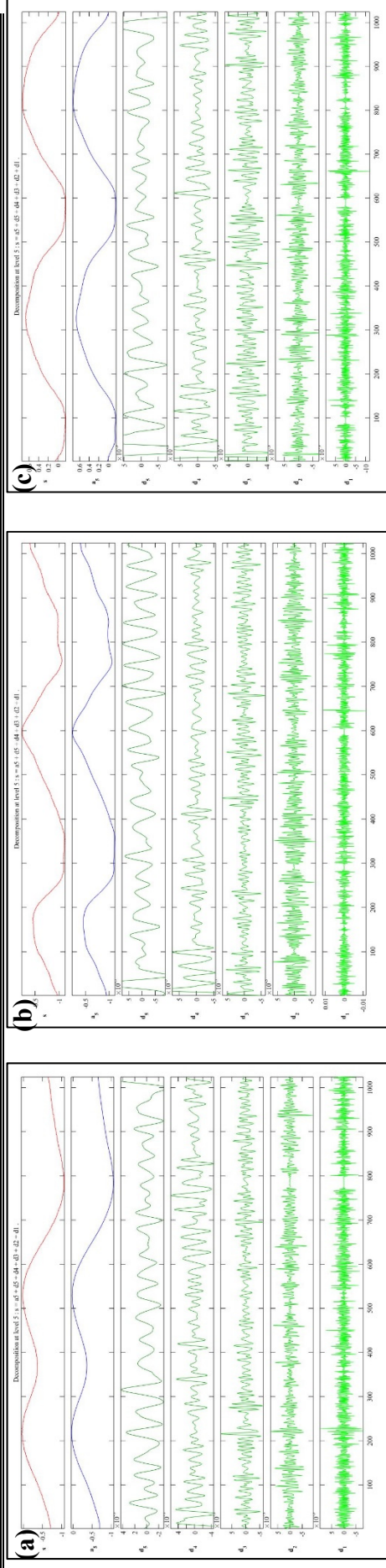


Figure B-6: Wavelet analysis for one bar rotor fault based on vibration signal a) no load, b) 50% load, and c) 100% load.

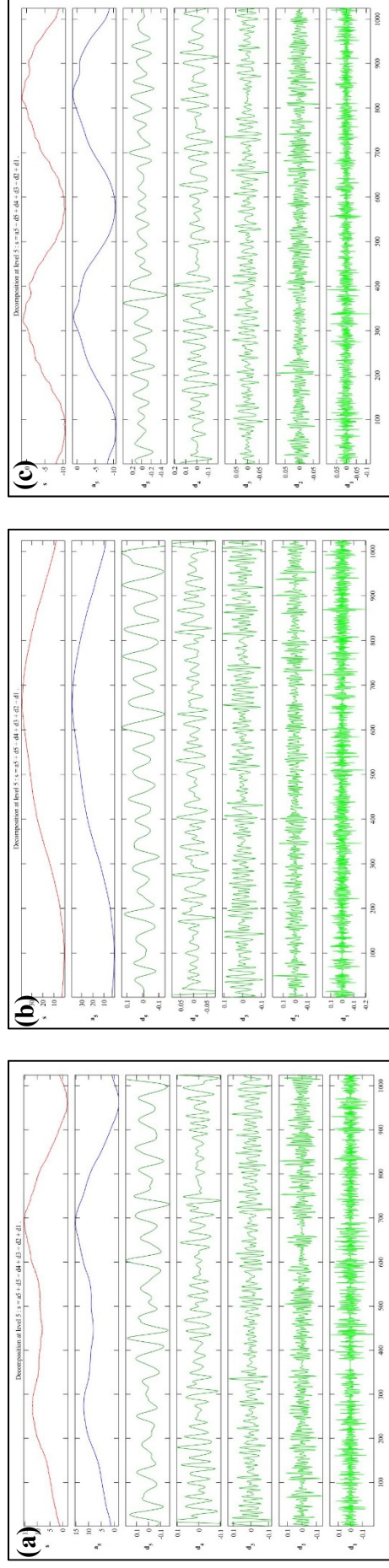


Figure B-7: Wavelet analysis for eight bars rotor fault based on vibration signal a) no load, b) 50% load, and c) 100% load.

Appendix B - CURRENT AND VIBRATION SIGNALS ANALYSIS

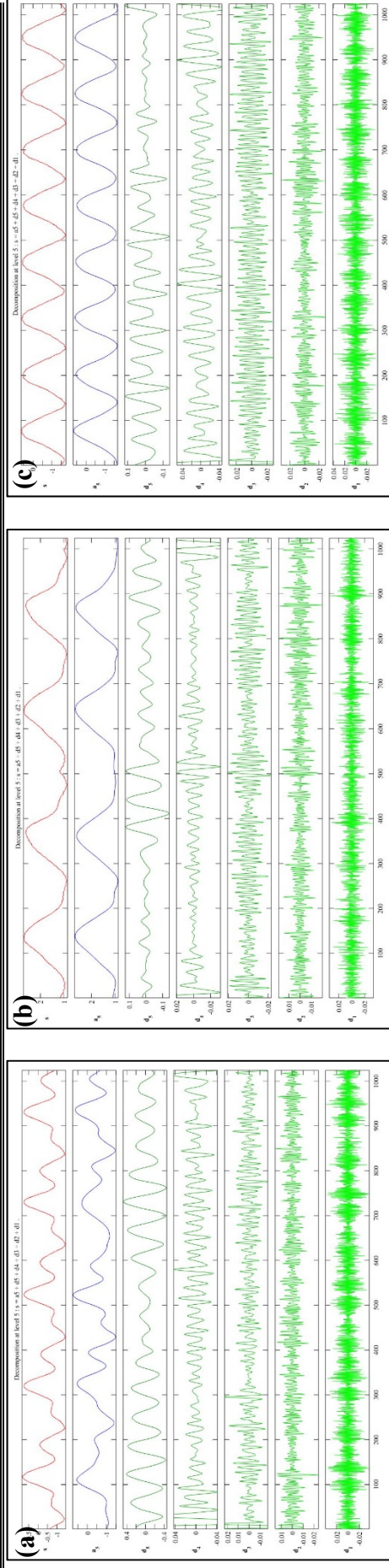


Figure B-8: Wavelet analysis for ball bearing vibration signal a) no load, b) 50% load, and c) 100% load.

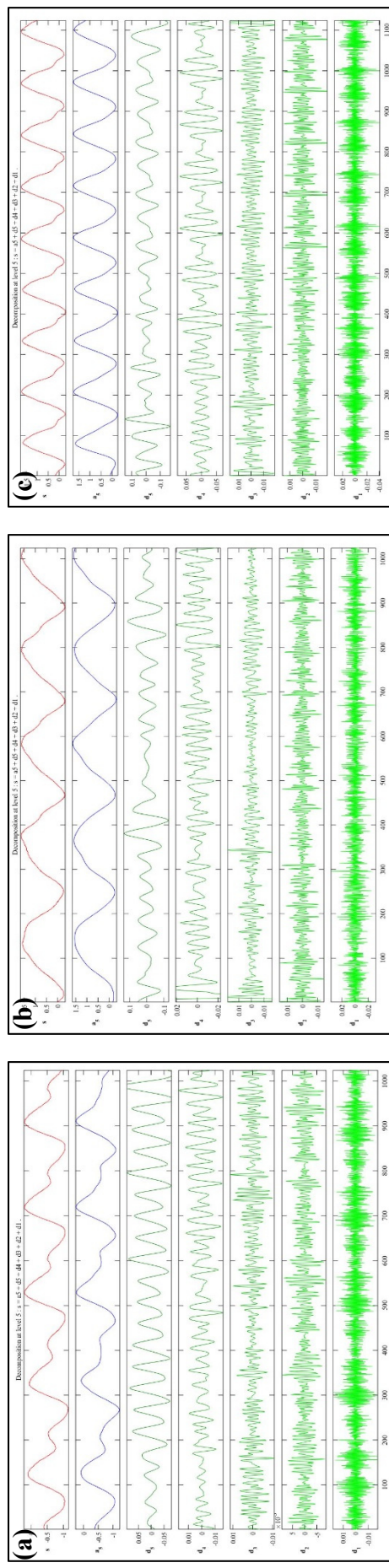


Figure B-9: Wavelet analysis for inner race bearing vibration signal a) no load, b) 50% load, and c) 100% load.

Appendix B - CURRENT AND VIBRATION SIGNALS ANALYSIS

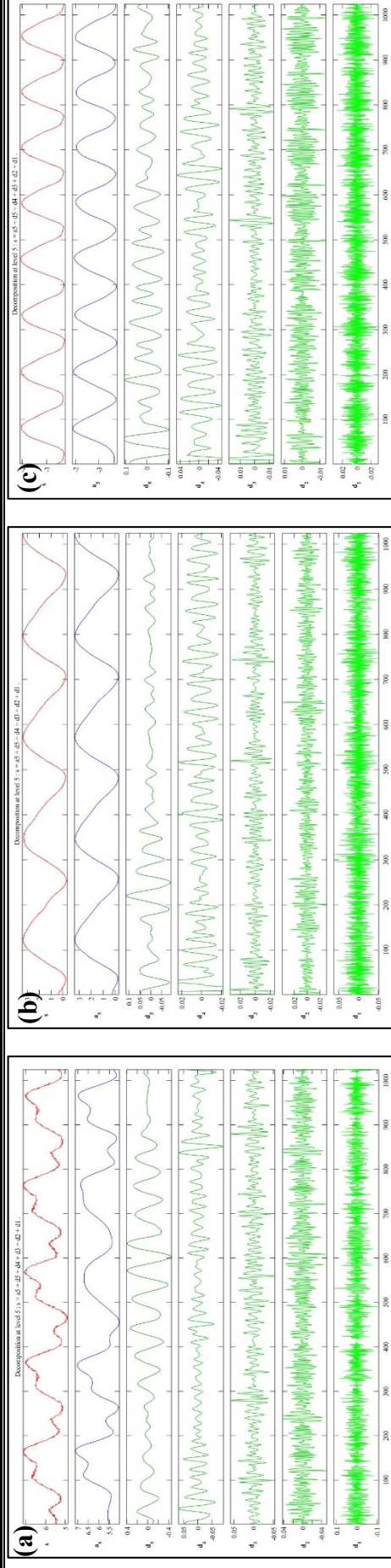


Figure B-10: Wavelet analysis for outer race bearing fault based on vibration signal a) no load, b) 50% load, and c) 100% load.

APPENDIX C – MATLAB CODE

1- MATLAB code for the proposed B4M

```
Clear all
clc
[num,txt,rows] = xlsread('Dataset.xlsx');
% import numerical data:
X = num;
[N,M] = size(X);
% calculate the minimum and maximum for each variables
Xmin = min(X);
Xmax = max(X);
% import category names:
category = txt(2:end,end);
categ = unique(category,'stable');
K = size(categ,1);
% convert category to group from 1 to k
[tf,group] = ismember(category,categ);
% calculate the minimum and maximum for each variables and for each categories
XmaxK = zeros(K,M);
XminK = zeros(K,M);
for i = 1:K
    XmaxK(i,:) = max(X(group==i,:));
    XminK(i,:) = min(X(group==i,:));
end;
XmaxK = reshape(XmaxK',1,K*M);
XminK = reshape(XminK',1,K*M);
%%%%%%%%%%%%%%%%%%%%%%%%%%%%%%%%%%%%%%%%%%%%%%%%%%%%%%%%%%%%%%%%%%%%%%%%
tic;
n = 100; % number of scout bees (e.g. 40-100)
itr = 10; % number of iterations (e.g. 1000-5000)
m = 10; % number of best selected patches (e.g. 10-50)
e = 10; % number of elite selected patches (e.g. 10-50)
n1 = 20; % number of recruited bees around best selected patches (e.g. 10-50)
n2 = 70; % number of recruited bees around elite selected patches (e.g.10-50)
ngh = 0.000000000234;
%%%%%%%%%%%%%%%%%%%%%%%%%%%%%%%%%%%%%%%%%%%%%%%%%%%%%%%%%%%%%%%%%%%%%%%%
%Scoutbees: random search (only once)%%%%%%%%
U = ones(n,1)*XmaxK + 2*ngh*(-rand(n,K*M));
L = ones(n,1)*XminK + 2*ngh*(rand(n,K*M));
Group = group*ones(1,n);
Par_Q = sortrows([U, L, fitnessfun(Group,categori(X,U,L))],-2*K*M-1);
XXXX=categori(X,U,L);
clear U L Best
%%%%%%%%%%%%%%%%%%%%%%%%%%%%%%%%%%%%%%%%%%%%%%%%%%%%%%%%%%%%%%%%%%%%%%%%
%Iterations of the algorithm %%%%%%%%%
for k=1:itr
    for j = 1:e % number of elite selected patches
        for i = 1:n2 % number of bees around elite patches
            U = beedance(ngh, Par_Q(j,1:K*M));
            LL = reshape((ones(K,1)*Xmin)',K*M,1)';
            L = LL + rand(1,K*M).*(U-LL);
            if fitnessfun(group,categori(X,U,L))> Par_Q(j,2*K*M+1)
                Par_Q(j,:)= [U, L, fitnessfun(group,categori(X,U,L))];
            end
        end
    end
end
```

```

for j = e+1:m % number of best selected patches
    for i = 1:n1 % number of bees around best patches
        U = beedance(ngh, Par_Q(j,1:K*M));
        LL = reshape((ones(K,1)*Xmin)',K*M,1)';
        L = LL + rand(1,K*M).*(U-LL);
        if fitnessfun(group,categori(X,U,L))> Par_Q(j,2*K*M+1)
            Par_Q(j,:)= [U, L, fitnessfun(group,categori(X,U,L))];
        end
    end
end
end
% Rule Pruning
U = ones(n-m,1)*XmaxK + 2*ngh*(-rand(n-m,K*M));
L = ones(n-m,1)*XminK + 2*ngh*(-rand(n-m,K*M));
Group = group*ones(1,n-m);
Par_Q(m+1:n,:) = sortrows([U, L, fitnessfun(Group,categori(X,U,L))],-2*K*M-1);
Par_Q = sortrows(Par_Q,-2*K*M-1);
Best(k,:) = Par_Q(1:15,2*K*M+1)';
if mod(k,1)==0
    disp(sprintf('Iteration Number: %02.0f,k));
end;
end
Xmax;
Xmin;
U = Par_Q(1,1:K*M);
L = Par_Q(1,K*M+1:2*K*M);
Lower = reshape(L,M,K)';
Upper = reshape(U,M,K)';
% Rules before optimization
disp("")
disp('Rules before optimization:')
disp("")
for i = 1:K
    str = ['if '];
    for j = 1:M
        str = [str '( x_' num2str(j) ' < ' num2str(Upper(i,j)) ' ) and '];
    end
    str = str(1:end-5);
    str = [str ' then class "" categ {i} ""'];
    disp(str)
end
% Rules after optimization
Lower = reshape(L,M,K)';
Upper = reshape(U,M,K)';
disp("")
disp('Pruning Rules:')
disp("")
for i = 1:K
    str = ['if '];
    for j = 1:M
        if Lower(i,j)>=Xmin(j)
            str = [str '( x_' num2str(j) ' >= ' num2str(Lower(i,j)) ' ) and '];
        end;
    end;
    str = str(1:end-5);
    str = [str ' then class "" categ {i} ""'];
    disp(str)
end;
% Testing the test data
[numb,txtt,rawss] = xlsread('test.xlsx');
XX = numb;

```

```
[MM,NN]=size(XX);
X1 = numb; % use all data for fitting
Y1 = category;
Conf_Mat = confusionmat(group,categori(X,U,L))
x = sum (diag(Conf_Mat));
y = sum (sum (Conf_Mat));
Accuracy = x/y*100
correctly = Accuracy * N /100
misclassified = N-correctly
toc;
```

2- MATLAB code for the all the proposed feature selection methods

```
function varargout = DEMO(varargin)
gui_Singleton = 1;
gui_State = struct('gui_Name',    mfilename, ...
    'gui_Singleton', gui_Singleton, ...
    'gui_OpeningFcn', @DEMO_OpeningFcn, ...
    'gui_OutputFcn', @DEMO_OutputFcn, ...
    'gui_LayoutFcn', [], ...
    'gui_Callback', []);
if nargin && ischar(varargin{1})
    gui_State.gui_Callback = str2func(varargin{1});
end
if nargout
    [varargout{1:nargout}] = gui_mainfcn(gui_State, varargin{:});
else
    gui_mainfcn(gui_State, varargin{:});
end
return
% --- Executes just before DEMO is made visible.
function DEMO_OpeningFcn(hObject, eventdata, handles, varargin)
global FSSettings StopByUser
FSSettings.ErrorEstMethod = 'SFS';
FSSettings.FSMethod = 'SFS';
%----- Classifier Settings -----
FSSettings.GammaParam = 0.025;
FSSettings.ConfMatSwitch = 0;
FSSettings.PercTest = 10;
%-- Sequential Selection Settings ----
FSSettings.MahalInfoLossMethod = 'on';
FSSettings.TotalNStepsThres = 250;
FSSettings.LogViewOfIntStep = 1;
%----- ReliefF -----
FSSettings.NCorePatterns = 250;
FSSettings.NHits = 10;
%-----
handles.output = hObject;
StopByUser = 0;
axes(handles.YelLinesAxes); set(gca, 'Visible', 'off');
handles.SliderValue = 10;
warning off all
guidata(hObject, handles);
% --- Outputs from this function are returned to the command line.
function varargout = DEMO_OutputFcn(hObject, eventdata, handles)
% varargout cell array for returning output args (see VARARGOUT);
% hObject handle to figure
varargout{1} = handles.output;
% -----Data Load and View -----
function OpenDataFile_ClickedCallback(hObject, eventdata, handles)
```

```
handles.file = uigetfile('*.*');
global StopByUser
if handles.file~=0
    % Only for viewing purpose
    [Patterns, Targets] = DataLoadAndPreprocess(handles.file);
    handles.PatternsToRunFS = Patterns;
    handles.TargetsToRunFS = Targets;
    StopByUser = 0;
    [NPatterns, KFeatures] = size(Patterns);
    axes(handles.FeatSelCurve); cla reset;
    axes(handles.ClassResAxes); cla reset;
    axes(handles.ClassesLegendAxes); cla reset;
    set(gca,'Visible','off');
    axes(handles.YelLinesAxes); set(gca, 'Visible', 'off');
    axis manual
    axes(handles.PatternsFeaturesAxes); cla reset;
    title(handles.file);
    colorbar;
    set(findobj(gcf,'Tag','ListSelFeats'), 'String','Press Start to select features');
    guidata(hObject, handles);
end
return
% -----
function RunFeatSelection_ClickedCallback(hObject, eventdata, handles)
global StopByUser FSSettings
set(findobj(gcf,'Tag','ListSelFeats'), 'String', []);
axes(handles.FeatSelCurve); cla reset;
axes(handles.YelLinesAxes); cla reset; set(gca,'Visible','off', 'YDir','reverse');
StopByUser = 0;
guidata(hObject, handles);
FSSettings.FSMethod
if strcmp(FSSettings.FSMethod,'SFS') || strcmp(FSSettings.FSMethod,'SFFS')
[ResultMat, ConfMatOpt, Tlapse, handles.OptimumFeatureSet, OptimumCCR]= ForwSel_main(handles.file,
FSSettings, handles);
elseif strcmp(FSSettings.FSMethod,'ReliefF')
[FeatureWeightsOrdered, FeaturesIndexOrdered, handles.OptimumFeatureSet] = ReliefF(handles.file,
FSSettings,handles);
elseif strcmp(FSSettings.FSMethod,'SBS') || strcmp(FSSettings.FSMethod,'SFBS')
[ResultMat, ConfMatOpt, Tlapse, handles.OptimumFeatureSet, OptimumCCR]= BackSel_main(handles.file,
FSSettings, handles);
end
handles.OptimumFeatureSet = sort(handles.OptimumFeatureSet);
guidata(hObject, handles);
% -----
function StopFeatSelButton_ClickedCallback(hObject, eventdata, handles)
global StopByUser
StopByUser = 1;
guidata(hObject, handles);
return
%-----
function ListSelFeats_CreateFcn(hObject, eventdata, handles)
if ispc && isequal(get(hObject,'BackgroundColor'), get(0,'defaultUicontrolBackgroundColor'));
    set(hObject,'BackgroundColor','white');
end
set(hObject,'String','None Selected yet');
%-----
function LoadAndClassifyButton_ClickedCallback(hObject, eventdata, handles)
handles.fileToClassify = uigetfile('*.*mat');
PatternsToClassify = DataLoadAndPreprocess(handles.fileToClassify);
handles.PatternsToClassify = PatternsToClassify(:, handles.OptimumFeatureSet);
```

```

NPatternsToClassify = size(PatternsToClassify,1);
if NPatternsToClassify >= 10
set(findobj(gcf,'Tag','ClassResSlider'), ...
    'Max', NPatternsToClassify,...
    'Min', 10, ...
    'Value', 10, ...
    'SliderStep',[1 1]/(NPatternsToClassify-10),'Enable', 'on');
else
set(findobj(gcf,'Tag','ClassResSlider'), 'Enable', 'off');
end
handles.SliderValue = 10;
guidata(hObject, handles);
DEMO('ClassifyAndPlot',guidata(gcbo));
guidata(hObject, handles);
%-----
function ClassResSlider_Callback(hObject, eventdata, handles)
handles.SliderValue = get(hObject,'Value');
guidata(hObject, handles);
DEMO('ClassifyAndPlot',guidata(gcbo));
guidata(hObject, handles);
%-----
function ClassResSlider_CreateFcn(hObject, eventdata, handles)
if isequal(get(hObject,'BackgroundColor'), ...
    get(0,'defaultUicontrolBackgroundColor'))
set(hObject,'BackgroundColor',[.9 .9 .9]);
end
%-----
function ClassifyAndPlot(handles)
PatternsToRunFS = handles.PatternsToRunFS(:, handles.OptimumFeatureSet);
ProbsClass = BayesClassValidationSet(PatternsToRunFS, handles.TargetsToRunFS,
handles.PatternsToClassify);
NPatternsToClassify = size(ProbsClass,1);
SumProbsClass = sum(ProbsClass,2);
for IndexPatterns = 1:NPatternsToClassify
    ProbsClass(IndexPatterns,:) = ProbsClass(IndexPatterns, :)/SumProbsClass(IndexPatterns);
end
[Dummy, PredictionClass] = max(ProbsClass, [], 2);
[NPatterns, CClasses] = size(ProbsClass);
axes(handles.ClassResAxes); cla reset;
set(gca,'YDir','reverse','Color',[.925 .914 .847]);
axis([-0.5 1.5 0.5 10.5]);
CumProbsClass = [zeros(NPatterns,1) cumsum(ProbsClass,2)];
ColorsToUse = 'rgbycmk';
YLocat = 0;
handles.SliderValue = 10 + NPatterns - ceil(handles.SliderValue);
for IndexPattern = (handles.SliderValue-9):handles.SliderValue
    YLocat = YLocat + 1;
    if IndexPattern <= NPatterns
        for IndexClass = 1:CClasses
            hold on
            text(-0.15, YLocat, num2str(IndexPattern), 'HorizontalAlignment', 'right');
            plot(CumProbsClass(IndexPattern, IndexClass:(IndexClass+1)), YLocat*ones(1,2),
ColorsToUse(IndexClass), 'LineWidth', 5);
        end
    end
end
text(-0.9 ,0.5,'Pattern #');
text(0.2 ,0.5,'P(x|\Omega_i)');
text(1 ,0.5,'Predict');
axis([-0.5 1.5 0.5 10.5]);

```

```
set(gca,'Visible','off');
drawnow
axes(handles.ClassesLegendAxes);
for IndexClass = 1:CClasses
    text(0.1, IndexClass*0.5, ['Class ' num2str(IndexClass)], 'Color', ColorsToUse(IndexClass));
end
axis([0 1.5 0.5 5])
% ----- Menu Functions -----
function OpenDataMenu_Callback(hObject, eventdata, handles)
DEMO('OpenDataFile_ClickedCallback',gcbo,[],guidata(gcbo));
function RunFsMenu_Callback(hObject, eventdata, handles)
DEMO('RunFeatSelection_ClickedCallback',gcbo,[],guidata(gcbo));
function StopFSMenu_Callback(hObject, eventdata, handles)
DEMO('StopFeatSelButton_ClickedCallback',gcbo,[],guidata(gcbo));
function StandardCrossMenu_Callback(hObject, eventdata, handles)
global FSSettings
FSSettings.ErrorEstMethod = 'Standard';
set(hObject,'Checked','on');
set(findobj(gcf,'Tag','ResubMenu'),'Checked','off');
set(findobj(gcf,'Tag','ProposedACrossMenu'),'Checked','off');
set(findobj(gcf,'Tag','ProposedABCrossMenu'),'Checked','off');
guidata(hObject, handles);
function ProposedACrossMenu_Callback(hObject, eventdata, handles)
global FSSettings
FSSettings.ErrorEstMethod = 'ProposedA';
set(hObject,'Checked','on');
set(findobj(gcf,'Tag','ResubMenu'),'Checked','off');
set(findobj(gcf,'Tag','ProposedABCrossMenu'),'Checked','off');
set(findobj(gcf,'Tag','StandardCrossMenu'),'Checked','off');
guidata(hObject, handles);
function ProposedABCrossMenu_Callback(hObject, eventdata, handles)
global FSSettings
FSSettings.ErrorEstMethod = 'ProposedAB';
set(hObject,'Checked','on');
set(findobj(gcf,'Tag','ResubMenu'),'Checked','off');
set(findobj(gcf,'Tag','ProposedACrossMenu'),'Checked','off');
set(findobj(gcf,'Tag','StandardCrossMenu'),'Checked','off');
guidata(hObject, handles);
function ResubMenu_Callback(hObject, eventdata, handles)
global FSSettings
FSSettings.ErrorEstMethod = 'Resubstitution';
set(hObject,'Checked','on');
set(findobj(gcf,'Tag','ProposedABCrossMenu'),'Checked','off');
set(findobj(gcf,'Tag','ProposedACrossMenu'),'Checked','off');
set(findobj(gcf,'Tag','StandardCrossMenu'),'Checked','off');
guidata(hObject, handles);
% ----- FS Menu Functions -----
function SFS_Callback(hObject, eventdata, handles)
global FSSettings
FSSettings.FSMethod = 'SFS';
FS_Method_ClearAllChecks(hObject, handles)
set(hObject,'Checked','on');
guidata(hObject, handles);
function SFFS_Callback(hObject, eventdata, handles)
global FSSettings
FSSettings.FSMethod = 'SFFS';
FS_Method_ClearAllChecks(hObject, handles)
set(hObject,'Checked','on');
guidata(hObject, handles);
function ReliefF_Callback(hObject, eventdata, handles)
```

```
global FSSettings
FSSettings.FSMethod = 'ReliefF';
FS_Method_ClearAllChecks(hObject, handles)
set(hObject,'Checked','on');
guidata(hObject, handles);
function SBS_Callback(hObject, eventdata, handles)
global FSSettings
FSSettings.FSMethod = 'SBS';
FS_Method_ClearAllChecks(hObject, handles)
set(hObject,'Checked','on');
guidata(hObject, handles);
function SFBS_Callback(hObject, eventdata, handles)
global FSSettings
FSSettings.FSMethod = 'SFBS';
FS_Method_ClearAllChecks(hObject, handles)
set(hObject,'Checked','on');
guidata(hObject, handles);
function FS_Method_ClearAllChecks(hObject, handles)
set(findobj(gcf,'Tag','ReliefF'),'Checked','off');
set(findobj(gcf,'Tag','SFBS'),'Checked','off');
set(findobj(gcf,'Tag','SFS'),'Checked','off');
set(findobj(gcf,'Tag','SFBS'),'Checked','off');
set(findobj(gcf,'Tag','SBS'),'Checked','off');
guidata(hObject, handles);
%-----
function SettingsMenu_Callback(hObject, eventdata, handles)
global FSSettings
FSSettings = SettingsMenuFig;
```

3- MATLAB code for GA-based feature selection

```
function Feat_Index = Genetic_Algorithm
clear all
% global Data
Data = load('Dataset.mat'); % This is available in Mathworks
GenomeLength = 8; % This is the number of features in the dataset
tournamentSize = 2;
options = gaoptimset('CreationFcn', {@PopFunction},...
    'PopulationSize',50,...
    'Generations',100,...
    'PopulationType', 'bitstring',...
    'SelectionFcn', {@selectiontournament,tournamentSize},...
    'MutationFcn', {@mutationuniform, 0.1},...
    'CrossoverFcn', {@crossoverarithmetic,0.8},...
    'EliteCount',2,...
    'StallGenLimit',100,...
    'PlotFcns', {@gaplotbestf},...
    'Display', 'iter');
rand('seed',1)
nVars = 8; %
FitnessFcn = @FitFunc_KNN;
[chromosome,~,~,~,~] = ga(FitnessFcn,nVars,options);
Best_chromosome = chromosome; % Best Chromosome
Feat_Index = find(Best_chromosome==1); % Index of Chromosome
end
%%% POPULATION FUNCTION
function [pop] = PopFunction(GenomeLength,~,options)
pop = (rand(options.PopulationSize, GenomeLength)> RD); % Initial Population
end
%%% FITNESS FUNCTION You may design your own fitness function here
```



```
function [FitVal] = FitFunc_KNN(pop)
% global Data
Data = load('vsv.mat');
FeatIndex = find(pop==1); %Feature Index
X1 = Data.X;% Features Set
Y1 = grp2idx(Data.Y);% Class Information
X1 = X1(:,[FeatIndex]);
NumFeat = numel(FeatIndex);
Compute = ClassificationKNN.fit(X1,Y1,'NSMethod','exhaustive','Distance','euclidean');
Compute.NumNeighbors = 3; % kNN = 3
FitVal = resubLoss(Compute)/(34-NumFeat);
end
```